QCD sum rule studies of Heavy Quarkonium-like states

A Thesis Submitted to the
College of Graduate Studies and Research
in Partial Fulfillment of the Requirements
for the degree of Doctor of Philosophy
in the Department of Physics and Engineering Physics
University of Saskatchewan
Saskatoon

By

Robin Thomas Kleiv

Permission to Use

In presenting this thesis in partial fulfilment of the requirements for a Postgraduate degree from the University of Saskatchewan, I agree that the Libraries of this University may make it freely available for inspection. I further agree that permission for copying of this thesis in any manner, in whole or in part, for scholarly purposes may be granted by the professor or professors who supervised my thesis work or, in their absence, by the Head of the Department or the Dean of the College in which my thesis work was done. It is understood that any copying or publication or use of this thesis or parts thereof for financial gain shall not be allowed without my written permission. It is also understood that due recognition shall be given to me and to the University of Saskatchewan in any scholarly use which may be made of any material in my thesis.

Requests for permission to copy or to make other use of material in this thesis in whole or part should be addressed to:

Head of the Department of Physics and Engineering Physics
116 Science Place
University of Saskatchewan
Saskatoon, Saskatchewan
Canada
S7N 5E2

Abstract

In 2003 the Belle collaboration announced the discovery of the $X(3872)$ particle. This was confirmed shortly thereafter by the CDF, D0 and BaBar collaborations, and later by the LHCb collaboration. Based on the decay modes that have been observed to date, it is clear that this particle is a hadron, that is, a composite particle that experiences the strong nuclear force. The $X(3872)$ was found within a family of well understood hadrons called charmonia. Interestingly, it is quite difficult to interpret the $X(3872)$ as a charmonium state. For this reason it has been widely speculated that the $X(3872)$ cannot be understood in terms of the quark model, unlike the vast majority of hadrons observed to date. Such hitherto unobserved particles are called exotic hadrons. Since the discovery of the $X(3872)$, many similarly anomalous charmonium-like particles have been discovered. As would be expected, some unanticipated hadrons have also been found in the closely related bottomonium spectrum. These particles are collectively referred to as heavy quarkonium-like. Evidence is growing that at least some of these particles are exotic hadrons. If confirmed, this would have dramatic implications for our understanding of the strong nuclear force.

A major experimental and theoretical effort is now underway in the field of hadron spectroscopy to determine the identities of the heavy quarkonium-like states. In order to investigate the possibility that some of these states could be exotic hadrons, theoretical calculations are needed to firmly establish their properties. One of the main arguments for the existence of exotic hadrons is that they are predicted by the fundamental theory of the strong interaction, Quantum Chromodynamics (QCD). Therefore it is desirable to predict the properties of exotic hadrons using a theoretical approach that is firmly based in QCD. One such method is QCD sum rules (QSR).

The research presented here uses the QSR technique to study exotic hadrons. There are several themes in this work. First is the use of QSR to predict the masses of exotic hadrons that may exist among the heavy quarkonium-like states. The second theme is the application of sophisticated loop integration methods in order to obtain more complete theoretical results. These in turn can be extended to higher orders in the perturbative expansion in order to predict the properties of exotic hadrons more accurately. The third

theme involves developing a renormalization methodology for these higher order calculations. This research has implications for the $Y(3940)$, $X(3872)$, $Z_c^{\pm}(3895)$, $Y_b(10890)$, $Z_b^{\pm}(10610)$ and $Z_b^{\pm}(10650)$ particles, thereby contributing to the ongoing effort to understand these and other heavy quarkonium-like states.

Acknowledgements

First, I wish to express my deepest gratitude to my supervisor, Dr. Tom Steele. His skilled guidance, thoughtful advice, constant support and deep knowledge of physics have benefited me enormously. I would also like to thank the members of my advisory committee, Dr. Murray Bremner, Dr. Rainer Dick, Dr. Glenn Hussey, and Dr. Kaori Tanaka, as well as my external examiner, Dr. Marcelo Loewe. I am grateful for their advice, support and encouragement. Thanks also to my collaborators on the articles included in this thesis: Ryan Berg, Dr. Ian Blokland, Dr. Derek Harnett, Dr. Hong-Ying Jin, Dr. Ken Moats, and Dr. Ailin Zhang. Part of this work was completed at Shanghai University, which I thank for its hospitality. I am also grateful to the National Science and Engineering Research Council (NSERC) and the University of Saskatchewan for financial support.

I am grateful to my family and friends for their unwavering support and encouragement. Without them, this thesis would not have been possible. Thanks to Ryan Berg, Brian Bewer, Yasmin Carter, Katie Knorr, Keith Kotyk, Martin Lepage, John McLeod, Denin Nienaber, Eric Nienaber, Kurt Nienaber, Percy Paul, Gareth Perry, Fred Sage, Zhi-Wei Wang, Mark Wurtz and Melissa Wurtz. *Mange Takk* to Margaret and Thor Kleiv for their kind hospitality when I first arrived in Saskatoon and for their constant encouragement since then. Special thanks are due to my teacher, mentor, colleague and friend Dr. Derek Harnett for setting me on this path in the first place. Above all I thank my family for their love and support.

To my family.

Contents

List of Tables

List of Figures

List of Abbreviations

MS	Minimal Subtraction
$\overline{\text{MS}}$	Modified-Minimal Subtraction
OPE	Operator Product Expansion
QCD	Quantum Chromodynamics
QED	Quantum Electrodynamics
QSR	QCD Sum Rules
SM	Standard Model

Chapter 1

Introduction

1.1 Motivation for Research

In 2003, the $X(3872)$ was discovered by the Belle collaboration [36]. The discovery was subsequently confirmed by the Babar [13], CDF [8], D0 [4] and LHCb collaborations [3]. The decays of this particle that have been observed to date clearly indicate that it is a hadron, that is, a composite particle composed of quarks that experiences the strong nuclear force. This particle was found within the mass region occupied by a well understood family of hadrons known as charmonia. However, the properties of the $X(3872)$ make it difficult to interpret it as a member of the charmonium spectrum [114]. Since 2003, more hadrons have been discovered in the charmonium mass region that are difficult to interpret as charmonium states. A few anomalous hadrons have also been found within the closely related bottomonium spectrum. These anomalous particles are called heavy quarkonium-like, or XYZ states. Table 1.1 includes basic information for experiments that have discovered XYZ states and Table 1.2 lists the XYZ states that have been confirmed by more than one experiment at a high level of statistical significance. Ref. [20] provides a more complete list that includes particles that have only been observed by a single experiment and particles that have been observed at a lower level of statistical significance.

Nearly all hadrons that have been observed to date can be classified according to the quark model. The quark model was introduced in Refs. [51, 131] to bring some order to the already large number of hadrons that were known at the time. The model introduces two families of hadrons: baryons such as the neutron and proton that are fermions, and mesons such as the pion that are bosons. Both baryons and mesons are composite particles composed of fundamental particles, called quarks. Baryons are composed of three quarks and

Experiment	Facility	Process
Babar	SLAC, Stanford, USA	Electron-Positron Collider
Belle	KEK, Tsukuba, Japan	Electron-Positron Collider
BES-III	BES, Beijing, China	Electron-Positron Collider
CDF	Fermilab, Chicago, USA	Proton-Antiproton Collider
CLEO	CESR, Ithaca, USA	Electron-Positron Collider
D0	Fermilab, Chicago, USA	Proton-Antiproton Collider
LHCb	CERN, Geneva, Switzerland	Proton-Proton Collider

Table 1.1: Experiments that have detected heavy quarkonium-like states.

mesons are composed of a quark and an antiquark. It should be emphasized that the quark model does not describe the dynamics of quarks. Rather, it is a classification scheme that successfully explains the large variety of hadrons as various combinations of a small number of quarks.

Quantum Chromodynamics (QCD) successfully describes the interactions of quarks, and as such, it is a fundamental theory of the strong nuclear force. However, it is not clear how the quark model of hadrons emerges from QCD. Interestingly, QCD seems to suggest that a much richer spectrum of hadrons is possible than the simple baryons and mesons of the quark model. These hadrons that exist outside the quark model are called exotic hadrons. To date there is no unambiguous proof for the existence of any exotic hadron, although the $Z_c^{\pm}(3895)$ is a very strong candidate. There are experimentally established hadrons that are difficult to interpret within the quark model and are often speculated to be exotic hadrons. It has been widely speculated that some of the heavy quarkonium-like states may be exotic hadrons. In order to investigate this possibility, theoretical calculations are needed to firmly establish the expected properties of exotic hadrons. The methods of QCD sum rules (QSR) can be used to predict the physical properties of exotic hadrons that may exist in the same mass region as heavy quarkonia. This is the main motivation for the research presented in

Particle	Experiments
$X(3872)$	Babar, Belle, CDF, D0, LHCb
$G(3900)$	Babar, Belle
$Y(4260)$	Babar, Belle, CLEO
$Y(4360)$	Babar, Belle
$Z_c^{\pm}(3895)$	Belle, BES-III, CLEO

Table 1.2: Experimentally confirmed heavy quarkonium-like states. In all cases the number in parentheses indicates the mass in units of MeV. This system of units is called natural units and is discussed in Appendix A.

this thesis.

1.2 Hadronic Physics

1.2.1 The Standard Model

The Standard Model (SM) of particle physics is an extremely successful theoretical framework that describes all fundamental interactions in nature at the quantum level, apart from gravity. The particle content of the SM is shown in Fig. 1.1. There are three main categories of particles: spin-1 gauge bosons (g, γ, W, Z), spin-1/2 leptons (e, μ, τ, ν_e, ν_μ, ν_τ), and spin-1/2 quarks (u, d, s, c, b, t). Because they mediate interactions between particles in quantum field theory, gauge bosons are often referred to as force carriers. Leptons are particles that do not experience the strong nuclear force, such as the electron. All of the particles in Fig. 1.1 have been confirmed experimentally. However, the SM also predicts the existence of an additional particle known as the Higgs boson. On July 4, 2012, the ATLAS [1] and CMS [30] collaborations announced the discovery of a particle that is likely to be the Higgs boson. Observation of the Higgs boson is a crucial test of the Higgs mechanism, which is essential to the SM. Experimental work to precisely determine the properties of this particle is ongoing.

Figure 1.1: The particle content of the Standard Model, excluding the Higgs boson. Figure from Ref. [61].

This thesis will focus on quarks and gluons, which are the only particles in the SM that directly experience the strong nuclear force. There are six types, or flavours of quarks: up (u), down (d), strange (s), charm (c), bottom (b) and top (t). These can be divided into light quarks ($u\,, d\,, s$) and heavy quarks ($c\,, b\,, t$), which have much greater masses than the light quarks (masses are given in Table 1.3). Gluons are massless and serve as the mediators of the strong interaction. Interestingly, quarks and gluons only occur within hadrons, and cannot be isolated or otherwise removed from hadrons. This peculiar feature of the strong interaction is known as confinement, and understanding how it emerges from QCD is one of the great problems of modern physics. All approaches to this problem must invariably deal with hadrons, which are how quarks and gluons manifest themselves in nature.

1.2.2 The Quark Model

In 1964, Gell-Mann [51] and Zweig [131] independently introduced the quark model, which proposes that hadrons are not fundamental particles. Rather, they are composite objects composed of more fundamental particles, which Gell-Mann called quarks. At the time, all known hadrons could be explained in terms of just three types of quarks ($u\,,\ d\,,\ s$), and their

Flavour	Mass (MeV)	Flavour	Mass (GeV)
u	2.3	c	1.28
d	4.8	b	4.18
s	95	t	173.07

Table 1.3: Phenomenological values of the light and heavy quark masses as given in Ref. [20].

corresponding antimatter counterparts, antiquarks. The quark model suggests that there are only two kinds of hadrons: baryons that contain three quarks (qqq), and mesons that contain a quark and an antiquark ($q\bar{q}$). Baryons and mesons naturally arrange themselves into multiplets containing hadrons with similar properties and masses that are roughly degenerate. This approximate flavour symmetry is the origin of the multiplets. The vector and pseudoscalar meson nonets are shown in Fig. 1.2.

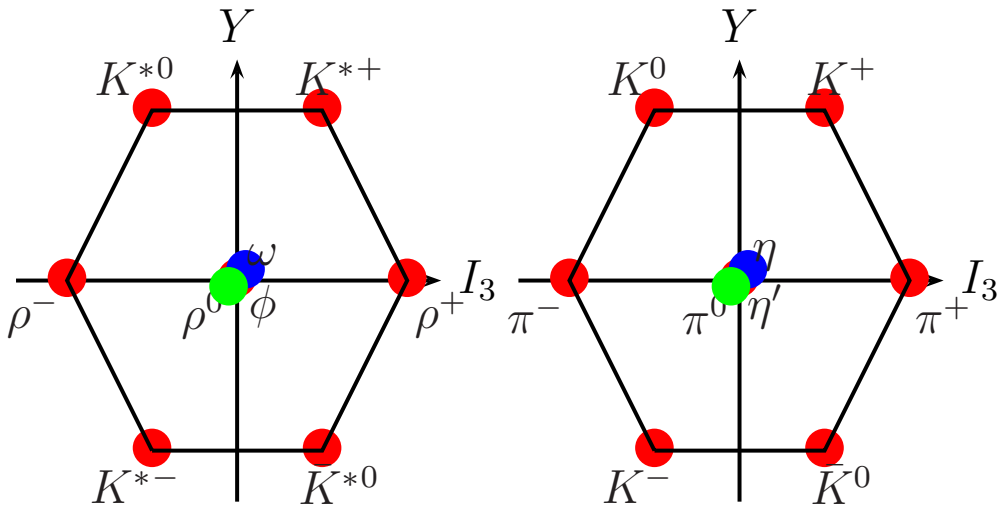

Figure 1.2: The vector (left) and pseudoscalar (right) meson nonets. The labels Y and I_3 indicate the hypercharge and isospin quantum numbers, respectively. The masses of all of these particles are less than about 1 GeV, and typically vary by a few hundred MeV within each nonet. However, the pions (π^-, π^0, π^+) are anomalously light. The reason for this emerges naturally from QCD. The figures are from Ref. [105].

In many ways, the quark model is analogous to the periodic table. Initially the periodic table served to classify the elements based on their physical and chemical properties, without

attempting to explain the underlying reasons for these properties. Of course, we now know that these properties ultimately derive from the electron shell structure of the elements as dictated by quantum mechanics. Similarly, the utility of the quark model lies in its explanation of the large number of hadrons in terms of a small number quarks.

The quark model also led to an important insight into the nature of hadrons. Consider for instance the Δ^{++} baryon, which has spin-3/2. In the quark model, it is composed of three identical spin-1/2 up quarks that are not orbitally excited with respect to one another. This means that the spin, flavour and spatial wave functions are symmetric under particle interchange, meaning that the total wave function is also. Because the Δ^{++} is a fermion, this violates the spin-statistics theorem. This observation led to the introduction of the colour quantum number for quarks [57], which in the case of the Δ^{++} has an anti-symmetric wave function, thus ensuring that the spin-statistics theorem is upheld. The name colour was chosen in order to emphasize a key feature of hadrons, and is only used as an analogy. The number of colours can be inferred from experimental data, such as from the decay rate of the neutral pion [89]. An individual quark may have one of three colours: red, green or blue. Each of the three quarks within a baryon must have a unique colour, thus the combination of red, green and blue is considered to have no net colour charge. All baryons and mesons are colourless, or colour singlets.

1.2.3 Exotic Hadrons

In QCD, the colour quantum number of quarks is understood as a kind of generalization of electric charge. Quantum Electrodynamics (QED) describes electromagnetic interactions between electrically charged particles that are mediated by electrically neutral photons. In QCD, quarks with colour charge interact via gluons, which also carry colour charge. This fact means that QCD is radically different from QED, and it is also responsible for many of the interesting features of QCD. Unlike QED, the fundamental degrees of freedom in QCD are not directly manifested in nature. Instead, quarks and gluons are realized in terms of hadrons.

QCD suggests the possibility of a far richer hadronic spectrum than the quark model. Exotic hadrons are colour singlet hadrons that are neither baryons nor mesons (see, *e.g.*

Ref. [72] for a review). One such possibility is a hadrons with four quarks ($qq\bar{q}\bar{q}$). Four-quark hadrons can be realized in two distinct ways. The first is as a weakly bound state of two colour singlet mesons $[(q\bar{q})\,(q\bar{q})]$, which is called a molecular state. The second is as a tetraquark, which is composed of diquark clusters that have a net colour charge $[(qq)\,(\bar{q}\bar{q})]$ and hence is more strongly bound than a molecular state. Diquarks are best thought of as a kind of strong correlation between two quarks within a hadron [11]. Because gluons also carry colour charge, colour singlet hadrons with explicit gluonic content are also possible. Hybrids are hadrons that can be thought of as a conventional meson with an excited gluon ($qG\bar{q}$). Perhaps the most exotic of all exotic hadrons are glueballs, which are composed entirely of gluons (GG or GGG). Note that four-quark states, hybrids and glueballs are all bosons. It should be noted that fermionic exotic hadrons are also possible, an example of which is a pentaquark ($qqqq\bar{q}$). However, these will not be discussed in this thesis. The majority of the candidates for exotic hadrons exist among heavy quarkonia, all of which are bosons.

1.2.4 Heavy Quarkonium-like States

A meson that is composed of two heavy quarks of the same flavour is called heavy quarkonium. Those that are composed of charm quarks ($c\bar{c}$) are called charmonia, while those that are composed of bottom quarks $\left(b\bar{b}\right)$ are called bottomonia. The top quark decays very rapidly via the weak interaction and does not form bound states. Because of the large masses of the charm and bottom quarks, relativistic effects are small, and hence heavy quarkonia can be approximated reasonably well using non-relativistic quantum mechanics. It is important to note that this approach does not derive directly from QCD. Rather, a potential is chosen that is inspired by QCD. The potential includes a short distance Coulombic term and a long distance term that models the effects of confinement. Spin dependent terms are crucial and relativistic corrections can also be included. The energy levels of the quarkonium system can be calculated using potential models. Each energy level, *i.e.* each charmonium or bottomonium state, is interpreted as a distinct meson. Ref. [74] provides a review of potential model methods.

Potential model predictions for the low-lying members of the charmonium and bottomonium spectra are in excellent agreement with experiment. However, in recent years experi-

ments have begun to probe the mass region that higher mass charmonium states are expected to occupy. The results of these experiments have been quite surprising: numerous states that were not predicted by potential models have been found in the $3.8-4.7\,\text{GeV}$ mass region, and a few unanticipated states have been found within the bottomonium mass region as well [28]. These anomalous states are called heavy quarkonium-like, or XYZ states. The current experimental situation is summarized in detail in Ref. [20]. Fig. 1.3 shows the charmonium spectrum, including many of the charmonium-like states.

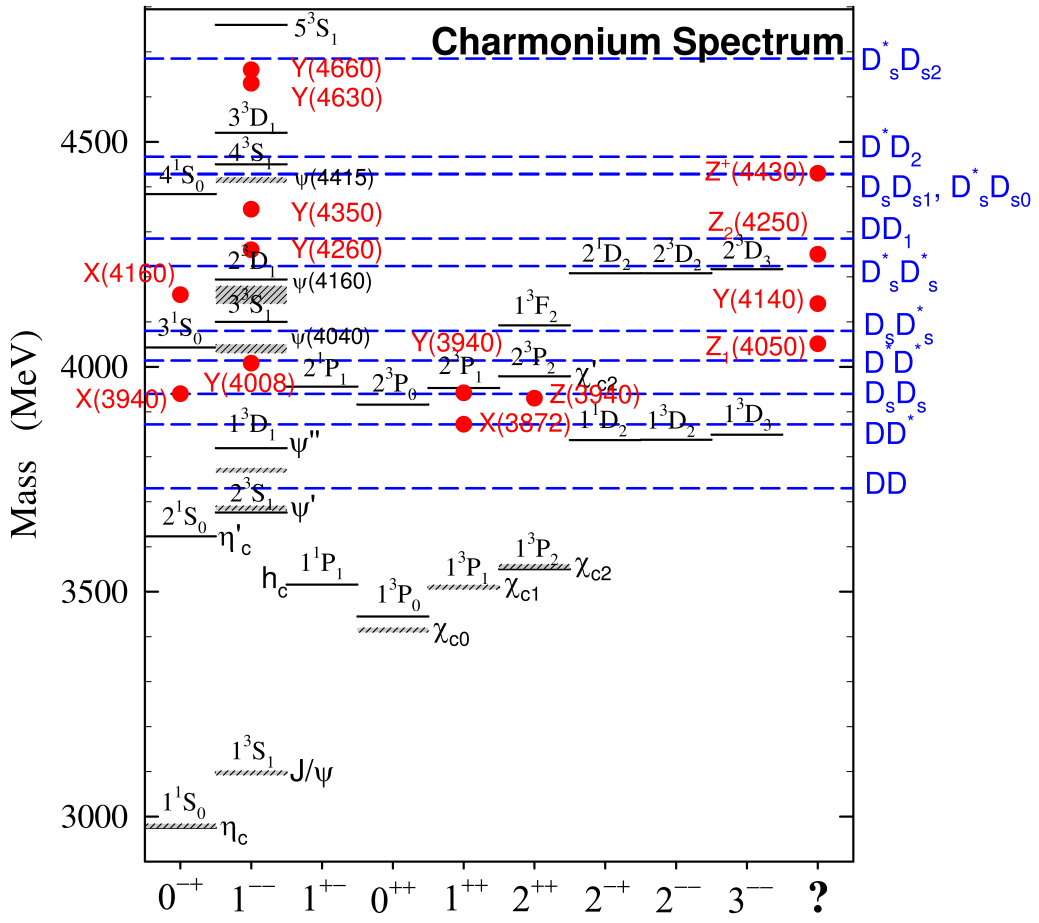

Figure 1.3: The charmonium spectrum. Black lines denote charmonium states, and red dots indicate charmonium-like states. Blue lines indicate the thresholds at which states can decay into a pair of D mesons, which contain a charm quark and a light quark. Note that most of the J^{PC} quantum numbers assigned to the XYZ states here are speculative (Ref. [20] lists the possible J^{PC} for each XYZ state). Figure taken from Ref. [53].

Charmonium states are labeled using spectroscopic notation $n^{2s+1}L_J$, where n is the

principal quantum number ($n = 1\,,2\,,\ldots$), $s = s_1 + s_2$ is the total spin ($s = 0\,,1$), L is the relative orbital angular momentum, and $J = L + S$ is the total angular momentum of the quark-antiquark pair. Following standard conventions, states with $L = 0\,,1\,,2$ are denoted as $S\,,P\,,D$, and so on. In addition, all hadrons can be classified according to their J^{PC} quantum numbers, where $P = (+,-)$ denotes parity and $C = (+,-)$ denotes charge conjugation (which is relevant to electrically neutral states). For quarkonia, it can be shown that the parity and charge conjugation quantum numbers are related to the spin and orbital angular momentum by $P = (-)^{L+1}$ and $C = (-)^{L+S}$, respectively [58]. Accordingly, heavy quarkonium states can have $J^{PC} = 0^{-+}$, 1^{--}, 1^{+-}, 0^{++}, 1^{++}, 2^{++}, for example. However, it is impossible for a heavy quarkonium state to have the quantum numbers $J^{PC} = 0^{--}$, 0^{+-}, 1^{-+}, or 2^{+-}. Quantum numbers that are forbidden for heavy quarkonia are called exotic quantum numbers.

It has been widely speculated that some of the heavy quarkonium-like states could be exotic hadrons (see [28, 114] for comprehensive reviews). This would explain why the XYZ states were unanticipated by potential models that consider only quark-antiquark hadrons. Experimentally, there are some simple signals for the existence of exotic hadrons. The first is that potential models predict a certain number of states for each J^{PC} channel, and any supernumerary states could be exotic hadrons. A more obvious signal would be the observation of a state with exotic J^{PC} quantum numbers, which cannot be realized by quark-antiquark bound states. To date, no hadrons with exotic quantum numbers have been definitively observed. Hadrons with unusual decay modes could also be exotic. For instance, states that are above open flavour thresholds in Fig. 1.3 are kinematically allowed to decay into pairs of D mesons. Hadrons that are kinematically allowed to undergo such decays but fail to do so could be exotic.

An overview of the exotic interpretations of the heavy quarkonium-like states is given in Ref. [28]. The most well known exotic hadron candidate is the $X(3872)$, whose quantum numbers have been confirmed to be $J^{PC} = 1^{++}$ by the LHCb collaboration [2]. Several of its decay modes involve a J/ψ, which is the lightest spin-1 charmonium state [20]. Therefore the quark content of the $X(3872)$ must be at least $\bar{c}c$. However, the properties of $X(3872)$ are incompatible with a charmonium interpretation [114]. Shortly after its discovery, it was

soon recognized that its mass is very close to the combined mass of the D^0 and $\bar{D}^{0*}$ mesons. For this reason the $X(3872)$ has been widely interpreted as a loosely bound $D^0\bar{D}^{0*}$ molecular state [37, 124, 113, 123, 9, 122, 80, 75]. Another interpretation is that the $X(3872)$ is a tetraquark, and is expected to be only one member of a nonet of tetraquarks [84, 44, 86, 121, 43]. Quite recently, the $Z_c^{\pm}(3895)$ was discovered by the BES-III collaboration [6] and confirmed by the Belle [81] and CLEO collaborations [128]. Because charmonium states cannot be electrically charged, this state cannot be a charmonium state. Like the $X(3872)$, the $Z_c^{\pm}(3895)$ decays to J/ψ, hence it must contain $\bar{c}c$. However, this combination cannot produce an electric charge. The simplest explanation for this state is that it is a four-quark state of the form $c\bar{c}q_i\bar{q}_j$, where q_i and $\bar{q}_j$ are light quarks with different flavours. In fact, Ref. [84] predicted the existence of the $Z_c^{\pm}(3895)$ on the basis of a tetraquark model of the $X(3872)$. The $X(3872)$ and $Z_c^{\pm}(3895)$ are discussed in Chapter 4.

1.3 Quantum Chromodynamics

Quantum Chromodynamics (QCD) is the fundamental theory of strong interactions. It is a quantum field theory, which is a generalization of quantum mechanics to describe physical processes involving particle creation or annihilation. It is important to stress that quantum mechanics is incapable of this: the wave function of a particle that has not yet been created or has been annihilated cannot be normalized, and thus is incompatible with the statistical interpretation of quantum mechanics. In quantum field theory particles are understood as being excitations, or quanta, of quantum fields. There are two distinct approaches that are used to construct a quantum field theory. Canonical quantization involves reinterpreting classical fields as operators that satisfy a certain algebra. A second approach utilizes the path integral formulation of quantum mechanics (see Ref. [50] for a review). Both methods will be utilized in this chapter to formulate QCD.

1.3.1 Canonical Quantization of Quark Fields

QCD begins with quantizing spin-1/2 fermion fields that represent quarks. These satisfy the Dirac equation,

$$\left[i\partial\!\!\!/ - m\right] Q\left(x\right) = 0\,, \quad \partial\!\!\!/ = \gamma^{\mu}\frac{\partial}{\partial x^{\mu}}\,, \tag{1.1}$$

where the quark field $Q\left(x\right)$ is a complex four-component spinor field and we are using natural units (see Appendix A). The set of four matrices γ^{μ} satisfy the algebra $\left\{\gamma^{\mu}\,,\,\gamma^{\nu}\right\} = 2\,g^{\mu\nu}$. A peculiarity of the Dirac equation is that it permits both positive and negative energy solutions for free particles. Negative energy solutions represent antiparticles, which are identical in every way to their particle counterparts, except that they have opposite electric charge. Particles and antiparticles can interact to annihilate one another and particle-antiparticle pairs can be created spontaneously. When interactions are included, the statistical interpretation of non-relativistic quantum theory cannot be applied to the Dirac equation.

The solution to this problem is to reinterpret the Dirac equation as a field equation, rather than a single particle wave equation, and then quantize the field. In this way, a consistent quantum field theory that incorporates interactions can be constructed. The dynamics of fields are governed by the principle of least action, where the action is defined as

$$S = \int d^{4}x\,\mathcal{L}\left(Q,\,\partial_{\mu}Q\right)\,, \tag{1.2}$$

where $\mathcal{L}\left(Q,\,\partial_{\mu}Q\right)$ is the Lagrangian density, which is commonly referred to as the Lagrangian. The principle of least action states that as the field $Q\left(x\right)$ evolves in spacetime it does so in a way that minimizes the action (1.2). It can be shown that in order to satisfy the principle of least action, the field must satisfy the Euler-Lagrange equation,

$$\frac{\partial\mathcal{L}}{\partial Q} - \partial_{\mu}\left(\frac{\partial\mathcal{L}}{\partial\left(\partial_{\mu}Q\right)}\right) = 0\,. \tag{1.3}$$

Note that this must be satisfied by each distinct field in a given Lagrangian. Given the Lagrangian for a field, the equations of motion for the field can be determined using (1.3). It is important to emphasize that at this stage the fields are still classical quantities. Only when the fields have been reinterpreted as operators that satisfy an appropriate algebra will

we pass to a quantum field theory.

Let us now consider canonical quantization of Dirac fields. Quantum theory uses the Hamiltonian to determine the time evolution of a system. In the Heisenberg picture of quantum theory, time-dependence is carried by operators governed by the Heisenberg equation of motion,

$$i\partial_0 Q\left(x\right) = \left[Q\left(x\right)\ ,\ H\right]\ . \tag{1.4}$$

In order to quantize the Dirac fields, we must first know what Hamiltonian operator to use in (1.4). Since the Hamiltonian and Lagrangian are related, we may determine a suitable Lagrangian for the Dirac fields and use this to find the corresponding Hamiltonian. The simplest form of the Lagrangian can be written as

$$\mathcal{L} = \bar{Q}\left[i\partial\!\!\!/ - m\right]Q\,, \tag{1.5}$$

where $\bar{Q} = Q^{\dagger}\gamma^0$. When this Lagrangian is substituted into the Euler-Lagrange equation (1.3) with Q and $\bar{Q}$ treated as dynamical fields, the correct equations of motion for Q and $\bar{Q}$ result, so this is a suitable Lagrangian for the quark fields. Using the relationship between the Hamiltonian and the Lagrangian along with (1.5), the Hamiltonian for Dirac fields can be shown to be

$$H = \int d^3x\,\mathcal{H} = \int d^3x\left[\frac{\partial\mathcal{L}}{\partial\left[\partial_0 Q\left(x\right)\right]}\partial_0 Q\ \left(x\right) - \mathcal{L}\right] = i\int d^3x\,\bar{Q}\left(x\right)\gamma^0\partial_0 Q\left(x\right)\ . \tag{1.6}$$

We may now use the Heisenberg equation of motion (1.4) to quantize Dirac fields. Using the Hamiltonian (1.6) and the identity $[A\,,\,BC] = \{A\,,\,B\}C - B\{A\,,\,C\}$,

$$\begin{aligned}
\left[Q\left(x\right)\ ,\ H\right] &= i\int d^3y\left[Q\left(x\right)\ ,\ \bar{Q}\left(y\right)\gamma^0\frac{\partial}{\partial y^0}Q\left(y\right)\right] \\
&= i\int d^3y\left(\left\{Q\left(x\right)\ ,\ \bar{Q}\left(y\right)\right\}\gamma^0\frac{\partial}{\partial y^0}Q\left(y\right) - \bar{Q}\left(y\right)\left\{Q\left(x\right)\ ,\ \gamma^0\frac{\partial}{\partial y^0}Q\left(y\right)\right\}\right) \\
&= i\int d^3y\left(\left\{Q\left(x\right)\ ,\ \bar{Q}\left(y\right)\right\}\gamma^0\frac{\partial}{\partial y^0}Q\left(y\right) - \bar{Q}\left(y\right)\gamma^0\frac{\partial}{\partial y^0}\left\{Q\left(x\right)\ ,\ Q\left(y\right)\right\}\right) \\
&= i\frac{\partial}{\partial x^0}Q\left(x\right)\ .
\end{aligned} \tag{1.7}$$

In order to satisfy the Heisenberg equation of motion, the quark fields must satisfy an equal time anticommutator algebra where

$$\{Q_j^\alpha(x)\ ,\ \bar{Q}_k^\beta(y)\} = \delta^3(\mathbf{x}-\mathbf{y})\ \gamma_{jk}^0\,, \tag{1.8}$$

and all other anticommutators are zero. Note that we have restored implicit spinor indices $j\,,k$ and used the property $(\gamma^0)^2 = 1$ as well as the Heisenberg equation of motion for $\bar{Q}$. It is important to note that the Heisenberg equation of motion can also be satisfied by operators that have a commutator algebra. However, the spin-statistics theorem requires that fermions satisfy an anticommutator algebra. Since Dirac fields are fermions, we must use the algebra (1.8). This issue is discussed in many standard texts, see for instance Ref. [100].

The Dirac fields can be expanded in a basis of plane wave states,

$$\begin{aligned} Q_j(x) &= \int \frac{d^3p}{(2\pi)^3}\frac{1}{\sqrt{2E_p}}\sum_s \left(a^s(\mathbf{p})\,u_j^s(p)\,e^{-ip\cdot x} + b^{s\dagger}(\mathbf{p})\,v_j^s(p)\,e^{ip\cdot x}\right) \\ \bar{Q}_k(x) &= \int \frac{d^3p}{(2\pi)^3}\frac{1}{\sqrt{2E_p}}\sum_s \left(b^s(\mathbf{p})\,\bar{v}_k^s(p)\,e^{-ip\cdot x} + a^{s\dagger}(\mathbf{p})\,\bar{u}_k^s(p)\,e^{ip\cdot x}\right) \end{aligned} \tag{1.9}$$

where $p^0 = E_p$ and s denotes the spin state. Using these expressions and the algebra (1.8) it is easy to show that

$$\{a_j^r(\mathbf{p})\ ,\ a_k^{s\dagger}(\mathbf{q})\} = \{b_j^r(\mathbf{p})\ ,\ b_k^{s\dagger}(\mathbf{q})\} = (2\pi)^3\,\delta^3(\mathbf{p}-\mathbf{q})\ \delta^{rs}\,\delta_{jk} \tag{1.10}$$

and all other anticommutators involving these operators are zero. The solutions (1.9) are linear combinations of the basis vectors of the Hamiltonian (1.6). In quantum field theory, the operators (1.9) are interpreted as creating and annihilating field quanta by acting on the vacuum (ground) state $|0\rangle$, which contains no field quanta. This requires that $a_j^r(\mathbf{p})\,|0\rangle = 0$. Particles and antiparticles are understood as field quanta and are represented by momentum eigenstates with an associated spin state s. For later convenience it is useful to define the normal-ordering operator. When acting on a product of creation and annihilation operators,

the normal-ordering operator moves all creation operators $a_k^{s\dagger}(\mathbf{q})$ to the left. For example,

$$: a_j^r(\mathbf{p})\, a_k^{s\dagger}(\mathbf{q}) := -a_k^{s\dagger}(\mathbf{q})\, a_j^r(\mathbf{p}) \,. \tag{1.11}$$

This can also be applied to the quark field operators (1.9). A crucial property is that

$$\langle 0| : \ldots : |0\rangle = 0 \,, \tag{1.12}$$

where the dots denote any combination of quantum fields.

The quark field operators can be used to determine the amplitude for a quark to propagate between two distinct locations in spacetime. In order to calculate this amplitude we must first define the time-ordering operator,

$$T\left[Q(x)\,\bar{Q}(y)\right] = \begin{cases} Q(x)\,\bar{Q}(y) \,, & x^0 > y^0 \\ -\bar{Q}(y)\,Q(x) \,, & x^0 < y^0 \end{cases} \tag{1.13}$$

which anticommutes a product of Dirac fields so that the field with the earliest time is the furthest right and the field with the latest time is the furthest left. The time-ordering operator ensures that particles only propagate forward in time. Explicitly calculating Eqn. (1.13) using the expressions for the quark fields (1.9) and their algebra (1.8), it can be shown that

$$\langle 0|\, T\left[\, Q(x)\,\bar{Q}(y)\,\right] |0\rangle = S(x-y) = i\int \frac{d^4p}{(2\pi)^4} \frac{\not{p}+m}{p^2-m^2+i\eta} e^{-ip\cdot(x-y)} \,, \tag{1.14}$$

where $\not{p} = \gamma^\mu p_\mu$ and $\eta \to 0^+$. Equation (1.14) is the Feynman quark propagator, which is also a Green's function of the Dirac equation (1.1). The $i\eta$ pole prescription ensures that time-ordering is respected. The Feynman propagator $S(x-y)$ is the quantum mechanical amplitude for a quark to travel between the spacetime points y and x, if $y^0 < x^0$.

1.3.2 Perturbation Theory

The S-matrix formalism relates physical quantities such as scattering cross sections and decay rates to correlation functions, which are also referred to as Green's functions or n-

point functions. Therefore correlation functions are of paramount importance in quantum field theory. As an example, consider the four-point function

$$\langle 0|T\left[Q\left(x_1\right)\bar{Q}\left(x_2\right)Q\left(x_3\right)\bar{Q}\left(x_4\right)\right]|0\rangle\,. \tag{1.15}$$

Correlation functions of this form can be evaluated using Wick's theorem, which can be used to express any time ordered product in terms of Feynman propagators and normal ordered products. For the time ordered product in (1.15), Wick's theorem yields

$$\begin{aligned} T\left[Q\left(x_1\right)\bar{Q}\left(x_2\right)Q\left(x_3\right)\bar{Q}\left(x_4\right)\right] = &:Q\left(x_1\right)\bar{Q}\left(x_2\right)Q\left(x_3\right)\bar{Q}\left(x_4\right): \\ &+\overbrace{Q\left(x_1\right)\bar{Q}}\left(x_2\right):Q\left(x_3\right)\bar{Q}\left(x_4\right): \\ &+:Q\left(x_1\right)\bar{Q}\left(x_2\right):\overbrace{Q\left(x_3\right)\bar{Q}}\left(x_4\right) \\ &+\overbrace{Q\left(x_1\right)\bar{Q}}\left(x_2\right)\overbrace{Q\left(x_3\right)\bar{Q}}\left(x_4\right) \\ &+\overbrace{Q\left(x_1\right)\bar{Q}\left(x_2\right)Q\left(x_3\right)\bar{Q}}\left(x_4\right)\,. \end{aligned} \tag{1.16}$$

The contraction of the quark fields is defined as

$$\overbrace{Q\left(x\right)\bar{Q}}\left(y\right) = S\left(x-y\right)\,, \tag{1.17}$$

where $S\left(x-y\right)$ is the quark propagator (1.14). Note that in the last line of Eq. (1.16) there are contractions where the fields are not adjacent and are not in the same order as those in (1.17). The quark fields can be moved so that they are adjacent and in the proper order using the anticommutator algebra (1.8). Wick's theorem yields the following for the correlation function:

$$\begin{aligned} \langle 0|T\left[Q\left(x_1\right)\bar{Q}\left(x_2\right)Q\left(x_3\right)\bar{Q}\left(x_4\right)\right]|0\rangle = &\,S\left(x_1-x_2\right)S\left(x_3-x_4\right) \\ &-S\left(x_3-x_2\right)S\left(x_1-x_4\right)\,, \end{aligned} \tag{1.18}$$

where we have used the fact that vacuum expectation values of normal ordered products are identically zero. Wick's theorem is valid for all quantum fields, and can be generalized to time ordered products involving any number of fields.

All physical theories involve interactions between quantum fields. When interactions are included correlation functions can be calculated via perturbation theory. It can be shown that correlation functions in the interacting theory are related to those in the non-interacting theory by

$$\langle\Omega|\, T\left[Q\left(x\right)\bar{Q}\left(y\right)\right]|\Omega\rangle = \lim_{t\to\infty(1-i\epsilon)} \frac{\langle 0|\, T\left[Q\left(x\right)\bar{Q}\left(y\right)e^{iS_{\text{int}}}\right]|0\rangle}{\langle 0|\, T\left[e^{iS_{\text{int}}}\right]|0\rangle}\,, \tag{1.19}$$

where $|\Omega\rangle$ and $|0\rangle$ denote the vacua of the interacting and free (non-interacting) theories, respectively [100]. The limit is needed in order to define $|\Omega\rangle$ as a perturbation of $|0\rangle$. The exponential is defined as

$$S_{\text{int}} = \int d^4x\, \mathcal{L}_{\text{int}}\,, \tag{1.20}$$

where $\mathcal{L}_{\text{int}}$ is the part of the interacting theory Lagrangian that defines an interaction between quantum fields. One of the fundamental assumptions of quantum field theory is that interactions between quantum fields are local, that is, fields interact at a single point in spacetime. For instance, in the next section we shall see that the interaction between quark and gluon fields is given by

$$\mathcal{L} = \frac{g}{2}\bar{Q}\left(x\right)\lambda^a\gamma^\mu A^a_\mu\left(x\right)Q\left(x\right)\,, \tag{1.21}$$

where A^a_μ denotes a gluon field and the coupling g characterizes the strength of the interaction. The interacting theory correlation function (1.19) can be calculated as a power series in the coupling g. Equation (1.19) can be generalized to calculate correlation functions involving any number of quark or gluon fields by simply adding these fields to both sides of the equation. Wick's theorem remains valid and can be used to calculate correlation functions in the interacting theory in terms of the propagators of the non-interacting theory (1.14). However, in the QCD vacuum $|\Omega\rangle$ there are some normal ordered products whose expectation values are non-zero. These are called condensates and will be discussed in Section 1.4.

Correlation functions can be represented in terms of Feynman diagrams. For instance, the perturbative expansion of the correlation function (1.19) involves quark and gluon propagators, as well as interactions between quarks and gluons due to the interaction term (1.21).

Some of these terms are shown in Fig. 1.4.

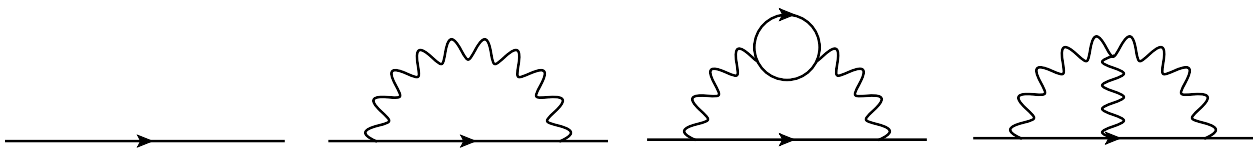

Figure 1.4: Examples of Feynman diagrams that contribution to the perturbative expansion of the correlation function in Eq. (1.19). Straight and wavy lines represent quark and gluon propagators, respectively. Each vertex represents the local interaction between quark and gluon fields given by (1.21), and hence introduces a factor of the coupling g. Diagrams with more vertices correspond to higher order terms in the perturbative expansion. Note that the first three diagrams can also occur in QED, where the gluons are replaced with photons. However, the fourth diagram includes a direct interaction between gluon fields and has no equivalent in QED. These Feynman diagrams were produced using JaxoDraw [23].

Note that the Feynman diagrams in Fig. (1.4) are connected, that is, all of the propagators are linked to one another. However, the perturbative expansion of the numerator in Eq. (1.19) includes disconnected diagrams. Diagrams of this type represent vacuum processes. It can be shown that the denominator of Eq. (1.19) serves to cancel all disconnected diagrams that arise in the perturbative expansion. In practice this cancellation can be implemented by simply ignoring terms in the perturbative expansion that correspond to disconnected diagrams.

Feynman diagrams can be used as mnemonics to keep track of terms in the perturbative expansion of a correlation function. Using Wick's theorem and the expression for the perturbative expansion (1.19), it is possible to relate each diagram component to a certain mathematical expression. These are called Feynman rules. One of the Feynman rules for QCD is that every quark line in a Feynman diagram mathematically corresponds to a quark propagator (1.14). Another is that every quark-gluon vertex is associated with a factor of $i\frac{g}{2}\lambda^a\gamma^\mu$. This vertex rule can be derived easily using Wick's theorem and the perturbative expansion. The Feynman rules for QCD are given in Ref. [100]. Note, however, that any correlation function can be calculated using Wick's theorem. It is important to emphasize that Wick's theorem is more fundamental than the Feynman rules.

1.3.3 Non-Abelian Gauge Theory

Correlation functions can be calculated perturbatively once the complete Lagrangian for a theory is known. In the SM, interactions are introduced through gauge symmetries. For instance, we have seen that the Lagrangian for free quark fields is given by

$$\mathcal{L}_{\text{quarks}} = \bar{Q}_j \left[i\partial\!\!\!/ - m \right] Q_j \,, \tag{1.22}$$

where we have introduced the index $j \in \{1\,,2\,,3\}$ to denote the colour degree of freedom of the quark fields. The Lagrangian (1.22) is invariant under the global gauge transformation

$$Q_i \to Q_i' = \exp\left[-igT^a_{ij}\theta^a\right] Q_j \,, \quad \bar{Q}_i \to \bar{Q}_i' = \exp\left[igT^a_{ij}\theta^a\right] \bar{Q}_j \,, \tag{1.23}$$

where T^a is a generator of the non-Abelian group $SU\,(3)$. The generators satisfy the Lie algebra $\left[T^a\,,T^b\right] = if^{abc}T^c$ where f^{abc} are the structure constants of $SU\,(3)$. The generators are related to the Gell-Mann matrices λ^a via $T^a = \frac{\lambda^a}{2}$. Now, suppose that we alter the gauge transformation (1.23) so that $\theta^a \to \theta^a\,(x)$. Clearly the Lagrangian (1.22) is not invariant under this local gauge transformation. However, it can be made so by introducing a gauge field. This can be done by replacing the derivative in (1.22) with a covariant derivative

$$D_\mu = \partial_\mu - igT^a A^a_\mu \,, \tag{1.24}$$

where A^a_μ is the gauge field. In fact, this is the gluon field, which has its own Lagrangian

$$\mathcal{L}_{\text{YM}} = -\frac{1}{4} G^a_{\mu\nu} G^{\mu\nu}_a \,, \quad G^c_{\mu\nu} = \partial_\mu A^c_\nu - \partial_\nu A^c_\mu + g f^{abc} A^a_\mu A^b_\nu \,, \tag{1.25}$$

where $G^a_{\mu\nu}$ is the gluon field strength tensor and the gluon field is massless. This is called the Yang-Mills Lagrangian. It can be shown that the following Lagrangian is invariant under local $SU(3)$ gauge transformations [111]:

$$\mathcal{L} = \bar{Q}\left[iD\!\!\!/ - m \right] Q - \frac{1}{4} G^a_{\mu\nu} G^{\mu\nu}_a \,. \tag{1.26}$$

The covariant derivative (1.24) leads to the quark-gluon interaction term (1.21) discussed earlier. Also, notice that the definition of the gluon field strength tensor (1.25) leads to self-interactions among gluon fields. Interactions between gauge fields with a universal coupling are a distinguishing feature of non-Abelian gauge theories.

1.3.4 Path Integral Quantization of Gluon Fields

Although the Lagrangian (1.25) contains interactions, the gluon field still has to be quantized. The methods of canonical quantization that was used in Section 1.3.1 to quantize quark fields are ill-suited for this purpose. Instead, we will utilize the path integral to quantize the gluon field. The discussion in this section closely follows that of Ref. [111].

The generating functional for a quantum field ϕ is defined as

$$Z[J] = \int D\phi \exp\left[i \int d^4x \left[\mathcal{L} + J(x)\,\phi(x)\right]\right], \tag{1.27}$$

where $\mathcal{L} = \mathcal{L}(\phi, \partial_\mu \phi)$ is the Lagrangian for the field ϕ. The integration in (1.27) is over the space of configurations of the field ϕ. An integral of this form is called a path integral. The path integral is a functional, that is, a function that acts upon functions and returns numbers. The term $J(x)$ in the exponential is known as a source term. It is useful to define the functional derivative

$$\frac{\delta}{\delta J(x)} J(y) = \delta^4(x - y)\ . \tag{1.28}$$

It can be shown that correlation functions involving the field ϕ can be calculated as functional derivatives of the generating functional [100]. For example,

$$\langle 0|T\left[\,\phi(x_1)\,\phi(x_2)\,\right]0\rangle = \frac{1}{Z_0}\left(-i\frac{\delta}{\delta J(x_1)}\right)\left(-i\frac{\delta}{\delta J(x_2)}\right) Z[J]\Big|_{J=0}, \tag{1.29}$$

where $Z_0 = Z[J=0]$. Correlation functions involving more ϕ fields can be calculated simply by calculating more functional derivatives of the generating functional. Note that the field ϕ has been quantized: the path integral can be used to calculate correlation functions of the field ϕ, which are quantum mechanical amplitudes. This procedure generalizes to any

quantum field, provided that the statistics of the field are incorporated. For instance, path integrals involving fermion fields require the use of Grassmann variables [100]. Once the generating function for a quantum field has been defined, the field has been quantized.

Now we will construct the generating functional for the gluon field. By analogy with the generating functional for the field ϕ (1.27), we might guess that the generating functional for the gluon field is given by

$$Z[J] = \int DA \exp\left[i \int d^4x \left[\mathcal{L}_{\mathrm{YM}} + J_a^\mu A_\mu^a\right]\right], \tag{1.30}$$

where $\mathcal{L}_{\mathrm{YM}}$ denotes the Yang-Mills Lagrangian (1.25). Unfortunately, the integration over the configurations of the gluon field is ill-defined. This is due to the gauge symmetry of $\mathcal{L}_{\mathrm{YM}}$. It can be shown that under an infinitesimal gauge transformation, the gluon field transforms as

$$A_\mu^a(x) \to \tilde{A}_\mu^a(x) = A_\mu^a(x) - D_\mu^{ab}\theta^b(x), \quad D_\mu^{ab} = \delta^{ab}\partial_\mu - g f^{abc} A_\mu^c. \tag{1.31}$$

This reflects a redundancy among the configurations of the field A_μ^a, which spoils the definition of the generating functional (1.30).

The generating functional given in Eq. (1.30) cannot be used to quantize the gluon fields in its present form. We will use a method introduced by Faddeev and Popov [49] to modify the generating functional so that quantization is possible. The redundancy in the integration over the field A_μ^a can be removed by introducing the gauge-fixing function

$$Z[J] = \int DA \det\left(\frac{\delta G}{\delta\theta}\right) \delta(G) \exp\left[i \int d^4x \left[\mathcal{L}_{\mathrm{YM}} + J_a^\mu A_\mu^a\right]\right], \tag{1.32}$$

where $G^a(x) = \partial^\mu A_\mu^a - \omega^a(x)$ for some arbitrary function ω^a. Using Eq. (1.31), it can be shown that the gauge-fixing function transforms as

$$G^a(x) \to \tilde{G}^a(x) = G^a(x) - \partial^\mu D_\mu^{ab}\theta^b(x). \tag{1.33}$$

Using this, the functional derivative in Eq. (1.32) is

$$\frac{\delta G^a(x)}{\delta \theta^b(y)} = -\partial^\mu D_\mu^{ab} \delta^4(x-y) \,. \tag{1.34}$$

Note that the Faddeev-Popov method can be used to quantize QED, but there Eq. (1.34) does not depend on the photon field and hence it cannot introduce any new dynamics into the theory. However, in QCD the functional determinant explicitly depends on the gluon field A_μ^a, because Eq. (1.34) contains the covariant derivative. The functional determinant that appears in (1.32) can be expressed in terms of a path integral involving Faddeev-Popov ghosts:

$$\begin{aligned} \det\left(\frac{\delta G}{\delta \theta}\right) &= \int Dc\, D\bar{c}\, \exp\left[i \int d^4x\, \mathcal{L}_{\rm gh}\right], \\ \mathcal{L}_{\rm gh} &= \bar{c}^a \partial^\mu D_\mu^{ab} c^b = -\partial^\mu \bar{c}^a \partial_\mu c^a + g f^{abc} A_\mu^c \partial^\mu \bar{c}^a c^b \,. \end{aligned} \tag{1.35}$$

The ghost fields c^a and $\bar{c}^a$ are unphysical, but are needed to defined the generating functional for the gluon field. The first term in $\mathcal{L}_{\rm gh}$ can be used to calculated the ghost propagator (given in Ref. [100], for instance) and the second term in $\mathcal{L}_{\rm gh}$ denotes an interaction between the ghost and gluon field. The delta functional appearing can be dealt with by multiplying the generating functional (1.32) by

$$\exp\left[-\frac{i}{2a}\int d^4x\, w^a(x)\, w^a(x)\right]. \tag{1.36}$$

This is permitted because $\omega^a(x)$ does not depend on the gluon field A_μ^a, and hence multiplying the generating functional (1.32) by Eq. (1.36) can only alter the overall normalization of the generating functional. The delta function in (1.32) can be used to evaluate the integral (1.36). This effectively introduces a new term into the generating functional that has the form

$$\mathcal{L}_{\rm gf} = -\frac{1}{2a}\partial^\mu A_\mu^a \partial^\nu A_\nu^a \,. \tag{1.37}$$

This is called the gauge-fixing Lagrangian, and a is the gauge parameter. Finally, the gener-

ating functional for the gluon field is

$$Z[J] = \int DA\, Dc\, D\bar{c}\, \exp\left[i \int d^4x \left[\mathcal{L}_{\rm YM} + J_a^\mu A_\mu^a + \mathcal{L}_{\rm gf} + \mathcal{L}_{\rm gh} \right] \right], \tag{1.38}$$

where $\mathcal{L}_{\rm YM}$ is the Yang-Mills Lagrangian (1.25), $\mathcal{L}_{\rm gf}$ is the gauge-fixing Lagrangian (1.37) and $\mathcal{L}_{\rm gh}$ is the ghost Lagrangian (1.35). Using (1.38), it can be shown that the gluon propagator is given by

$$\langle 0 | \, T\left[\, A_\mu^a(x) \, A_\nu^b(y) \, \right] | 0 \rangle = D_{\mu\nu}^{ab}(x-y) = -i\delta^{ab} \int \frac{d^4p}{(2\pi)^4} \left[g_{\mu\nu} - (1-a) \frac{p_\mu p_\nu}{p^2 + i\eta} \right] \frac{e^{-ip\cdot(x-y)}}{p^2 + i\eta} \,. \tag{1.39}$$

1.3.5 Regularization and Renormalization

Now that the quark and gluon fields have been quantized, the complete QCD Lagrangian is given by

$$\begin{aligned} \mathcal{L}_{\rm QCD} = {} & \bar{Q}\left[i\partial\!\!\!/ - m \right] Q - \frac{1}{4}\left[\partial_\mu A_\nu^b - \partial_\nu A_\mu^b \right] \left[\partial^\mu A_b^\nu - \partial^\nu A_b^\mu \right] - \frac{1}{2a} \partial^\mu A_\mu^b \partial^\nu A_\nu^b \\ & + \frac{g}{2} \bar{Q} \lambda^a \gamma^\mu A_\mu^a Q - \frac{g}{4}\left[\partial_\mu A_\nu^a - \partial_\nu A_\mu^a \right] f^{abc} A_b^\mu A_c^\nu - \frac{g^2}{4} f^{abc} f^{ade} A_\mu^a A_\nu^b A_d^\mu A_e^\nu \\ & - \partial^\mu \bar{c}^a \partial_\mu c^a + g f^{abc} A_\mu^c \partial^\mu \bar{c}^a c^b \,. \end{aligned} \tag{1.40}$$

The terms in Eq. (1.40) can be interpreted as follows: the first term can be used to derive the quark propagator, the second and third terms can be used to derive the gluon propagator, the fourth term represents an interaction between quark and gluon fields, the fifth term represents an interaction between three gluon fields, the sixth term represents an interaction between four gluon fields, the seventh term can be used to derive the ghost propagator, while the eighth term represents an interaction between ghost and gluon fields. It is important to note that the gauge-fixing Lagrangian in Eq. (1.37) is not gauge invariant. Although the QCD Lagrangian (1.40) is not gauge invariant, it is invariant under a generalized form of gauge symmetry known as BRST symmetry [18, 64]. This can be used to prove the Slavnov-Taylor identities which relate various correlation functions in QCD [109, 120].

Any QCD correlation function can be calculated to any order in g using the perturbative

expansion (1.19), the interaction terms in the QCD Lagrangian (1.40), as well as the quark, gluon and ghost propagators. In practice, this can be done via Wick's theorem or using the Feynman rules for QCD, which can be derived from the QCD Lagrangian (1.40). Higher order terms in the expansion can be represented by Feynman diagrams that contain loops. For instance, consider the correlation function $\langle\Omega|T\left[\,Q\left(x\right)\bar{Q}\left(y\right)\,\right]|\Omega\rangle$, which is related to the amplitude for a quark to propagate between the spacetime points y and x in the presence of interactions. We will consider the next-to-leading order term in the perturbative expansion of this correlation function, which is $\mathcal{O}\left(g^2\right)$. This is called the quark self-energy and can be represented by the Feynman diagram shown in Fig. 1.5. It is conventional to depict Feynman diagrams in momentum space, with the four-momentum of each propagator uniquely labeled. For brevity we will refer to four-momenta as momenta in what follows.

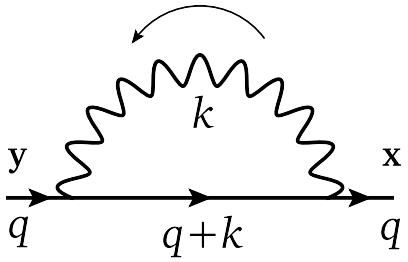

Figure 1.5: Feynman diagram representing the quark self-energy. The quark propagates between the spacetime points y and x, and has momentum q at these locations. The quark interacts with a gluon that has momentum k, which flows from right to left in the diagram. Momentum is conserved at each vertex in the diagram.

The quark self-energy is represented by the Feynman diagram in Fig. 1.5 and is proportional to an integral over the momentum of the gluon. Schematically, the quark self-energy is given by

$$\Sigma\left(q\right)\simeq g^2\int\frac{d^4k}{\left(2\pi\right)^4}\frac{1}{k^2\left[\,\left(k+q\right)^2-m^2\,\right]}\,. \tag{1.41}$$

Momentum integrals such as this are called loop integrals, because they emerge naturally from Feynman diagrams that contain loops. It should be understood that we are integrating over the entire infinite range of each integration variable, that is, the integration in (1.41) is over the entire volume of the four-dimensional momentum space. In what follows we will suppress the limits of integration in loop integrals. For brevity we have also omitted the $i\eta$

pole prescription in the propagators in Eq. (1.41). In addition, we have ignored the leftmost and rightmost quark propagators with momentum q in Fig. 1.5. It is customary to remove (or amputate) external propagators in Feynman diagrams. The integral in Eq. (1.41) can be evaluated in spherical coordinates [100]. However, the result is surprising: the integral diverges at large values of the gluon momentum k. Integrals that diverge in this way are called ultraviolet divergent.

In order to extract meaningful physical information from the integral (1.41), the ultraviolet divergence must first be brought under control, or regulated. In order to do this, we will utilize dimensional regularization [115, 25]. With this method, integrals in four dimensional Minkowski space are reinterpreted as integrals in d-dimensions. For example, the integral above is reinterpreted as

$$\Sigma\left(q\right) \simeq \left(g^2\mu^{d-4}\right) \frac{1}{\mu^{d-4}} \int \frac{d^dk}{(2\pi)^d} \frac{1}{k^2\left[\,\left(k+q\right)^2 - m^2\,\right]}\,. \tag{1.42}$$

In dimensional regularization the number of dimensions, d, is best thought of as a parameter that can be adjusted such that the integral (1.42) converges. Integrals that are formally divergent in a certain number of dimensions can be uniquely defined through analytic continuation in the parameter d. In four dimensions, the coupling g is dimensionless and hence is suitable to be used as an expansion parameter. However, in d-dimensions the combination $g^2\mu^{d-4}$ is dimensionless, where μ is the renormalization scale. This can be used to define the d-dimensional expansion parameter

$$\alpha = \frac{g^2\mu^{d-4}}{4\pi}\,. \tag{1.43}$$

The remaining factor of the renormalization scale in the denominator of Eq. (1.42) ensures that the d-dimensional integral has the same dimensions as the original four dimensional integral (1.41). The integral (1.42) can be evaluated in d-dimensions using the methods described in Chapter 2. The result naturally depends on d, and we may examine the behaviour of the integral near four dimensions by setting $d = 4 + 2\epsilon$ and expanding around $\epsilon = 0$. The methods used to perform this expansion are discussed in Section 2.6. For the integral (1.42),

the result is

$$\Sigma\left(q\right) \simeq -\frac{i}{4}\left(\frac{\alpha}{\pi}\right)\left[\frac{1}{\epsilon} - \log\left(4\pi\right) + \gamma_E - \log\left[\frac{Q^2}{\mu^2}\right] + f\left(\frac{Q^2}{m^2}\right)\right], \tag{1.44}$$

where γ_E is the Euler-Mascheroni constant (see Appendix B), $Q^2 = -q^2$ is the Euclidean momentum and f is a function of the dimensionless ratio Q^2/m^2. The divergence has been regulated and appears as a simple pole at $\epsilon = 0$.

Theories in which divergences can be removed systematically order by order in perturbation theory are called renormalizable. The proof that QCD is renormalizable was given in Refs. [115, 116]. Renormalization is the process of canceling these divergences. Formally, this can be achieved by rescaling the parameters of the QCD Lagrangian (1.40) as follows:

$$\begin{array}{lll}
\left[A_a^\mu\right]_B = Z_{3\mathrm{YM}}^{1/2}\left[A_a^\mu\right]_R & \left[Q\right]_B = Z_{2\mathrm{F}}^{1/2}\left[Q\right]_R & \left[c_a\right]_B = \tilde{Z}_3^{1/2}\left[c_a\right]_R \\
\left[g_{1\mathrm{YM}}\right]_B = Z_{1\mathrm{YM}}Z_{3\mathrm{YM}}^{-3/2}\left[g\right]_R & \left[\tilde{g}\right]_B = \tilde{Z}_1\tilde{Z}_3^{-1}Z_{3\mathrm{YM}}^{-1/2}\left[g\right]_R & \left[g_{\mathrm{F}}\right]_B = Z_{1\mathrm{F}}Z_{3\mathrm{YM}}^{-1/2}Z_{2\mathrm{F}}^{-1}\left[g\right]_R \\
\left[g_5\right]_B = Z_5^{1/2}Z_{3\mathrm{YM}}^{-1}\left[g\right]_R & \left[m\right]_B = Z_4Z_{2\mathrm{F}}^{-1}\left[m\right]_R & \left[a\right]_B = Z_6^{-1}Z_{3\mathrm{YM}}\left[a\right]_R ,
\end{array} \tag{1.45}$$

where we have used the notations of Ref. [97]. The constants Z_i are called renormalization factors, and the subscripts B and R denote bare and renormalized quantities, respectively. The bare couplings $\left[g_{\mathrm{YM}}\right]_B$, $\left[\tilde{g}\right]_B$, $\left[g_{\mathrm{F}}\right]_B$, and $\left[g_5\right]_B$ are associated with the three-gluon, ghost-gluon, quark-gluon and four-gluon interaction terms in the bare QCD Lagrangian (1.40). However, all of these couplings must be identical in order for the QCD Lagrangian to be BRST invariant. This implies the that renormalization factors satisfy

$$\frac{Z_{3\mathrm{YM}}}{Z_{1\mathrm{YM}}} = \frac{\tilde{Z}_3}{\tilde{Z}_1}, \quad \frac{Z_{3\mathrm{YM}}}{Z_{1\mathrm{YM}}} = \frac{Z_{2\mathrm{F}}}{Z_{1\mathrm{F}}}, \quad Z_5 = \frac{Z_{1\mathrm{YM}}^2}{Z_{3\mathrm{YM}}}. \tag{1.46}$$

These identities are closely related to the Slavnov-Taylor identities that are needed in order to prove that QCD is renormalizable.

The Lagrangian given above in Eq. (1.40) is implicitly in terms of bare parameters, hence it is called the bare Lagrangian. The renormalized Lagrangian has the same form as the bare Lagrangian, and can be obtained using the relations given in Eq. (1.45). Because QCD is a

renormalizable theory, all correlation functions calculated with the renormalized Lagrangian must be free of divergences. The renormalization factors are of the form

$$Z = 1 + \frac{\alpha}{\pi}\frac{A}{\epsilon} + \mathcal{O}\left(\alpha^2\right) , \tag{1.47}$$

where A is a constant and dimensional regularization is used with $d = 4 + 2\epsilon$. In practice, a correlation function can be calculated using the bare Lagrangian (1.40), and the result in terms of the bare parameters will contain divergences. The bare parameters can be rewritten in terms of the renormalization factors and renormalized parameters using (1.45). When this is done, the divergences in the bare correlation function are canceled by compensating divergences in the renormalization factors. The resulting renormalized correlation function is purely in terms of the renormalized parameters and is free of divergences. This approach is called bare perturbation theory, because it involves calculating correlation functions in terms of bare parameters which are then renormalized. A complementary approach is renormalized perturbation theory, where correlation functions are calculated in terms of renormalized parameters. This procedure involves inverting the relations (1.45), leading to the introduction of counterterms. Renormalized perturbation theory is described in Ref. [100].

The renormalization process is somewhat arbitrary because there are many ways that it can be implemented. The minimal subtraction (MS) scheme is often used in conjunction with dimensional regularization. In the MS scheme the renormalization factors Z_i are defined such that only the poles at $\epsilon = 0$ are canceled, while the γ_E and $\log(4\pi)$ terms appearing in Eq. (1.44) remain. However, these terms are merely artifacts of dimensional regularization and are unphysical. In the modified minimal subtraction ($\overline{\text{MS}}$) scheme the renormalization constants are defined so that these terms are also canceled. A convenient method of partially implementing the $\overline{\text{MS}}$ renormalization scheme is discussed in Chapter 2.

Renormalization factors can be calculated as an expansion in the coupling α. This can be done to one-loop order as follows. First, all possible one-loop connected correlation functions are calculated in terms of bare parameters. Second, the bare parameters are eliminated in favor of the renormalized parameters using Eq. (1.45). Finally, the requirement that the renormalized correlation functions must be finite can be used to determine the renormaliza-

tion factors. As an example, consider the quark self-energy represented by Fig. 1.5. The renormalized and bare quark self-energy are related by

$$\Sigma_R\left(q\,;m_R\,,a_R\,,\alpha_R\right)=\lim_{\epsilon\to 0}\left[Z_{2\mathrm{F}}^{-1}\Sigma_B\left(q\,;m_B\,,a_B\,,\alpha_B\right)\right]\,, \tag{1.48}$$

where Σ_B denotes the bare quark self-energy (1.44) which is in terms of bare parameters. Using the relationships between the bare and renormalized parameters given in Eq. (1.45), the bare parameters can be expressed in terms of renormalized parameters along with the corresponding renormalization factors. The renormalization factors are defined such that the limit in Eq. (1.48) can be taken order by order in α. Ref. [97] provides expressions for the renormalization factors in Eq. (1.45) to two-loop order.

So far, we have only considered correlation functions that involve multiple quark or gluon fields at distinct spacetime locations. However, in QSR calculations correlation functions involving composite local operators are needed. For instance, the following correlation function can be used to study a heavy-light pseudoscalar meson:

$$\Pi\left(Q^2\right)=i\int d^4x\,e^{iq\cdot x}\langle\Omega|\,T\left[J\left(x\right)J^\dagger\left(0\right)\right]|\Omega\rangle\,,\quad Q^2=-q^2\,. \tag{1.49}$$

The current $J\left(x\right)=i\bar{q}\left(x\right)\gamma_5 Q\left(x\right)$, where q and Q respectively denote light and heavy quark fields, is a composite local operator that couples to the heavy-light pseudoscalar mesons [66]. In order to extend QSR calculations to higher orders, we must consider the renormalization of correlation functions that involve composite operators.

The renormalization of composite operators is complicated by the fact that multiple composite operators may share the same quantum numbers. Because the fields in the QCD Lagrangian (1.40) have distinct quantum numbers, they must renormalize separately. However, this is not the case with composite operators: those with the same quantum numbers can mix under renormalization. The renormalization of composite operators is discussed in detail in Ref. [39]. In general, in order to study the renormalization of an operator $\mathcal{O}_a$ with dimension a, one must also consider operators $\mathcal{O}_b$ with the same quantum numbers and dimension $b<a$ (the dimensions of quark and gluon fields are given in Appendix A). The

renormalization factors of these operators are formally defined as

$$[\mathcal{O}_i]_R = Z_{ij} [\mathcal{O}_j]_B \tag{1.50}$$

where the vector $\mathcal{O}_i = \left(\mathcal{O}_a\,, \Lambda^{a-b}\mathcal{O}_b\,, \dots\right)$ and the parameters Λ ensure that all elements of the vector have the same dimension. The matrix Z_{ij} is an upper diagonal matrix containing the renormalization factors. The renormalization factors Z_{ij} can be determined by calculating correlation functions composed of the operators $\mathcal{O}_i$.

In Chapter 6 mixing between scalar $\left(J^{PC} = 0^{++}\right)$ glueballs and quark mesons is studied using the currents

$$J_g = \alpha G^2\,, \quad G^2 = G^a_{\mu\nu} G^{\mu\nu}_a\,, \quad J_q = m_q \left(\bar{u}u + \bar{d}d\right)\,. \tag{1.51}$$

The scalar glueball operator J_g mixes under renormalization with the scalar quark meson operator J_q, which has the same dimension and quantum numbers. In Refs. [97, 89] the renormalization of the scalar glueball operator is studied using background field techniques. The resulting renormalized scalar glueball operator is given by

$$G^2_R = \left[1 + \frac{1}{\epsilon}\frac{\alpha}{\pi}\left(\frac{11}{4} - \frac{n_f}{6}\right)\right] G^2_B - \frac{4}{\epsilon}\frac{\alpha}{\pi}\left[m_u \bar{u}u + m_d \bar{d}d\right]_B\,, \tag{1.52}$$

where n_f is the number of active quark flavours. The mixing between the operators J_g and J_q under renormalization is signaled by the second term in Eq. (1.52). This second term leads to a crucial renormalization-induced contribution in the mixing analysis in Chapter 6.

A somewhat simpler example of composite operator renormalization is considered in Chapter 5. There the renormalization of the scalar diquark current is considered, which is given by

$$J^d_\alpha(x) = \epsilon_{\alpha\beta\gamma} Q_\beta(x)\, C\gamma_5 q_\gamma(x)\,, \tag{1.53}$$

where $\alpha\,,\ \beta\,,\ \gamma$ are colour indices, C is the charge conjugation operator and γ_5 is a Dirac matrix (both are defined in Appendix A). There are no composite operators of lower dimension

with the same quantum numbers as the scalar diquark current, hence it cannot mix under renormalization with any other operators. This greatly simplifies the task of determining the renormalization factor of the scalar diquark current. Composite operators typically require an additional renormalization beyond that of their component fields and parameters. In Chapter 5 the scalar diquark operator renormalization factor is determined to two-loop order by considering the correlation function

$$\Gamma^d = \langle\Omega|\, T\left[Q\,(x)\, J^d\,(0)\, q\,(y)\right]|\Omega\rangle\,, \tag{1.54}$$

where J^d is the scalar diquark current (1.53) and colour indices have been omitted for brevity. Conventionally the correlation in Eq. (1.54) is calculated in momentum space and the external quark propagators are amputated, in an identical fashion to the quark self-energy (1.44) However, in the case of Eq. (1.54) the scalar diquark operator is inserted with zero momentum. This is justified because renormalization factors are momentum independent. Then the renormalized correlation function is related to the bare correlation function by

$$\Gamma^d_R\,(q\,; m_R\,, a_R\,, \alpha_R) = \lim_{\epsilon\to 0}\left[Z_{\rm d}\, Z^{-1}_{\rm 2F}\Gamma^d_B\,(q\,; m_B\,, a_B\,, \alpha_B)\right]\,. \tag{1.55}$$

Notice that this expression is identical to Eq. (1.48), apart from the factor of $Z_{\rm d}$. This extra factor is the additional renormalization that is required in order to evaluate the limit in Eq. (1.55). This extra factor is precisely the scalar diquark current renormalization factor. In Chapter 5 the scalar diquark operator renormalization factor is calculated to two-loop order using Eq. (1.55).

Renormalized correlation functions explicitly depend on the renormalization scale μ. However, bare correlation functions which are calculated prior to renormalization do not. For instance, consider an amputated bare correlation function with $n = n_{\rm YM} + \tilde{n} + n_{\rm F}$ external gluon, ghost and quark propagators. Then the bare correlation function must satisfy

$$\mu\frac{d}{d\mu}\Gamma_B\left(q_1\,, q_2\,, \ldots\,, q_n\,; \alpha_B\,, a_B\,, m^i_B\,; \epsilon\right) = 0\,, \tag{1.56}$$

where q_i denote the momenta of each external propagator and m_i is to distinguish distinct

quark flavours. The bare and renormalized correlation functions are related by

$$\Gamma_R\left(q_1\,,q_2\,,\ldots\,,q_n\,;\alpha_R\,,a_R\,,m_R^i\,;\mu\right)=\lim_{\epsilon\to 0}\left[Z_\Gamma\left(\mu\,,\epsilon\right)\Gamma_B\left(q_1\,,q_2\,,\ldots\,,q_n\,;\alpha_B\,,a_B\,,m_B^i\,;\epsilon\right)\right]\,, \tag{1.57}$$

$$Z_\Gamma\left(\mu\,,\epsilon\right)=Z_{3\mathrm{YM}}^{-n_{\mathrm{YM}}/2}\left(\mu\,,\epsilon\right)\tilde{Z}_3^{-\tilde{n}/2}\left(\mu\,,\epsilon\right)Z_{2\mathrm{F}}^{-n_{\mathrm{F}}/2}\left(\mu\,,\epsilon\right)\,. \tag{1.58}$$

Using Eqs. (1.56) and (1.58) it can be shown that the renormalized correlation function must satisfy the differential equation

$$\left[\mu\frac{\partial}{\partial\mu}+\beta\left(\alpha\right)\alpha\frac{\partial}{\partial\alpha}+\delta\left(\alpha\right)a\frac{\partial}{\partial a}-\gamma_i\left(\alpha\right)x_i\frac{\partial}{\partial x_i}-\gamma_\Gamma\left(\alpha\right)\right]\Gamma_R\left(\alpha\,,a\,,m_i\,;\mu\right)=0\,, \tag{1.59}$$

$$x_i=\frac{m_i}{\mu}\,,\quad \gamma_\Gamma\left(\alpha\right)=-\frac{1}{2}\left[n_{\mathrm{YM}}\gamma_{\mathrm{YM}}\left(\alpha\right)+n_{\mathrm{F}}\gamma_{\mathrm{F}}\left(\alpha\right)+\tilde{n}\tilde{\gamma}\left(\alpha\right)\right]\,, \tag{1.60}$$

where all parameters should be interpreted as renormalized parameters and we have omitted the momentum dependence of the renormalized correlation function. The parameter x_i is implicitly summed over all quark flavours. The differential equation above is called the renormalization group equation. The renormalization group functions in Eq. (1.60) are defined as

$$\mu\frac{d\alpha}{d\mu}=\alpha\beta\left(\alpha\,,a\,,x_i\right)\,,\quad \frac{\mu}{m_i}\frac{dm_i}{d\mu}=-\gamma_i\left(\alpha\,,a\,,x_i\right)\,,\quad \mu\frac{da}{d\mu}=a\delta\left(\alpha\,,a\,,x_i\right)\,, \tag{1.61}$$

$$\frac{\mu}{Z_{3\mathrm{YM}}}\frac{dZ_{3\mathrm{YM}}}{d\mu}=\gamma_{\mathrm{YM}}\left(\alpha\,,a\,,x_i\right)\,,\quad \frac{\mu}{Z_{2\mathrm{F}}}\frac{dZ_{2\mathrm{F}}}{d\mu}=\gamma_{\mathrm{F}}\left(\alpha\,,a\,,x_i\right)\,,\quad \frac{\mu}{\tilde{Z}_3}\frac{d\tilde{Z}_3}{d\mu}=\tilde{\gamma}\left(\alpha\,,a\,,x_i\right)\,. \tag{1.62}$$

Note that the a and x_i dependence of these functions was suppressed in Eq. (1.60). In the MS and $\overline{\mathrm{MS}}$ renormalization schemes all renormalization group functions are independent of the mass parameter x_i, and the β function is also independent of that gauge parameter a [97].

An important consequence of the renormalization process is that parameters of the renormalized QCD Lagrangian depend on the renormalization scale, and hence are called running parameters. The renormalization group equation can be used to determine how the running parameters vary with the renormalization scale. First, however, the renormalization group

functions must be calculated. For instance, the β function is calculated to $\mathcal{O}(\alpha^3)$ in Ref. [97]. We will now outline the calculation of the leading order term in the expansion. First, the Slavnov-Taylor identities (1.46) allow us to write

$$\alpha = \frac{(g\mu)^{2\epsilon}}{4\pi}\,, \quad \alpha_R = Z_\alpha^{-1}\alpha_B\,, \quad Z_\alpha = \tilde{Z}_1^2\tilde{Z}_3^{-2}Z_{3\mathrm{YM}}^{-1}\,. \tag{1.63}$$

The renormalization factor Z_α can be determined using the methods described previously. To one-loop order,

$$Z_\alpha = 1 + \frac{\alpha}{\pi}\left[\frac{11}{4} - \frac{n_f}{6}\right]\frac{1}{\epsilon}\,, \tag{1.64}$$

where n_f denotes the number of quark flavours. In Ref. [97] it is shown that to lowest order in α,

$$\beta(\alpha) = -2\alpha\frac{\partial Z_\alpha^{(1)}}{\partial\alpha}\,, \quad \beta(\alpha) = \frac{\alpha}{\pi}\beta_1\,, \quad \beta_1 = -\frac{11}{2} + \frac{n_f}{3}\,, \tag{1.65}$$

where $Z_\alpha^{(1)}$ denotes the divergent term in Eq. (1.64). In a similar fashion it can be shown that to lowest order

$$\gamma(\alpha) = \frac{\alpha}{\pi}\gamma_1\,, \quad \gamma_1 = 2\,. \tag{1.66}$$

The differential equations defining the renormalization group functions in Eq (1.62) can be solved to determine how the QCD Lagrangian parameters depend on the renormalization scale. For instance, using the one-loop expression for the β function (1.65), we find

$$\mu\frac{d\alpha}{d\mu} = \alpha^2\frac{\beta_1}{\pi} \quad \rightarrow \quad \alpha(\mu) = \frac{\alpha(M)}{1 - \frac{\beta_1\alpha(M)}{2\pi}\log\left[\frac{\mu^2}{M^2}\right]}\,, \tag{1.67}$$

The value of β_1 depends on the number of active quark flavours n_f, as can be seen from Eq. (1.65). In QSR calculations n_f is chosen to encompass the heaviest quark in the hadron being studied. For instance, if the heaviest quark is the charm quark $n_f = 4$, whereas if it is the bottom quark $n_f = 5$. This is justified by the decoupling theorem, which states that

contributions from quarks that are much heavier than the characteristic scale of the problem are suppressed by the heavy quark mass [12]. In the $\overline{\rm MS}$ scheme the value of the coupling at the reference scale is taken to be

$$\begin{aligned} n_f = 4 &: \quad \alpha(M) = \alpha(M_\tau) = 0.33 \pm 0.01\,, \qquad M_\tau = 1.77\,\text{GeV}\,, \\ n_f = 5 &: \quad \alpha(M) = \alpha(M_Z) = 0.1184 \pm 0.0007\,, \quad M_Z = 91.118\,\text{GeV}\,, \end{aligned} \tag{1.68}$$

where all numerical values have been taken from Ref. [20]. Similarly, using the one-loop expression for the γ function (1.66), it can be shown that

$$\frac{\mu}{m}\frac{dm}{d\mu} = -\alpha\frac{\gamma_1}{\pi} \quad \to \quad m(\mu) = \overline{m}\left[\frac{\alpha(\mu)}{\alpha(\overline{m})}\right]^{-\frac{\gamma_1}{\beta_1}}\,, \quad \overline{m} = m(\mu = m)\,. \tag{1.69}$$

In the $\overline{\rm MS}$ scheme the value of the quark mass at the reference scale is taken to be

$$\begin{aligned} n_f = 4 &: \quad \overline{m} = \overline{m}_c = m(\mu = m_c) = 1.28 \pm 0.03\,\text{GeV}\,, \\ n_f = 5 &: \quad \overline{m} = \overline{m}_b = m(\mu = m_b) = 4.18 \pm 0.03\,\text{GeV}\,, \end{aligned} \tag{1.70}$$

where the numerical values are taken again from Ref. [20] and $\alpha(\overline{m})$ can be determined using Eq. (1.67).

The β function signals an essential feature of QCD. Because $\beta_1 < 0$, the one-loop QCD coupling decreases with increasing energy scale. This defining characteristic of QCD is called asymptotic freedom. Fig. 1.6 compares theoretical predictions and experimental measurements of $\alpha(\mu)$ at several different energy scales μ. The predicted and measured values are in excellent agreement. Because asymptotic freedom is a prediction of QCD, this agreement is a strong experimental confirmation of QCD [22].

1.4 QCD Laplace sum rules

The QCD coupling is small at high energies due to asymptotic freedom. This means that perturbative expansions in QCD converge rapidly at high energies. However, at low energies the coupling increases, and the convergence of the perturbative expansion suffers. In practical terms this means that perturbative techniques alone are insufficient to describe QCD at low

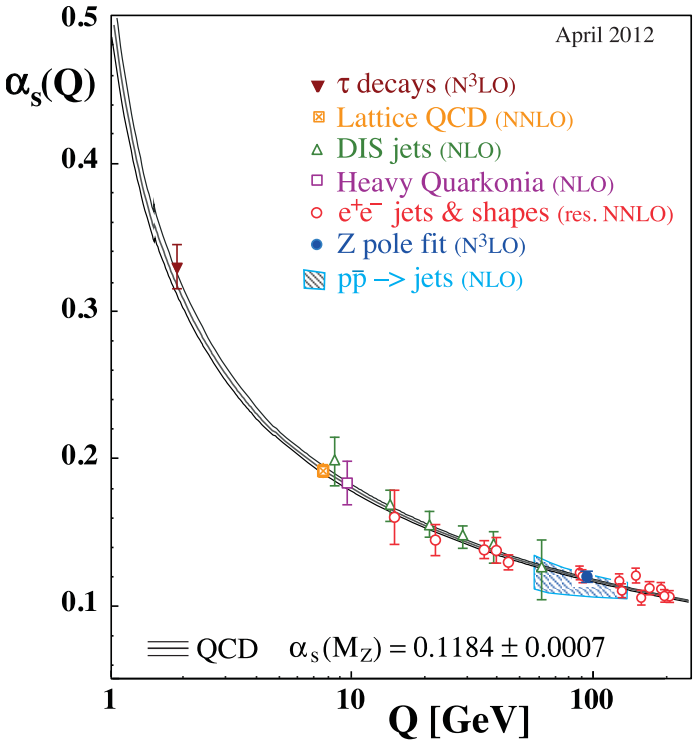

Figure 1.6: Experimental and theoretical predictions for the running QCD coupling $\alpha(\mu)$. Figure taken from Ref. [20].

energies.

There are two broad classes of theoretical techniques that are used to study hadrons: those that are inspired by QCD and those that are based in QCD. The key distinction between these two is that the latter utilize the QCD Lagrangian (1.40) while the former do not. Most QCD-inspired techniques are based on effective field theory methods, such as chiral perturbation theory [45] or heavy quark effective theory [93]. Additional QCD-inspired methods include potential models [74] and techniques based on the AdS/CFT correspondence in string theory [69]. Methods that are based in QCD typically augment perturbation theory in some way or avoid it entirely. In lattice QCD the path integral is calculated numerically in a discretized Euclidean space [73]. The Dyson-Schwinger equations are an infinite set of coupled integral equations relating various correlation functions in the interacting theory. When truncated, the equations can be solved and used to determine hadronic parameters [85]. Another QCD-based approach is QCD sum rules (QSR).

The QSR method is based upon the concept of quark-hadron duality and on the operator product expansion (OPE). Refs. [106, 107] are the original papers outlining the QSR tech-

nique and reviews of its methodology are given in Refs. [104, 38, 89]. QSR depends critically on the concept of quark-hadron duality, which asserts that hadrons can be described equally well in terms resonances or in terms of bound states composed of quarks and gluons. This duality is realized globally rather than locally, in the sense that the two descriptions agree when suitably averaged. Calculations on the QCD side of the duality relation can be performed using the OPE, which naturally includes both perturbative and non-perturbative effects. The hadron side of the duality can be invoked using an experimentally known hadronic spectral function, or a suitable resonance model. Ultimately there are two main applications of QSR that utilize this duality in opposite directions. The first uses experimentally known hadronic parameters to determine unknown QCD parameters, such as quark masses (see *e.g.* Ref. [91]). The second involves determining unknown hadronic parameters in terms of known QCD parameters, using an appropriate model for the hadronic spectral function. The research presented in Chapters 3, 4 and 6 uses the second approach to predict the properties of exotic hadrons.

1.4.1 Dispersion Relation

All QSR calculations begin with a QCD correlation function of the form

$$\Pi\left(Q^2\right) = i \int d^4x \, e^{iq\cdot x} \left\langle \Omega \right| \left[\, J\left(x\right) J^{\dagger}\left(0\right) \, \right] \left| \Omega \right\rangle , \quad Q^2 = -q^2 \, , \tag{1.71}$$

where the current J is a composite operator that couples to the hadron being studied. Techniques for calculating the correlation function will be discussed in Section 1.4.3. The analytic properties of the correlation function (1.71) can be used to show that $\Pi\left(Q^2\right)$ and its imaginary part $\mathrm{Im}\Pi\left(Q^2\right)$ are related by a dispersion relation. In turn, $\mathrm{Im}\Pi\left(Q^2\right)$ is related to a hadronic spectral function. Quark-hadron duality is therefore encoded through this dispersion relation.

We will now demonstrate how the dispersion relation can be derived by appealing to the analytic properties of the correlation function. To do so, we will calculate the contour integral

$$I = \oint_C \frac{dz}{2\pi i} \frac{\Pi\left(z\right)}{z^n \left(z - Q^2\right)} \, , \tag{1.72}$$

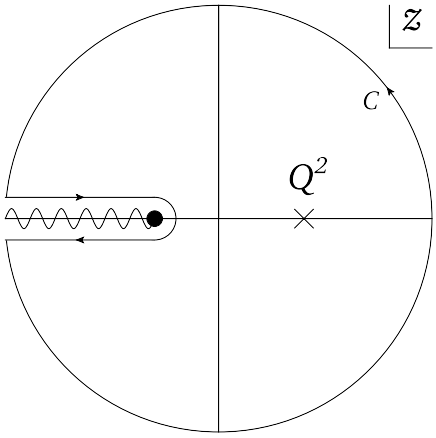

Figure 1.7: Integration contour used to derive the dispersion relation between the correlation function and its imaginary part. The correlation function has a branch cut on the interval $z \in (-\infty\,, -t_0]$, where t_0 is the hadronic threshold.

which is depicted in Fig. 1.7. The branch cut singularity is due to the correlation function and the integrand has poles at $z = 0$ and $z = Q^2$ as depicted in the figure. The value of n is chosen to ensure that the contribution of the radial contour vanishes as its radius is taken to infinity. As an example, we will derive the dispersion relation used in Chapter 4, where the correlation function satisfies

$$\lim_{z\to\infty} \Pi\,(z) \sim z \log^2 (z)\,. \tag{1.73}$$

The dispersion relation can be derived by evaluating the contour integral (1.72) in two ways and equating the results. First, we will evaluate the contribution from each portion of the contour C. The radial portion of the contour can be bounded using (1.73):

$$|I_R| \leq \lim_{R\to\infty} \frac{\Pi\,(R)}{R^n} = \lim_{R\to\infty} \frac{R \log^2 (R)}{R^n} = \lim_{R\to\infty} \frac{\log^2 (R)}{R} = 0\,, \tag{1.74}$$

where we have set $n = 2$ to ensure that the contribution of the radial contour is zero. In order to determine the contribution of the portion of C that circles the branch point, we must know the behaviour of the correlation function near the hadronic threshold t_0. The correlation function in Chapter 4 is regular at this point, therefore the contribution of the portion of the contour that circles the branch point is zero. The only remaining portions of the contour C are those that are above and below the branch cut in Fig. 1.7. For these, we

find

$$I = \int_{t_0}^{\infty} \frac{dt}{2\pi i} \frac{\Pi\left(te^{-i\pi}\right) - \Pi\left(te^{i\pi}\right)}{t^2\left(t+Q^2\right)}\,, \tag{1.75}$$

where $\Pi\left(te^{-i\pi}\right)$ and $\Pi\left(te^{i\pi}\right)$ are the values of the correlation function at points below and above the branch cut, respectively. Therefore Eq. (1.75) effectively requires the discontinuity of the correlation function across the branch cut. However, the correlation function satisfies Schwarz reflection [101], which implies that

$$\left[\Pi\left(z^*\right)\right]^* = \Pi\left(z\right) \quad \rightarrow \quad \Pi\left(te^{-i\pi}\right) - \Pi\left(te^{i\pi}\right) = 2i\,\mathrm{Im}\Pi\left(te^{-i\pi}\right)\,, \tag{1.76}$$

where z^* denotes the complex conjugate of z and $\mathrm{Im}\Pi\left(te^{-i\pi}\right)$ is the imaginary part of the correlation function evaluated at a point below the branch cut. The imaginary part of the correlation function is equivalent to the hadronic spectral function $\rho^{\mathrm{had}}\left(t\right)$ (see Ref. [89] for a proof of this). Using this and substituting Eq. (1.76) into Eq. (1.75) yields

$$I = \frac{1}{\pi}\int_{t_0}^{\infty} dt\, \frac{\rho^{\mathrm{had}}\left(t\right)}{t^2\left(t+Q^2\right)}\,. \tag{1.77}$$

The contour integral (1.72) can also be evaluated using the residue theorem, with the result

$$I = \frac{1}{Q^4}\left[\Pi\left(Q^2\right) - \Pi\left(0\right) - Q^2\Pi'\left(0\right)\right]\,, \quad \Pi'\left(0\right) = \left.\frac{d}{dQ^2}\Pi\left(Q^2\right)\right|_{Q^2=0}\,. \tag{1.78}$$

Equating the results for the contour integral given in Eq. (1.77) and Eq. (1.78), the following dispersion relation results:

$$\Pi\left(Q^2\right) = \Pi\left(0\right) + Q^2\Pi'\left(0\right) + \frac{Q^4}{\pi}\int_{t_0}^{\infty} dt\, \frac{\rho^{\mathrm{had}}\left(t\right)}{t^2\left(t+Q^2\right)}\,. \tag{1.79}$$

1.4.2 Borel Transform

The dispersion relation (1.79) relates the correlation function $\Pi\left(Q^2\right)$ that can be calculated in QCD to the hadronic spectral function $\rho^{\mathrm{had}}\left(t\right)$ which can be parametrized in terms of the hadronic parameters. In principle this can be used to calculate hadronic parameters, such

as masses, in terms of QCD parameters. However, in practice this approach fails. In general we are interested in the ground state hadron in a certain J^{PC} channel. The spectral function will include this state, along with excited states and the continuum. Hence it is difficult to isolate the ground state contribution when such a dispersion relation is used. In addition, the correlation function $\Pi\left(Q^2\right)$ often contains field theoretical divergences and its value at $Q^2 = 0$ is usually unknown.

The critical insight of Refs. [106, 107] is that these difficulties can be overcome by applying the Borel transform to the dispersion relation (1.79), which is defined as

$$\hat{B} \equiv \lim_{\substack{N,\ Q^2\to\infty \\ N/Q^2\equiv\tau}} \frac{\left(-Q^2\right)^N}{\Gamma(N)} \left(\frac{\mathrm{d}}{\mathrm{d}Q^2}\right)^N \quad . \tag{1.80}$$

The Borel transform has the following properties:

$$\hat{B}\left[Q^{2n}\right] = 0\,, \quad \hat{B}\left[\frac{Q^{2n}}{t+Q^2}\right] = \tau\left(-1\right)^n e^{-t\tau}\,, \tag{1.81}$$

where $n > 0$. In Ref. [21] it was shown that the Borel transform is related to the inverse Laplace transform via

$$\frac{\hat{B}}{\tau}\left[f\left(Q^2\right)\right] = \mathcal{L}^{-1}\left[f\left(Q^2\right);\tau\right] = \frac{1}{2\pi i}\int_{b-i\infty}^{b+i\infty} dQ^2 f\left(Q^2\right) e^{Q^2\tau}\,, \tag{1.82}$$

where b is defined such that $f\left(Q^2\right)$ is analytic to the right of the integration contour. Multiplying both sides of Eq. (1.79) by $\left(-Q^2\right)^k$ and taking the Borel transform using Eq. (1.81), the dispersion relation becomes

$$\frac{\hat{B}}{\tau}\left[\left(-Q^2\right)^k \Pi\left(Q^2\right)\right] = \frac{1}{\pi}\int_{t_0}^{\infty} dt\, t^k\, e^{-t\tau}\, \rho^{\mathrm{had}}\left(t\right)\,. \tag{1.83}$$

Note that the Borel transform has removed the $\Pi\left(0\right)$ and $\Pi'\left(0\right)$ terms. In addition, any terms in the explicit field-theoretic expression for $\Pi\left(Q^2\right)$ that are polynomials in Q^2 will be removed by the Borel transform. Note that this includes any divergences of the form $\epsilon^{-n} f\left(Q^2\right)$ where $f\left(Q^2\right)$ is a polynomial in Q^2. However, such terms will not be eliminated

by the Borel transform when the function $f(Q^2)$ is not a polynomial in Q^2. These are called non-local divergences and must be dealt with through renormalization. Furthermore, the Borel transform has introduced an exponential factor which serves to suppress excited state contributions to the hadronic spectral function. In order to isolate the ground state contribution, it is conventional to parametrize the hadronic spectral function in terms of a resonance and continuum:

$$\rho^{\text{had}}(t) = \rho^{\text{res}}(t) + \theta(t - s_0)\,\rho^{\text{cont}}(t)\ , \quad \rho^{\text{cont}}(t) = \text{Im}\Pi\left(te^{-i\pi}\right)\ , \tag{1.84}$$

where $\theta(t - s_0)$ is the Heaviside step function and s_0 is the continuum threshold ($s_0 > t_0$). The continuum contribution is related to the imaginary part of the QCD correlation function through the optical theorem [100]. Inserting this into Eq. (1.83) yields

$$\mathcal{R}_k(\tau, s_0) = \frac{1}{\pi}\int_{t_0}^{\infty} dt\, t^k\, e^{-t\tau}\,\rho^{\text{res}}(t)\ , \tag{1.85}$$

$$\mathcal{R}_k(\tau, s_0) = \frac{\hat{B}}{\tau}\left[\left(-Q^2\right)^k \Pi\left(Q^2\right)\right] - \frac{1}{\pi}\int_{s_0}^{\infty} dt\, t^k\, e^{-t\tau}\,\text{Im}\Pi\left(te^{-i\pi}\right)\ . \tag{1.86}$$

The quantity $\mathcal{R}_k(\tau, s_0)$ can be calculated in QCD, and is related to the spectral function $\rho^{\text{res}}(t)$. The spectral function $\rho^{\text{res}}(t)$ can be measured experimentally, or it can be modeled in terms of the physical properties of the hadron being studied. Therefore, Eq. (1.86) provides a direct relationship between QCD calculations and hadronic parameters. This is the central identity of QCD Laplace sum rules.

Before proceeding it is useful to consider possible forms that $\mathcal{R}_k(\tau, s_0)$ can take. Typically, the correlation function $\Pi(Q^2)$ involves functions that have a branch cut on the interval $Q^2 \in (-\infty, -t_0]$ and functions that have a pole at $Q^2 = -t_0$. Those that have a pole generally have the form

$$\Pi^{\text{pole}}\left(Q^2\right) \sim \frac{1}{\left(Q^2 + t_0\right)^n}\ , \tag{1.87}$$

where n is a positive integer. Because Eq. (1.87) has no imaginary part, the contribution of

such a function to the sum rule is given by

$$\mathcal{R}_k^{\text{pole}}(\tau) = \frac{\hat{B}}{\tau}\left[\left(-Q^2\right)^k \Pi^{\text{pole}}\left(Q^2\right)\right], \tag{1.88}$$

which is independent of the continuum threshold s_0. The following result is useful in order to calculate the Borel transform [97]:

$$\frac{\hat{B}}{\tau}\left[\frac{(-Q^2)^k}{Q^2+t_0}\right] = t_0^{2k} e^{-t_0\tau}. \tag{1.89}$$

Note that Eq. (1.89) can be extended to cases where the denominator is raised to a higher power by differentiating with respect to t_0.

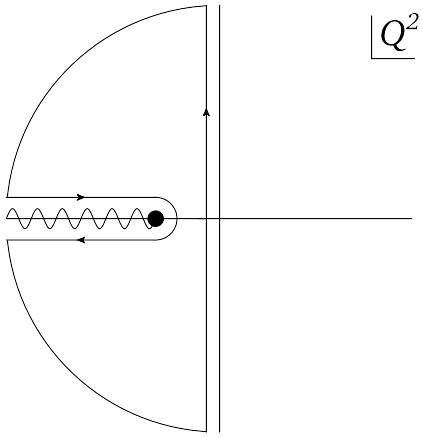

Figure 1.8: Contour integral used to calculate the inverse Laplace transform in Eq. (1.91). The function has a branch cut on the interval $Q^2 \in (-\infty, -t_0]$, where t_0 is the hadronic threshold.

Functions that have a branch cut can be dealt with using the relationship between the Borel transform and the inverse Laplace transform (1.82). The contribution to the sum rule is given by

$$\mathcal{R}_k^{\text{branch}}(\tau, s_0) = \frac{\hat{B}}{\tau}\left[\left(-Q^2\right)^k \Pi^{\text{branch}}\left(Q^2\right)\right] - \frac{1}{\pi}\int_{s_0}^{\infty} dt\, t^k\, e^{-t\tau}\, \text{Im}\Pi^{\text{branch}}\left(te^{-i\pi}\right), \tag{1.90}$$

The first term in Eq. (1.90) is an inverse Laplace transform

$$\mathcal{L}^{-1}\left[\left(-Q^2\right)^k \Pi^{\text{branch}}\left(Q^2\right) ; \tau\right] = \frac{1}{2\pi i}\int_{b-i\infty}^{b+i\infty} dQ^2 \left(-Q^2\right)^k \Pi^{\text{branch}}\left(Q^2\right) e^{Q^2\tau} . \tag{1.91}$$

This can be calculated using the residue theorem. For instance, consider the contour integral

$$I = \frac{1}{2\pi i}\oint_C dQ^2 \left(-Q^2\right)^k \Pi^{\text{branch}}\left(Q^2\right) e^{Q^2\tau} , \tag{1.92}$$

where the integration contour C is depicted in Fig. 1.8. By the residue theorem $I = 0$, and hence

$$I_{\mathcal{L}} = -I_R - I_{\text{top}} - I_\eta - I_{\text{bottom}} , \tag{1.93}$$

where $I_{\mathcal{L}}$, I_R, I_{top}, I_η and I_{bottom} denote the portion of contour C in Fig 1.8 parallel to the imaginary axis, the radial contour, the portion above the branch cut, the portion that circles the branch cut, and the portion below the branch cut, respectively. The exponential factor in Eq. (1.91) ensures that $I_R = 0$ for $R \to \infty$ and $I_\eta = 0$ provided that $\Pi^{\text{branch}}\left(-t_0\right)$ is regular. It can be shown that the remaining portions of the contour give

$$I_{\mathcal{L}} = \frac{1}{2\pi i}\int_{t_0}^{\infty} dt\, t^k \left[\Pi^{\text{branch}}\left(te^{-i\pi}\right) - \Pi^{\text{branch}}\left(te^{i\pi}\right)\right] e^{-t\tau} = \frac{1}{\pi}\int_{t_0}^{\infty} dt\, t^k \text{Im}\Pi\left(te^{-i\pi}\right) e^{-t\tau} , \tag{1.94}$$

where we have used the fact that $\Pi^{\text{branch}}\left(Q^2\right)$ must satisfy Schwarz reflection. Inserting this into Eq. (1.90), we find

$$\mathcal{R}_k^{\text{branch}}\left(\tau , s_0\right) = \frac{1}{\pi}\int_{t_0}^{s_0} dt\, t^k\, e^{-t\tau}\, \text{Im}\Pi^{\text{branch}}\left(te^{-i\pi}\right) . \tag{1.95}$$

In general, the field theoretic correlation function $\Pi\left(Q^2\right)$ will contain functions that have a branch cut, and in order to formulate the contribution of these to the sum rule we must evaluate the imaginary part of these functions below the branch cut. In principle, only the imaginary part of the correlation function is needed in order to use Eq. (1.95). However, there

are some situations in which the entire correlation function is needed in order to properly formulate the sum rule. For example, some terms in the correlation function may be singular at the branch point. This occurs in Chapter 3, for instance. In this case, the integrand in Eq. (1.95) is singular at the lower limit of integration. However, this difficulty can be overcome by noting that contribution to the inverse Laplace transform from the integration contour I_η in Eq. (1.93) is singular as the radius of the contour is taken to zero. This compensates for the integration divergence in Eq. (1.95). In this way a limiting procedure can be developed such that the integration in Eq. (1.95) is well-defined. In order to do so the entire correlation function $\Pi\left(Q^2\right)$ must be known, however.

1.4.3 Operator Product Expansion

In QSR analyses we typically wish to study a hadronic state $|h\rangle$ with certain J^{PC} quantum numbers. To do so, we define a current J with the same quantum numbers that couples to the hadronic state

$$\langle\Omega|J|h\rangle = \Lambda f_h \tag{1.96}$$

where Λ is a dimensionful constant and f_h is a dimensionless factor that measures how strongly the hadronic state $|h\rangle$ couples to the current J. The current is a local composite operator composed of quark and gluon fields that approximate the valence quark and gluon content of the hadronic state $|h\rangle$. However, it is important to note that more than one current J may couple to a single hadronic state. Chapter 6 explores such a scenario. Once the current J has been constructed, we form the correlation function

$$\Pi\left(Q^2\right) = i\int d^4x\, e^{iq\cdot x}\langle\Omega|\, T\left[J\left(x\right)J^\dagger\left(0\right)\right]|\Omega\rangle\,, \quad Q^2 = -q^2\,, \tag{1.97}$$

which can be calculated using the perturbative expansion (1.19). However, as mentioned previously the QCD coupling becomes large at hadronic energy scales and hence a purely perturbative approach cannot adequately describe low energy phenomena.

In QSR, confinement is assumed to exist, and its effects are parametrized through the

operator product expansion (OPE) [127]:

$$\lim_{x\to 0} J(x)\, J^{\dagger}(0) = \sum_{n} C_n(x) : \mathcal{O}_n(0) :, \tag{1.98}$$

where the Wilson coefficients $C_n(x)$ are functions of x and $: \mathcal{O}_n(0) :$ are normal ordered composite operators of dimension n (the dimensions of quark and gluon fields are discussed in Appendix A). Taking the vacuum expectation value and moving to momentum space, the OPE reads

$$\lim_{Q^2\to\infty} \int d^4x\, e^{iq\cdot x} J(x)\, J^{\dagger}(0) = \sum_{n} \langle\Omega| : \mathcal{O}_n(0) : |\Omega\rangle \int d^4x\, e^{iq\cdot x} C_n(x)\ . \tag{1.99}$$

The lowest dimensional operator in the OPE is the identity operator, which corresponds to purely perturbative contributions. Each higher dimensional operator $\mathcal{O}_n(0)$ is a normal ordered combination of quark and gluon fields whose vacuum expectation value does not vanish. These are called condensates and represent non-trivial features of the QCD vacuum $|\Omega\rangle$. Through the OPE, QSR analyses naturally include both perturbative and non-perturbative effects. The OPE involves an implicit separation of scales: the condensates and Wilson coefficients represent low and high energy phenomena, respectively. As such, the Wilson coefficients can be calculated perturbatively. The condensates are gauge invariant and Lorentz invariant combinations of quark and gluon fields. The two most important condensates are the quark and gluon condensates

$$m_q\langle\bar{q}q\rangle = m_q\langle\Omega| : \bar{q}(0)\, q(0) : |\Omega\rangle\,, \quad \alpha\langle G^2\rangle = \alpha\langle\Omega| : G^a_{\mu\nu}(0)\, G^{\mu\nu}_a(0) : |\Omega\rangle\,, \tag{1.100}$$

both of which have dimension four. Note that the quark condensate does not include heavy flavours because the heavy quark condensate can be related to the gluon condensate. It is important to stress that the numerical values of condensates cannot be calculated directly within QCD. Rather, they must be determined empirically. One such method involves using QSR duality relations to relate condensates to experimental data, for instance. The quark condensate can be defined in terms of the pion mass and decay constant via the Gell-Mann-

Oakes-Renner relation [52]:

$$m_q\langle\bar{q}q\rangle = -\frac{1}{2}f_\pi^2 m_\pi^2\,, \quad f_\pi = 0.093\,\text{GeV}\,, \quad m_\pi = 0.139\,\text{GeV}\,, \tag{1.101}$$

where the numerical values have been taken from Ref. [20]. The gluon condensate can be extracted from a QSR analysis of charmonium [90], which yields

$$\langle\alpha G^2\rangle = (7.5 \pm 2.0) \times 10^{-2}\,\text{GeV}^4\,. \tag{1.102}$$

Higher-dimensional condensates involving more quark and gluon fields also exist. For instance, the mixed condensate has dimension-five and is given by

$$\langle\Omega| : g\,\bar{q}\,(0)\,\frac{\lambda^a}{2}\sigma^{\mu\nu}G^a_{\mu\nu}\,(0)\,q\,(0) : |\Omega\rangle = \langle\bar{q}\sigma Gq\rangle = M_0^2\langle\bar{q}q\rangle\,, \tag{1.103}$$

where $M_0^2 = (0.8 \pm 0.1)\ \text{GeV}^2$, which was determined from baryon sum rules [41]. The dimension-six gluon condensate is given by

$$\langle\Omega| : g^3\,f_{abc}\,G^a_{\alpha\beta}\,(0)\,G^b_{\beta\gamma}\,(0)\,G^c_{\gamma\alpha}\,(0) : |\Omega\rangle = \langle g^3G^3\rangle = (8.2 \pm 1.0)\ \text{GeV}^2\,\langle\alpha G^2\rangle\,, \tag{1.104}$$

which was also determined in Ref. [90]. Additional condensates include the dimension-six quark condensate and the dimension-eight gluon condensate, which are given in Ref. [89].

In QSR calculations the correlation function (1.97) is evaluated using the OPE (1.99). Contributions that are proportional to the identity operator correspond to purely perturbative effects, while contributions from higher dimensional operators in the OPE correspond to non-perturbative effects that are represented through condensates. In practice, the simplest way to calculate these contributions is with the aid of Wick's theorem (1.16). For instance, consider the calculation of a correlation function of the form

$$\Pi\left(Q^2\right) = i\int d^4x\,e^{iq\cdot x}\langle\Omega|\,T\left[J\,(x)\,J^\dagger\,(0)\right]|\Omega\rangle\,, \quad Q^2 = -q^2\,, \tag{1.105}$$

where $J\,(x) = \bar{q}\,(x)\,q\,(x)$. The correlation function can be calculated using the perturbative expansion (1.19). The lowest order term in the perturbative expansion involves the following

time ordered product, which can be evaluated using Wick's theorem (1.16):

$$\begin{aligned} T\left[q\left(x\right)\bar{q}\left(x\right)\bar{q}\left(0\right)q\left(0\right)\right] = & :q\left(x\right)\bar{q}\left(x\right)\bar{q}\left(0\right)q\left(0\right): \\ & -\overbrace{q\left(x\right)\bar{q}}\left(0\right)\overbrace{q\left(0\right)\bar{q}}\left(x\right) \\ & +\overbrace{q\left(0\right)\bar{q}}\left(x\right):\bar{q}\left(0\right)q\left(x\right): \\ & +:\bar{q}\left(x\right)q\left(0\right):\overbrace{q\left(x\right)\bar{q}}\left(0\right)\,. \end{aligned} \tag{1.106}$$

Note that the first term in Eq. (1.106) corresponds to a disconnected diagram and can be ignored. The second term in Eq. (1.106) is the $\mathcal{O}\left(g^0\right)$ contribution to the $n = 0$ Wilson coefficient in the OPE. That is, the second term represents the leading-order perturbative contribution to the correlation function (1.105). The third and fourth terms in Eq. (1.106) involve the normal ordered product of two quark fields at distinct locations. Ultimately, the normal ordered products will be related to condensate contributions, *i.e.* terms in the OPE with $n > 0$. The propagators that multiply these terms will lead to the corresponding Wilson coefficients.

Note that because of the limit the definition of the perturbative expansion (1.19), the vacuum expectation value of these terms is taken using $|\Omega\rangle$. For instance, the fourth term in Eq. (1.106) involves the vacuum expectation value

$$\langle\Omega|:\bar{q}\left(x\right)q\left(0\right):|\Omega\rangle = \langle\Omega|:\bar{q}\left(0\right)q\left(0\right):|\Omega\rangle + x^{\mu}\partial_{\mu}\left\langle\Omega\right|:\bar{q}\left(x\right)q\left(0\right):\left|\Omega\right\rangle\big|_{x=0} + \mathcal{O}\left(x^2\right) \tag{1.107}$$

The first term in this expansion can be identified with the quark condensate $\langle\bar{q}q\rangle$ (1.101). The second term is problematic because it involves the derivative ∂_{μ} and hence is not gauge invariant. Ultimately the higher order terms in this expansion will be related to higher dimensional condensates, which are gauge invariant by definition. Therefore the expansion in Eq. (1.107) must be performed in a gauge invariant fashion. This can be achieved using fixed-point gauge techniques [95], or equivalently using plane wave methods [16]. Here we will use fixed-point gauge, where the gluon field satisfies

$$x^{\mu}A_{\mu}^{a}\left(x\right) = 0\,. \tag{1.108}$$

Using this gauge, the derivative in Eq. (1.107) can be replaced by a covariant derivative. In Ref. [97] the fixed-point gauge expansion of the vacuum expectation value in Eq. (1.107) is explicitly calculated to third order in x. Higher order terms in the expansion can expressed naturally in terms of higher dimensional condensates. For instance, $\mathcal{O}\left(x^2\right)$ terms in the expansion are proportional to the mixed condensate (1.103) while $\mathcal{O}\left(x^3\right)$ terms are proportional to the dimension-six quark condensate.

So far we have only considered the leading order term in the perturbative expansion of the correlation function (1.105). Higher order terms that are generated by the perturbative expansion (1.19) can be evaluated within the OPE using an approach identical to that described above. However, this naturally leads to time ordered products that include not only the quark fields of the currents in Eq. (1.105), but also quark and gluon fields from the QCD action. This means that vacuum expectation values involving gluon fields will be encountered. Fixed point gauge techniques can be used to express the gluon field in terms of the gluon field strength, and hence a manifestly gauge invariant expansion of vacuum expectation values involving gluon fields can be constructed. Fixed point expansions of vacuum expectation values involving gluons are discussed in Ref. [97]. Ultimately, the terms in the resulting expansion will lead to contributions from the gluon condensate (1.100) and dimension-six gluon condensate (1.104), for instance.

In QSR calculations the OPE is usually truncated at some order and the Wilson coefficients are calculated to a certain order in the coupling α. For instance, Chapter 3 studies heavy quarkonium hybrids which are probed by the current

$$J_\mu = \frac{g}{2}\bar{Q}\lambda^a\gamma^\nu\tilde{G}^a_{\mu\nu}Q\,, \quad \tilde{G}^a_{\mu\nu} = \frac{1}{2}\epsilon_{\mu\nu\alpha\beta}G^{\alpha\beta}_a\,, \tag{1.109}$$

where Q and $G^{\alpha\beta}_a$ denote a heavy quark field and the gluon field strength, respectively. In Chapter 3 the perturbative, dimension-four $\langle\alpha G^2\rangle$ and dimension-six $\langle g^3G^3\rangle$ gluon condensate contributions are included in the OPE. Because the hybrid current (1.109) contains only heavy quarks, condensates that include light quark fields contribute at higher orders in the expansion and are suppressed. The Wilson coefficients for the perturbative, dimension-four and dimension-six gluon condensate are calculated to leading order in the coupling α. The

evaluation of leading order contributions to the Wilson coefficients involves the calculation of multiple two-loop momentum integrals. These loop integrals are often quite difficult to evaluate and constitute a significant technical barrier to extending QSR calculations to higher orders. Chapter 2 discusses techniques for evaluating loop integrals.

1.4.4 Hadronic Spectral Function

As mentioned previously, the hadronic spectral function can be measured experimentally. For instance, the spectral function for hadronic states with $J^{PC} = 1^{--}$ is related to the ratio of the cross sections

$$R(s) = \frac{\sigma\left(e^- e^+ \to \text{ hadrons }\right)}{\sigma\left(e^- e^+ \to \mu^- \mu^+\right)} \,. \tag{1.110}$$

This spectral function is shown in Fig. 1.9.

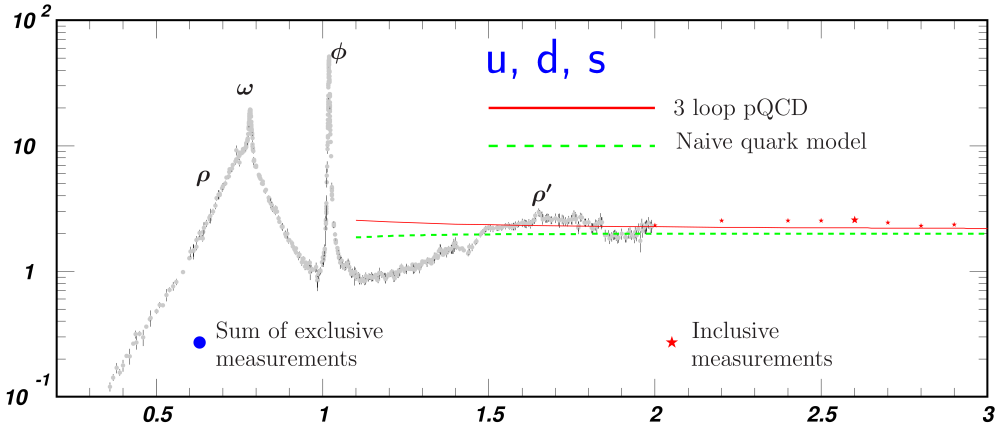

Figure 1.9: The hadronic spectral function $R(s)$. The horizontal axis is the center of mass frame collision energy of the electron and positron in units of GeV and the vertical axis is the dimensionless number $R(s)$. The resonances labeled ρ, ω and ϕ correspond to distinct hadrons. The electron and positron annihilate through a virtual photon or Z boson, both of which have the quantum numbers $J^{PC} = 1^{--}$. Therefore all of these hadrons must have these quantum numbers. The horizontal location of each resonance peak is the mass of the hadron corresponding to the resonance. The region between 1.5 GeV and 3.0 GeV is the continuum which is described well by the three-loop perturbative QCD calculation. Note that in the region below 1.5 GeV the QCD prediction and resonance features agree in the sense of a global average. This is an example of the concept of quark-hadron duality which is crucial to QSR. Figure taken from Ref. [20].

Experimentally known spectral functions such as that shown in Fig. 1.9 can be related to a theoretically calculated correlation function $\Pi(Q^2)$ via Eq. (1.86). In this way, QSR techniques can be used to extract QCD parameters in terms of experimentally measured quantities.

Alternatively, a resonance model can be used to calculate hadron properties in terms of QCD parameters. This must be done in order to study exotic hadrons with QSR. For instance, a single narrow resonance can be parametrized as

$$\rho^{\text{res}}(t) = \pi f^2 \delta\left(t - M^2\right) \tag{1.111}$$

where f and M are the decay constant and mass of the hadron corresponding to the resonance. It is natural to question accuracy of this admittedly rather simple resonance model. However, it is important to remember that in QCD Laplace sum rules the resonance is multiplied by an exponential factor which tends to obscure any detailed features of the resonance. In addition, methods described in Ref. [46] can be used to estimate resonance width effects. The most basic quantity of interest in any QSR analysis is the hadron mass which can be determined using this model. Inserting Eq. (1.111) into Eq. (1.86) yields

$$\mathcal{R}_k(\tau, s_0) = f^2 M^{2k} e^{-M^2\tau}. \tag{1.112}$$

The hadron mass M can be isolated and is given by

$$M(\tau, s_0) = \sqrt{\frac{\mathcal{R}_1(\tau, s_0)}{\mathcal{R}_0(\tau, s_0)}}. \tag{1.113}$$

Using this result a hadron mass M can be extracted from the theoretically calculated quantity $\mathcal{R}_k(\tau, s_0)$.

Note that the hadron mass given in Eq. (1.113) is a function of the Borel parameter τ and continuum threshold s_0. The Borel parameter τ probes the hadronic spectral function at various energies while the continuum threshold s_0 is built into the model of the hadronic spectral function 1.84 and is predicted in the QSR analysis. We must first find a region where the mass prediction (1.113) varies little with the Borel parameter. For a given value of s_0 we

first determine a range of τ values for which the sum rule is considered reliable, called the sum rule window. In order to do this it is convenient to define the Borel mass $M_B = 1/\sqrt{\tau}$. There are multiple ways in which the sum rule window can be defined. All approaches involve fixing lower and upper limits on the Borel mass. Typically contributions from condensates become significant at small values of M_B whereas contributions from the continuum become important at large values of M_B. Therefore placing restrictions on condensate contributions to the sum rule can be used to place a lower bound on M_B, whereas restrictions on continuum contributions can be used to place an upper bound on M_B. The resulting range of M_B values is where the sum rule is considered to be reliable, or the sum rule window. However, the width of the sum rule window varies with the value of s_0.

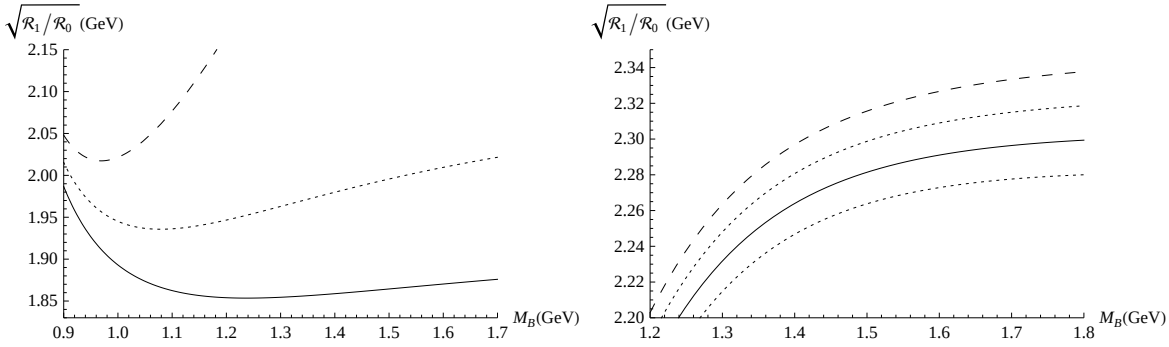

Figure 1.10: Examples of stable (left) and unstable (right) sum rules. The stable sum rule exhibits τ stability within the sum rule window whereas the unstable sum rule does not. In the unstable case there is no region in the sum rule window where the mass prediction given by Eq. (1.113) displays weak dependence on the Borel parameter. Mass predictions made from unstable sum rules are unreliable for this reason. The left and right figures correspond to the scalar and pseudoscalar charm-light diquark sum rules from Chapter 4, respectively.

The value of s_0 can be constrained through the requirement of τ stability [89]:

$$\frac{d}{d\tau} M\left(\tau\,, s_0\right) = 0\,. \tag{1.114}$$

Examples of stable and unstable sum rules are shown in Fig. 1.10. The smallest value of s_0 in which the mass prediction (1.113) exhibits τ stability within the sum rule window is taken

to be the minimum value $s_0^{\min}$. The optimal value of s_0 is determined using

$$\chi^2(s_0) = \sum_j \left(\frac{1}{M} \sqrt{\frac{\mathcal{R}_1(\tau_j, s_0)}{\mathcal{R}_0(\tau_j, s_0)}} - 1 \right)^2 , \quad s_0 \geq s_0^{\min} . \tag{1.115}$$

The optimal value of s_0 is that which minimizes (1.115). The sum in Eq. (1.115) is calculated over the sum rule window corresponding to $s_0^{\min}$. Once the optimal value s_0^{opt} has been determined, the mass can be extracted by fitting $M\left(s_0^{\text{opt}}, \tau\right)$ to a constant over the sum rule window.

1.4.5 QCD sum rules and Heavy Quarkonium-like states

The QSR method has been applied to a wide variety of problems in hadronic physics. In particular, QSR calculations provide crucial information on the properties of exotic hadrons. This theoretical input helps to guide the experimental search for such states. The majority of QSR studies of exotic hadrons have focused on those that are much lighter than the heavy quarkonium-like states (see Ref. [89] for a detailed review).

However, the recently discovered XYZ states have motivated QSR studies of exotic hadrons that may exist within the same mass region as heavy quarkonia. Nearly all of this work has considered four-quark states, which can be realized as molecules or tetraquarks (Ref. [94] provides a review). A common feature of all of these studies is the use of currents that contain four quark fields. However, for reasons discussed in Chapter 4, QSR studies that use four-quark currents cannot distinguish between the molecular and tetraquark configurations. An alternate approach is to use diquark currents, which are relevant to tetraquarks only. This approach was first applied to diquarks containing a heavy quark in Ref. [125]. The research presented in Chapter 4 serves to extend this work.

Hybrid mesons could also exist in the heavy quarkonium mass region. Surprisingly, this possibility has been little explored by QSR practitioners. Refs. [55, 56, 54] comprise the earliest QSR studies of heavy quarkonium hybrids. These studies examined a wide variety of J^{PC} channels. However, the sum rules for many channels exhibited instabilities, and hence the resulting mass predictions in those channels are unreliable. Ref. [102] recently performed

an updated analysis of the 1^{--} channel. The research presented in Chapter 3 updates the 1^{++} and 0^{-+} heavy hybrid sum rules and extracts reliable mass predictions in both cases.

QSR analyses of heavy quarkonium-like states necessarily use currents containing heavy quarks. In practice, this means that the loop integrals that must be evaluated in order to determine the Wilson coefficients are quite complicated. This is in contrast to QSR studies of hadrons composed of light quarks, which are often performed in the chiral limit where the light quark masses are neglected. However, the heavy quark mass cannot be neglected and the resulting loop integrals lead to complicated functions in the dimensionless ratio of the external momentum and the heavy quark mass. Chapter 2 discusses techniques for evaluating these integrals.

1.5 Outline of Thesis

This thesis has been prepared in the manuscript style. Chapter 2 develops techniques for evaluating loop integrals that are essential in subsequent chapters. Chapter 3 includes two closely related manuscripts that have been published in the Journal of Physics G and Physical Review D. Chapters 4, 5 and 6 each consist of individual manuscripts that have been published in Physical Review D, Journal of Physics G and Nuclear Physics A, respectively. The copyright agreements of the respective journals grant permission for articles to be reproduced in a thesis. Chapters 3, 4, 5 and 6 each include an introduction to the research presented therein, along with a discussion of the results of the research and its relation to the thesis as a whole. Chapter 7 discusses the themes of the research presented in this thesis and their relation to the field of hadron spectroscopy in general. Appendices A and B discuss conventions and mathematical functions used in this thesis, respectively.

The research presented in Chapters 3, 4, 5 and 6 involves three overarching themes. The first theme is the use of QSR techniques to extract mass predictions for exotic hadrons containing heavy quarks, and the comparison of these mass predictions with the XYZ states. The second theme involves the application of sophisticated loop integration techniques, which are described in Chapter 2. These techniques are essential for all of the research in this thesis. The third theme is the development of the renormalization methodology used in higher-order

QSR calculations. Table 1.4 summarizes the research presented in subsequent chapters.

Chapter	Description and Key Results	Themes 1	2	3
3	QSR study of $J^{PC} = 1^{++}, 0^{-+}$ heavy quarkonium hybrids. $M(1^{++}, c\bar{c}g) = 5.13 \pm 0.25\,\text{GeV}$, $M(0^{-+}, c\bar{c}g) = 3.82 \pm 0.13\,\text{GeV}$. These results preclude the pure charmonium hybrid interpretation of the $X(3872)$ and support the charmonium hybrid interpretation of the $Y(3940)$.	✓	✓	
4	QSR study of $J^{PC} = 0^{\pm}, 1^{\pm}$ heavy-light diquarks. $M(0^{+}, cq) = 1.86 \pm 0.05\,\text{GeV}$, $M(1^{+}, cq) = 1.87 \pm 0.10\,\text{GeV}$, $M(0^{+}, bq) = M(1^{+}, bq) = 5.20 \pm 0.10\,\text{GeV}$. These masses are consistent with constituent diquark models, providing QCD-based support for the tetraquark interpretation of the $X(3872)$, $Z_c^{\pm}(3895)$, $Y_b(10890)$, $Z_b^{\pm}(10610)$ and $Z_b^{\pm}(10650)$. The renormalization methodology needed for next-to-leading order QSR calculations is also developed.	✓	✓	✓
5	Calculation of two-loop scalar diquark operator renormalization factor. The renormalization factor and anomalous dimension are calculated to $\mathcal{O}(\alpha^2)$. These results are utilized in Chapter 4.		✓	✓
6	QSR analysis of mixing between scalar gluonium and quark mesons. The perturbative contribution to the non-diagonal scalar gluonium-quark meson correlation function is calculated. The renormalization methodology needed for QSR studies involving non-diagonal correlation functions is developed.		✓	✓

Table 1.4: Summary of thesis research.

Chapter 2

Loop Integrals

Correlation functions of quantum fields are related to experimentally observable quantities and as such they are the building blocks of all calculations in quantum field theory. When the perturbative expansion of a correlation function is extended to higher orders, integrals over the momentum variables that circulate in Feynman diagrams are encountered. These integrals can be rather difficult and many powerful techniques have been developed to evaluate them. Much of this activity is driven by steady increases in experimental accuracy: as experimental measurements become more precise, so must theoretical calculations. Refs. [110, 112] provide reviews of modern techniques for evaluating loop integrals. This chapter will focus on the integrals and techniques that are used in Chapters 3, 4, 5 and 6.

2.1 Properties of Loop Integrals

Ref. [39] provides a careful exposition of the properties of dimensionally regularized momentum integrals. As we shall see in Section 2.2, the $i\eta$ pole prescription in the Feynman propagator permits a transition from Minkowski space to Euclidean space, thus without loss of generality we may consider all momentum integrals as existing in a d-dimensional Euclidean space. Dimensionally regularized integrals are completely analogous with integrals in a Euclidean space with an arbitrary integer number of dimensions. The integration operation is linear so that

$$\int d^d k \left[a_1 f_1(k) + a_2 f_2(k)\right] = a_1 \int d^d k f_1(k) + a_2 \int d^d k f_2(k) \,. \tag{2.1}$$

Integration variables may be rescaled, leading to the definition

$$\int d^d k f(ak) = a^{-d} \int d^d k f(k)\,, \tag{2.2}$$

which is consistent with the d-dimensional definition of the Jacobian. The integration operation also respects translation invariance:

$$\int d^d k f(k+q) = \int d^d k f(k)\,. \tag{2.3}$$

The normalization of the integrals is fixed through the Gaussian integral

$$\int d^d k \, \exp\left[-\frac{k^2}{a^2}\right] = a^d \, \pi^{\frac{d}{2}}\,, \quad a^2 > 0\,. \tag{2.4}$$

An important property is that integrals that do not involve a mass or external momenta are identically zero, that is

$$\int d^d k \, k^{2n} = 0\,, \tag{2.5}$$

for all values of n. This result is proven in Ref. [39]. Integrals such as (2.5) that do not depend on any external scales are called massless tadpoles.

2.2 Integrals with at most one massive propagator

The most basic loop integral is the one-loop massive tadpole, which is given by

$$A\,(d\,;n\,,m) = \lim_{\eta\to 0^+} \frac{1}{\mu^{d-4}} \int \frac{d^d k}{(2\pi)^d} \frac{1}{\left[k^2 - m^2 + i\eta\right]^n}\,. \tag{2.6}$$

where μ denotes the renormalization scale. A Feynman diagram representing this loop integral is shown in Fig. 2.1. The momentum of the particle with mass m that circulates the loop is k, as such k is called the loop momentum. There is a correspondence between the topology of a Feynman diagram and the structure of the loop integral that it represents. In particular, the flow of momenta through a diagram is closely related to the form of the

corresponding integral. The Feynman diagrams in this chapter are intended to emphasize this correspondence, therefore they do not specify the spin or mass of any given particle and only serve to indicate the flow of momenta through the diagram.

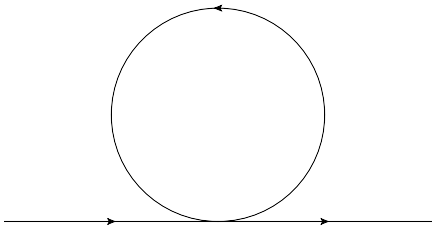

Figure 2.1: Feynman diagram representing the A-type massive tadpole integral.

The $i\eta$ pole prescription is related to causality and is implicitly included in all propagators. As we are in Minkowski space, so the momentum k has one temporal component k_0 and $d-1$ spatial components k_i. Thus the integral can be written as

$$A\left(d\,;n\,,m\right) = \lim_{\eta\to 0^+} \frac{1}{\mu^{d-4}} \prod_{i=1}^{d-1} \int \frac{dk_i}{2\pi} \int \frac{dk_0}{2\pi} \frac{1}{\left[k_0^2 - k_i^2 - m^2 + i\eta\right]^n} \,. \tag{2.7}$$

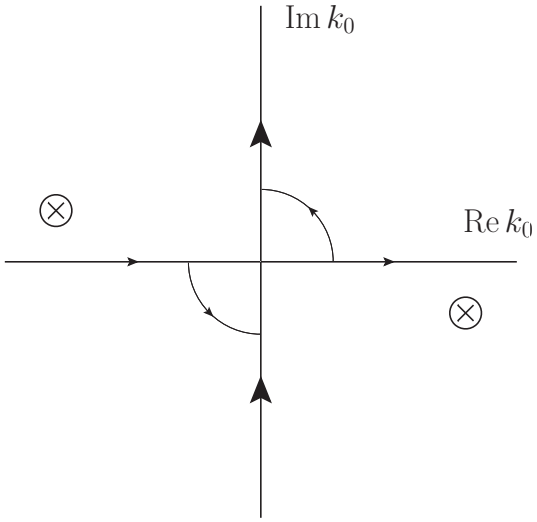

Figure 2.2: Integration contours for the k_0 integral in (2.7). Poles are indicated by $\otimes$ symbols.

The k_0 integral has poles at $k_0 = \pm\sqrt{k_i^2 + m^2} \mp i\eta$, as shown in Fig. 2.2. The locations of the poles permit the integration contour to be shifted as shown in Fig. 2.2. Rather than integrating along the real k_0 axis, we perform a Wick rotation and integrate along the

imaginary k_0 axis. This is equivalent to the following change of variables:

$$k_0 = i\,\ell_d\,, \quad dk_0 = i\,d\ell_d\,, \quad k_i = \ell_i\,, \quad d^dk = i\,d^d\ell\,, \quad \ell^2 = \sum_{i=1}^{d} \ell_i^2\,. \tag{2.8}$$

Formally this is equivalent to moving to a d-dimensional Euclidean space, therefore we can evaluate the integral in d-dimensional spherical coordinates. In these coordinates the volume element is given by

$$d^d\ell = \ell^{d-1} d\ell\, d\Omega_d\,, \tag{2.9}$$

where $d\ell$ denotes the integration over the radial coordinate and $d\Omega_d$ denotes the integrations over the $d-1$ angular coordinates. The $\eta \to 0^+$ limit can now be safely evaluated, and the integral (2.7) becomes

$$A\,(d\,;n\,,m) = \frac{i}{(2\pi)^d} \frac{(-1)^n}{\mu^{d-4}} \int d\Omega_d \int_0^\infty d\ell \frac{\ell^{d-1}}{\left[\ell^2+m^2\right]^n}\,. \tag{2.10}$$

The angular integration can be performed using the d-dimensional Euclidean space Gaussian integral (2.4) and converting to spherical coordinates [100]. The result is

$$\int d\Omega_d = \frac{2\pi^{\frac{d}{2}}}{\Gamma\left(\frac{d}{2}\right)}\,. \tag{2.11}$$

Making the change of variables $z = \frac{\ell^2}{m^2}$, the radial integral can be evaluated in terms of the Beta function (B.11):

$$\frac{1}{2}\left(m^2\right)^{\frac{d}{2}-n} \int_0^\infty dz\, \frac{z^{\frac{d}{2}-1}}{[1+z]^n} = \frac{1}{2}\left(m^2\right)^{\frac{d}{2}-n} \frac{\Gamma\left(\frac{d}{2}\right)\Gamma\left(n-\frac{d}{2}\right)}{\Gamma\left(n\right)}\,. \tag{2.12}$$

The final result for the one-loop massive tadpole integral (2.6) is

$$A\,(d\,;n\,,m) = \frac{i}{(4\pi)^2}\left(-m^2\right)^{2-n} \left[\frac{m^2}{4\pi\mu^2}\right]^{\frac{d}{2}-2} \frac{\Gamma\left(n-\frac{d}{2}\right)}{\Gamma\left(n\right)}\,. \tag{2.13}$$

Note that the mass dimension of this result is the same as that of the original integral (2.6),

namely $4-2n$. Typically, we will be interested in the behaviour of this integral near $d=4$, which can be determined by setting $d=4+2\epsilon$ and expanding around $\epsilon=0$. However, we will refrain from doing so until Section 2.6. By itself, this integral is not particularly useful in QCD sum rule analyses because it has no momentum dependence. However, it is extraordinarily useful as a means for deriving more complicated integrals.

Now consider the one-loop integral

$$B\left(d\,;n_1\,,0\,;n_2\,,m\right)=\frac{1}{\mu^{d-4}}\int\frac{d^dk}{(2\pi)^d}\frac{1}{k^{2n_1}\left[\,(k-q)^2-m^2\,\right]^{n_2}}\,, \tag{2.14}$$

which is depicted in Fig. 2.3. This integral is reminiscent of a quark self-energy contribution, therefore it is called a self-energy integral.

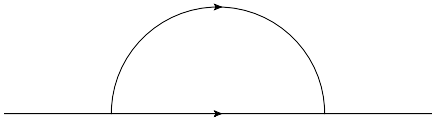

Figure 2.3: Feynman diagram representing the B-type self-energy integral.

This integral can be evaluated with the aid of the following identity [97]:

$$\frac{1}{A^\alpha B^\beta}=\frac{\Gamma(\alpha+\beta)}{\Gamma(\alpha)\Gamma(\beta)}\int_0^1 dx\,\frac{x^{\alpha-1}(1-x)^{\beta-1}}{[Ax+B(1-x)]^{\alpha+\beta}}\,. \tag{2.15}$$

The variable x is called a Feynman parameter. This identity can be used to combine the two propagators in (2.14) so that the integral can be performed using the result (2.13). For instance, let $A=(k-q)^2-m^2$, $\alpha=n_2$, $B=k^2$, and $\beta=n_1$, then we can write

$$Ax+B(1-x)=x(k^2+q^2-2k\cdot q-m^2)+(1-x)k^2=(k-xq)^2-\left[xm^2-x(1-x)q^2\right]\,. \tag{2.16}$$

Using this and making the change of variables $p=k-xq$,

$$\begin{aligned}B\left(d\,;n_1\,,0\,;n_2\,,m\right)=\frac{\Gamma(n_1+n_2)}{\Gamma(n_1)\Gamma(n_2)}\int_0^1 dx\,x^{n_2-1}(1-x)^{n_1}\\ \frac{1}{\mu^{d-4}}\int\frac{d^dp}{(2\pi)^d}\frac{1}{\left[\,p^2-(xm^2-x(1-x)q^2)\,\right]^{n_1+n_2}}\,,\end{aligned} \tag{2.17}$$

where the momentum integral can be evaluated using (2.13). The result is

$$B\left(d\,;n_1\,,0\,;n_2\,,m\right)=\frac{i}{(4\pi)^2}\left(q^2\right)^{2-n_1-n_2}\left[-\frac{q^2}{4\pi\mu^2}\right]^{\frac{d}{2}-2}\frac{\Gamma\left(n_1+n_2-\frac{d}{2}\right)}{\Gamma(n_1)\Gamma(n_2)}$$
$$\int_0^1 dx\,x^{n_2-1}(1-x)^{n_1-1}\left[x(1-x)-\frac{xm^2}{q^2}\right]^{\frac{d}{2}-n_1-n_2}. \tag{2.18}$$

Setting $m=0$, the Feynman parameter integral can be evaluated in terms of the Beta function (B.11). The result is

$$B\left(d\,;n_1\,,0\,;n_2\,,0\right)=\frac{i}{(4\pi)^2}\left(q^2\right)^{2-n_1-n_2}\left[-\frac{q^2}{4\pi\mu^2}\right]^{\frac{d}{2}-2}\frac{\Gamma\left(\frac{d}{2}-n_1\right)\Gamma\left(\frac{d}{2}-n_2\right)\Gamma\left(n_1+n_2-\frac{d}{2}\right)}{\Gamma\left(n_1\right)\Gamma\left(n_2\right)\Gamma\left(d-n_1-n_2\right)}. \tag{2.19}$$

This result agrees with an expression given for this integral in Ref. [97]. Also note that the result requires $n_1\geq 0$ and $n_2\geq 0$; if either of these is not satisfied the integral is a massless tadpole of the form (2.5) and is identically zero. In order to evaluate (2.18) when the mass is non-zero, note that it can be written as

$$B\left(d\,;n_1\,,0\,;n_2\,,m\right)=\frac{i}{(4\pi)^2}\left(q^2\right)^{2-n_1-n_2}\left[-\frac{q^2}{4\pi\mu^2}\right]^{\frac{d}{2}-2}\frac{\Gamma\left(n_1+n_2-\frac{d}{2}\right)}{\Gamma(n_1)\Gamma(n_2)}z^{n_1+n_2-\frac{d}{2}}$$
$$\int_0^1 dx\,x^{\frac{d}{2}-n_1-1}(1-x)^{n_1-1}\left(1-zx\right)^{\frac{d}{2}-n_1-n_2}, \tag{2.20}$$
$$z=\frac{1}{1-\frac{m^2}{q^2}}.$$

The Feynman parameter integral can be evaluated in terms of the Gauss hypergeometric function (B.16). The result is

$$B\left(d\,;n_1\,,0\,;n_2\,,m\right)=\frac{i}{(4\pi)^2}\left(q^2\right)^{2-n_1-n_2}\left[-\frac{q^2}{4\pi\mu^2}\right]^{\frac{d}{2}-2}z^{n_1+n_2-\frac{d}{2}}\frac{\Gamma\left(\frac{d}{2}-n_1\right)\Gamma\left(n_1+n_2-\frac{d}{2}\right)}{\Gamma(n_1)\Gamma(\frac{d}{2})}$$
$${}_2F_1\left[n_1+n_2-\frac{d}{2}\,,\frac{d}{2}-n_1\,;\frac{d}{2}\,;z\right]. \tag{2.21}$$

This result agrees with an expression for this integral that is given in Ref. [97]. As an additional check, we can verify that this result reproduces (2.19) when $m = 0$. Setting $z = 1$ and using the identity (B.17), it is easy to verify that (2.21) is consistent with the massless result (2.19). Note that the mass dimension of the result is carried by the term $(q^2)^{2-n_1-n_2}$ and agrees with that of the integral (2.14), as it must. However, for future convenience it will be helpful to recast this mass dependence in terms of the mass m. This can be done using the definition of the dimensionless variable z given in (2.20). Doing so, the final result for the one-loop self-energy integral with one massive propagator is

$$B\left(d\,;n_1\,,0\,;n_2\,,m\right) = \frac{i}{(4\pi)^2}\left[-\frac{m^2}{1-z}\right]^{2-n_1-n_2}\exp\left[\frac{d-4}{2}\left(\log\left[\frac{m^2}{4\pi\mu^2}\right]-\log\left[1-z\right]\right)\right] \\ \frac{\Gamma\left(\frac{d}{2}-n_1\right)\Gamma\left(n_1+n_2-\frac{d}{2}\right)}{\Gamma(n_1)\Gamma(\frac{d}{2})}{}_2F_1\left[n_1+n_2-\frac{d}{2}\,,\frac{d}{2}-n_1\,;\frac{d}{2}\,;z\right]\,, \tag{2.22}$$

where z is defined as in Eq. (2.20). Note that $\log\left[1-z\right] = -\log\left[1+\frac{Q^2}{m^2}\right]$, which has a branch cut on $Q^2 \in (-\infty\,,-m^2]$. It can also be shown that the hypergeometric function has the same branch cut. Therefore the result (2.22) has the branch cut structure that is appropriate for a correlation function of a currents containing one massive quark with mass m.

The results above can be used to calculate some two-loop integrals. For instance, consider the following integral

$$V\left(d\,;n_1\,,0\,;n_2\,,0\,;n_3\,,0\,;n_4\,,0\right) \\ = \frac{1}{\mu^{2(d-4)}}\int\frac{d^dk_1}{(2\pi)^d}\int\frac{d^dk_2}{(2\pi)^d}\frac{1}{k_1^{2n_1}\left(k_1-q\right)^{2n_2}\left(k_2-q\right)^{2n_3}\left(k_1-k_2\right)^{2n_4}}\,, \tag{2.23}$$

which is represented in Fig. 2.4.

Note that in (2.23) the momentum k_2 only appears in the third and fourth propagators, therefore the k_2 integral can be performed using the result (2.19). Specifically, if we make the change of variables $\tilde{k}_2 = k_2 - q$, the $\tilde{k}_2$ integral is proportional to $(k_1-q)^{2\left(\frac{d}{2}-n_3-n_4\right)}$. Because the integrations can be performed in an iterative fashion, these are called nested

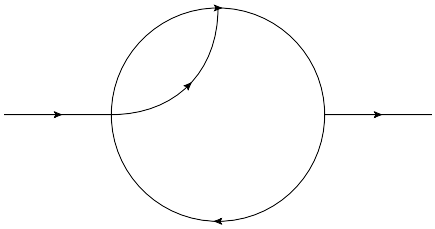

Figure 2.4: Feynman diagram representing the V-type two-loop nested integral.

loop integrals. Finally, the result for (2.23) is

$$\begin{aligned}
&V\left(d\,;n_1\,,0\,;n_2\,,0\,;n_3\,,0\,;n_4\,,0\right)\\
&=-\frac{1}{(4\pi)^4}\left(q^2\right)^{4-n_1-n_2-n_3-n_4}\left[-\frac{q^2}{4\pi\mu^2}\right]^{d-4}\frac{\Gamma\left(\frac{d}{2}-n_1\right)\Gamma\left(\frac{d}{2}-n_3\right)\Gamma\left(\frac{d}{2}-n_4\right)}{\Gamma\left(n_1\right)\Gamma\left(n_3\right)\Gamma\left(n_4\right)}\\
&\frac{\Gamma\left(n_1+n_2+n_3+n_4-d\right)\Gamma\left(d-n_2-n_3-n_4\right)\Gamma\left(n_3+n_4-\frac{d}{2}\right)}{\Gamma\left(n_2+n_3+n_4-\frac{d}{2}\right)\Gamma\left(\frac{3d}{2}-n_1-n_2-n_3-n_4\right)\Gamma\left(d-n_3-n_4\right)}\,.
\end{aligned}\tag{2.24}$$

From the definition (2.23) it is clear that this result has the proper mass dimension. Interestingly, the result is also valid for any value of n_2, including $n_2 = 0$. This technique can be extended to integrals containing one massive propagator. For example, consider the integral

$$\begin{aligned}
&V\left(d\,;n_1\,,m\,;n_2\,,0\,;n_3\,,0\,;n_4\,,0\right)\\
&=\frac{1}{\mu^{2(d-4)}}\int\frac{d^dk_1}{(2\pi)^d}\int\frac{d^dk_2}{(2\pi)^d}\frac{1}{\left(k_1^2-m^2\right)^{n_1}\left(k_1-q\right)^{2n_2}\left(k_2-q\right)^{2n_3}\left(k_1-k_2\right)^{2n_4}}\,.
\end{aligned}\tag{2.25}$$

This integral occurs in Chapter 4, and also in Ref. [66]. Once again the k_2 integral can be integrated immediately, and the resulting k_1 integral can be evaluated using (2.22). Expressing the overall scale dependence in terms of the mass m, the result is

$$\begin{aligned}
&V\left(d\,;n_1\,,m\,;n_2\,,0\,;n_3\,,0\,;n_4\,,0\right)\\
&=-\frac{1}{(4\pi)^4}\left[-\frac{m^2}{1-z}\right]^{4-n_1-n_2-n_3-n_4}\exp\left[(d-4)\left(\log\left[\frac{m^2}{4\pi\mu^2}\right]-\log\left[1-z\right]\right)\right]\\
&\frac{\Gamma\left(\frac{d}{2}-n_3\right)\Gamma\left(\frac{d}{2}-n_4\right)\Gamma\left(n_3+n_4-\frac{d}{2}\right)\Gamma\left(d-n_2-n_3-n_4\right)\Gamma\left(n_1+n_2+n_3+n_4-d\right)}{\Gamma\left(n_1\right)\Gamma\left(n_3\right)\Gamma\left(n_4\right)\Gamma\left(\frac{d}{2}\right)\Gamma\left(d-n_3-n_4\right)}\\
&{}_2F_1\left[n_1+n_2+n_3+n_4-d\,,d-n_2-n_3-n_4\,;\frac{d}{2}\,;z\right]\,,
\end{aligned}\tag{2.26}$$

where z is as defined in Eq. (2.20). Note that this result is valid for all values of n_2, and that the dimension of the result (2.26) is the same as that of the integral (2.23). The method that we have used to calculate (2.25) cannot be extended to integrals with more than one massive propagator. For instance, suppose that the third propagator in (2.25) contained a mass m. In this case, the k_2 integral could be evaluated using the one-loop result (2.22). However, the resulting k_1 integral would involve a hypergeometric function in the argument k_2, and this integral cannot be evaluated in closed form. A new method is required in order to consider integrals containing external momenta and more than one massive propagator.

2.3 Integrals with two massive propagators

Consider a generalization of the integral (2.14) where both propagators are massive

$$B\left(d\,;n_1\,,m\,;n_2\,,m\right)=\frac{1}{\mu^{d-4}}\int\frac{d^dk}{(2\pi)^d}\frac{1}{\left(k^2-m^2\right)^{n_1}\left[\,\left(k-q\right)^2-m^2\,\right]^{n_2}}\,. \tag{2.27}$$

This integral can be evaluated using Feynman parameters (see, *e.g.* Ref. [97]). Instead, we will utilize an approach developed in Ref. [40, 27], which makes use of the Mellin-Barnes contour integral representation of the hypergeometric function ${}_1F_0$ (B.14) to represent a massive propagator in terms of a massless propagator. In this way, massive propagators can be represented in terms of massless propagators, at the cost of introducing a contour integration. The resulting massless integrals can be evaluated in terms of Gamma functions, and then the contour integrals involving these Gamma functions can be evaluated. The result of the contour integration is typically a generalized hypergeometric function whose argument is a dimensionless ratio of the external momentum and the mass.

In order to illustrate the Mellin-Barnes technique, we will use it to evaluate the integral (2.27). Applying the Mellin-Barnes representation to the integral (2.27) gives

$$\begin{aligned}B\left(d\,;n_1\,,m\,;n_2\,,m\right)=\frac{1}{\Gamma\left(n_1\right)\Gamma\left(n_2\right)}\int_{-i\infty}^{i\infty}\frac{ds}{2\pi i}\int_{-i\infty}^{i\infty}\frac{dt}{2\pi i}\left(-m^2\right)^{s+t}\Gamma\left(-s\right)\Gamma\left(-t\right)\\ \Gamma\left(s+n_1\right)\Gamma\left(t+n_2\right)\frac{1}{\mu^{d-4}}\int\frac{d^dk}{(2\pi)^d}\frac{1}{k^{2(n_1+s)}\left(k-q\right)^{2(n_2+t)}}\,.\end{aligned} \tag{2.28}$$

The loop integral can be evaluated immediately using (2.19), which gives

$$B\left(d\,;n_1\,,m\,;n_2\,,m\right)=\frac{i}{(4\pi)^2}\left[-\frac{q^2}{4\pi\mu^2}\right]^{\frac{d}{2}-2}\frac{\left(q^2\right)^{2-n_1-n_2}}{\Gamma\left(n_1\right)\Gamma\left(n_2\right)}\int_{-i\infty}^{i\infty}\frac{ds}{2\pi i}\int_{-i\infty}^{i\infty}\frac{dt}{2\pi i}\left[-\frac{m^2}{q^2}\right]^{s+t}$$
$$\Gamma\left(-s\right)\Gamma\left(-t\right)\frac{\Gamma\left(\frac{d}{2}-n_1-s\right)\Gamma\left(\frac{d}{2}-n_2-t\right)\Gamma\left(n_1+n_2+s+t-\frac{d}{2}\right)}{\Gamma\left(d-n_1-n_2-s-t\right)}\,. \tag{2.29}$$

Now, making the change of variables $v=s$, $w=\frac{d}{2}-n_1-n_2-s-t$, the integral becomes

$$B\left(d\,;n_1\,,m\,;n_2\,,m\right)=\frac{i}{(4\pi)^2}\left[\frac{m^2}{4\pi\mu^2}\right]^{\frac{d}{2}-2}\frac{\left(-m^2\right)^{2-n_1-n_2}}{\Gamma\left(n_1\right)\Gamma\left(n_2\right)}\int_{-i\infty}^{i\infty}\frac{dv}{2\pi i}\int_{-i\infty}^{i\infty}\frac{dw}{2\pi i}\left(-\frac{q}{m^2}\right)^{w}$$
$$\Gamma\left(n_1+w+v\right)\Gamma\left(n_1+n_2-\frac{d}{2}+w+v\right)\Gamma\left(-v\right)\Gamma\left(\frac{d}{2}-n_1-v\right) \tag{2.30}$$
$$\frac{\Gamma\left(-w\right)}{\Gamma\left(\frac{d}{2}+w\right)}\,.$$

The contour integral over the variable v can now be evaluated using Barnes' Lemma (B.15). Doing so, the integral becomes

$$B\left(d\,;n_1\,,m\,;n_2\,,m\right)=\frac{i}{(4\pi)^2}\left[\frac{m^2}{4\pi\mu^2}\right]^{\frac{d}{2}-2}\frac{\left(-m^2\right)^{2-n_1-n_2}}{\Gamma\left(n_1\right)\Gamma\left(n_2\right)}\int_{-i\infty}^{i\infty}\frac{dw}{2\pi i}\left(-\frac{q}{m^2}\right)^{w}\Gamma\left(-w\right)$$
$$\frac{\Gamma\left(n_1+w\right)\Gamma\left(n_1+n_2-\frac{d}{2}+w\right)\Gamma\left(n_2+w\right)}{\Gamma\left(n_1+n_2+2w\right)}\,. \tag{2.31}$$

The Gamma function in the denominator of (2.31) can be simplified using Eq. (B.4), which gives

$$B\left(d\,;n_1\,,m\,;n_2\,,m\right)=\frac{i}{(4\pi)^2}\left[\frac{m^2}{4\pi\mu^2}\right]^{\frac{d}{2}-2}\frac{\left(-m^2\right)^{2-n_1-n_2}}{\Gamma\left(n_1\right)\Gamma\left(n_2\right)}2^{1-n_1-n_2}\pi^{\frac{1}{2}}\int_{-i\infty}^{i\infty}\frac{dw}{2\pi i}\left(-\frac{q}{4m^2}\right)^{w}$$
$$\Gamma\left(-w\right)\frac{\Gamma\left(n_1+w\right)\Gamma\left(n_1+n_2-\frac{d}{2}+w\right)\Gamma\left(n_2+w\right)}{\Gamma\left(\frac{1}{2}\left(n_1+n_2\right)+w\right)\Gamma\left(\frac{1}{2}\left(n_1+n_2+1\right)+w\right)}\,. \tag{2.32}$$

Note that the remaining contour integral can be evaluated in terms of the generalized hyper-

geometric function ${}_3F_2$. The result is

$$B\left(d\,;n_1\,,m\,;n_2\,,m\right)=\frac{i}{(4\pi)^2}\left(-m^2\right)^{2-n_1-n_2}\left[\frac{m^2}{4\pi\mu^2}\right]^{\frac{d}{2}-2}\frac{\Gamma\left(n_1+n_2-\frac{d}{2}\right)}{\Gamma\left(n_1+n_2\right)}$$
$$\left.{}_3F_2\left[\begin{array}{c} n_1\,,n_2\,,n_1+n_2-\frac{d}{2} \\ \frac{1}{2}\left(n_1+n_2\right)\,,\frac{1}{2}\left(n_1+n_2+1\right)\end{array}\right|\frac{q^2}{4m^2}\right]. \tag{2.33}$$

which agrees with an expression given for this integral in Ref. [27]. Note that this technique can be used to calculate integrals such as (2.27) where the masses in each propagator are distinct. In Ref. [27] this is done, and the results are given in terms of multivariable generalized hypergeometric functions functions. However, these functions are somewhat unwieldy and are not widely implemented in computer algebra systems. Fortunately, all of the integrals in Chapters 3, 4, 5 and 6 can be evaluated in terms of only two scales, the external momentum q and the heavy quark mass m.

Consider now a two-loop integral with two massive propagators

$$\begin{aligned} &J\left(d\,;n_1\,,m\,;n_2\,,m\,;n_3\,,0\right)\\ &=\frac{1}{\mu^{2(d-4)}}\int\frac{d^dk_1}{(2\pi)^d}\int\frac{d^dk_2}{(2\pi)^d}\frac{1}{\left(k_1^2-m^2\right)^{n_1}\left[\,\left(k_2-q\right)^2-m^2\,\right]^{n_2}\left(k_1-k_2\right)^{2n_3}}\,. \end{aligned} \tag{2.34}$$

This integral occurs in Chapter 3, and is represented by the Feynman diagram in Fig. 2.5.

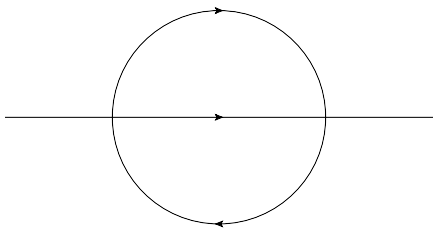

Figure 2.5: Feynman diagram representing the J-type two-loop sunset integral.

This integral can also be evaluated using Mellin-Barnes techniques. The result is

$$J\left(d\,;n_1\,,m\,;n_2\,,m\,;n_3\,,0\right)=-\frac{1}{(4\pi)^4}\left(-m^2\right)^{4-n_1-n_2-n_3}\left[\frac{m^2}{4\pi\mu^2}\right]^{d-4}$$
$$\frac{\Gamma\left(\frac{d}{2}-n_3\right)\Gamma\left(n_2+n_3-\frac{d}{2}\right)\Gamma\left(n_1+n_3-\frac{d}{2}\right)\Gamma\left(n_1+n_2+n_3-d\right)}{\Gamma\left(\frac{d}{2}\right)\Gamma\left(n_1\right)\Gamma\left(n_2\right)\Gamma\left(n_1+n_2+2n_3-d\right)}$$
$${}_4F_3\left[\begin{array}{c} n_1+n_2+n_3-d\,,n_2+n_3-\frac{d}{2}\,,n_1+n_3-\frac{d}{2}\,,n_3 \\ \frac{d}{2}\,,n_3+\frac{1}{2}\left(n_1+n_2-d\right)\,,n_3+\frac{1}{2}\left(n_1+n_2-d+1\right)\end{array}\,\middle|\,\frac{q^2}{4m^2}\right]. \tag{2.35}$$

Note that this result agrees with results given for this integral in Ref. [29]. This is the most complicated integral that we will evaluate in this chapter. In the next section we will consider a technique that can be used to construct recurrence relations among loop integrals. Using this approach, all integrals encountered in Chapters 3, 4, 5 and 6 can be evaluated in terms of the integrals given so far in this chapter.

2.4 Integration By Parts

Consider the two-loop integral

$$F\left(d\,;n_1\,,m\,;n_2\,,m\,;n_3\,,0\,;n_4\,,0\,;n_5\,,0\right)$$
$$=\frac{1}{\mu^{2(d-4)}}\int\frac{d^dk_1}{(2\pi)^d}\int\frac{d^dk_2}{(2\pi)^d}\frac{1}{\left(k_1^2-m^2\right)^{n_1}\left(k_2^2-m^2\right)^{n_2}\left(k_1-q\right)^{2n_3}\left(k_2-q\right)^{2n_4}\left(k_1-k_2\right)^{2n_5}}. \tag{2.36}$$

This integral is represented by the Feynman diagram in Fig. 2.6. Note that this is the most complex loop integral that can occur when calculating two-point functions at two-loop level, because at most five independent propagators can be constructed from the two loop momenta k_1, k_2, and the external momentum q. For this reason, the integral (2.36) is occasionally referred to as the "master" two-loop integral for two-point functions [29].

This integral cannot be evaluated using the methods discussed so far. However, it can be evaluated by appealing to one of the properties of dimensionally regularized momentum

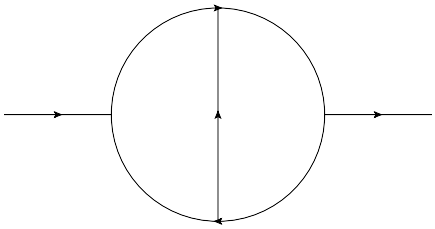

Figure 2.6: Feynman diagram representing the F-type two-loop master integral.

integrals. Specifically, loop integrals satisfy the relation

$$\frac{1}{\mu^{d-4}} \int \frac{d^d k}{(2\pi)^d} \frac{\partial}{\partial v_\mu} \left[w_\mu f\left(k\,,q\,,m\right)\right] = 0\,, \quad v_\mu = k_\mu\,, \quad w_\mu \in \left\{ k_\mu\,, (k \pm q)_\mu \right\}\,, \tag{2.37}$$

which is proven in Ref. [39]. This identity is commonly referred to as integration by parts. The identity generalizes to multi-loop integrals, the restriction being that v_μ must be one of the loop momenta. The technique was developed in Ref. [35] and used to calculate the renormalization group functions in scalar ϕ^4 theory to four-loop order. In order to illustrate the technique, we will use it to calculate the integral (2.36). Using the identity (2.37), we have

$$\int \frac{d^d k_1}{(2\pi)^d} \int \frac{d^d k_2}{(2\pi)^d} \frac{\partial}{\partial k_1^\mu} \left[\frac{(k_1 - k_2)^\mu}{\left(k_1^2 - m^2\right)^{n_1} \left(k_2^2 - m^2\right)^{n_2} \left(k_1 - q\right)^{2n_3} \left(k_2 - q\right)^{2n_4} \left(k_1 - k_2\right)^{2n_5}} \right] = 0\,, \tag{2.38}$$

where the derivatives can be calculated using the result

$$\frac{\partial}{\partial k^\mu} \frac{1}{k^{2n}} = -\frac{2nk^\mu}{k^{2(n+1)}}\,. \tag{2.39}$$

Explicitly calculating the derivatives, we arrive at the following recurrence relation

$$\begin{aligned} &\left(d - n_1 - n_3 - 2n_5\right) F\left(d\,; n_1\,, m\,; n_2\,, m\,; n_3\,, 0\,; n_4\,, 0\,; n_5\,, 0\right) \\ &= \left[n_1 \left(\mathbf{5}^- - \mathbf{2}^- \right) \mathbf{1}^+ + n_3 \left(\mathbf{5}^- - \mathbf{4}^- \right) \mathbf{3}^+ \right] F\left(d\,; n_1\,, m\,; n_2\,, m\,; n_3\,, 0\,; n_4\,, 0\,; n_5\,, 0\right)\,. \end{aligned} \tag{2.40}$$

For convenience we have defined the operators $\mathbf{N}^+$ and $\mathbf{N}^-$ that increase and decrease the index n_i by one unit when acting on the integral (2.36). Essentially, equation (2.40) is a recurrence relation for integrals of the form (2.36). For instance, consider an integral of the

form (2.36) where each $n_i = 1$. Inserting this into the recurrence relation (2.40), we find

$$\begin{aligned} F\left(d\,;1\,,m\,;1\,,m\,;1\,,0\,;1\,,0\,;1\,,0\right) = \frac{1}{d-4}\,[&F\left(d\,;2\,,m\,;1\,,m\,;1\,,0\,;1\,,0\,;0\,,0\right) \\ &- F\left(d\,;2\,,m\,;0\,,m\,;1\,,0\,;1\,,0\,;1\,,0\right) \\ &+ F\left(d\,;1\,,m\,;1\,,m\,;2\,,0\,;1\,,0\,;0\,,0\right) \\ &- F\left(d\,;1\,,m\,;1\,,m\,;2\,,0\,;0\,,0\,;1\,,0\right)]\ . \end{aligned} \tag{2.41}$$

This is a very important result. The integral on the left hand side of Eq., (2.41) cannot be evaluated using results given so far. However, the integrals on the right hand side can be calculated using (2.19) and (2.24). The recurrence relation allows us to calculate an integral that cannot be calculated directly by expressing it as a linear combination of integrals that we can evaluate. This is the power of the integration by parts method: integrals that are incalculable by themselves can be expressed in terms of calculable integrals. Several unique recurrence relations can be developed by choosing different vectors v^μ and w^μ in (2.37). With the aid of (2.41), all integrals that occur in the heavy-light diquark calculation in Chapter 4 can be evaluated in terms of results given in this chapter. In addition, we have used these methods to reproduce the result given in Ref. [66] for the next-to-leading order heavy-light pseudoscalar meson correlation function.

2.5 Generalized Recurrence Relations

Using the integration by parts technique, we can construct many recurrence relations for a certain class of loop integrals. In practice, it is often enough to use recurrence relations to calculate unknown integrals in terms of known integrals, as we did in order to calculate the integral (2.36) above. However, the question arises, given all possible recurrence relations, can we determine a minimal set of basis integrals from which all others can be calculated? As we shall see, this is possible, although we must discuss some technicalities first.

So far, we have only considered scalar integrals. However, in order to determine a minimal set of basis integrals, we must first consider how to deal with integrals that include tensors composed of the loop momenta. These can always be dealt with by appealing to the Lorentz

invariant nature of loop integrals. A simple example is as follows:

$$\frac{1}{\mu^{2(d-4)}}\int\frac{d^dk_1}{(2\pi)^d}\int\frac{d^dk_2}{(2\pi)^d}\frac{k_2^\mu}{k_2^2\left(k_1-q\right)^2\left(k_1-k_2\right)^2}\equiv q^\mu f\left(q^2\right)\,. \tag{2.42}$$

Due to Lorentz invariance, the integral must be proportional to the external momentum q^μ and a function of the Lorentz scalar q^2. Contracting both sides of (2.42) with q_μ, the function $f\left(q^2\right)$ can be determined and hence the integral on the left hand side of (2.42) can be calculated. This technique can be easily generalized to accommodate more complicated tensor structures. Ref. [98] constructs an algorithm to solve this problem in general. However, we will use a far more powerful method to deal with tensor integrals such as (2.42).

The method that we will utilize was developed in Ref. [117] and relates tensor integrals in d-dimensions to scalar integrals in $d+2N$-dimensions. In Ref. [118] the method was applied to two-point propagator-type integrals, that is, integrals of the type A, B, J, V and F that we have considered so far. This method can be used to find a truly minimal set of basis integrals for the family of two-loop two-point integrals that we have studied so far. The key idea of the method is that it is possible to express an arbitrary tensor integral as

$$\int\frac{d^dk_1}{(2\pi)^d}\int\frac{d^dk_2}{(2\pi)^d}\frac{k_1^{\mu_1}\ldots k_1^{\mu_r}k_2^{\lambda_1}\ldots k_2^{\mu_s}}{c_1^{n_1}c_2^{n_2}c_3^{n_3}c_4^{n_4}c_5^{n_5}}\equiv T^{\mu_1\ldots\mu_r\lambda_1\ldots\lambda_s}\int\frac{d^dk_1}{(2\pi)^d}\int\frac{d^dk_2}{(2\pi)^d}\frac{1}{c_1^{n_1}c_2^{n_2}c_3^{n_3}c_4^{n_4}c_5^{n_5}}\,, \tag{2.43}$$

$$c_1=k_1^2-m_1^2\,,\quad c_2=k_2^2-m_2^2\,,\quad c_3=\left(k_1-q\right)^2-m_3^2\,, \tag{2.44}$$

$$c_4=\left(k_2-q\right)^2-m_4^2\,,\quad c_5=\left(k_1-k_2\right)^2-m_5^2\,. \tag{2.45}$$

where we have omitted the renormalization scale for brevity. The tensor operator $T^{\mu_1\ldots\mu_r\lambda_1\ldots\lambda_s}$ is a function of the external momentum q^μ, derivatives with respect to each mass m_i, and an operator $\mathbf{d}^+$ that increases the dimension of any given loop integral by two units, *i.e.* $\mathbf{d}^+I^{(d)}=I^{(d+2)}$. We will now construct the explicit form of this operator. We will follow the derivation given in Ref. [118], although we will retain the loop integral normalization convention that has been used in this chapter. Introducing the auxiliary vectors a_1 and a_2,

we can write

$$T_{\mu_1\ldots\mu_r\lambda_1\ldots\lambda_s} = \frac{1}{i^{r+s}}\frac{\partial}{\partial a_1^{\mu_1}}\cdots\frac{\partial}{\partial a_1^{\mu_r}}\frac{\partial}{\partial a_2^{\lambda_1}}\cdots\frac{\partial}{\partial a_2^{\lambda_s}}\exp\left[i\left(a_1\cdot k_1 + a_2\cdot k_2\right)\right]\Big|_{a_1=a_2=0}. \tag{2.46}$$

Now, consider the integral

$$G^{(d)}\left(q^2\right) = \int\frac{d^dk_1}{(2\pi)^d}\int\frac{d^dk_2}{(2\pi)^d}\frac{\exp\left[i\left(a_1\cdot k_1 + a_2\cdot k_2\right)\right]}{c_1^{n_1}c_2^{n_2}c_3^{n_3}c_4^{n_4}c_5^{n_5}}. \tag{2.47}$$

To evaluate this integral we will use the following identity [110, 118]

$$\frac{1}{\left(k^2-m^2\right)^n} = \frac{1}{i^n\,\Gamma\left(n\right)}\int_0^\infty d\alpha\,\alpha^{n-1}\exp\left[i\alpha\left(k^2-m^2\right)\right]. \tag{2.48}$$

The integration variable α is called an alpha parameter and serves a similar purpose to the Feynman parameters introduced earlier. The resulting k_1 and k_2 loop integrals can be evaluated using the integral [118]

$$\int d^dk\exp\left[i\left(Ak^2+2q\cdot k\right)\right] = i\left[\frac{\pi}{iA}\right]^{\frac{d}{2}}\exp\left[-\frac{iq^2}{A}\right]. \tag{2.49}$$

Doing this, the result is

$$G^{(d)}\left(q^2\right) = \frac{i^{2-d}}{(4\pi)^d}\prod_{i=1}^{5}\frac{1}{i^{n_i}\,\Gamma\left(n_i\right)}\int_0^\infty\frac{d\alpha_i}{\left[D\left(\alpha\right)\right]^{\frac{d}{2}}}\alpha_i^{n_i-1}\exp\left[i\left(\frac{Q\left(\alpha_i\,,a_1\,,a_2\right)}{D\left(\alpha\right)}-\sum_{j=1}^{5}\alpha_jm_j^2\right)\right]. \tag{2.50}$$

The functions $D\left(\alpha\right)$ and $Q\left(\alpha\,,a_1\,,a_2\right)$ are

$$D\left(\alpha\right) = \alpha_5\left(\alpha_1+\alpha_2+\alpha_3+\alpha_4\right)+\left(\alpha_1+\alpha_3\right)\left(\alpha_2+\alpha_4\right), \tag{2.51}$$

$$\begin{aligned}Q\left(\alpha_i\,,a_1\,,a_2\right) = {}& \left[\left(\alpha_1+\alpha_2\right)\left(\alpha_3+\alpha_4\right)\alpha_5+\alpha_1\alpha_2\left(\alpha_3+\alpha_4\right)+\alpha_3\alpha_4\left(\alpha_1+\alpha_2\right)\right]q^2\\ &+\left(a_1\cdot q\right)Q_1+\left(a_2\cdot q\right)Q_2+a_1^2Q_{11}^2+a_2^2Q_{22}^2+\left(a_1\cdot a_2\right)Q_{12}\,,\end{aligned} \tag{2.52}$$

$$
\begin{aligned}
&Q_1 = \alpha_3\alpha_5 + \alpha_4\alpha_5 + \alpha_2\alpha_3 + \alpha_3\alpha_4\,, \quad Q_2 = \alpha_4\alpha_5 + \alpha_3\alpha_5 + \alpha_1\alpha_4 + \alpha_3\alpha_4\,, \\
&Q_{11} = -\frac{1}{4}\left(\alpha_2 + \alpha_4 + \alpha_5\right)\,, \quad Q_{22} = -\frac{1}{4}\left(\alpha_1 + \alpha_3 + \alpha_5\right)\,, \quad Q_{12} = -\frac{1}{2}\alpha_5\,.
\end{aligned}
\tag{2.53}
$$

The explicit form of the operator $T^{\mu_1\ldots\mu_r\lambda_1\ldots\lambda_s}$ can be determined by taking derivatives of (2.50) with respect to a_1, a_2, and then setting $a_1 = a_2 = 0$. For instance, consider the operator corresponding to the tensor structure k_1^μ:

$$
T_\mu = \frac{1}{i}\frac{\partial}{\partial a_1^\mu} G^{(d)}\left(q^2\right)\Big|_{a_1=a_2=0} = q_\mu\left[\alpha_3\alpha_5 + \alpha_4\alpha_5 + \alpha_2\alpha_3 + \alpha_3\alpha_4 + \ldots\right]\frac{G^{(d)}\left(q^2\right)}{D\left(\alpha\right)}\Big|_{a_1=a_2=0}\,,
\tag{2.54}
$$

where the ellipses indicate additional terms that vanish when a_1 and a_2 are set to zero. Notice that each factor of α_i multiplying $G^{(d)}\left(q^2\right)$ is proportional to a derivative of $G^{(d)}\left(q^2\right)$ with respect to m_i^2. In addition, we can absorb the factor of $D\left(\alpha\right)$ in (2.54) into $G^{(d)}\left(q^2\right)$, effectively sending $d \to d+2$ in (2.50). Finally, note that when a_1 and a_2 are set to zero in $G^{(d)}\left(q^2\right)$ (*i.e.* in Eq., (2.47)), what remains is the loop integral that the T operator acts upon in Eq., (2.45). Therefore, the T operator corresponding to the tensor k_1^μ is given by

$$
\begin{aligned}
T_\mu = -\left(4\pi\right)^2 q_\mu \Bigg[&\left(i\frac{\partial}{\partial m_3^2}\right)\left(i\frac{\partial}{\partial m_5^2}\right) + \left(i\frac{\partial}{\partial m_4^2}\right)\left(i\frac{\partial}{\partial m_5^2}\right) \\
&+ \left(i\frac{\partial}{\partial m_2^2}\right)\left(i\frac{\partial}{\partial m_3^2}\right) + \left(i\frac{\partial}{\partial m_3^2}\right)\left(i\frac{\partial}{\partial m_4^2}\right)\Bigg]\mathbf{d}^+\,,
\end{aligned}
\tag{2.55}
$$

Generalizing this result, the T operator corresponding to the tensor $k_1^{\mu_1}\ldots k_1^{\mu_r}k_2^{\lambda_1}\ldots k_2^{\lambda_s}$ is given by

$$
\begin{aligned}
&T_{\mu_1\ldots\mu_r\lambda_1\ldots\lambda_s}\left(q^\mu\,,\partial_k\,,\mathbf{d}^+\right) = \frac{1}{i^{r+s}}\prod_{i=1}^{r}\frac{\partial}{\partial a_1^{\mu_i}}\prod_{j=1}^{s}\frac{\partial}{\partial a_2^{\lambda_j}} \\
&\exp\left[i\left(Q_1\left(a_1\cdot q\right) + Q_2\left(a_2\cdot q\right) + Q_{11}a_1^2 + Q_{22}a_2^2 + Q_{12}\left(a_1\cdot a_2\right)\right)\rho\right]\Bigg|\begin{array}{l} a_k = 0 \\ \alpha_k = i\partial_k \end{array}\,, \\
&\partial_k = \frac{\partial}{\partial m_k^2}\,, \quad \rho = -\left(4\pi\right)^2\mathbf{d}^+\,.
\end{aligned}
\tag{2.56}
$$

Using T operators, any d-dimensional tensor integral which is of the same form as (2.45)

can be expressed as a linear combination of scalar integrals in $d + 2N$-dimensions. Therefore, without loss of generality we can focus entirely on scalar integrals. Although this is a very helpful result, it is not the most important use of the T operators. Notice that the loop integral recurrence relations derived from integration by parts identities (2.37) can only alter the indices n_i of a given loop integral, and cannot change the number of dimensions d. However, T operators effectively lead to loop integral recurrence relations in the number of dimensions. These two distinct forms of recurrence relations can be combined, creating generalized recurrence relations that shift not only the indices n_i of loop integrals, but also the dimension d of the loop integrals. In Ref. [118] generalized recurrence relations are developed and used to determine a minimal set of basis integrals for the family of integrals that includes the A, B, J, V, and F type integrals that we have considered so far. These generalized recurrence relations have been implemented in the Mathematica package Tarcer [88]. This package was utilized in the heavy quarkonium hybrid calculations in Chapter 3, and in the heavy-light diquark calculation in Chapter 4. After using Tarcer, all of the Wilson coefficients in the hybrid calculations can be expressed in terms of the following set of integrals: $A\,(d\,;1\,,m)$(2.13), $B\,(d\,;1\,,m\,;1\,,m)$ (2.33), $J\,(d\,;2\,,m\,;1\,,m\,;1\,,0)$ and $J\,(d\,;1\,,m\,;1\,,m\,;1\,,0)$ (2.35). Similarly, the integrals required in the heavy-light diquark calculation are $A\,(d\,;1\,,m)$ (2.13), $B\,(d\,;1\,,m\,;1\,,0)$ (2.22), $J\,(d\,;2\,,m\,;1\,,0\,;1\,,0)$ and $J\,(d\,;1\,,m\,;1\,,0\,;1\,,0)$. Note that the last two of these can be calculated using (2.26). Tarcer can be applied to any two-loop calculation, with any combination of masses.

2.6 The Epsilon Expansion

We now have explicit d-dimensional results for all of the loop integrals that are encountered in Chapters 3, 4, 5 and 6. Now we shall see that divergent integrals can be regulated by setting $d = 4 + 2\epsilon$ and expanding around $\epsilon = 0$. First we will consider the massive tadpole integral (2.13). Setting $n = 1$, $d = 4 + 2\epsilon$ and using the properties of the Gamma

function (B.9), this integral gives

$$\begin{aligned} A\left[4+2\epsilon\,;1\right] &= -\frac{im^2}{\left(4\pi\right)^2}\left[\frac{m^2}{4\pi\mu^2}\right]^{\epsilon}\Gamma\left(-1-2\epsilon\right) \\ &= -\frac{im^2}{\left(4\pi\right)^2}\exp\left(\epsilon\log\left[\frac{m^2}{4\pi\mu^2}\right]\right)\left(\frac{1}{\epsilon}+\gamma_E-1+\mathcal{O}\left(\epsilon\right)\right) \\ &= -\frac{im^2}{\left(4\pi\right)^2}\left[\frac{1}{\epsilon}+\gamma_E-\log\left(4\pi\right)-1+\log\left[\frac{m^2}{\mu^2}\right]\right]. \end{aligned} \tag{2.57}$$

Notice that the integral is divergent, and the divergence is parametrized as a simple pole at $\epsilon = 0$. Ultimately, this divergence can be traced back to the radial integral (2.10). For $\ell \gg m$, the integral goes like ℓ^{d-2n}, and hence is divergent for $d > 2n$. When this is the case, the radial integral is ill-defined. However, the expression in terms of the Gamma function (2.13) uniquely defines the loop integral when $d > 2n$.

The divergence that arises in (2.57) can be canceled through renormalization, which was discussed in Chapter 1. Recall that in the $\overline{\text{MS}}$ scheme the renormalization constants are defined so that γ_E and $\log\left(4\pi\right)$ terms are canceled in addition to poles at $\epsilon = 0$. A convenient way of partially implementing this to rescale $\mu^2 \to \mu^2 e^{-\gamma_E}/4\pi$. Doing this, all one-loop integrals will contain a factor of

$$\left[\frac{M^2}{4\pi\mu^2}\right]^{\frac{d-4}{2}} \equiv \exp\left(\frac{d-4}{2}\left[\log\left[\frac{M^2}{\mu^2}\right]-\gamma_E\right]\right), \tag{2.58}$$

where M^2 is the external scale, *i.e.* the mass m^2 or the external momentum $-q^2$. The benefit of this replacement is that it automatically cancels all factors of γ_E and $\log\left(4\pi\right)$ that would otherwise emerge when performing the epsilon expansion. This replacement easily generalizes to multi-loop integrals: an n-loop integral would have n factors of (2.58). All calculations in Chapters 3, 4, 5 and 6 use the $\overline{\text{MS}}$ renormalization scheme, therefore all loop integrals encountered there implicitly include (2.58).

Now let us consider a more complicated example. For example, consider the integral

$$\begin{aligned} &F\left(d\,;1\,,0\,;1\,,0\,;1\,,0\,;1\,,0\,;1\,,0\right) \\ &= \frac{1}{\mu^{2(d-4)}}\int\frac{d^dk_1}{\left(2\pi\right)^d}\int\frac{d^dk_2}{\left(2\pi\right)^d}\frac{1}{k_1^2\,k_2^2\left(k_1-q\right)^2\left(k_2-q\right)^2\left(k_1-k_2\right)^2}\,, \end{aligned} \tag{2.59}$$

which corresponds to the integral (2.36) with $m = 0$. This integral occurs in Chapter 6. Setting the mass to zero does not change the recurrence relation (2.40), and therefore the integral above can be written as

$$\begin{aligned} F\left(d\,;1\,,0\,;1\,,0\,;1\,,0\,;1\,,0\,;1\,,0\right) = \frac{1}{d-4}\,[&F\left(d\,;2\,,0\,;1\,,0\,;1\,,0\,;1\,,0\,;0\,,0\right) \\ &- F\left(d\,;2\,,0\,;0\,,0\,;1\,,0\,;1\,,0\,;1\,,0\right) \\ &+ F\left(d\,;1\,,0\,;1\,,0\,;2\,,0\,;1\,,0\,;0\,,0\right) \\ &- F\left(d\,;1\,,0\,;1\,,0\,;2\,,0\,;0\,,0\,;1\,,0\right)]\ . \end{aligned} \tag{2.60}$$

The integrals on the right hand side can be calculated using (2.19) and (2.24). Setting $d = 4 + 2\epsilon$ and expanding using the properties of the Gamma function to perform the expansion, we find

$$F\left(d\,;1\,,0\,;1\,,0\,;1\,,0\,;1\,,0\,;1\,,0\right) = -\frac{1}{(4\pi)^4}\frac{1}{q^2}\left[-\frac{q^2}{4\pi\mu^2}\right]^{\epsilon}\zeta\left(3\right)\ , \tag{2.61}$$

where ζ denotes the Riemann Zeta function. This integral is calculated in Ref. [97] using position space methods [34], and is in complete agreement with (2.61). Note that loop integrals that do not involve massive propagators can always be expressed in terms of Gamma functions which can be expanded easily using any computer algebra system.

As we have seen, integrals that involve an external momentum and massive propagators tend to lead to hypergeometric functions whose indices are d-dependent. Therefore, after setting $d = 4 + 2\epsilon$ we are required to expand around $\epsilon = 0$ in the indices of a hypergeometric function, which can often be a non-trivial task. For example, consider the integral

$$\begin{aligned} &V\left(d\,;1\,,m\,;1\,,0\,;1\,,0\,;1\,,0\right) \\ &= \frac{1}{\mu^{2(d-4)}}\int\frac{d^dk_1}{(2\pi)^d}\int\frac{d^dk_2}{(2\pi)^d}\frac{1}{\left(k_1^2-m^2\right)\left(k_1-q\right)^2\left(k_2-q\right)^2\left(k_1-k_2\right)^2} \end{aligned} \tag{2.62}$$

Using the result (2.26), setting $d = 4 + 2\epsilon$, and working in the $\overline{\text{MS}}$ scheme, we find

$$\begin{aligned} V\left(d\,;1\,,m\,;1\,,0\,;1\,,0\,;1\,,0\right) = & -\frac{1}{(4\pi)^4}\exp\left[2\epsilon\left(\log\left[\frac{m^2}{\mu^2}\right]-\gamma_E-\log\left[1-z\right]\right)\right] \\ & \frac{\Gamma^2\left(1+\epsilon\right)\Gamma\left(-\epsilon\right)\Gamma\left(1+2\epsilon\right)\Gamma\left(-2\epsilon\right)}{\Gamma\left(2+2\epsilon\right)\Gamma\left(2+\epsilon\right)} \\ & {}_2F_1\left[-2\epsilon\,,1+2\epsilon\,;2+\epsilon\,;z\right]\,, \quad z=\frac{1}{1-\frac{m^2}{q^2}}\,. \end{aligned} \tag{2.63}$$

In order to expand the hypergeometric function, it is useful to write it in series form

$$\begin{aligned} V\left(d\,;1\,,m\,;1\,,0\,;1\,,0\,;1\,,0\right) = & -\frac{1}{(4\pi)^4}\exp\left[2\epsilon\left(\log\left[\frac{m^2}{\mu^2}\right]-\gamma_E-\log\left[1-z\right]\right)\right] \\ & \frac{\Gamma^2\left(1+\epsilon\right)\Gamma\left(-\epsilon\right)}{\Gamma\left(2+2\epsilon\right)}\sum_{n=0}^{\infty}\frac{\Gamma\left(-2\epsilon+n\right)\Gamma\left(1+2\epsilon+n\right)}{\Gamma\left(2+\epsilon+n\right)}\frac{z^n}{n!}\,. \end{aligned} \tag{2.64}$$

Now we must expand the sum around $\epsilon = 0$, and because of the overall $\Gamma\left(-\epsilon\right)$ term we must expand the sum to $\mathcal{O}\left(\epsilon\right)$ in order to expand the entire integral to $\mathcal{O}\left(\epsilon^0\right)$. First, note that for $n \geq 1$ we may safely set $\epsilon = 0$ in the sum. Extracting the $n = 0$ term, we have

$$\begin{aligned} \sum_{n=0}^{\infty} f\left(\epsilon\,,n\right)\frac{z^n}{n!} = f\left(\epsilon\,,0\right) + \sum_{n=1}^{\infty}\left[f\left(0\,,n\right)+\epsilon\frac{d}{d\epsilon}f\left(\epsilon\,,n\right)\Big|_{\epsilon=0}\right]\frac{z^n}{n!}\,, \\ f\left(\epsilon\,,n\right) = \frac{\Gamma\left(-2\epsilon+n\right)\Gamma\left(1+2\epsilon+n\right)}{\Gamma\left(2+\epsilon+n\right)}\,. \end{aligned} \tag{2.65}$$

Using the properties of the Gamma function, this can be written as

$$\sum_{n=0}^{\infty} f\left(\epsilon\,,n\right)\frac{z^n}{n!} = \frac{\Gamma\left(-2\epsilon\right)\Gamma\left(1+2\epsilon\right)}{\Gamma\left(2+\epsilon\right)} + \sum_{n=1}^{\infty}\frac{z^n}{n\left(n+1\right)} + \epsilon\sum_{n=1}^{\infty}\left[\frac{1}{n^2\left(1+n\right)^2}-\frac{\psi\left(n\right)}{n\left(1+n\right)}\right]z^n\,, \tag{2.66}$$

where $\psi\left(n\right)$ is the Polygamma function (B.6). Evaluating the sums and performing the

epsilon expansion, the result for this integral is

$$
\begin{aligned}
V\left(d\,;1\,,m\,;1\,,0\,;1\,,0\,;1\,,0\right) = \frac{1}{512\pi^4}\Bigg[& -\frac{1}{\epsilon^2} + \frac{1}{\epsilon}\left(5 + \frac{2\log\left[1-z\right]}{z} - 2\log\left[\frac{m^2}{\mu^2}\right]\right) \\
& - \frac{1}{2}\left(38 + \pi^2 - 20\log\left[\frac{m^2}{\mu^2}\right] + 4\log^2\left[\frac{m^2}{\mu^2}\right]\right) \\
& + \frac{2\log\left[1-z\right]}{z}\left(2\log\left[\frac{m^2}{\mu^2}\right] - 5\right) \\
& + 2\left(1+\frac{1}{z}\right)\mathrm{Li}_2\left(z\right) + \left(1-\frac{3}{z}\right)\log^2\left[1-z\right]\Bigg],
\end{aligned}
\tag{2.67}
$$

where $\mathrm{Li}_2\left(z\right)$ denotes the dilogarithm function (B.18). Polylogarithm functions often appear when hypergeometric functions such as (2.62) are expanded. Note the divergent terms proportional to ϵ^{-2} and ϵ^{-1}. In a QCD sum rule calculation most of these terms would correspond to dispersion relation subtraction constants that would be eliminated when the Borel transform is applied. However, the divergent term proportional to $\log\left[1-z\right]$ is a non-local divergence that will not be eliminated by the Borel transform. Such a divergence must be dealt with through renormalization.

Using the same method as was used to expand the integral (2.62), the epsilon expansion can be performed for all of the integrals that occur in Chapter 4, and for all those in Ref. [66]. Ref. [68] provides a result for the epsilon expansion of the ${}_2F_1$ hypergeometric function up to fifth order in epsilon. In conjunction with hypergeometric function identities, this result has be used to verify the results in Chapter 4 and in Ref. [66]. In addition, the Mathematica package HypExp [62, 63] can perform epsilon expansions of many different hypergeometric functions. This package has also been used to verify the results in Chapter 4 and Ref. [66].

Finally, we will consider a typical integral occurring in the hybrid calculations in Chapter 3,

$$
J\left(d\,;1\,,m\,;1\,,m\,;1\,,0\right) = \frac{1}{\mu^{2(d-4)}}\int\frac{d^dk_1}{(2\pi)^d}\int\frac{d^dk_2}{(2\pi)^d}\frac{1}{\left(k_1^2-m^2\right)\left[\,\left(k_2-q\right)^2-m^2\,\right]\left(k_1-k_2\right)^2}\,.
\tag{2.68}
$$

Using the result (2.35), setting $d = 4 + 2\epsilon$ and working in the $\overline{\text{MS}}$ renormalization scheme,

$$J\left(d\,;1\,,m\,;1\,,m\,;1\,,0\right) = \frac{m^2}{(4\pi)^4}\exp\left[2\epsilon\left(\log\left[\frac{m^2}{\mu^2}\right]-\gamma_E\right)\right]\frac{\Gamma^2\left(-\epsilon\right)\Gamma\left(1+\epsilon\right)\Gamma\left(-1-2\epsilon\right)}{\Gamma\left(2+\epsilon\right)\Gamma\left(-2\epsilon\right)} \\ {}_4F_3\left[\left.\begin{array}{c} -1-2\epsilon\,,-\epsilon\,,-\epsilon\,,1 \\ 2+\epsilon\,,-\epsilon\,,\frac{1}{2}-\epsilon \end{array}\right| w\right], \\ w = \frac{q^2}{4m^2}\,. \tag{2.69}$$

Because the ${}_4F_3$ hypergeometric function has one common upper and lower index, it reduces to a ${}_3F_2$ hypergeometric function. Using the series representation of the hypergeometric function, the result can be written as

$$J\left(d\,;1\,,m\,;1\,,m\,;1\,,0\right) = \frac{m^2}{(4\pi)^4}\exp\left[2\epsilon\left(\log\left[\frac{m^2}{\mu^2}\right]-\gamma_E\right)\right]\frac{\Gamma\left(-\epsilon\right)\Gamma\left(1+\epsilon\right)\Gamma\left(\frac{1}{2}-\epsilon\right)}{\Gamma\left(-2\epsilon\right)} \\ \sum_{n=0}^{\infty}\frac{\Gamma\left(-1-2\epsilon+n\right)\Gamma\left(-\epsilon+n\right)\Gamma\left(1+n\right)}{\Gamma\left(2+\epsilon+n\right)\Gamma\left(\frac{1}{2}-\epsilon+n\right)}\frac{w^n}{n!}\,. \tag{2.70}$$

Noting that the factor multiplying the sum is $\mathcal{O}\left(\epsilon^0\right)$, we only need to expand the sum to this order. Also, note that the for $n \geq 2$ we may safely set $\epsilon = 0$ in the sum, so we can extract the $n = 0$ and $n = 1$ terms. Doing so, we have

$$J\left(d\,;1\,,m\,;1\,,m\,;1\,,0\right) = \frac{m^2}{(4\pi)^4}\exp\left[2\epsilon\left(\log\left[\frac{m^2}{\mu^2}\right]-\gamma_E\right)\right]\Gamma\left(-\epsilon\right)\Gamma\left(\frac{1}{2}-\epsilon\right) \\ \left[\frac{\Gamma\left(-1-2\epsilon\right)\Gamma\left(-\epsilon\right)}{\Gamma\left(2+\epsilon\right)\Gamma\left(\frac{1}{2}-\epsilon\right)}+\frac{\Gamma\left(-2\epsilon\right)\Gamma\left(1-\epsilon\right)}{\Gamma\left(3+\epsilon\right)\Gamma\left(\frac{3}{2}-\epsilon\right)}w\right. \\ \left.+\sum_{n=2}^{\infty}\frac{\Gamma\left(-1-2\epsilon+n\right)\Gamma\left(-\epsilon+n\right)\Gamma\left(1+n\right)}{\Gamma\left(2+\epsilon+n\right)\Gamma\left(\frac{1}{2}-\epsilon+n\right)}\frac{w^n}{n!}\right]. \tag{2.71}$$

Letting $k = n-2$ and using the properties of the Gamma function, the sum can be expressed as a hypergeometric function

$$w^2\sum_{k=0}^{\infty}\frac{\Gamma\left(1+k\right)\Gamma\left(2+k\right)\Gamma\left(3+k\right)}{\Gamma\left(4+k\right)\Gamma\left(\frac{5}{2}+k\right)}\frac{w^k}{\Gamma\left(3+k\right)} = \frac{2w^2}{9\sqrt{\pi}}\,{}_3F_2\left[1\,,1\,,2\,;4\,,\frac{5}{2}\,;w\right]. \tag{2.72}$$

Finally, expanding the remaining functions we find

$$J\left(d\,;1\,,m\,;1\,,m\,;1\,,0\right)=\frac{m^2}{256\pi^4}\left[-\frac{1}{6}\left(42+\pi^2+3w+12\log\left[\frac{m^2}{\mu^2}\right]\left[w-3+\log\left[\frac{m^2}{\mu^2}\right]\right]\right)\right.$$
$$-\frac{1}{\epsilon^2}+\frac{1}{\epsilon}\left(3-w-2\log\left[\frac{m^2}{\mu^2}\right]\right)$$
$$\left.+\frac{4w^2}{9}{}_3F_2\left[1\,,1\,,2\,;4\,,\frac{5}{2}\,;w\right]\right]. \tag{2.73}$$

Note that the hypergeometric function can be expressed in terms of inverse sine functions. However, there are several reasons for leaving the result in terms of a hypergeometric function. First, all hypergeometric functions with argument x have a branch cut on $x\in[1\,,\infty)$, therefore it is clear that the result (2.73) has appropriate branch cut structure, namely a branch cut on $q^2\in[4m^2\,,\infty)$. However, when the result is expressed in terms of inverse sine functions, this branch cut structure is obscured. Second, the result is very compact. Apart from the hypergeometric function, all terms in (2.73) are dispersion relation subtraction constants.

2.7 Analytic Continuation

The methods discussed so far in this chapter are sufficient to calculate the correlation functions that are studied in Chapters 3, 4 and 6. However, it is the singularities of the Wilson coefficients in the complex Euclidean momentum plane that are of interest in QSR analyses. Typically, these singularities appear as isolated poles or as branch cuts. Fig. 2.7 shows a typical branch cut singularity.

The branch point corresponds to the hadronic threshold, which is related to the total mass of the hadronic constituents. For instance, in the heavy quarkonium hybrid calculations in Chapter 3, the currents used contain two identical heavy quarks so that $t_0=4m^2$. In calculations that involve light quarks we work in the chiral limit, ignoring the light quark mass. Accordingly, $t_0=m^2$ in the heavy-light diquark calculation in Chapter 4, while in the glueball quark meson mixing calculation in Chapter 6, $t_0=0$. Recall that in QSR analyses

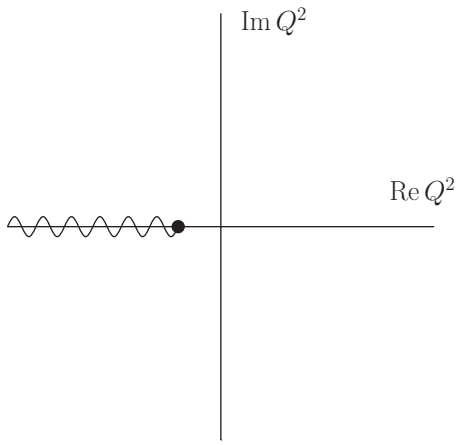

Figure 2.7: A branch cut singularity in the complex Euclidean momentum plane. The branch cut is on the interval $Q^2 \in (-\infty\,, -t_0]$, where t_0 is the hadronic threshold.

the discontinuity of the correlation function across the branch cut is required. As discussed in Chapter 1, due to the analytic properties of the correlation function, the discontinuity is related to the imaginary part. Therefore, once the correlation function has been calculated, the imaginary part must be extracted. This can be achieved via analytic continuation.

The complexity of the functions that arise in QCD sum rule calculations depends on the number of external scales involved in the calculation. In the chiral limit, typically only logarithms involving dimensionless ratios of the Euclidean external momentum Q^2 and renormalization scale μ occur. In order to deal with these, we define the complex logarithm as follows:

$$\log(w) \equiv \log|w| + i\mathrm{Arg}(w)\ , \quad \mathrm{Arg}(w) \in [-\pi\,, \pi)\ . \tag{2.74}$$

Using this, we can define

$$\log\left[\frac{Q^2}{\mu^2}\right]\Bigg|_{Q^2 = te^{-i\pi}\,, t>0} \equiv \log\left[\frac{t}{\mu^2}\right] - i\pi, \tag{2.75}$$

where we have considered a point below the branch cut, as described in Chapter 1. From (2.75) it can be shown that

$$\mathrm{Im}\log\left[\frac{Q^2}{\mu^2}\right] = -\pi\,, \quad \mathrm{Im}\log^2\left[\frac{Q^2}{\mu^2}\right] = -2\pi\log\left[\frac{t}{\mu^2}\right], \tag{2.76}$$

for example. In the heavy-light diquark calculation in Chapter 4 , more complicated functions involving dimensionless ratios of the external momentum Q^2 and the quark mass m occur. For instance, in the integral (2.67) the logarithms can be written as

$$\log\left[1-z\right] = -\log\left[1+\frac{Q^2}{m^2}\right], \quad z = \frac{1}{1+\frac{m^2}{Q^2}}\,. \tag{2.77}$$

which has the appropriate branch cut structure. Using (2.74), we can define

$$\log\left[1+\frac{Q^2}{m^2}\right]\Bigg|_{Q^2=te^{-i\pi}\,,\,t>m^2} \equiv \log\left[\frac{t}{m^2}-1\right] - i\pi\,, \tag{2.78}$$

so that, for instance,

$$\mathrm{Im}\log\left[1+\frac{Q^2}{m^2}\right] = -\pi\,, \quad \mathrm{Im}\log^2\left[1+\frac{Q^2}{m^2}\right] = -2\pi\log\left[\frac{t}{m^2}-1\right]. \tag{2.79}$$

Note the occurrence of the dilogarithm function in the integral (2.67). Using the definition of the dilogarithm function (B.18) and the properties of the logarithm above, the imaginary part can be shown to be

$$\mathrm{Im}\,\mathrm{Li}_2\left[\frac{1}{1+\frac{m^2}{Q^2}}\right]\Bigg|_{Q^2=te^{-i\pi}\,,\,t>m^2} = i\pi\log\left[1-\frac{m^2}{t}\right]. \tag{2.80}$$

Finally, we will consider the hypergeometric functions occurring in the heavy quarkonium hybrid calculations in Chapter 3. As mentioned previously, the hypergeometric function that occurs in (2.73) can be expressed in terms of inverse sine functions. Once this has been done, the imaginary part can be extracted using the identity

$$\sin^{-1}(w) = -i\log\left[iw+\sqrt{1-w^2}\right], \tag{2.81}$$

where the logarithm can be dealt with as above. Using these techniques, closed form expressions for the imaginary parts of the correlation functions in Chapters 3, 4 and 6 can be determined.

Chapter 3

Heavy Quarkonium Hybrid mass predictions

3.1 Introduction

The research presented in this chapter involves two closely related publications:

- D. Harnett, R.T. Kleiv, T.G. Steele, and Hong-Ying Jin, Axial Vector $J^{PC} = 1^{++}$ Charmonium and Bottomonium Hybrid Mass Predictions with QCD Sum-Rules, J. Phys. G39 (2012) 125003.

- R. Berg, D. Harnett, R.T. Kleiv, and T.G. Steele, Mass Predictions for Pseudoscalar $J^{PC} = 0^{-+}$ Charmonium and Bottomonium Hybrids in QCD Sum-Rules, Phys. Rev. D86 (2012) 034002.

The publications above (Refs. [60, 19]) extract mass predictions for heavy quarkonium hybrids with the quantum numbers $J^{PC} = 1^{++}$ and 0^{-+}, respectively. Heavy quarkonium hybrids are widely suspected to exist in the same mass region as charmonia and bottomonia, so it is entirely possible that some of the heavy quarkonium-like states that have been discovered so far could be heavy quarkonium hybrids. For instance, the $Y(4260)$ is considered to be a strong candidate for a charmonium hybrid [130].

Surprisingly, this possibility has been little explored by QSR practitioners. The original QSR studies of heavy quarkonium hybrids were performed by Govaerts *et al.* in Refs. [55, 56, 54]. Many different heavy quarkonium hybrid J^{PC} channels were examined, however, only the perturbative and dimension-four gluon condensate $\langle \alpha G^2 \rangle$ were included in the OPE of the correlation functions. Consequently many of the sum rules that were derived were unstable, meaning that the resulting heavy quarkonium hybrid mass predictions are unreliable. However, the authors of Ref. [102] recently updated the sum rule for the vector (1^{--}) channel,

which was unstable in Refs. [55, 56, 54]. It was found that inclusion of the dimension-six gluon condensate $\langle g^3 G^3 \rangle$ stabilizes the sum rule in this channel, permitting reliable mass predictions to be made. The publications in this chapter update the $J^{PC} = 1^{++}$ and 0^{-+} heavy quarkonium hybrid sum rules to include the effects of the dimension-six gluon condensate.

3.2 Results

The axial vector (1^{++}) and pseudoscalar (0^{-+}) heavy quarkonium hybrids can be studied within QSR using the following current and correlation function [55, 56, 54]:

$$\Pi_{\mu\nu}(q) = i \int d^4x \, e^{iq\cdot x} \langle \Omega | T \left[J_\mu(x) J_\nu(0) \right] | \Omega \rangle \,, \tag{3.1}$$

$$J_\mu = \frac{g}{2} \bar{Q} \lambda^a \gamma^\nu \tilde{G}^a_{\mu\nu} Q \,, \quad \tilde{G}^a_{\mu\nu} = \frac{1}{2} \epsilon_{\mu\nu\alpha\beta} G_a^{\alpha\beta} \,, \tag{3.2}$$

where q is the external momentum, Q denotes a heavy (charm or bottom) quark field and $G^a_{\mu\nu}$ denotes the gluon field strength tensor. Because the correlation function is Lorentz invariant, it can be decomposed into

$$\Pi_{\mu\nu}(q) = \left[\frac{q_\mu q_\nu}{q^2} - g_{\mu\nu} \right] \Pi_V\left(q^2\right) + \frac{q_\mu q_\nu}{q^2} \Pi_S\left(q^2\right) \,, \tag{3.3}$$

where $\Pi_V(q^2)$ and $\Pi_S(q^2)$ couple to axial vector and pseudoscalar heavy quarkonium hybrids, respectively [54]. These functions can be isolated by contracting Eq. (3.3) with appropriate combinations of the metric and the external momentum. Note that the contractions must be performed in d-dimensions when dimensional regularization is used.

The axial vector channel sum rule analysis resulted in mass predictions of $5.13 \pm 0.25\,\text{GeV}$ and $11.32 \pm 0.32\,\text{GeV}$ for the charmonium and bottomonium hybrids, respectively. Interestingly, the dimension-six gluon condensate had little effect on the sum rules in this channel. Although the axial vector channel sum rule was stable in the original analysis [55, 56, 54], it was important to examine the effects of the dimension-six condensate on this channel. Furthermore, because the quantum numbers of the $X(3872)$ are now firmly established to be 1^{++} [2], clear mass predictions for all axial vector exotic hadrons are needed. As dis-

cussed in Chapter 1, the $X(3872)$ is most often interpreted as a four-quark state. There has also been an attempt to describe it as a charmonium hybrid [77]. However, the hybrid interpretation has been largely set aside due to the fact that several different theoretical approaches predict an axial vector charmonium hybrid mass that is much greater than that of the $X(3872)$ [17, 99, 79, 78]. With the mass predictions that we have extracted, QSR is now in agreement with these other theoretical approaches. Therefore this work has helped to rule out the pure charmonium hybrid interpretation of the $X(3872)$. However, it should be noted that the results of this work cannot exclude the possibility that the $X(3872)$ could be a mixture of various hadronic structures, perhaps with a hybrid component. The latter possibility is explored in Ref. [32].

The pseudoscalar channel sum rule analysis lead to mass predictions of $3.82 \pm 0.13\,\text{GeV}$ and $10.64 \pm 0.19\,\text{GeV}$ for the charmonium and bottomonium hybrids, respectively. Both of these mass predictions are significantly lower than the mass predictions of the original studies of Govaerts *et al.* which were derived from unstable sum rules. Similar to the recent work in the vector channel, inclusion of the dimension-six gluon condensate was found to stabilize the pseudoscalar channel sum rules. Including the theoretical uncertainty, the pseudoscalar charmonium hybrid mass prediction is comparable to the mass of the $Y(3940)$ [5, 14]. This particle has been identified as a charmonium hybrid candidate [5], and our mass prediction supports this claim. However, to date the quantum numbers of this state have not yet been firmly established. More experimental work is needed to determine the true nature of the $Y(3940)$.

The research in this chapter contributes to several of the themes of this thesis. First, the heavy quarkonium hybrid mass predictions presented here will help to unravel the true nature of the enigmatic heavy quarkonium-like states. It is also interesting to note that the vector [102], axial vector [60] and pseudoscalar [19] charmonium hybrid mass predictions derived from QSR are in qualitative agreement with the charmonium hybrid multiplet structure predicted using lattice QCD [78]. Second, the calculations of the axial vector and pseudoscalar heavy quarkonium hybrid correlation functions profitably apply the loop integration techniques discussed in Chapter 2. In order to properly formulate the contributions of the dimension-six gluon condensate to the sum rules the entire correlation function must be

calculated explicitly. Specifically, $\Pi_{\mathrm{GGG}}(Q^2)$ is singular at the hadronic threshold $t_0 = 4m^2$. This singularity also appears in the imaginary part $\mathrm{Im}\Pi_{\mathrm{GGG}}(Q^2)$, and hence when the sum rules are formulated the integration in Eq. (1.95) is singular at the lower limit. This difficulty can be overcome by noting that Laplace sum rules (1.86) involve the inverse Laplace transform of the entire correlation function. The inverse Laplace transform can be calculated via a limiting procedure so that the sum rules are well defined at the hadronic threshold. However, the imaginary part of the correlation function alone is insufficient to do this. Therefore the the entire correlation function must be calculated explicitly, and the loop integration techniques discussed in Chapter 2 are indispensable for this.

3.3 Published Articles

The $J^{PC} = 1^{++}$ heavy quarkonium hybrid paper was published in the Journal of Physics G in 2012, while the $J^{PC} = 0^{-+}$ heavy quarkonium hybrid paper was published in Physical Review D in 2012. The papers are included on the following pages, with the second paper following immediately after the first. Each paper is presented in the journal format.

- D. Harnett, R.T. Kleiv, T.G. Steele, and Hong-Ying Jin, Axial Vector $J^{PC} = 1^{++}$ Charmonium and Bottomonium Hybrid Mass Predictions with QCD Sum-Rules, J. Phys. G39 (2012) 125003.

- R. Berg, D. Harnett, R.T. Kleiv, and T.G. Steele, Mass Predictions for Pseudoscalar $J^{PC} = 0^{-+}$ Charmonium and Bottomonium Hybrids in QCD Sum-Rules, Phys. Rev. D86 (2012) 034002.

Axial vector ($J^{PC} = 1^{++}$) charmonium and bottomonium hybrid mass predictions with QCD sum-rules

2012 J. Phys. G: Nucl. Part. Phys. 39 125003

(http://iopscience.iop.org/0954-3899/39/12/125003)

IOP PUBLISHING JOURNAL OF PHYSICS G: NUCLEAR AND PARTICLE PHYSICS

J. Phys. G: Nucl. Part. Phys. **39** (2012) 125003 (11pp) doi:10.1088/0954-3899/39/12/125003

Axial vector ($J^{PC} = 1^{++}$) charmonium and bottomonium hybrid mass predictions with QCD sum-rules

D Harnett[1], **R T Kleiv**[2], **T G Steele**[2] **and Hong-ying Jin**[3]

[1] Department of Physics, University of the Fraser Valley, Abbotsford, BC V2S 7M8, Canada
[2] Department of Physics and Engineering Physics, University of Saskatchewan, Saskatoon, SK S7N 5E2, Canada
[3] Zhejiang Institute of Modern Physics, Zhejiang University, Zhejiang, People's Republic of China

E-mail: Tom.Steele@usask.ca

Received 17 August 2012
Published 6 November 2012
Online at stacks.iop.org/JPhysG/39/125003

Abstract
Axial vector ($J^{PC} = 1^{++}$) charmonium and bottomonium hybrid masses are determined via QCD Laplace sum-rules. Previous sum-rule studies in this channel did not incorporate the dimension-six gluon condensate, which has been shown to be important for 1^{--} and 0^{-+} heavy quark hybrids. An updated analysis of axial vector charmonium and bottomonium hybrids is presented, including the effects of the dimension-six gluon condensate. The axial vector charmonium and bottomonium hybrid masses are predicted to be 5.13 and 11.32 GeV, respectively. We discuss the implications of this result for the charmonium-like 'XYZ' states and the charmonium hybrid multiplet structure observed in recent lattice calculations.

1. Introduction

A long-standing problem in hadron spectroscopy is to determine what role is played, if any, by explicit gluonic constituents in the hadronic spectrum. Quantum chromodynamics (QCD) suggests the possibility of the existence of glueballs which are composed entirely of gluons, as well as hybrids which are composed of a quark, an anti-quark and a gluon. An interesting feature of hybrids is that they can have J^{PC} quantum numbers that are not possible for conventional quark mesons. Consequently, the observation of a state with so-called exotic quantum numbers would be a 'smoking gun' for the existence of hadrons with explicit gluonic content. Hybrids with non-exotic meson quantum numbers are possible as well; these could signal their presence through supernumerary states in conventional J^{PC} channels. In this work we consider the latter scenario.

Hybrids with non-exotic J^{PC} that contain heavy quarks could coexist with conventional heavy quarkonia states. The large number of anomalous heavy quarkonium-like states

0954-3899/12/125003+11$33.00

discovered above open flavour thresholds has provided an ideal place to look for heavy quark hybrids [1–5]. A recent review [6] lists nineteen states discovered since 2003, and many of these states are difficult to accommodate as conventional charmonia [7] leading to numerous suggestions that some of them may be of an exotic nature (see e.g. [3, 8, 9] for reviews).

In this paper we use QCD Laplace sum-rules to investigate axial vector ($J^{PC} = 1^{++}$) charmonium and bottomonium hybrids. The constituent gluon model [10] was used for the earliest studies of heavy quark hybrids. Charmonium hybrids have also been studied using the flux tube model [11] which predicts the lightest charmonium hybrids at 4.1–4.2 GeV, as well as lattice QCD [12–14] which gives quenched predictions of about 4.0 GeV and unquenched predictions of about 4.4 GeV for 1^{++} hybrid charmonium. The authors of [14] perform a comprehensive study of the charmonium spectrum up to approximately 4.5 GeV and finds evidence for a ground state multiplet of hybrids which contains the 0^{-+} and 1^{--} states, as well as an excited multiplet containing the 1^{++}. As far as we are aware, [15–17] comprise the only QCD sum-rules studies of axial vector charmonium and bottomonium hybrids. Several other channels were examined in this work, and many of the resulting sum-rules exhibited instabilities, leading to unreliable mass predictions. The 1^{++} channel led to well-behaved sum-rules resulting in mass predictions in the range 4.7–5.7 GeV for hybrid charmonium and 10.9–11.5 GeV for hybrid bottomonium.

In recent sum-rule studies of vector (1^{--}) [18] and pseudoscalar (0^{-+}) [19] heavy quark hybrids it was shown that including the dimension-six gluon condensate can have significant effects on the resulting sum-rules. Specifically, in these channels it was found that inclusion of the dimension-six gluon condensate is sufficient to remove the instabilities observed in [15–17]. With this paper, we explore the effects of the dimension-six gluon condensate on the sum-rules for axial vector heavy quark hybrids and provide updated mass predictions.

In section 2, we calculate the appropriate two-point function, including leading-order perturbative contributions and contributions from the dimension-four and dimension-six gluon condensates. In section 3, we analyse the sum-rules using the single narrow resonance model and then determine ground state mass predictions. Finally, in section 4, we discuss the implications of our results for the charmonium-like and bottomonium-like states. With our result for the 1^{++} and previous results for the 1^{--} [18] and 0^{-+} [19] charmonium hybrid mass predictions, we comment on the hybrid multiplet structure identified in [14].

2. Laplace sum-rules for axial vector heavy quark hybrids

The axial vector ($J^{PC} = 1^{++}$) heavy quark hybrids may be examined using the following correlation function [15]

$$\Pi_{\mu\nu}(q) = \mathrm{i}\int d^4x\, \mathrm{e}^{\mathrm{i}q\cdot x}\langle 0|T[j_\mu(x)j_\nu(0)]|0\rangle, \tag{1}$$

$$j_\mu = \frac{g}{2}\bar{Q}\lambda^a\gamma^\nu\tilde{G}^a_{\mu\nu}Q,\ \tilde{G}^a_{\mu\nu} = \frac{1}{2}\epsilon_{\mu\nu\alpha\beta}G^a_{\alpha\beta}, \tag{2}$$

with Q representing a heavy quark field. Here we examine the transverse part Π_v of (1), which couples to 1^{++} states

$$\Pi_{\mu\nu}(q) = \left(\frac{q_\mu q_\nu}{q^2} - g_{\mu\nu}\right)\Pi_v(q^2) + \frac{q_\mu q_\nu}{q^2}\Pi_s(q^2). \tag{3}$$

In [15, 16] the perturbative and gluon condensate $\langle\alpha G^2\rangle = \langle\alpha G^a_{\mu\nu}G^a_{\mu\nu}\rangle$ contributions to the imaginary part of Π_v were calculated to leading order. Here we extend these results by including the contributions of the dimension-six gluon condensate $\langle g^3G^3\rangle = \langle g^3 f_{abc}G^a_{\mu\nu}G^b_{\nu\alpha}G^c_{\alpha\mu}\rangle$, which

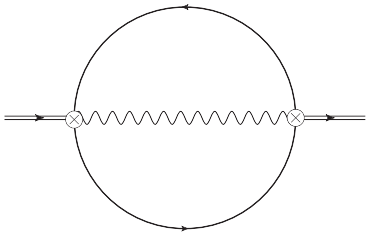

Figure 1. Feynman diagram for the leading-order perturbative contribution to Π_v. The current is represented by the $\otimes$ symbol. This and all subsequent Feynman diagrams were created with JaxoDraw [20].

were shown to have important consequences for heavy quark hybrid sum-rule studies in different channels [18, 19].

First, we verify the leading-order perturbative and $\langle\alpha G^2\rangle$ results [15, 16] for Π_v. We have opted to calculate the full expression for Π_v rather than only its imaginary part as in [15, 16]. This was found to be necessary in order to correctly formulate the sum-rules for the pseudoscalar heavy quark hybrid [19]. In addition, verifying existing results using a different approach provides a further consistency check of our results.

The leading-order perturbative contribution to Π_v is represented in figure 1. We have made use of the Tarcer [21] implementation of loop-integral recurrence relations and tensor structures [22, 23] to express Π_v in terms of a small number of basic integrals. Results for these basic integrals are provided in [24–26]. In $D = 4 + 2\epsilon$ dimensions in the $\overline{\text{MS}}$ scheme, the perturbative result is

$$\Pi_v^{\text{pert}}(q^2) = \frac{m^6\alpha}{8100\pi^3}[180(z-1)\left(12z^2-3z+5\right){}_3F_2\,(1,1,1;3/2,3;z) + 20z\left(24z^3-96z^2+7z-5\right){}_3F_2\,(1,1,2;5/2,4;z)], \quad z = \frac{q^2}{4\,m^2}, \tag{4}$$

where terms corresponding to dispersion relation subtraction constants have been omitted. The coupling α and quark mass m implicitly depend on the renormalization scale μ in the $\overline{\text{MS}}$ scheme. The generalized hypergeometric functions [27] in (4) are particularly convenient for sum-rule applications since they clearly reveal the analytic structure of Π_v, namely a branch cut starting at the threshold $q^2 = 4m^2$. In addition, the imaginary part may be easily extracted via analytic continuation of the hypergeometric functions. Doing so, we find

$$\text{Im}\Pi_v^{\text{pert}}(q^2) = \frac{\alpha m^6}{180\pi^2 z^2}(\sqrt{z-1}\sqrt{z}\left(15-35z-22z^2-216z^3+48z^4\right) + 15(1-3z+16z^3)\log[\sqrt{z-1}+\sqrt{z}]\Big), \quad z>1. \tag{5}$$

We find complete agreement between the integral representation for $\text{Im}\Pi_v^{\text{pert}}$ given in [15, 16] and (5).

The leading-order $\langle\alpha G^2\rangle$ contribution to Π_v is represented in figure 2. Due to the presence of the field strength in the current (2) this contribution is most easily calculated using fixed-point gauge methods (see e.g. [28] for examples of this technique). However, plane wave methods could be also be used as they have been proven to be equivalent to fixed-point gauge when gauge-invariant currents such as (2) are used [29]. For the $\langle\alpha G^2\rangle$ contribution we find

$$\Pi_v^{\text{GG}}(q^2) = -\frac{\langle\alpha G^2\rangle}{27\pi}m^2 z(1+2z){}_2F_1\,(1,1;5/2;z)\,, \tag{6}$$

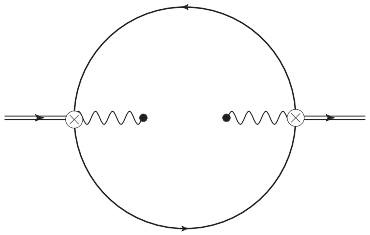

Figure 2. Feynman diagram for the leading-order $\langle \alpha G^2 \rangle$ contribution to Π_v.

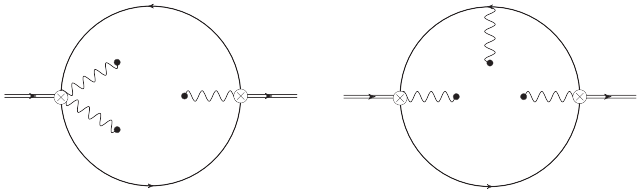

Figure 3. Feynman diagram for the leading-order $\langle g^3 G^3 \rangle$ contribution to Π_v. Additional diagrams related by symmetry are not shown.

where non-physical terms corresponding to dispersion relation subtraction constants have been omitted. The imaginary part of (6) is

$$\mathrm{Im}\Pi_v^{\mathrm{GG}}(q^2) = -\frac{m^2\langle \alpha G^2 \rangle}{18}(1+2z)\frac{\sqrt{z-1}}{\sqrt{z}}, \quad z > 1. \tag{7}$$

This again agrees with the result given in [15, 16].

Finally we consider the dimension-six gluon condensate contributions which were not calculated in [15, 16]. These are represented by the diagrams in figure 3. Again utilizing fixed-point gauge methods, we find

$$\begin{aligned}\Pi_v^{\mathrm{GGG}}(q^2) = {} & \frac{\langle g^3 G^3 \rangle}{1152\pi^2(z-1)^2}[2z(2-9z+6z^2) - 4z(z-1)(3z-1)]_2F_1(1,1;5/2;z) \\ & + \frac{\langle g^3 G^3 \rangle}{1152\pi^2(z-1)^2}[3(17z-9)(z-1) - 3(17-46z+27z^2)].\end{aligned} \tag{8}$$

The resulting imaginary part of (8) is

$$\mathrm{Im}\Pi_v^{\mathrm{GGG}}(q^2) = \frac{\langle g^3 G^3 \rangle}{384\pi(z-1)^2}\frac{\sqrt{z-1}}{\sqrt{z}}\left[2(1-3z)(z-1) + (2-9z+6z^2)\right], \quad z > 1. \tag{9}$$

The singularity at $z = 1$ in (9) must be dealt with carefully. Although (9) can be extracted from the purely hypergeometric terms in (8), it is not well-defined at $z = 1$. This problem is addressed through inclusion of the non-hypergeometric terms in (8). These contribute compensating terms which ensure that the contributions of $\Pi^{\mathrm{GGG}}(q^2)$ to the sum-rules are well-defined when $\mathrm{Im}\Pi_v^{\mathrm{GGG}}(q^2)$ is integrated from $z = 1$. Thus the imaginary part (9) by itself is insufficient to construct the contribution of the dimension-six gluon condensate to the QCD Laplace sum-rules.

Now that we have calculated the correlation function, we can proceed with the QCD Laplace sum-rules analysis [30, 31] (for reviews of the methodology see e.g. [32, 33]).

Utilizing the standard resonance plus continuum model for the hadronic spectral function, the Laplace sum-rules take the form

$$\mathcal{L}_k^{\rm QCD}(\tau, s_0) = \frac{1}{\pi}\int_{t_0}^{\infty} t^k \exp\left[-t\tau\right] \rho^{\rm had}(t)\, {\rm d}t, \tag{10}$$

where t_0 is the hadronic threshold. The quantity on the left hand side of (10) is given by

$$\mathcal{L}_k^{\rm QCD}(\tau, s_0) \equiv \frac{1}{\tau}\hat{B}\left[(-1)^k Q^{2k}\Pi_v\left(Q^2\right)\right] - \frac{1}{\pi}\int_{s_0}^{\infty} t^k \exp\left[-t\tau\right] {\rm Im}\Pi_v(t)\, {\rm d}t, \tag{11}$$

where s_0 is the continuum threshold, $Q^2 = -q^2$ is the Euclidean momentum and $\Pi_v\left(Q^2\right)$ is the axial vector heavy quark hybrid correlation function. The Borel transform operator $\hat{B}$ is closely related to the inverse Laplace transform [34]

$$\frac{1}{\tau}\hat{B}[f(Q^2)] = F(\tau) = \mathcal{L}^{-1}[f(Q^2)], \tag{12}$$

$$\mathcal{L}^{-1}[f(Q^2)] = \frac{1}{2\pi {\rm i}}\int_{b-{\rm i}\infty}^{b+{\rm i}\infty} f(Q^2)\, {\rm e}^{Q^2\tau}\, {\rm d}Q^2, \tag{13}$$

where b is chosen such that $f\left(Q^2\right)$ is analytic to the right of the integration contour in the complex plane.[4] Therefore any terms in the full expression for the correlation function $\Pi_v\left(Q^2\right)$ that contribute to the inverse Laplace transform (13) must be included in the construction of the Laplace sum-rules. The singular terms in (8) that do not contribute to the imaginary part (9) fall into this category, and thus they are an essential element of the QCD Laplace sum-rules.

Using the results for the leading order perturbative (5), $\langle\alpha G^2\rangle$ (7) and $\langle g^3G^3\rangle$ (8),(9) contributions, we find

$$\mathcal{L}_0^{\rm QCD}(\tau, s_0) = \frac{4m^2}{\pi}\int_1^{s_0/4m^2} \left[{\rm Im}\Pi_v^{\rm pert}\left(4m^2x\right) + {\rm Im}\Pi_s^{\rm GG}\left(4m^2x\right)\right]\exp\left(-4m^2\tau x\right){\rm d}x$$
$$+ \lim_{\eta\to 0^+}\left[\frac{4m^2}{\pi}\int_{1+\eta}^{s_0/4m^2} {\rm Im}\Pi_v^{\rm GGG}(4m^2x)\exp\left(-4m^2\tau x\right){\rm d}x + \frac{4m^2\langle g^3G^3\rangle}{192\pi^2\sqrt{\eta}}\exp\left(-4m^2\tau\right)\right], \tag{14}$$

$$\mathcal{L}_1^{\rm QCD}(\tau, s_0) = -\frac{\partial}{\partial\tau}\mathcal{L}_0^{\rm QCD}(\tau, s_0)\,. \tag{15}$$

The terms involving η in (15) render the integration in (14) well-defined for the $x \to 1$ ($\eta \to 0$) limit, and are natural consequence of the inverse Laplace transform of the full expression (8). Again, we stress that this expression cannot be obtained with ${\rm Im}\Pi_v^{GGG}$ alone. As before, the mass and coupling in (14) and (15) are functions of the renormalization scale μ in the $\overline{\rm MS}$-scheme. After evaluating the τ derivative in (15), renormalization group improvement may be implemented by setting $\mu = 1/\sqrt{\tau}$ [36].

3. Analysis: mass predictions for axial vector heavy quark hybrids

In order to extract ground state mass predictions for the 1^{++} heavy quark hybrids, we use a single narrow resonance model

$$\frac{1}{\pi}\rho^{\rm had}(t) = f^2\delta\left(t - M^2\right). \tag{16}$$

Using this in equation (10) yields

$$\mathcal{L}_k^{\rm QCD}(\tau, s_0) = f^2M^{2k}\exp\left(-M^2\tau\right), \tag{17}$$

[4] The work [35] contains detailed examples applying inverse Laplace transform techniques in sum-rule calculations.

from which the ground state mass M can be determined via the ratio

$$M^2 = \frac{\mathcal{L}_1^{\rm QCD}(\tau, s_0)}{\mathcal{L}_0^{\rm QCD}(\tau, s_0)}. \tag{18}$$

It should be noted that the narrow resonance model (16) results in a smaller mass prediction M compared to resonance models including width effects [37]. Additionally, an upper bound on the ground state mass prediction M can be obtained by taking the limit as $s_0 \to \infty$. The resulting upper bound on M is quite robust as it does not depend on the resonance model or how the QCD continuum is modelled.

To extract a ground state mass prediction the sum-rule parameters must be fixed. In the interest of self-consistency, we have chosen to utilize sum-rule estimates of quark masses. For the charm and bottom quark masses we take

$$m_c(\mu = m_c) = \overline{m}_c = (1.28 \pm 0.02)\ \text{GeV}, \tag{19}$$

$$m_b(\mu = m_b) = \overline{m}_b = (4.17 \pm 0.02)\ \text{GeV}, \tag{20}$$

corresponding to the full range of $\overline{\rm MS}$ charm and bottom quark mass estimates of [38–41] and in agreement with the ranges recommended by the Particle Data Group [42]. We have used one-loop $\overline{\rm MS}$ expressions for the coupling and quark masses. The coupling is evolved from the τ and Z mass for charmonium and bottomonium hybrids, respectively:

$$\alpha(\mu) = \frac{\alpha(M_\tau)}{1 + \frac{25\alpha(M_\tau)}{12\pi}\log\left(\frac{\mu^2}{M_\tau^2}\right)}, \quad \alpha(M_\tau) = 0.33, \tag{21}$$

$$\alpha(\mu) = \frac{\alpha(M_Z)}{1 + \frac{23\alpha(M_Z)}{12\pi}\log\left(\frac{\mu^2}{M_Z^2}\right)}, \quad \alpha(M_Z) = 0.118. \tag{22}$$

The numerical values of $\alpha(M_\tau)$ and $\alpha(M_Z)$ are taken from [43], and we use Particle Data Group values of the τ and Z masses [42]. At one-loop order, the $\overline{\rm MS}$ charm and bottom quark masses are given by

$$m_c(\mu) = \overline{m}_c\left(\frac{\alpha(\mu)}{\alpha(\overline{m}_c)}\right)^{12/25}, \tag{23}$$

$$m_b(\mu) = \overline{m}_b\left(\frac{\alpha(\mu)}{\alpha(\overline{m}_b)}\right)^{12/23}. \tag{24}$$

For the purposes of the sum-rule analysis we set $\mu = 1/\sqrt{\tau}$ as described above. We use the following values of the QCD condensates, extracted from heavy-quark systems [40]:

$$\langle g^3 G^3\rangle = (8.2 \pm 1.0)\,\text{GeV}^2\langle \alpha G^2\rangle, \tag{25}$$

$$\langle \alpha G^2\rangle = (7.5 \pm 2.0) \times 10^{-2}\ \text{GeV}^4. \tag{26}$$

We find that $\eta = 10^{-4}$ is sufficient to numerically evaluate the limit in (14).

Now that the numerical values of the physical parameters have been fixed, we may proceed with the sum-rule analysis beginning with hybrid charmonium. First we must establish a region of validity for the sum-rule analysis. To do so, we follow [31] and define the functions

$$f_{\rm cont}(\tau, s_0) = \frac{\mathcal{L}_1^{\rm QCD}(\tau, s_0)/\mathcal{L}_0^{\rm QCD}(\tau, s_0)}{\mathcal{L}_1^{\rm QCD}(\tau, \infty)/\mathcal{L}_0^{\rm QCD}(\tau, \infty)}, \tag{27}$$

$$f_{\rm pow}(\tau, s_0) = \frac{\mathcal{L}_1^{\rm QCD}(\tau, s_0)/\mathcal{L}_0^{\rm QCD}(\tau, s_0)}{\mathcal{L}_1^{\rm pert}(\tau, s_0)/\mathcal{L}_0^{\rm pert}(\tau, s_0)}, \tag{28}$$

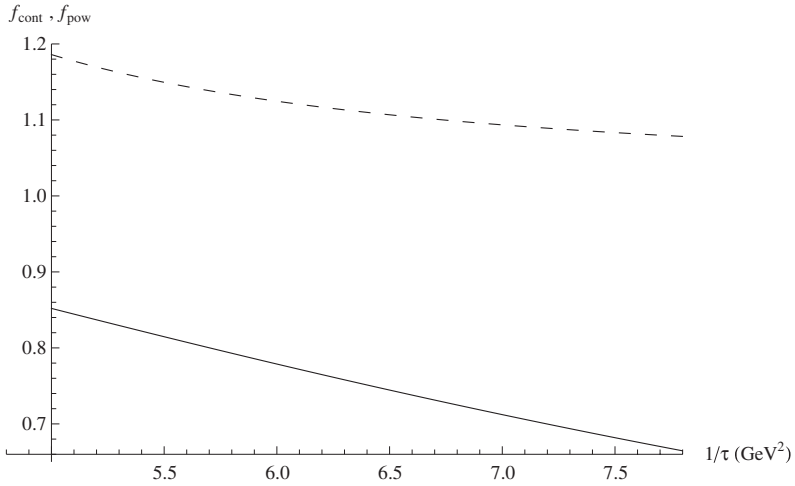

Figure 4. The quantities $f_{\rm cont}(\tau, s_0)$ (solid line) and $f_{\rm pow}(\tau, s_0)$ (dashed line) for hybrid charmonium are shown as a function of the Borel scale $1/\tau$ for the optimized value $s_0 = 33.0\,{\rm GeV}^2$. Central values of the QCD parameters have been used.

where $\mathcal{L}_k^{\rm pert}$ represents the perturbative contributions to (14) and (15). The functions (27) and (28) measure the relative importance of the respective continuum and non-perturbative contributions to the sum-rule. These two functions can be used to constrain the Borel parameter τ and define a window of reliability for the sum-rule. Inspired by [31], we impose the constraints $f_{\rm cont} > 0.7$ (i.e. continuum contributions must be less than 30%) and $|f_{\rm pow} - 1| < 0.15$ (i.e. non-perturbative contributions do not exceed 15%). The purpose of these constraints is to control uncertainties associated with non-perturbative effects (such as truncation of the operator-product expansion at dimension-six) and the continuum model. Figure 4 depicts the functions $f_{\rm cont}$ and $f_{\rm pow}$ for the optimal value of s_0 which is determined below. We have also performed the analysis in the pole scheme, with a charm quark pole mass of $m_c^{\rm pole} = 1.71\,{\rm GeV}$ [42]. As in the pseudoscalar charmonium hybrid analysis [19], we find that the sum-rule window closes rapidly in the pole scheme, and hence the $\overline{\rm MS}$ scheme is more suitable for this analysis. The advantage of the $\overline{\rm MS}$ scheme is also seen in [44].

The optimal s_0 value is determined as follows. First, the lowest value of s_0 where the mass prediction (18) stabilizes (exhibits a minimum) within its sum-rule window is identified. In this case, we find the minimum value of s_0 to be $32\,{\rm GeV}^2$, with a corresponding sum-rule window of $5.3\,{\rm GeV}^2 < 1/\tau < 7.3\,{\rm GeV}^2$. Figure 5 shows the mass prediction (18) within this sum-rule window for several values of s_0. Second, we define

$$\chi^2(s_0) = \sum_j \left(\frac{1}{M} \sqrt{\frac{\mathcal{L}_1^{\rm QCD}(\tau_j, s_0)}{\mathcal{L}_0^{\rm QCD}(\tau_j, s_0)}} - 1 \right)^2, \tag{29}$$

summed over the window $5.3\,{\rm GeV}^2 < 1/\tau < 7.3\,{\rm GeV}^2$, and then search for the value of s_0 that minimizes (29). The width of the sum-rule window increases slowly as s_0 is increased from the minimum value, so this approach guarantees that (29) is calculated in a region where the sum-rule is reliable for all values of s_0. This procedure results in an optimal $s_0 = 33\,{\rm GeV}^2$ and a corresponding charmonium hybrid mass prediction of 5.13 GeV. Note that the limit as $s_0 \to \infty$ cannot be used here to obtain a demonstrable upper bound on the charmonium hybrid mass since the mass prediction (18) does not stabilize within the sum-rule window, as

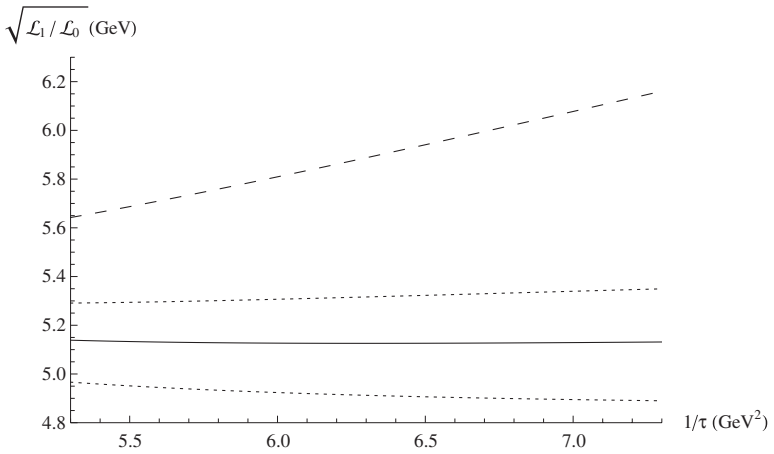

Figure 5. The ratio $\mathcal{L}_1^{\rm QCD}(\tau, s_0)/\mathcal{L}_0^{\rm QCD}(\tau, s_0)$ for hybrid charmonium is shown as a function of the Borel scale $1/\tau$ for the optimized value $s_0 = 33\,{\rm GeV}^2$ (solid curve). The ratio is also shown for $s_0 = 38\,{\rm GeV}^2$ (upper dotted curve), $s_0 = 28\,{\rm GeV}^2$ (lower dotted curve) and $s_0 \to \infty$ (uppermost dashed curve). Central values of the QCD parameters have been used.

can be seen from figure 5. On the Borel window, the optimized curve in figure 5 is virtually τ-independent; this provides us with strong *a posteriori* justification for the use of a single narrow resonance model. Hence any excited states are either exponentially suppressed by τ relative to the ground state or are weakly coupled and absorbed into the continuum.

We now estimate the uncertainty in the charmonium hybrid mass prediction due to uncertainties in the QCD input parameters. Interestingly, the uncertainty in the mass prediction is dominated by $\langle\alpha G^2\rangle$ (26), while the uncertainties due to the charm quark mass (19) and $\langle g^3 G^3\rangle$ (25) are significantly smaller. This is in contrast with the pseudoscalar heavy quark hybrid, where the uncertainty in the mass prediction is dominated by the dimension-six gluon condensate. We have made no attempt to estimate contributions to these uncertainties from higher loop effects. Since we are interested in hybrids that may exist among the established charmonium-like states, we have explored the effect of resonance widths on our mass predictions with a 200 MeV width, corresponding to the widest of these established resonances [42]. Using methods described in [37], we find that our mass prediction changes by less than 1%, which is negligible compared to the uncertainty due to the QCD input parameters. Adding the QCD parameter uncertainties in quadrature, we predict the charmonium hybrid mass to be $5.13 \pm 0.25\,{\rm GeV}$. This prediction is in good agreement with the range of results of 4.7–5.7 GeV found in [15, 17], all of which were derived from stable sum-rules that did not include effects of the dimension-six gluon condensate. Thus we can conclude that the dimension-six condensate is not as significant in the 1^{++} channel as it is in the 0^{-+} and 1^{--} channels of hybrid charmonium.

The sum-rule analysis of hybrid bottomonium is very similar. The sum-rule is reliable in the region $s_0 > 145\,{\rm GeV}^2$ and $7.8\,{\rm GeV}^2 < 1/\tau < 25.0\,{\rm GeV}^2$. The functions $f_{\rm cont}$ (27) and $f_{\rm pow}$ (28) are shown in this region in figure 6, and we again use the constraints $0.85 < f_{\rm pow} < 1.15$ and $f_{\rm cont} > 0.7$. As in the hybrid charmonium analysis, it is not possible to obtain a demonstrable upper bound on the mass prediction since the ratio (18) for $s_0 \to \infty$ does not stabilize within the sum rule window. Using (29), we find the optimal $s_0 = 150\,{\rm GeV}^2$. Figure 7 shows the mass prediction (18) within the sum-rule window for several values of s_0. The uncertainty analysis again shows that the error in $\langle\alpha G^2\rangle$ dominates the error in the

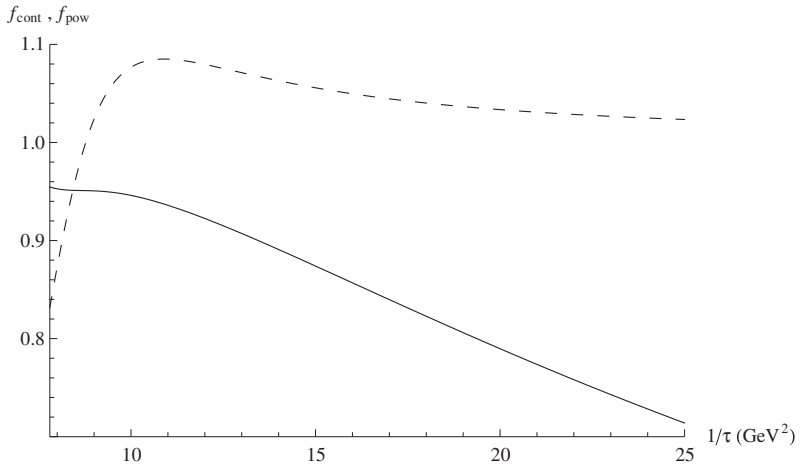

Figure 6. The quantities $f_{\rm cont}(\tau, s_0)$ (solid line) and $f_{\rm pow}(\tau, s_0)$ (dashed line) for hybrid bottomonium are shown as a function of the Borel scale $1/\tau$ for the optimized value $s_0 = 150\,\text{GeV}^2$. Central values of the QCD parameters have been used.

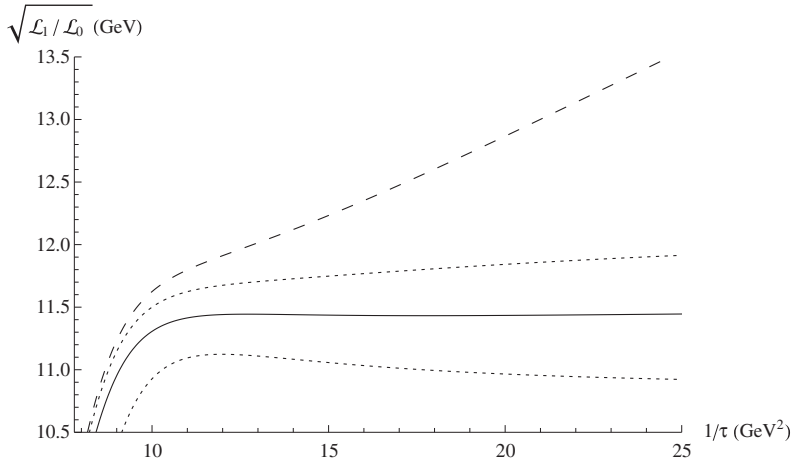

Figure 7. The ratio $\mathcal{L}_1^{\rm QCD}(\tau, s_0)/\mathcal{L}_0^{\rm QCD}(\tau, s_0)$ for hybrid bottomonium is shown as a function of the Borel scale $1/\tau$ for the optimized value $s_0 = 150\,\text{GeV}^2$ (solid curve). For comparison the ratio is also shown for $s_0 = 170\,\text{GeV}^2$ (upper dotted curve), $s_0 = 130\,\text{GeV}^2$ (lower dotted curve) and $s_0 \to \infty$ (uppermost dashed curve). Central values of the QCD parameters have been used.

bottomonium hybrid mass prediction and that resonance width effects are negligible. Adding the errors in quadrature, we predict a bottomonium hybrid mass of 11.32 ± 0.32 GeV. This result is in good agreement with the range of 10.9–11.5 GeV for hybrid bottomonium predicted in [15, 17].

4. Conclusions

In this paper we have studied axial vector ($J^{PC} = 1^{++}$) heavy quark hybrids via QCD Laplace sum-rules. We have calculated the full expressions for the leading order perturbative and $\langle \alpha G^2 \rangle$

contributions to the correlation function, and have noted that the corresponding imaginary parts of these expressions agree with the results given in [15, 17]. For the first time, we have also determined the contributions from $\langle g^3G^3\rangle$, which were not included in previous work. For these it was shown that the imaginary part alone was insufficient to formulate the QCD Laplace sum-rules, and the full expression for the $\langle g^3G^3\rangle$ contribution to the correlation function was needed.

In [15, 17], many of the sum-rules for various J^{PC} heavy quark hybrids exhibited instabilities, and hence the resulting mass predictions for those channels are unreliable. Recent sum-rule analyses of vector (1^{--}) [18] and pseudoscalar (0^{-+}) [19] heavy quark hybrids have shown that the inclusion of the dimension-six gluon condensate stabilizes the sum-rules for these channels. Although no instabilities were found for 1^{++} heavy quark hybrids in [15, 17], it is nevertheless of interest to examine the effects of the dimension-six gluon condensate in this channel given the significant effect observed in other channels. Including the $\langle g^3G^3\rangle$ contributions in our analysis results in the predictions of 5.13 ± 0.25 GeV for hybrid charmonium and 11.32 ± 0.32 GeV for hybrid bottomonium. Our results are in agreement with the predictions of [15, 17] which ranged from 4.7–5.7 GeV and 10.9–11.5 GeV for axial vector charmonium and bottomonium hybrids, respectively. The uncertainties in the mass predictions are dominated by the uncertainty in $\langle \alpha G^2\rangle$ while the uncertainty due to $\langle g^3G^3\rangle$ is less significant, in contrast to the uncertainty in the pseudoscalar hybrid mass predictions [19]. This, together with our agreement with the mass predictions of [15, 17], suggests that unlike the vector [18] and pseudoscalar [19] channels, the effects of the dimension-six gluon condensate are less significant for the axial vector channel.

To date, all of the charmonium-like 'XYZ' states have been discovered in the mass range 3.8–4.7 GeV [6]. Clearly our prediction of 5.13 GeV does not support the identification of any of these states as an axial vector charmonium hybrid. The first discovered charmonium-like state was the X(3872), whose possible J^{PC} assignments are 1^{++} or 2^{-+} [45, 46], although the 1^{++} option is strongly favoured [9]. Many different proposals have been made regarding the nature of the X(3872): a conventional charmonium state, a $D^0\bar{D}^{0*}$ molecule, a tetraquark and a hybrid (see e.g. [8] for a review). The hybrid interpretation was suggested in [47], but has now been largely set aside. The reason for this seems to be that both flux-tube model [11] and lattice QCD [12–14] predict that the lightest charmonium hybrids have masses significantly greater than that of the X(3872). If its quantum numbers are shown to be 1^{++}, our mass prediction of 5.13 GeV is in agreement with the results of other theoretical approaches that seem to preclude a charmonium hybrid interpretation of the X(3872).

It is interesting to note the large difference between the predicted masses of 3.82 GeV for 0^{-+} [19] and 4.12–4.79 for 1^{--} [18] hybrid charmonium compared to the 1^{++} prediction of 5.13 GeV. In [14] it is suggested that 0^{-+} and 1^{--} are members of a ground state charmonium hybrid multiplet, while 1^{++} is a member of a multiplet of excited charmonium hybrids. Although the mass splittings are significantly larger, the present result and those of [18, 19] seem to be in approximate agreement with this multiplet structure. Future work to update remaining unstable sum-rule channels in [15–17] to include the effects of the dimension-six gluon condensate would clarify the predictions for the spectrum of charmonium hybrids from a QCD sum-rules standpoint.

Acknowledgment

We are grateful for financial support from the Natural Sciences and Engineering Research Council of Canada (NSERC).

References

[1] Olsen S L 2009 *Nucl. Phys.* A **827** 53C (arXiv:0901.2371 [hep-ex])
[2] Olsen S L 2009 arXiv:0909.2713 [hep-ex]
[3] Godfrey S and Olsen S L 2008 *Annu. Rev. Nucl. Part. Sci.* **58** 51 (arXiv:0801.3867 [hep-ph])
[4] Pakhlova G V 2008 arXiv:0810.4114 [hep-ex]
[5] Close F E 2007 *Proc. Fifth Flavor Physics Comp.* eConf C **070512** 020 (arXiv:0706.2709 [hep-ph])
[6] Eidelman S, Heltsley B K, Hernandez-Rey J J, Navas S and Patrignani C 2012 arXiv:1205.4189 [hep-ex]
[7] Barnes T, Godfrey S and Swanson E S 2005 *Phys. Rev.* D **72** 054026 (arXiv:hep-ph/0505002)
[8] Swanson E S 2006 *Phys. Rep.* **429** 243 (arXiv:hep-ph/0601110)
[9] Brambilla N *et al* 2011 *Eur. Phys. J.* C **71** 1534 (arXiv:1010.5827 [hep-ph])
[10] Horn D and Mandula J 1978 *Phys. Rev.* D **17** 898
[11] Barnes T, Close F E and Swanson E S 1995 *Phys. Rev.* D **52** 5242 (arXiv:hep-ph/9501405)
[12] Perantonis S and Michael C 1990 *Nucl. Phys.* B **347** 854
[13] Liu L, Ryan S M, Peardon M, Moir G and Vilaseca P 2011 arXiv:1112.1358 [hep-lat]
[14] Liu L *et al* 2012 arXiv:1204.5425 [hep-ph]
[15] Govaerts J, Reinders L J and Weyers J 1985 *Nucl. Phys.* B **262** 575
[16] Govaerts J, Reinders L J, Rubinstein H R and Weyers J 1985 *Nucl. Phys.* B **258** 215
[17] Govaerts J, Reinders L J, Francken P, Gonze X and Weyers J 1987 *Nucl. Phys.* B **284** 674
[18] Qiao C -F, Tang L, Hao G and Li X-Q 2012 *J. Phys. G: Nucl. Part. Phys.* **39** 015005 (arXiv:1012.2614 [hep-ph])
[19] Berg R, Harnett D, Kleiv R T and Steele T G 2012 *Phys. Rev.* D **86** 034002
[20] Binosi D and Theussl L 2004 *Comput. Phys. Commun.* **161** 76 (arXiv:hep-ph/0309015)
[21] Mertig R and Scharf R 1998 *Comput. Phys. Commun.* **111** 265 (arXiv:hep-ph/9801383)
[22] Tarasov O V 1997 *Nucl. Phys.* B **502** 455 (arXiv:hep-ph/9703319)
[23] Tarasov O V 1996 *Phys. Rev.* D **54** 6479 (arXiv:hep-th/9606018)
[24] Boos E E and Davydychev A I 1991 *Theor. Math. Phys.* **89** 1052
Boos E E and Davydychev A I 1991 *Teor. Mat. Fiz.* **89** 56
[25] Davydychev A I 1992 *J. Math. Phys.* **33** 358
[26] Broadhurst D J, Fleischer J and Tarasov O V 1993 *Z. Phys.* C **60** 287 (arXiv:hep-ph/9304303)
[27] Erdélyi A (ed) 1953 Higher transcendental functions *Bateman Manuscript Project* vol 1 (New York: McGraw-Hill)
[28] Elias V, Steele T G and Scadron M D 1988 *Phys. Rev.* D **38** 1584
[29] Bagan E, Ahmady M R, Elias V and Steele T G 1994 *Z. Phys.* C **61** 157
[30] Shifman M A, Vainshtein A I and Zakharov V I 1979 *Nucl. Phys.* B **147** 385
[31] Shifman M A, Vainshtein A I and Zakharov V I 1979 *Nucl. Phys.* B **147** 448
[32] Reinders L J, Rubinstein H and Yazaki S 1985 *Phys. Rep.* **127** 1
[33] Narison S 2002 QCD as a theory of hadrons from partons to confinement *Camb. Monogr. Part. Phys. Nucl. Phys. Cosmol.* **17** 1 (arXiv:hep-ph/0205006)
[34] Bertlmann R A, Launer G and de Rafael E 1985 *Nucl. Phys.* B **250** 61
[35] Harnett D, Steele T G and Elias V 2001 *Nucl. Phys.* A **686** 393 (arXiv:hep-ph/0007049)
[36] Narison S and de Rafael E 1981 *Phys. Lett.* B **103** 57
[37] Elias V, Fariborz A H, Shi F and Steele T G 1998 *Nucl. Phys.* A **633** 279 (arXiv:hep-ph/9801415)
[38] Chetyrkin K G, Kuhn J H, Maier A, Maierhofer P, Marquard P, Steinhauser M and Sturm C 2009 *Phys. Rev.* D **80** 074010 (arXiv:0907.2110 [hep-ph])
[39] Narison S 2012 *Phys. Lett.* B **707** 259 (arXiv:1105.5070 [hep-ph])
[40] Narison S 2010 *Phys. Lett.* B **693** 559 (arXiv:1004.5333 [hep-ph])
Narison S 2011 *Phys. Lett.* B **705** 544 (erratum)
[41] Kuhn J H, Steinhauser M and Sturm C 2007 *Nucl. Phys.* B **778** 192 (arXiv:hep-ph/0702103)
[42] Nakamura K *et al* (Particle Data Group) 2010 *J. Phys. G: Nucl. Part. Phys.* **37** 075021
Beringer J *et al* (Particle Data Group) 2012 *Phys. Rev.* D **86** 010001
[43] Bethke S 2009 *Eur. Phys. J.* C **64** 689 (arXiv:0908.1135 [hep-ph])
[44] Jamin M and Lange B O 2002 *Phys. Rev.* D **65** 056005 (arXiv:hep-ph/0108135)
[45] Abulencia A *et al* (CDF Collaboration) 2007 *Phys. Rev. Lett.* **98** 132002 (arXiv:hep-ex/0612053)
[46] Abe K *et al* (Belle Collaboration) 2005 arXiv:hep-ex/0505038
[47] Li B A 2005 *Phys. Lett.* B **605** 306 (arXiv:hep-ph/0410264)

PHYSICAL REVIEW D **86,** 034002 (2012)

Mass predictions for pseudoscalar ($J^{PC} = 0^{-+}$) charmonium and bottomonium hybrids in QCD sum-rules

R. Berg,[1] D. Harnett,[1] R. T. Kleiv,[2] and T. G. Steele[2]

[1]*Department of Physics, University of the Fraser Valley, Abbotsford, British Columbia, V2S 7M8, Canada*
[2]*Department of Physics and Engineering Physics, University of Saskatchewan, Saskatoon, Saskatchewan, S7N 5E2, Canada*

(Received 23 May 2012; published 2 August 2012)

Masses of the pseudoscalar ($J^{PC} = 0^{-+}$) charmonium and bottomonium hybrids are determined using QCD Laplace sum-rules. The effects of the dimension-six gluon condensate are included in our analysis and result in a stable sum-rule analysis, whereas previous studies of these states were unable to optimize mass predictions. The pseudoscalar charmonium hybrid is predicted to have a mass of approximately 3.8 GeV and the corresponding bottomonium prediction is 10.6 GeV. Calculating the full correlation function, rather than only the imaginary part, is shown to be necessary for accurate formulation of the sum-rules. The charmonium hybrid mass prediction is discussed within the context of the *XYZ* resonances.

DOI: 10.1103/PhysRevD.86.034002 PACS numbers: 12.39.Mk, 12.38.−t, 14.40.Rt

I. INTRODUCTION

Quantum chromodynamics (QCD) seems to allow for hadrons which contain explicit gluonic degrees of freedom i.e., glueballs and hybrids. Despite decades of dedicated effort by experimentalists and theoreticians, no such state has been conclusively identified. Within the context of heavy quarkonia, hybrids can make their presence known in two ways: through J^{PC} quantum numbers that are not permissible for conventional quarkonia (so-called exotic hybrids), and through an overpopulation of states with conventional (nonexotic) quantum numbers. In this work we focus on the latter scenario.

A promising area in which to search for such hybrid states has been provided by the recent population boom in the charmonium sector above $D\bar{D}$-threshold [1–6]. Since 2002, more than a dozen new resonances have been discovered, the so-called *XYZ* resonances, mainly by the Belle and *BABAR* Collaborations; however, few of these particles fit neatly with a conventional charmonium meson interpretation [7]. Not surprisingly, there has been much speculation that some of the new states lie outside the constituent quark model.

In this article, we analyze pseudoscalar ($J^{PC} = 0^{-+}$) charmonium and bottomonium hybrids using a QCD Laplace sum-rules approach. The pioneering calculations for heavy quark hybrids were handled with a constituent gluon model [8]. Additional computational approaches (relevant to the pseudoscalar sector) include the flux tube model [9] which predicts the lightest charmonium hybrids at 4.1–4.2 GeV as well as lattice QCD [10–12] which yields a quenched prediction of 4.01 GeV and unquenched predictions of about 4.2 GeV. To our knowledge, the only sum-rules literature concerning heavy quark pseudoscalar hybrids is Refs. [13–15]. As noted therein, the sum-rules that were derived demonstrated instabilities when analyzed. With this paper, we aim to address these instabilities and update the sum-rule mass prediction by extending previous work [13,14] to include dimension-six gluon condensate effects.

In Sec. II, we compute the relevant two-point correlation function. We include leading-order perturbative contributions as well as contributions stemming from the dimension-four and dimension-six gluon condensates. Using these results, we then derive the needed Laplace sum-rules. In Sec. III, we analyze the sum-rules using the single narrow resonance model and extract ground state mass predictions. Finally, in Sec. IV, we comment on our charmonium hybrid results and interpret them within the context of current experimental data.

II. LAPLACE SUM-RULES FOR THE PSEUDOSCALAR HEAVY QUARK HYBRIDS

The pseudoscalar ($J^{PC} = 0^{-+}$) heavy quark hybrid states can be studied from the following correlation function [13]

$$\Pi_{\mu\nu}(q) = i\int d^4x e^{iq\cdot x}\langle 0|T[j_\mu(x)j_\nu(0)]|0\rangle, \tag{1}$$

$$j_\mu = \frac{g}{2}\bar{Q}\lambda^a\gamma^\nu\tilde{G}^a_{\mu\nu}Q, \qquad \tilde{G}^a_{\mu\nu} = \frac{1}{2}\epsilon_{\mu\nu\alpha\beta}G^a_{\alpha\beta}, \tag{2}$$

where Q denotes a heavy (charm or bottom) quark field. Within (1), the longitudinal part Π_s is of primary interest in this work because it probes the 0^{-+} states

$$\Pi_{\mu\nu}(q) = \left(\frac{q_\mu q_\nu}{q^2} - g_{\mu\nu}\right)\Pi_v(q^2) + \frac{q_\mu q_\nu}{q^2}\Pi_s(q^2). \tag{3}$$

The leading-order perturbative and gluon condensate $\langle\alpha G^2\rangle = \langle\alpha G^a_{\mu\nu}G^a_{\mu\nu}\rangle$ contributions to the imaginary part of Π_S have previously been calculated [13,14], but the resulting sum-rule analysis for the 0^{-+} mass was unstable [14,15]. We extend these results by calculating the leading-order dimension-six gluon condensate $\langle g^3G^3\rangle = \langle g^3 f_{abc}G^a_{\mu\nu}G^b_{\nu\alpha}G^c_{\alpha\mu}\rangle$ contributions to Π_s. As will be seen

below, the $\langle g^3G^3\rangle$ contribution is sufficient to stabilize the sum-rule 0^{-+} mass prediction. The stabilizing effect of $\langle g^3G^3\rangle$ has also been observed for the sum-rule analysis of 1^{--} heavy quark hybrids [16].

We begin by verifying the leading-order perturbative and $\langle\alpha G^2\rangle$ results [13,14] for Π_s. Reference [17] advocates the desirability of an independent confirmation of the Ref. [13,14] results; as such we have calculated the full expression for Π_s as opposed to simply reproducing the previously calculated imaginary part [13,14].

The leading-order perturbative contribution to Π_s is represented in Fig. 1. We use the Tarcer [18] implementation of loop-integral recurrence relations and tensor structures [19,20] to express Π_s in terms of the small set of basic integrals given in Refs. [21–23]. In $D = 4 + 2\epsilon$ dimensions in the $\overline{\text{MS}}$ scheme, the perturbative result is

$$\begin{aligned}\Pi_s^{\text{pert}}(q^2) &= \frac{m^6\alpha}{5400\pi^3}[180(z-1)(4z^2-21z+10)\\ &\quad\times {}_3F_2(1,1,1;3/2,3;z)\\ &\quad+20z(8z^3+8z^2+29z-10)\\ &\quad\times {}_3F_2(1,1,2;5/2,4;z)],\\ z &= \frac{q^2}{4m^2},\end{aligned} \tag{4}$$

where m is the quark mass, and nonphysical terms corresponding to dispersion relation subtraction constants have been omitted. The quantities α and m are implicitly evaluated at the renormalization scale μ in the $\overline{\text{MS}}$ scheme. Standard conventions for generalized hypergeometric functions have been used (see for example Ref. [24]). The analytic structure of Π_s (i.e., a branch starting at $q^2 = 4m^2$) is clearly evident from the hypergeometric functions. Analytic continuation of the hypergeometric functions in (4) gives

$$\begin{aligned}\text{Im}\Pi_s^{\text{pert}}(q^2) &= \frac{\alpha m^6}{120\pi^2 z^2}(\sqrt{z-1}\sqrt{z}(30-115z+166z^2\\ &\quad+8z^3+16z^4)-15(-2+9z-16z^2\\ &\quad+16z^3)\log[\sqrt{z-1}+\sqrt{z}]), \qquad z>1.\end{aligned} \tag{5}$$

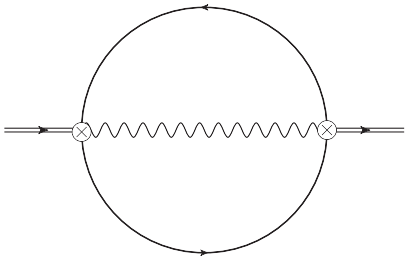

FIG. 1. Feynman diagram for the leading-order perturbative contribution to Π_s. The current is represented by the ⊗ symbol. This and all subsequent Feynman diagrams were created with JaxoDraw [51].

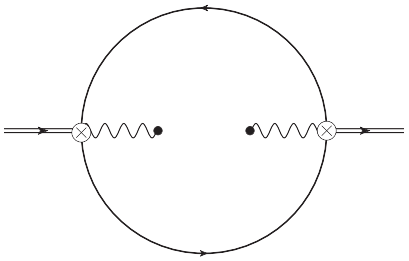

FIG. 2. Feynman diagram for the leading-order $\langle\alpha G^2\rangle$ contribution to Π_s.

Calculating the integral representations for $\text{Im}\Pi_s^{\text{pert}}$ given in [13,14] we find complete agreement with (5).

The leading order $\langle\alpha G^2\rangle$ contribution to Π_s is represented in Fig. 2. We choose to calculate this contribution using fixed-point gauge methods (see, e.g., Ref. [25] for examples applying these methods), which have been proven to be equivalent to plane-wave techniques for correlation functions of gauge-invariant currents [26].[1] Using the same loop-calculation methods as for the perturbative contributions, the $\langle\alpha G^2\rangle$ result is

$$\Pi_s^{\text{GG}}(q^2) = \frac{\langle\alpha G^2\rangle}{36\pi}m^2z(4z+2)_2F_1(1,1;5/2;z), \tag{6}$$

where nonphysical terms corresponding to dispersion relation subtraction constants have been omitted. The imaginary part of (6)

$$\text{Im}\,\Pi_s^{\text{GG}}(q^2) = \frac{m^2\langle\alpha G^2\rangle}{12}(1+2z)\frac{\sqrt{z-1}}{\sqrt{z}}, \qquad z>1, \tag{7}$$

again agrees with the explicit result of Refs. [13,14].

The dimension-six gluon condensate contributions represented by the diagrams in Fig. 3 were not calculated in Refs. [13,14]. Using the fixed-point gauge and loop-calculation techniques described above, we find

$$\begin{aligned}\Pi_s^{\text{GGG}}(q^2) &= \frac{\langle g^3G^3\rangle}{384\pi^2(z-1)^2}[4z^2(z-1)\\ &\quad-(4z^3-6z^2+2z-1)]_2F_1(1,1;5/2;z)\\ &\quad+\frac{\langle g^3G^3\rangle}{384\pi^2(z-1)^2}[31z^2-50z+16\\ &\quad+(z-1)(9-21z)].\end{aligned} \tag{8}$$

The corresponding imaginary part of (8) is

$$\begin{aligned}\text{Im}\Pi_s^{\text{GGG}}(q^2) &= \frac{\langle g^3G^3\rangle}{256\pi z(z-1)^2}\frac{\sqrt{z-1}}{\sqrt{z}}[4z^2(z-1)\\ &\quad-(4z^3-6z^2+2z-1)], \qquad z>1.\end{aligned} \tag{9}$$

[1]Implementation of fixed-point gauge methods is trivial because the field strength appears in the current (2).

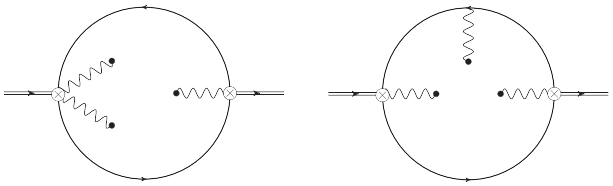

FIG. 3. Feynman diagram for the leading-order $\langle g^3G^3\rangle$ contribution to Π_s. Additional diagrams related by symmetry are not shown.

At this stage, we note that only the hypergeometric terms contribute to the imaginary part, but as will be shown below, the remaining terms do contribute to the QCD Laplace sum-rules because of the single and double poles at $z = 1$. Thus if only the imaginary parts are calculated (as in Refs. [13,14]), there exists the possibility that the resulting sum-rule will be inaccurate.

The dispersion relation appropriate to the asymptotic (perturbative) behavior of Π_s is

$$\Pi_s(Q^2) = \Pi_s(0) + Q^2\Pi_s'(0) + \frac{1}{2}Q^4\Pi_s''(0) + \frac{1}{6}Q^6\Pi_s'''(0) + Q^8\frac{1}{\pi}\int_{t_0}^{\infty} dt\frac{\rho(t)}{t^4(t+Q^2)}. \tag{10}$$

where $Q^2 = -q^2$ is the Euclidean momentum and $\rho(t)$ is the hadronic spectral function with physical threshold t_0. Note that the high-energy behavior of (5) ensures convergence of the integral. Direct application of the dispersion relation is not possible because Π_s contains field-theoretical divergences that are polynomials in Q^2 and the associated subtraction constants on the right-hand side of (10) are unknown. A related problem is the contribution of excited states and the QCD continuum to the integral of $\rho(t)$ in (10). Enhancement of the lowest-lying resonance contribution in hadronic systems requires greater high-energy suppression of this integral.

The established technique for dealing with these issues is the Laplace sum-rules [27,28]. A family of Laplace sum-rules can be obtained from the dispersion relation (10) through the Borel transform operator $\hat{B}$

$$\hat{B} \equiv \lim_{\substack{N,Q^2\to\infty \\ N/Q^2=\tau}} \frac{(-Q^2)^N}{\Gamma(N)}\left(\frac{d}{dQ^2}\right)^N, \tag{11}$$

which has the following useful properties in the construction of the Laplace sum-rules:

$$\hat{B}[a_0 + a_1Q^2 + \ldots a_mQ^{2m}] = 0 \qquad (m \text{ finite}), \tag{12}$$

$$\hat{B}\left[\frac{Q^{2n}}{t+Q^2}\right] = \tau(-1)^n t^n e^{-t\tau}, \qquad n = 0, 1, 2, \ldots \ (n \text{ finite}). \tag{13}$$

The Borel transform is related to the inverse Laplace transform via [29]

$$f(Q^2) = \int_0^{\infty} d\tau F(\tau)e^{-Q^2\tau} \equiv \mathcal{L}[F(\tau)] \Rightarrow \frac{1}{\tau}\hat{B}[f(Q^2)] = F(\tau) = \mathcal{L}^{-1}[f(Q^2)], \tag{14}$$

$$\mathcal{L}^{-1}[f(Q^2)] = \frac{1}{2\pi i}\int_{b-i\infty}^{b+i\infty} f(Q^2)e^{Q^2\tau}dQ^2, \tag{15}$$

where $f(Q^2)$ is analytic to the right of the integration contour in the complex plane.

The theoretically determined quantity

$$\mathcal{L}_k(\tau) \equiv \frac{1}{\tau}\hat{B}[(-1)^kQ^{2k}\Pi_s(Q^2)], \tag{16}$$

leads to the following family of Laplace sum-rules, after application of $\hat{B}$ to the dispersion relation (10) weighted by the appropriate power of Q^2:

$$\mathcal{L}_k(\tau) = \frac{1}{\pi}\int_{t_0}^{\infty} dt t^k e^{-t\tau}\rho(t), \qquad k \geq 0. \tag{17}$$

On the right-hand side of (17), we impose the standard resonance plus continuum model

$$\rho(t) = \rho^{\text{had}}(t) + \theta(t - s_0)\,\text{Im}\Pi^{\text{QCD}}(t), \tag{18}$$

where s_0 represents the onset of the QCD continuum. The resulting continuum contribution

$$\mathcal{L}_k^{\text{cont}}(\hat{s}, \tau, s_0) = \frac{1}{\pi}\int_{s_0}^{\infty} t^k \exp[-t\tau]\text{Im}\Pi^{\text{QCD}}(t)dt \tag{19}$$

is then moved to the left-hand side of (17). The total QCD contribution

$$\mathcal{L}_k^{\text{QCD}}(\tau, s_0) \equiv \mathcal{L}_k(\tau) - \mathcal{L}_k^{\text{cont}}(\tau, s_0) \tag{20}$$

is then related to the hadronic spectral function

$$\mathcal{L}_k^{\text{QCD}}(\tau, s_0) = \frac{1}{\pi}\int_{t_0}^{\infty} t^k \exp[-t\tau]\rho^{\text{had}}(t)dt. \tag{21}$$

We also note that the tensor decomposition in (3) could have been chosen without the overall factor of $1/q^2$, as is done for axial-vector and vector correlators (for examples of each see Ref. [17]). If this convention had been used, the perturbative calculation would have a $1/q^2\epsilon^2$ divergence, which must be eliminated by additional weights of Q^2 in the Laplace sum-rule (16). In other words, knowledge of the divergence structure, which is not revealed in the imaginary part, places a bound on the lowest-possible weight k in the Laplace sum-rule (16).

The Laplace sum-rule can now be calculated using the methods described above (see, e.g., Ref. [30] for detailed examples of applying inverse Laplace transform techniques), leading to the following results

$$\mathcal{L}_0^{\rm QCD}(\tau, s_0) = \frac{4m^2}{\pi}\int_1^{s_0/4m^2}[{\rm Im}\Pi_s^{\rm pert}(4m^2x) + {\rm Im}\Pi_s^{\rm GG}(4m^2x)]\exp(-4m^2\tau x)dx + \lim_{\eta\to 0^+}\left[\frac{4m^2}{\pi}\int_{1+\eta}^{s_0/4m^2}{\rm Im}\Pi_s^{\rm GGG}(4m^2x) \times \exp(-4m^2\tau x)dx - \frac{4m^2\langle g^3G^3\rangle}{128\pi^2\sqrt{\eta}} \times \exp(-4m^2\tau)\right], \quad (22)$$

$$\mathcal{L}_1^{\rm QCD}(\tau, s_0) = -\frac{\partial}{\partial\tau}\mathcal{L}_0^{\rm QCD}(\tau, s_0). \quad (23)$$

Several clarifying remarks on Eqs. (22) and (23) are needed. First, the mass m and strong coupling α are implicitly $\overline{\rm MS}$-scheme running quantities evaluated at a scale μ. However, one often implements renormalization-group improvement by setting $\mu = 1/\sqrt{\tau}$ [31], which must be done after calculating the τ partial derivative in (23). Second, the η limiting procedure naturally originates from the inverse Laplace transform approach applied to the full result (8), and ensures cancellation of integration divergences arising from the $1/(z-1)$ poles of (9). Thus, as mentioned earlier, the last term in (22) requires knowledge of the full $\langle g^3G^3\rangle$ contributions and cannot be obtained solely from ${\rm Im}\Pi_s^{\rm GGG}$.

III. ANALYSIS: MASS PREDICTIONS FOR THE PSEUDOSCALAR HEAVY QUARK HYBRIDS

We analyze the QCD Laplace sum-rules using a single narrow resonance model

$$\frac{1}{\pi}\rho^{\rm had}(t) = f^2\delta(t-M^2). \quad (24)$$

In this approximation, the sum-rules become

$$\mathcal{L}_k^{\rm QCD}(\tau, s_0) = f^2M^{2k}\exp(-M^2\tau), \quad (25)$$

and the 0^{-+} hybrid mass M is given by the ratio of the first two Laplace sum-rules

$$M^2 = \frac{\mathcal{L}_1^{\rm QCD}(\tau, s_0)}{\mathcal{L}_0^{\rm QCD}(\tau, s_0)}. \quad (26)$$

Using fairly general arguments, one can demonstrate that the narrow-width mass estimate would overestimate the actual mass when resonance width effects are included [32]. Furthermore, the $s_0 \to \infty$ limit provides an upper bound on the ratio (26), permitting a very robust upper bound on the ground state mass prediction that is essentially independent of the QCD continuum approximation and resonance model.

Before proceeding with the detailed analysis, the QCD parameters will be specified. It is easy to see that the quark mass m sets the basic scale of the mass prediction, so it is the most crucial parameter in our analysis. We have chosen to focus on sum-rule estimates of quark masses as they would provide the greatest possibility of a self-consistent prediction for the hybrid mass. In particular, the following values encompass the $\overline{\rm MS}$ quark masses of Refs. [33–36]:

$$m_c(\mu = m_c) = \bar{m}_c = (1.28 \pm 0.02)\ {\rm GeV}, \quad (27)$$

$$m_b(\mu = m_b) = \bar{m}_b = (4.17 \pm 0.02)\ {\rm GeV}. \quad (28)$$

These values are within the Particle Data Group's recommended ranges [37].

Since our calculation is leading-order, one-loop $\overline{\rm MS}$ expressions for the renormalization-group evolution of the strong coupling and quark masses are appropriate. For the hybrid charmonium analysis, the strong coupling is best determined by evolution from the τ mass, and in the hybrid bottomonium case by evolution from the Z mass:

$$\alpha(\mu) = \frac{\alpha(M_\tau)}{1+\frac{25\alpha(M_\tau)}{12\pi}\log(\frac{\mu^2}{M_\tau^2})}, \qquad \alpha(M_\tau) = 0.33; \quad (29)$$

$$\alpha(\mu) = \frac{\alpha(M_Z)}{1+\frac{23\alpha(M_Z)}{12\pi}\log(\frac{\mu^2}{M_Z^2})}, \qquad \alpha(M_Z) = 0.118. \quad (30)$$

The numerical values of $\alpha(M_\tau)$ and $\alpha(M_Z)$ are based on the determinations of [38], and we use Particle Data Group values of the τ and Z masses [37]. The scale dependence of the $\overline{\rm MS}$ masses can then be expressed to the same leading-order as

$$m_c(\mu) = \bar{m}_c\left(\frac{\alpha(\mu)}{\alpha(\bar{m}_c)}\right)^{12/25}, \quad (31)$$

$$m_b(\mu) = \bar{m}_b\left(\frac{\alpha(\mu)}{\alpha(\bar{m}_b)}\right)^{12/23}. \quad (32)$$

We set $\mu = 1/\sqrt{\tau}$ in our sum-rule analysis [31].

For the QCD condensates, we use the following determinations of the QCD condensates from heavy-quark systems [35]:

$$\langle g^3G^3\rangle = (8.2 \pm 1.0)\ {\rm GeV}^2\langle\alpha G^2\rangle, \quad (33)$$

$$\langle\alpha G^2\rangle = (7.5 \pm 2.0)\times 10^{-2}\ {\rm GeV}^4. \quad (34)$$

For the $\langle g^3G^3\rangle$ contributions to (22) we find that $\eta = 10^{-4}$ is sufficient to evaluate the limit.

We begin with the analysis of hybrid charmonium. We first establish a window for the Borel parameter τ for which the sum-rule analysis is considered reliable. Following [28], we define the quantities

$$f_{\rm cont}(\tau, s_0) = \frac{\mathcal{L}_1^{\rm QCD}(\tau, s_0)/\mathcal{L}_0^{\rm QCD}(\tau, s_0)}{\mathcal{L}_1^{\rm QCD}(\tau, \infty)/\mathcal{L}_0^{\rm QCD}(\tau, \infty)}, \quad (35)$$

$$f_{\rm pow}(\tau, s_0) = \frac{\mathcal{L}_1^{\rm QCD}(\tau, s_0)/\mathcal{L}_0^{\rm QCD}(\tau, s_0)}{\mathcal{L}_1^{\rm pert}(\tau, s_0)/\mathcal{L}_0^{\rm pert}(\tau, s_0)}, \quad (36)$$

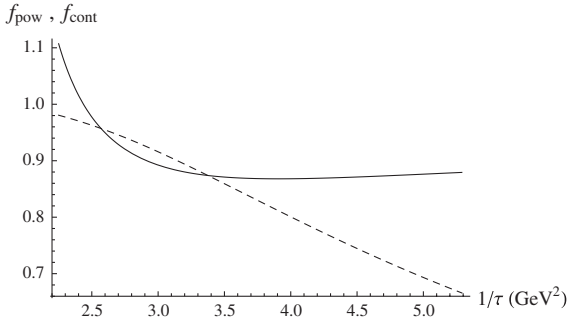

FIG. 4. The quantities $f_{pow}(\tau, s_0)$ (solid line) and $f_{cont}(\tau, s_0)$ (dashed line) for hybrid charmonium are shown as a function of the Borel scale $1/\tau$ for the optimized value $s_0 = 23.0$ GeV^2. Central values of the QCD parameters have been used.

where $\mathcal{L}_k^{pert}$ includes only the perturbative corrections arising from (22). The ratio (35) represents the relative importance of the continuum to the sum-rule ratio (26) while (36) represents the relative importance of nonperturbative (power-law) effects. Consistent with [28], we define the window of sum-rule validity by $f_{cont} > 0.7$ (i.e., the continuum contribution does not exceed 30%) and $0.9 < f_{pow} < 1.1$ (i.e., the nonperturbative contributions do not exceed 10%). Figure 4 show the resulting constraints on the Borel parameter τ for the optimum value of s_0 to be discussed below. The resulting region of validity 2.6 GeV$^2 < 1/\tau < 4.8$ GeV^2 is comparable to the window established for the 1^{--} charmonium hybrid [16]. If we change to the pole scheme for the charm quark (with a pole mass $m_c^{pole} = 1.71$ GeV [37]), the sum-rule window diminishes considerably and thus the sum-rule is less reliable than in the $\overline{MS}$ quark mass scheme, consistent with the findings of [39].

The optimized value of s_0 and mass prediction is obtained by finding the minimum value $s_0 = 19$ GeV^2 for which the ratio (26) stabilizes (in this case, a minimum) at a τ value within the s_0-dependent region of validity. We thereby establish a region $s_0 > 19$ GeV^2 and 1.6 GeV $< 1/\sqrt{\tau} < 2.0$ GeV for locating an optimized prediction. We then search for the optimized mass prediction M and s_0 that minimize the quantity[2]

$$\chi^2(s_0) = \sum_j \left(\frac{1}{M} \sqrt{\frac{\mathcal{L}_1^{QCD}(\tau_j, s_0)}{\mathcal{L}_0^{QCD}(\tau_j, s_0)}} - 1 \right)^2, \qquad (37)$$

where $1.6 \text{ GeV} < 1/\sqrt{\tau_j} < 2.0$ GeV. This procedure results in $s_0 = 23.0$ GeV^2 and the predicted charmonium hybrid mass 3.82 GeV. In Fig. 5 we show the optimized ratio for $s_0 = 23$ GeV^2 in addition to larger and smaller values, including the $s_0 \to \infty$ limit used for obtaining mass bounds.

[2]A fit based on the quantity $\frac{1}{M^2} \frac{\mathcal{L}_1^{QCD}(\tau_j, s_0)}{\mathcal{L}_0^{QCD}(\tau_j, s_0)}$ leads to virtually identical optimizations.

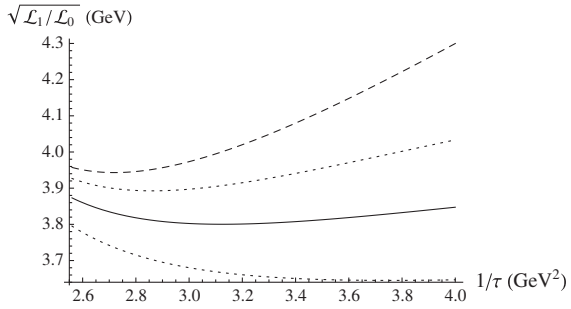

FIG. 5. The ratio $\mathcal{L}_1^{QCD}(\tau, s_0)/\mathcal{L}_0^{QCD}(\tau, s_0)$ for hybrid charmonium is shown as a function of the Borel scale $1/\tau$ for the optimized value $s_0 = 23$ GeV^2 (solid curve). For comparison the ratio is also shown for $s_0 = 28$ GeV^2 (upper dotted curve) and $s_0 = 19$ GeV^2 (lower dotted curve). The uppermost dashed curve represents the $s_0 \to \infty$ limit corresponding to the bound $M < 3.96$ GeV. Central values of the QCD parameters have been used.

Uncertainties in the mass prediction resulting from the QCD input parameters are dominated by variations of the charm quark mass (27) and $\langle g^3 G \rangle$ (33), while $\langle \alpha G^2 \rangle$ variations (34) are relatively stable. The analysis is also stable under an alternative choice of renormalization scale ($\mu = m_c^{pole} = 1.71$ GeV). Adding the uncertainties in quadrature, we find the predicted value of the charmonium hybrid mass to be $M = (3.82 \pm 0.13)$ GeV. The influence of $\langle g^3 G \rangle$ on the mass prediction corroborates our key observation that the dimension-six condensate effects are essential for stabilizing the mass prediction. The basic scales of our analysis align well with Ref. [16] which also included effects of $\langle g^3 G^3 \rangle$ to find a 1^{--} charmonium hybrid mass of approximately 4.4 GeV for $s_0 \approx 26$ GeV^2. By contrast, Ref. [13] was not able to obtain optimized mass predictions for 0^{-+} and 1^{--} hybrid charmonium, so we speculate that the dimension-six condensate $\langle g^3 G^3 \rangle$ is a necessary component of sum-rule analyses for heavy quark hybrids.

For hybrid bottomonium a simple scaling behavior in moving from the hybrid charmonium to bottomonium systems will not occur because in addition to a function of q^2/m^2 that would lead to scaling behavior, there are

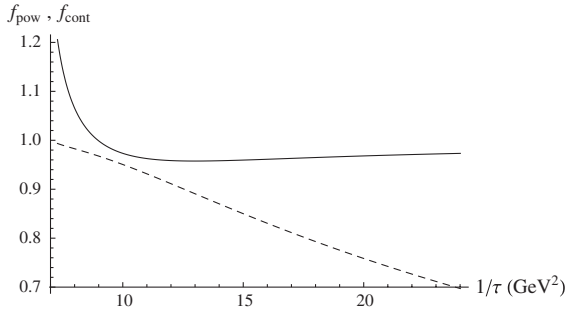

FIG. 6. The quantities $f_{pow}(\tau, s_0)$ (solid line) and $f_{cont}(\tau, s_0)$ (dashed line) for hybrid bottomonium are shown as a function of the Borel scale $1/\tau$ for the optimized value $s_0 = 140$ GeV^2. Central values of the QCD parameters have been used.

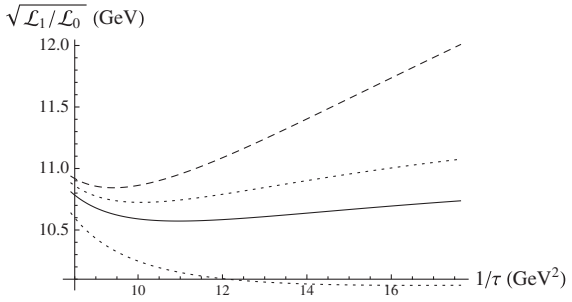

FIG. 7. The ratio $\mathcal{L}_1^{\rm QCD}(\tau, s_0)/\mathcal{L}_0^{\rm QCD}(\tau, s_0)$ for hybrid bottomonium is shown as a function of the Borel scale $1/\tau$ for the optimized value $s_0 = 140$ GeV^2 (solid curve). For comparison the ratio is also shown for $s_0 = 155$ GeV^2 (upper dotted curve) and $s_0 = 116$ GeV^2 (lower dotted curve). The uppermost dashed curve represents the $s_0 \to \infty$ limit corresponding to the bound $M < 10.84$ GeV. Central values of the QCD parameters have been used.

differing prefactors of the quark mass for each contribution [see Eqs. (4), (6), and (8)]. This will lead to differing weights of the various perturbative and nonperturbative contributions, and hence there are intrinsic field-theoretical differences between hybrid charmonium and bottomonium systems.

The details of the bottomonium hybrid analysis proceeds in a very similar fashion as the charmonium hybrid case. The sum-rule window of validity for the optimized $s_0 = 140$ GeV^2 is shown in Fig. 6, and using the same methodology described above, we establish the region $s_0 > 115$ GeV^2 and 2.9 GeV $< 1/\sqrt{\tau} < 4.2$ GeV for locating an optimized prediction. The optimization procedure described above yields $s_0 = 140$ GeV^2 and the predicted bottomonium hybrid mass 10.64 GeV shown in Fig. 7 in addition to larger and smaller s_0 values, including the $s_0 \to \infty$ limit used for obtaining mass bounds. The bottom quark mass and $\langle g^3G^3\rangle$ variations (28) and (33) still dominate uncertainties resulting in the final mass prediction $M = (10.64 \pm 0.19)$ GeV. Once again, the basic scales of our predictions are in good agreement with the 1^{--} results [16].

IV. CONCLUSIONS

In this paper we have calculated the leading-order perturbative, $\langle \alpha G^2\rangle$, and $\langle g^3G^3\rangle$ contributions to the pseudoscalar ($J^{\rm PC} = 0^{-+}$) heavy quark hybrid correlation function. A full calculation of the perturbative and $\langle \alpha G^2\rangle$ terms has been performed, and the imaginary parts confirm the results of Refs. [13,14]. However, the $\langle g^3G^3\rangle$ contributions have not previously been calculated, and the full contribution to the correlation function was needed because the imaginary part was not sufficient to determine the Laplace sum-rules.

In the absence of the $\langle g^3G^3\rangle$ contributions, a stable Laplace sum-rule prediction of the 0^{-+} charmonium and bottomonium hybrids was not achieved even with sophisticated coupled sum-rule methods [14,15]. However, the $\langle g^3G^3\rangle$ effects are able to stabilize the Laplace sum-rule mass analysis and result in the predictions $M = (3.82 \pm 0.13)$ GeV for the charmonium hybrid and $M = (10.64 \pm 0.19)$ GeV for hybrid bottomonium. The uncertainties in our mass predictions only include effects of the QCD input parameters; we make no attempt to estimate the effect of higher-loop or other theoretical uncertainties. We emphasize that the $\langle g^3G^3\rangle$ uncertainty is clearly observable, demonstrating that the dimension-six contributions are significant enough to stabilize the analysis. Reference [16] previously found a similar stabilizing effect of the $\langle g^3G^3\rangle$ contributions for mass predictions of 1^{--} hybrid charmonium and bottomonium, and the sum-rule scales of the 1^{--} and 0^{-+} systems are in qualitative agreement.

The results of our analysis may have implications concerning the Y(3940) first observed by the Belle Collaboration [40] and seemingly verified by the *BABAR* Collaboration [41] although at the significantly lower mass of 3915 MeV. There seems to be an emerging consensus that the Y(3940) and the X(3915) [42] are the same particle whereas the Y(3940) and the X(3940) [43] are distinct [44–46]. In what follows, we adopt this point of view.

As first noted in the paper announcing its discovery [40], the Y(3940) is a legitimate charmonium hybrid candidate. It is observed in B decays which, as argued in [47], are thought to be prime charmonium hybrid hunting grounds. Also, to date, the only hadronic decay mode detected is to $\omega J/\psi$ [45,46], an observation difficult to reconcile with a conventional charmonium meson assignment considering the kinematically allowed $D\bar{D}$ and $D\bar{D}^*$ channels. Such peculiar decay signatures are, however, consistent with a hybrid interpretation as there exists a flux tube model-inspired selection rule which heavily suppresses hybrid decays to pairs of S-wave mesons [48–50].

The $\omega J/\psi$ decay mode allows for a straightforward identification of the Y(3940) as an isosinglet with $C = +$. Unfortunately, the J^P assignment is not so simple; additional effort is required to identify the needed spin and parity quantum numbers.

Optimistically assuming that the Y(3940) will eventually be identified as a pseudoscalar state, comparing our mass prediction of 3820 MeV (and 130 MeV uncertainty) to the measured value of 3915 MeV provides additional evidence in favor of an interpretation of the Y(3940) as a charmonium hybrid or at least as a resonance admitting a significant hybrid component.

ACKNOWLEDGMENTS

We are grateful for financial support from the Natural Sciences and Engineering Research Council of Canada (NSERC). We thank John Gracey for generously providing his advice on loop-calculations.

[1] S. L. Olsen, Nucl. Phys. **A827**, 53c (2009).
[2] S. L. Olsen, arXiv:0909.2713.
[3] S. Godfrey and S. L. Olsen, Annu. Rev. Nucl. Part. Sci. **58**, 51 (2008).
[4] G. V. Pakhlova, arXiv:0810.4114.
[5] F. E. Close, in *Proceedings of the Flavor Physics Conference*, eConf C070512, 020 (2007).
[6] A. G. Mokhtar (unpublished).
[7] T. Barnes, S. Godfrey, and E. S. Swanson, Phys. Rev. D **72**, 054026 (2005).
[8] D. Horn and J. Mandula, Phys. Rev. D **17**, 898 (1978).
[9] T. Barnes, F. E. Close, and E. S. Swanson, Phys. Rev. D **52**, 5242 (1995).
[10] S. Perantonis and C. Michael, Nucl. Phys. **B347**, 854 (1990).
[11] L. Liu, S. M. Ryan, M. Peardon, G. Moir, and P. Vilaseca, Proc. Sci., LATTICE2011 (2011) 140.
[12] L. Liu *et al.*, arXiv:1204.5425.
[13] J. Govaerts, L. J. Reinders, and J. Weyers, Nucl. Phys. **B262**, 575 (1985).
[14] J. Govaerts, L. J. Reinders, H. R. Rubinstein, and J. Weyers, Nucl. Phys. **B258**, 215 (1985).
[15] J. Govaerts, L. J. Reinders, P. Francken, X. Gonze, and J. Weyers, Nucl. Phys. **B284**, 674 (1987).
[16] C.-F. Qiao, L. Tang, G. Hao, and X.-Q. Li, J. Phys. G **39**, 015005 (2012).
[17] S. Narison, Cambridge Monogr. Part. Phys., Nucl. Phys., Cosmol. **17**, 1 (2004).
[18] R. Mertig and R. Scharf, Comput. Phys. Commun. **111**, 265 (1998).
[19] O. V. Tarasov, Nucl. Phys. **B502**, 455 (1997).
[20] O. V. Tarasov, Phys. Rev. D **54**, 6479 (1996).
[21] E. E. Boos and A. I. Davydychev, Teor. Mat. Fiz. **89**, 56 (1991) [Theor. Math. Phys. **89**, 1052 (1991)].
[22] A. I. Davydychev, J. Math. Phys. (N.Y.) **33**, 358 (1992).
[23] D. J. Broadhurst, J. Fleischer, and O. V. Tarasov, Z. Phys. C **60**, 287 (1993).
[24] *Higher Transcendental Functions*, edited by A. Erdelyi, Bateman Manuscript Project, Vol. 1 (McGraw-Hill, New York, 1953).
[25] V. Elias, T. G. Steele, and M. D. Scadron, Phys. Rev. D **38**, 1584 (1988).
[26] E. Bagan, M. R. Ahmady, V. Elias, and T. G. Steele, Z. Phys. C **61**, 157 (1994).
[27] M. A. Shifman, A. I. Vainshtein, and V. I. Zakharov, Nucl. Phys. **B147**, 385 (1979).
[28] M. A. Shifman, A. I. Vainshtein, and V. I. Zakharov, Nucl. Phys. **B147**, 448 (1979).
[29] R. A. Bertlmann, G. Launer, and E. de Rafael, Nucl. Phys. **B250**, 61 (1985).
[30] D. Harnett, T. G. Steele, and V. Elias, Nucl. Phys. **A686**, 393 (2001).
[31] S. Narison and E. de Rafael, Phys. Lett. **103B**, 57 (1981).
[32] V. Elias, A. H. Fariborz, F. Shi, and T. G. Steele, Nucl. Phys. **A633**, 279 (1998).
[33] K. G. Chetyrkin, J. H. Kuhn, A. Maier, P. Maierhofer, P. Marquard, M. Steinhauser, and C. Sturm, Phys. Rev. D **80**, 074010 (2009).
[34] S. Narison, Phys. Lett. B **707**, 259 (2012).
[35] S. Narison, Phys. Lett. B **693**, 559 (2010); **705**, 544(E) (2011).
[36] J. H. Kuhn, M. Steinhauser, and C. Sturm, Nucl. Phys. **B778**, 192 (2007).
[37] K. Nakamura *et al.* (Particle Data Group) J. Phys. G **37**, 075021 (2010).
[38] S. Bethke, Eur. Phys. J. C **64**, 689 (2009).
[39] M. Jamin and B. O. Lange, Phys. Rev. D **65**, 056005 (2002).
[40] S.-K. Choi *et al.* (Belle Collaboration), Phys. Rev. Lett. **94**, 182002 (2005).
[41] B. Aubert *et al.* (*BABAR* Collaboration), Phys. Rev. Lett. **101**, 082001 (2008).
[42] S. Uehara *et al.* (Belle Collaboration), Phys. Rev. Lett. **104**, 092001 (2010).
[43] K. Abe *et al.* (Belle Collaboration), Phys. Rev. Lett. **98**, 082001 (2007).
[44] P. del Amo Sanchez *et al.* (*BABAR* Collaboration), Phys. Rev. D **82**, 011101 (2010).
[45] T. Aushev *et al.* (Belle Collaboration), Phys. Rev. D **81**, 031103(R) (2010).
[46] B. Aubert *et al.* (*BABAR* Collaboration), Phys. Rev. D **77**, 011102 (2008).
[47] F. E. Close, I. Dunietz, P. R. Page, S. Veseli, and H. Yamamoto, Phys. Rev. D **57**, 5653 (1998).
[48] P. R. Page, Phys. Lett. B **402**, 183 (1997).
[49] F. E. Close and P. R. Page, Nucl. Phys. **B443**, 233 (1995).
[50] N. Isgur, R. Kokoski, and J. Paton, Phys. Rev. Lett. **54**, 869 (1985).
[51] D. Binosi and L. Theussl, Comput. Phys. Commun. **161**, 76 (2004).

Chapter 4

Heavy-Light Diquark mass predictions

4.1 Introduction

The research in this chapter is based upon the following publication:

- R.T. Kleiv, T.G. Steele, Ailin Zhang, and Ian Blokland, Heavy-light diquark masses from QCD sum rules and constituent diquark models of tetraquarks, Phys. Rev. D87 (2013) 125018.

The manuscript above (Ref. [71]) uses QSR to determine the masses of diquarks with $J^P = 0^\pm\,, 1^\pm$ that are composed of one heavy (charm or bottom) quark and one light quark. As described in Chapter 1, many of the heavy quarkonium-like states have been interpreted as four-quark states. These can be realized as weakly bound molecular states, or as tightly bound tetraquarks composed of diquark clusters. Heavy quarkonium-like four-quark states have been widely studied using QSR (see Ref. [94] for a review). A universal feature of these approaches has been the use of currents containing four quark fields, which are in either the molecule or tetraquark configurations

$$J_{\text{molecule}} = \left(\bar{Q}\Gamma Q\right)\left(\bar{q}\Gamma q\right)\,, \quad J_{\text{tetraquark}} = \left[\bar{Q}\tilde{\Gamma}\bar{q}\right]\left[Q\tilde{\Gamma}q\right]\,, \tag{4.1}$$

where Q and q denote heavy and light quark fields, respectively. The Dirac matrices Γ and $\tilde{\Gamma}$ are related to the quantum numbers of the hadrons probed by each current. The composite operator in the round brackets in Eq. (4.1) is a current that couples to heavy-light mesons, while that in the square brackets is a current that couples to heavy-light diquarks. However, the two currents in Eq. (4.1) are not truly independent because they can be transformed

into one another through Fierz transformations. In Ref. [129] it was pointed out that this ambiguity obscures the nature of the hadronic states that are probed by these currents. For this reason QSR studies that utilize currents containing four quark fields cannot distinguish between the molecular and tetraquark scenarios.

An alternative approach to studying four-quark states within QSR is to use diquark currents. Using QSR the diquark mass can be calculated and can be thought of as a constituent diquark mass. This in turn can be used in constituent diquark models of tetraquarks. This approach was first used in Ref. [129] to study tetraquarks composed of light quarks. There are several benefits to this approach for studying four-quark states in QSR. First, it avoids the Fierz transformation ambiguities associated with four-quark currents. This is perhaps the only way that pure tetraquark states can be studied using QSR. Second, the composite operators in Eq. (4.1) mix under renormalization [92, 65]. For this reason it is challenging to extend QSR studies using four-quark currents to higher orders. However, as discussed in Chapter 1, the diquark current does not mix with other operators under renormalization. The renormalization factor of the scalar ($J^P = 0^+$) diquark operator is determined to two-loop order in Ref. [70] and is the subject of Chapter 5. For these reasons QSR studies using diquark currents can be extended to higher order in the perturbative expansion much more easily than those that use four-quark currents.

In Ref. [84] the $X(3872)$ is interpreted as a tetraquark using a constituent diquark model where the scalar (0^+) and axial vector (1^+) charm-light diquark masses are assumed to be degenerate due to heavy quark symmetry. The constituent charm-light diquark mass is determined to be 1.93 GeV from a fit to the $X(3872)$. The model also predicts the existence of electrically charged tetraquarks that are members of the same nonet as the $X(3872)$. The recently discovered $Z_c^{\pm}(3895)$ appears to be compatible with this prediction [48]. A similar analysis was performed in Ref. [10] where a bottom-light constituent diquark mass of 5.20 GeV was extracted from a fit to the tetraquark candidate $Y_b(10890)$ [31]. The results of the analysis support the tetraquark interpretation of the charged bottomonium-like states $Z_b^{\pm}(10610)$ and $Z_b^{\pm}(10650)$ which were discovered by the Belle collaboration [26]. Essential features of these constituent diquark models are that the masses of the scalar (0^+) and axial vector (1^+) diquarks are assumed to be identical, and that the constituent diquark masses

are extracted from fits to tetraquark candidates among the XYZ states.

The main goal of the research in this chapter was to calculate the constituent heavy-light diquark mass using QSR, so as to provide a QCD-based test of the constituent diquark models used in Refs. [84, 10]. Constituent masses of diquarks composed of light quarks only were determined in Refs. [42, 67, 129, 126]. In Ref. [125] heavy-light diquarks with $J^P = 0^+ , 1^+$ were studied using QSR, however, only leading-order perturbative contributions to the OPE were considered. The research presented in this chapter builds upon the work of Ref. [125] by including next-to-leading order perturbative contributions and diquarks with $J^P = 0^- , 1^-$.

4.2 Results

The correlation function and currents used to study heavy-light diquarks with $J^P = 0^\pm , 1^\pm$ are given by

$$\Pi\left(Q^2\right) = i \int d^4x \, e^{iq\cdot x} \langle \Omega | T \left[\, J_\alpha \left(x\right) S_{\alpha\omega} \left[x \, , 0\right] J^\dagger_\omega \left(0\right) \, \right] | \Omega \rangle \, , \tag{4.2}$$

where α, ω are color indices. The heavy-light diquark currents are

$$J_\alpha = \epsilon_{\alpha\beta\gamma} Q^T_\beta C \mathcal{O} q_\gamma \, , \tag{4.3}$$

where the Lorentz structures $\mathcal{O} = \gamma_5 \, , I \, , \gamma_\mu \, , \gamma_\mu\gamma_5$ respectively probe scalar $\left(J^P = 0^+\right)$, pseudoscalar (0^-), axial vector (1^+), and vector (1^-) heavy-light diquarks [42, 67]. In Eq. (4.3) C is the charge conjugation operator (A.4), T denotes the transpose, Q is a heavy (charm or bottom) quark field, and q is a light quark field. The axial vector and vector correlation functions are given by

$$\Pi^{(\mathrm{A,V})}\left(q\right) = \frac{1}{d-1} \left(\frac{q^\mu q^\nu}{q^2} - g^{\mu\nu} \right) \Pi^{(\mathrm{A,V})}_{\mu\nu} \left(q\right) \, , \tag{4.4}$$

where the number of spacetime dimensions d is kept arbitrary because dimensional regularization is used. The correlation function in Eq. (4.2) includes a path-ordered exponential,

also known as a Schwinger string, defined as

$$S_{\alpha\omega}\left[x\,,0\right]=P\exp\left[ig\frac{\lambda^{a}_{\alpha\omega}}{2}\int_{0}^{x}dz^{\mu}\;A^{a}_{\mu}\left(z\right)\right]\,, \tag{4.5}$$

where P denotes path-ordering and g is the strong coupling. In Ref. [42] the correlation function (4.2) was calculated for diquarks composed of light quarks, and it was demonstrated that the correlation function is gauge invariant to next-to-leading order in the strong coupling. Because physical observables are gauge invariant, only gauge invariant correlation functions can be used in QSR analyses. Therefore, in order to extract physically meaningful heavy-light diquark masses, it is crucial to verify the gauge invariance of the heavy-light diquark correlation function. In this chapter we perform an explicit calculation that confirms that Eq. (4.2) is gauge invariant to next-to-leading order in the strong coupling. Using a straight line geometry, the Schwinger string is given by

$$S_{\alpha\omega}\left[x\,,0\right]=\delta_{\alpha\omega}+ig\frac{\lambda^{a}_{\alpha\omega}}{2}\int_{0}^{1}d\xi A^{a}_{\mu}\left(\xi x\right)x^{\mu}+\mathcal{O}\left(g^{2}\right)\,. \tag{4.6}$$

The first term in Eq. (4.6) simply generates a trace over the colour indices in the correlation function (4.2). However, the second term in Eq. (4.6) leads to a non-trivial contribution. Note that this term is not calculated in the leading-order analysis performed in Ref. [125]. In order to verify that the heavy-light correlation function is gauge invariant, all calculations must be performed in a general covariant gauge. That is, the gauge parameter a in the gluon propagator (1.39) must be retained in all calculations.

The next-to-leading order perturbative contributions to the heavy-light diquark correlation function also introduce gauge dependent terms. In this chapter it is shown that the gauge dependent contributions of the Schwinger string (4.6) exactly cancel the gauge dependence in the next-to-leading order perturbative contribution. Therefore the heavy-light diquark correlation function (4.2) is gauge invariant to next-to-leading order in the strong coupling and can be utilized in QSR to determine the heavy-light diquark mass.

Once the gauge invariance of the heavy-light diquark correlation has been established the bare correlation function must be renormalized. This can be achieved by renormalizing the heavy quark mass and the diquark current, whose renormalization factor is calculated

in Chapter 5. The renormalization can be implemented using the methods discussed in Chapter 1. However, in order to perform the renormalization in a self-consistent fashion, renormalization-induced contributions must be included. In practical terms this means that the explicit $\mathcal{O}(\epsilon)$ terms in the leading order perturbative contribution must be calculated. These terms can be calculated using the loop integration methods discussed in Chapter 2. After the correlation function has been renormalized, the imaginary part is needed for the QSR analysis. A closed form expression for the imaginary part can be determined using methods discussed in Chapter 2.

Mass predictions were successfully extracted for all positive parity diquarks. However, mass predictions could not be extracted for any negative parity diquarks due to instabilities in those sum rules. The scalar and axial vector charm-light diquark masses were found to be $1.86 \pm 0.05\,\text{GeV}$ and $1.87 \pm 0.10\,\text{GeV}$, respectively. These mass predictions are degenerate within uncertainty as expected by heavy quark symmetry and in excellent agreement with the constituent charm-light diquark mass of $1.93\,\text{GeV}$ predicted by Maiani *et al.* [84]. Similarly, the scalar and axial vector bottom-light diquark masses were both found to be $5.08 \pm 0.04\,\text{GeV}$, which is in reasonable agreement with the mass of $5.20\,\text{GeV}$ determined by Ali *et al.* [10]. Therefore, these heavy-light diquark mass predictions support interpreting the $X(3872)$ and the $Y_b(10890)$ as tetraquarks. This QCD-based test supports the constituent diquark model of tetraquarks, and provides indirect support for the tetraquark interpretation of the charged heavy quarkonium-like states $Z_c^{\pm}(3895)$, $Z_b^{\pm}(10610)$ and $Z_b^{\pm}(10650)$.

The research presented in this chapter will contribute to the ongoing effort to understand the $X(3872)$, $Y_b(10890)$ and the electrically charged heavy quarkonium-like states. There are several technical challenges that are involved in calculating the next-to-leading order perturbative contributions to the heavy-light diquark correlation function. Although only the imaginary part of the correlation function is required for the QSR analysis, the entire correlation function must be calculated in order to properly deal with the gauge invariance and renormalization issues that arise in this calculation. The loop integration techniques discussed in Chapter 2 are essential for this. In order to verify that the heavy-light diquark correlation function is gauge invariant, and hence is suitable for use in a QSR analysis, the entire correlation function must be calculated in a general covariant gauge. In addition, the

entire correlation function is needed in order to renormalize the next-to-leading order perturbative contributions. The research in this chapter develops a renormalization methodology that can be applied to next-to-leading order QSR calculations. Key features of this methodology are the renormalization of the diquark current, which is discussed in Chapter 5, and the generation of renormalization-induced contributions to the correlation function.

4.3 Published Article

The Heavy-light diquark article was published in Physical Review D in 2013. The manuscript is included on the following pages and is presented in the journal format.

- R.T. Kleiv, T.G. Steele, Ailin Zhang, and Ian Blokland, Heavy-light diquark masses from QCD sum rules and constituent diquark models of tetraquarks, Phys. Rev. D87 (2013) 125018.

Heavy-light diquark masses from QCD sum rules and constituent diquark models of tetraquarks

R. T. Kleiv,[1] T. G. Steele,[1] Ailin Zhang,[2] and Ian Blokland[3]

[1]*Department of Physics and Engineering Physics, University of Saskatchewan, Saskatoon, Saskatchewan S7N 5E2, Canada*
[2]*Department of Physics, Shanghai University, Shanghai 200444, China*
[3]*Department of Science, University of Alberta Augustana Campus, Camrose, Alberta T4V 2R3, Canada*

(Received 8 May 2013; published 10 June 2013)

Diquarks with $J^P = 0^{\pm}$, $1^{\pm}$ containing a heavy (charm or bottom) quark and a light quark are investigated using QCD Laplace sum rules. Masses are determined using appropriately constructed gauge invariant correlation functions, including for the first time next-to-leading order perturbative contributions. The $J^P = 0^+$ and 1^+ charm-light diquark masses are, respectively, found to be 1.86 ± 0.05 and 1.87 ± 0.10 GeV, while those of the 0^+ and 1^+ bottom-light diquarks are both determined to be 5.08 ± 0.04 GeV. The sum rules derived for heavy-light diquarks with negative parity are poorly behaved and do not permit unambiguous mass predictions, in agreement with previous results for negative parity light diquarks. The scalar and axial vector heavy-light diquark masses are degenerate within uncertainty, as expected by heavy quark symmetry considerations. Furthermore, these mass predictions are in good agreement with masses extracted in constituent diquark models of the tetraquark candidates $X(3872)$ and $Y_b(10890)$. Thus these results provide QCD support for the interpretation of the $X(3872)$ and $Y_b(10890)$ as $J^{\mathrm{PC}} = 1^{++}$ tetraquark states composed of diquark clusters. Further implications for tetraquarks among the heavy quarkoniumlike XYZ states are discussed.

DOI: 10.1103/PhysRevD.87.125018 PACS numbers: 14.40.Rt, 14.40.Pq, 12.38.−t

I. INTRODUCTION

The discovery of the $X(3872)$ by the Belle Collaboration [1] and its subsequent confirmation by the CDF [2], D0 [3], *BABAR* [4], and LHCb [5] Collaborations initiated a new era in hadron spectroscopy. Since then, hadrons have been found in the charmonium and bottomonium spectra that are difficult to reconcile as conventional heavy quarkonia. These are called heavy quarkoniumlike or XYZ states, and a comprehensive review of the current experimental situation is given in Ref. [6]. The $X(3872)$ exemplifies the difficulties in interpreting these states: its mass is $M = 3871.68 \pm 0.17$ MeV, its width is $\Gamma < 1.2$ MeV [6], and the LHCb Collaboration has clearly established that its quantum numbers are $J^{\mathrm{PC}} = 1^{++}$ [7]. These properties pose problems for a conventional charmonium interpretation of the $X(3872)$ [8]. Given the proximity of its mass to that of $\bar{D}D^*$, the $X(3872)$ has been widely interpreted as a four-quark molecular state [9–16]. A complementary interpretation is that the $X(3872)$ is a tetraquark [17–21]. In addition to the $X(3872)$, several XYZ states that are four-quark candidates are discussed in Ref. [22].

Molecules and tetraquarks have very different internal quark structures. In the molecular scenario, two color-singlet mesons form a weakly bound conglomerate, whereas in the tetraquark scenario a diquark and antidiquark form a tightly bound four-quark state. A diquark is a strongly correlated pair of quarks within a hadron (see Ref. [23] for a review of applications). Because single gluon exchange leads to an attractive interaction between quarks in a color antitriplet configuration, diquarks are identical to antiquarks in terms of color. In Ref. [24] all possible diquark configurations were classified, and it was shown that due to spin interactions, the scalar is the most strongly bound, followed by the vector. However, these spin interactions scale as the inverse of the quark mass, and hence scalar and vector diquarks that contain one or more heavy quarks should be degenerate.

The tetraquark and molecular currents used in QCD sum rule analyses are related through Fierz transformations, leading to ambiguities in their interpretation which can be addressed through the diquark scenario [25] (Ref. [26] provides a review of the numerous QCD sum rule studies of tetraquarks and molecules among the XYZ states). In addition, the renormalization of four-quark operators is complicated by operator mixing [27,28]. Conversely, the renormalization of the diquark operator is multiplicative and has been studied to two-loop order [29]. For this reason, QCD sum rule studies of diquarks can be extended to higher orders much more easily. The first QCD sum rule studies of diquarks were given in Refs. [30,31], followed by Refs. [25,32,33]. The Bethe-Salpeter [34,35], Dyson-Schwinger [36], and effective field theory approaches [37] have also been used to determine diquark masses. Reference [33] used QCD sum rules to investigate heavy-light diquarks with $J^P = 0^+$ and 1^+. In this paper we will build upon previous work by including next-to-leading order perturbative contributions and negative parity diquarks in our analysis.

Diquarks are clearly not hadrons, thus their masses must be regarded as constituent masses. Constituent diquark models have been used to study tetraquarks among the XYZ states. In Ref. [17] Maiani *et al.* interpret the $X(3872)$ as a tetraquark composed of charm-light diquarks,

and using its mass determine both the scalar and vector charm-light constituent diquark masses to be 1.93 GeV. Reference [38] points out that the $Z_c^{\pm}(3895)$, which was very recently discovered by the BESIII [39] Collaboration and quickly confirmed by the Belle [40] and CLEO [41] Collaborations, was predicted in Ref. [17]. The confirmation of this charged charmoniumlike state strongly supports the existence of hadrons outside the constituent quark model. Similarly, Ali *et al.* [42] interpret the $Y_b(10890)$ discovered by Belle [43] as a tetraquark composed of bottom-light diquarks, determining the scalar and vector bottom-light diquark masses to be 5.20 GeV. The charged bottomoniumlike states $Z_b^{\pm}(10610)$ and $Z_b^{\pm}(10650)$ [44] are also suggested to be tetraquarks. Important features of the analyses in Refs. [17,42] are the use of heavy-light diquarks whose constituent masses are extracted from fits to tetraquark candidates and the equality of scalar and vector heavy-light diquark masses. In this paper we seek to determine if these heavy-light diquark masses are supported by QCD sum rule analyses, thereby providing a QCD-based test of the heavy-light diquark model of tetraquark states. Because our aim is to compare our results with the heavy-light diquark masses determined in Refs. [17,42], our focus is on heavy-light diquarks.

The remainder of the paper is organized as follows: in Sec. II we calculate the $J^P = 0^{\pm}$, $1^{\pm}$ heavy-light diquark correlation functions, in Sec. III we construct and analyze the corresponding QCD Laplace sum rules, and in Sec. IV we make concluding remarks and discuss the phenomenological implications of our results.

II. HEAVY-LIGHT DIQUARK CORRELATION FUNCTION

The heavy-light diquark correlation function is defined as

$$\Pi(Q^2) = i\int d^4x e^{iq\cdot x}\langle 0|T[J_\alpha(x)S_{\alpha\omega}[x,0]J^\dagger_\omega(0)]|0\rangle, \quad (1)$$

where $Q^2 = -q^2$ is the Euclidean momentum, and α, ω are color indices. The heavy-light diquark currents are

$$J_\alpha = \epsilon_{\alpha\beta\gamma}Q^T_\beta C\mathcal{O}q_\gamma, \quad (2)$$

where C is the charge conjugation operator, T denotes the transpose, Q is a heavy (charm or bottom) quark field, and q is a light quark field [30,31]. The Lorentz structures $\mathcal{O} = \gamma_5, I, \gamma_\mu, \gamma_\mu\gamma_5$, respectively, couple to scalar ($J^P = 0^+$), pseudoscalar (0^-), axial vector (1^+), and vector (1^-) heavy-light diquarks. We denote these as S, P, A, and V, respectively. The axial vector and vector correlation functions are given by

$$\Pi^{(\mathrm{A,V})}(q) = \frac{1}{d-1}\left(\frac{q^\mu q^\nu}{q^2} - g^{\mu\nu}\right)\Pi^{(\mathrm{A,V})}_{\mu\nu}(q), \quad (3)$$

where d is the number of spacetime dimensions. Following Refs. [25,30–33], the diquark correlation function (1) includes a path-ordered exponential, or Schwinger string, defined as

$$S_{\alpha\omega}[x,0] = P\exp\left[ig\frac{\lambda^a_{\alpha\omega}}{2}\int_0^x dz^\mu A^a_\mu(z)\right], \quad (4)$$

where P denotes path-ordering and $g = \sqrt{4\pi\alpha}$ is the strong coupling. Reference [30] demonstrated that the correlation function (1) is gauge invariant to leading order for light quark currents. We will show that this is also true for heavy-light diquark currents (2).

First we calculate perturbative contributions to the heavy-light diquark correlation function, which are shown in Fig. 1. We include $\mathcal{O}(\alpha)$ perturbative contributions that have not been calculated previously. To leading order the Schwinger string (4) generates a trace over the color indices in (1), and this trace has been performed in calculating perturbative contributions. We will also consider a higher order contribution from the Schwinger string that is gauge dependent and should cancel the gauge dependence of the perturbative contributions. Thus perturbative contributions are calculated in a general covariant gauge in order to verify the gauge independence of the correlation function (1). The gluon propagator is taken to be

$$D^{AB}_{\mu\nu}(k) = -i\delta^{AB}[D^{(0)}_{\mu\nu}(k) - D^{(1)}_{\mu\nu}(k)];$$
$$D^{(0)}_{\mu\nu}(k) = \frac{g_{\mu\nu}}{k^2}, \qquad D^{(1)}_{\mu\nu}(k) = (1-a)\frac{k_\mu k_\nu}{k^4}, \quad (5)$$

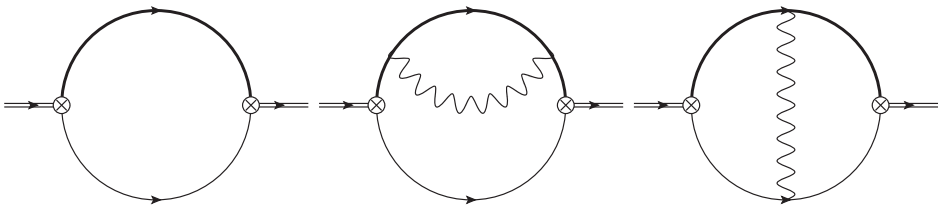

FIG. 1. Feynman diagrams representing the leading order and next-to-leading order perturbative contributions to the heavy-light diquark correlation function (1). An insertion of the diquark current is represented by the ⊗ symbol, bold lines represent heavy quark propagators, thin lines represent light quark propagators, and wavy lines represent gluon propagators. An additional diagram where the light and heavy quark propagators are exchanged is not shown. These and all subsequent Feynman diagrams were created using JAXODRAW [75].

where a denotes the gauge parameter and the functions $D^{(0)}_{\mu\nu}$, $D^{(1)}_{\mu\nu}$ are defined for later convenience. As in Refs. [45,46] we calculate the entire correlation function, rather than only the imaginary part. This approach is essential in order to deal with gauge invariance and renormalization issues properly in this calculation. Results for the loop integrals that are encountered are given in Refs. [47–49]. The number of distinct integrals to be calculated can be significantly reduced using the MATHEMATICA package TARCER [50], which implements the generalized recurrence relations developed in Refs. [51,52]. Finally, the epsilon expansion can be performed using the MATHEMATICA package HypExp [53,54]. Using the $\overline{\text{MS}}$ scheme and working in $d = 4 + 2\epsilon$ dimensions, the perturbative result for each channel can be parametrized as

$$\begin{aligned}\Pi^{(i)}_{\text{pert,B}}(w) = \frac{m_B^2}{\pi^2}\frac{w+1}{w^2}\Bigg[& b_0 \log(1+w) + \epsilon\Bigg\{b_1 \log(1+w) + b_2 \log^2(1+w) + b_3 \text{Li}_2\left(\frac{w}{1+w}\right)\Bigg\} \\ & + \frac{\alpha}{\pi}\Bigg[\frac{b_4}{\epsilon}\log(1+w) + b_5 \log(1+w)\text{Li}_2\left(\frac{w}{1+w}\right) + b_6 \log(1+w) + b_7 \log^2(1+w) + b_8 \log^3(1+w) \\ & + b_9 \text{Li}_3(-w) + b_{10}\text{Li}_2\left(\frac{w}{1+w}\right) + b_{11}\text{Li}_3\left(\frac{w}{1+w}\right) + a\Bigg\{\frac{b_{12}}{\epsilon}\log(1+w) + b_{13}\log(1+w) \\ & + b_{14}\log^2(1+w) + b_{15}\text{Li}_2\left(\frac{w}{1+w}\right)\Bigg\}\Bigg]\Bigg], \\ w = \frac{Q^2}{m^2}. & \end{aligned} \tag{6}$$

Here the subscript B indicates bare quantities, $i = S, P, A, V$ denotes each distinct channel, Li_3 and Li_2 denote the trilogarithm and dilogarithm functions [55], and we have omitted terms corresponding to dispersion relation subtraction constants. The coefficients b_i are functions of w, which are given for each channel in Table I.

Some comments must be made regarding the form of (6). First, terms proportional to the gauge parameter a have been retained to allow comparison with contributions from the path-ordered exponential (4), so as to ensure that the correlation function (1) is gauge invariant. Second, the term b_4 in (6) is a nonlocal divergence that cannot be removed through application of the Borel transform when the sum rules are constructed. This term must be dealt with through renormalization, necessitating inclusion of the terms b_1, b_2, and b_3 which will lead to renormalization-induced

TABLE I. Coefficient functions b_i for the bare perturbative result (6). Here $L_m = \log[\frac{m^2}{\mu^2}]$.

J^P	$0^\pm$	$1^\pm$
b_0	$\frac{3}{4}w(1+w)$	$\frac{1}{4}(1+w)(2w-1)$
b_1	$\frac{3}{4}w(1+w)(L_m-2)$	$\frac{1}{12}(1+w)[8-10w+(6w-3)L_m]$
b_2	$\frac{3}{8}w(1+w)$	$\frac{1}{8}(1+w)(2w-1)$
b_3	$-\frac{3}{4}w(1+w)$	$-\frac{1}{4}(1+w)(2w-1)$
b_4	$-\frac{3}{4}w(5+w)$	$-\frac{3}{2}(w-1)$
b_5	$w(1+w)$	$\frac{1}{3}(1+w)(2w-1)$
b_6	$\frac{w}{24}[273+87w+2\pi^2(1+w)-36(5+w)L_m]$	$\frac{1}{36}[9w^2+90w-201+\pi^2(2w^2+w-1)-108(w-1)L_m]$
b_7	$-\frac{2+27w+34w^2+6w^3}{8(1+w)}$	$\frac{13+2w-16w^2}{12(1+w)}$
b_8	$\frac{1}{4}w(1+w)$	$\frac{1}{12}(1+w)(2w-1)$
b_9	$\frac{3}{2}w(1+w)$	$\frac{1}{2}(1+w)(2w-1)$
b_{10}	$\frac{w(15+20w+8w^2)}{4(1+w)}$	$\frac{5w^3+8w^2-w-9}{6(1+w)}$
b_{11}	$\frac{3}{2}w(1+w)$	$\frac{1}{2}(1+w)(2w-1)$
b_{12}	$\frac{1}{4}w(1+w)$	$\frac{1}{12}(1+w)(2w-1)$
b_{13}	$\frac{1}{8}w[4(1+w)L_m-7-9w]$	$\frac{1}{24}[11-3w-16w^2+4(2w^2+w-1)L_m]$
b_{14}	$\frac{w(3+4w+2w^2)}{8(1+w)}$	$\frac{4w^3+6w^2-3}{24(1+w)}$
b_{15}	$-\frac{w(1+4w+2w^2)}{4(1+w)}$	$\frac{1-6w^2-4w^3}{12(1+w)}$

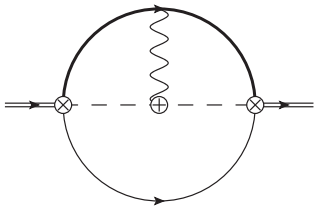

FIG. 2. Feynman diagrams representing the contribution of the Schwinger string to the heavy-light diquark correlation function. An insertion of the Schwinger string operator is represented by the ⊕ symbol. The dashed line is not a particle propagator. Instead, it indicates the straight line integration path between points 0 and x used in equation (7). An additional diagram where the light and heavy quark propagators are exchanged is not shown. All other notations are identical to Fig. 1.

contributions. A similar methodology was also needed in Ref. [56]. Finally, note that (6) has a branch cut on $w \in (-\infty, -1]$, as it must. However, after using the package HypExp some functions are generated that do not have this branch structure. This anomalous branch structure is spurious and is eliminated when polylogarithm identities are used [55].

We now turn our attention to contributions from the Schwinger string (4). Following Refs. [30,31], we define

$$S_{\alpha\omega}[x,0] = \delta_{\alpha\omega} + ig\frac{\lambda^a_{\alpha\omega}}{2}\int_0^1 d\xi A^a_\mu(\xi x)x^\mu - g^2\frac{\lambda^a_{\alpha\beta}}{2}\frac{\lambda^b_{\beta\omega}}{2}\int_0^1 d\xi\int_0^\xi d\xi' :A^a_\mu(\xi x) \times A^b_\nu(\xi' x):x^\mu x^\nu + \mathcal{O}(g^3), \tag{7}$$

where : : denotes normal ordering. As in [30,31] the integration path between points 0 and x in (4) has been chosen to be a straight line.[1] As mentioned earlier, the leading order term in (7) leads to a trace over the diquark current color indices in (1), which was done in calculating (6). To the order that we are working, the quadratic term in g is irrelevant because it cannot be used to form a gluon propagator. However, the linear term leads to a nontrivial contribution to the correlation function, which is shown in Fig. 2. This contribution has the form

$$\Pi^{(i)}_{\text{string}}(Q^2) \sim \int d^4x e^{iq\cdot x}\int d^4z\int_0^1 d\xi x^\mu D^{AB}_{\mu\nu}(\xi x - z)\ldots, \tag{8}$$

where q is the external momentum, z denotes the location of the quark-gluon interaction in Fig. 2, and the ellipses indicate ξ-independent terms that are not shown. The ξ integration in (8) cannot be evaluated readily. In momentum space the gluon propagator in (8) unavoidably leads to terms of the form

$$\Pi^{(i)}_{\text{string}}(Q^2) \sim \int\frac{d^dk_1}{(2\pi)^d}\int\frac{d^dk_2}{(2\pi)^d} \times\int_0^1 d\xi D^{AB}_{\mu\nu}(k_1)\frac{\partial}{\partial q_\mu}S(q-k_2-\xi k_1)\ldots, \tag{9}$$

where the ξ and loop integrations are coupled. Most of these integrals can be decoupled using the scaling properties of d-dimensional momentum integrals [57], but unfortunately a few cannot be. However, for the gauge dependent terms in (9) this obstacle can be circumvented. Note that the quark propagator in (9) satisfies the identity

$$k_1\cdot\frac{\partial}{\partial q}S(q-k_2-\xi k_1) = -\frac{d}{d\xi}S(q-k_2-\xi k_1). \tag{10}$$

The $D^{(1)}_{\mu\nu}(k_1)$ part of the gluon propagator (5) provides a factor of k_1^μ, and hence the ξ integration in (9) can be performed using (10). Note that this approach cannot be used to calculate terms in (9) that correspond to the $D^{(0)}_{\mu\nu}(k_1)$ piece of the gluon propagator (5). Based upon the result of Ref. [30] we have assumed that there is no contribution from the Schwinger string in Landau gauge. The remaining loop integrations can be performed using the same methods that were used to calculate the perturbative contributions. It should be noted that because of the bosonic nature of the diquark currents and gauge field, the integration over ξ in (7) must be symmetric about the point $\xi = \frac{1}{2}$, meaning that the gauge configurations corresponding to ξ and $1-\xi$ are equivalent. Thus the ξ integration double counts and we have introduced an overall factor of $\frac{1}{2}$ accordingly.

In order to check the validity of the methods described, we have used them to reproduce the result of Ref. [30], verifying that the correlation function (1) for light diquark currents is gauge independent to order α. Using the approach described above we have calculated the gauge dependent contributions of the Schwinger string (7) to the heavy-light diquark correlation function (1). We find that these precisely cancel the gauge dependent terms b_{12}, b_{13}, b_{14}, and b_{15} in the perturbative contribution (6). This verification of gauge independence emerges from the manifestly gauge invariant formalism of the Schwinger string, confirming that the heavy-light diquark correlation function (1) is suitable for use in a QCD sum rule analysis.

Now we must renormalize the bare result (6). To the order that we are working, this can be done through renormalization of the heavy quark mass and the diquark current. The one-loop expression for the renormalized quark mass is [49]

$$m_B = Z_m m, \qquad Z_m = 1 + \frac{\alpha}{\pi\epsilon}. \tag{11}$$

The renormalization of the scalar diquark current was studied in Ref. [29]. A distinct benefit of using a diquark current rather than a four quark current is that, unlike four quark currents, the diquark current renormalizes multiplicatively. In Ref. [29] it was shown that the renormalization factors of the scalar diquark and meson operators are

[1] In Ref. [31] it was argued that any deviations from a straight line would correspond to additional Wilson loops and hence would not correspond to the lowest energy configuration.

TABLE II. Coefficient functions c_i for the renormalized perturbative result (13). All notations are identical to those in Table I.

J^P	$0^{\pm}$	$1^{\pm}$
c_0	$\frac{3}{4}w(1+w)$	$\frac{1}{4}(1+w)(2w-1)$
c_1	$\frac{1}{24}w[165+51w+2\pi^2(1+w)-18(5+w)L_m]$	$\frac{1}{36}[9w^2+90w-93+\pi^2(2w^2+w-1)-54(w-1)L_m]$
c_2	$-\frac{2+12w+16w^2+3w^3}{8(1+w)}$	$\frac{4+2w-7w^2}{12(1+w)}$
c_3	$\frac{1}{4}w(1+w)$	$\frac{1}{12}(1+w)(2w-1)$
c_4	$w(1+w)$	$\frac{1}{3}(1+w)(2w-1)$
c_5	$\frac{w^2(2+5w)}{4(1+w)}$	$\frac{5w^3-w^2-w}{6(1+w)}$
c_6	$\frac{3}{2}w(1+w)$	$\frac{1}{2}(1+w)(2w-1)$
c_7	$\frac{3}{2}w(1+w)$	$\frac{1}{2}(1+w)(2w-1)$

proportional at one-loop level. This relationship can be extended to the pseudoscalar, axial vector, and vector channels in order to determine the renormalization factors of those diquark operators. Given our explicit demonstration of gauge independence and that the Schwinger string contributions are zero in Landau gauge [30], we calculate the renormalization factors in Landau gauge.[2] The results are as follows:

$$[J_\alpha^{(\mathrm{i})}]_R = Z_d^{(\mathrm{i})}[J_\alpha^{(\mathrm{i})}]_B; \qquad Z_d^{(\mathrm{S})} = 1+\frac{\alpha}{2\pi\epsilon}, \qquad Z_d^{(\mathrm{P})} = 1+\frac{\alpha}{2\pi\epsilon}, \qquad Z_d^{(\mathrm{A})} = 1, \qquad Z_d^{(\mathrm{V})} = 1. \tag{12}$$

Note that the axial vector and vector diquark operator renormalization factors are trivial, in analogy with the corresponding meson operators. Finally, the renormalized perturbative result for each distinct heavy-diquark channel can be expressed as

$$\begin{aligned}\Pi_{\mathrm{pert}}^{(i)}(w) = \frac{m^2}{\pi^2}\frac{w+1}{w^2}\Bigg[c_0\log(1+w)+\frac{\alpha}{\pi}\Bigg[c_1\log(1+w)&\\ +c_2\log^2(1+w)+c_3\log^3(1+w)&\\ +c_4\log(1+w)\mathrm{Li}_2\left(\frac{w}{1+w}\right)+c_5\mathrm{Li}_2\left(\frac{w}{1+w}\right)&\\ +c_6\mathrm{Li}_3(-w)+c_7\mathrm{Li}_3\left(\frac{w}{1+w}\right)\Bigg]\Bigg].&\end{aligned} \tag{13}$$

The heavy quark mass and strong coupling are implicitly functions of the renormalization scale μ, and the coefficients c_i are functions of w that are given in Table II.

The imaginary part of (13) can be easily determined via analytic continuation. The result is

$$\begin{aligned}\mathrm{Im}\Pi_{\mathrm{pert}}^{(i)}(x) = \frac{m^2}{4\pi x}\Bigg[f_0+\frac{\alpha}{\pi}\Bigg(f_1+f_2\log(x)+f_3\log(1-x)&\\ +f_4\log(x)\log(1-x)+f_5\mathrm{Li}_2(x)&\\ +f_6\log\left[\frac{m^2}{\mu^2}\right]\Bigg)\Bigg], \quad 0<x<1,&\end{aligned} \tag{14}$$

[2]This is the approach that was implicitly used in Refs. [30,31].

where the coefficients f_i are functions of x as given in Table III.

Now we consider contributions to the heavy-light diquark correlation function from the QCD condensates. Following Ref. [30,31], we calculate these contributions using fixed-point gauge techniques because the Schwinger string (7) does not contribute to the condensates due to the $x^\mu A_\mu^a = 0$ gauge condition. We note that the manifestly gauge invariant nature of the correlation function (1) containing the Schwinger string implies that the fixed-point gauge results will be equivalent to those obtained in other methods [58]. First we consider the contribution from the quark condensate $\langle\bar{q}q\rangle$, which is shown in Fig. 3. For this contribution we find

$$\Pi_{\bar{\mathrm{q}}\mathrm{q}}^{(\mathrm{S,A})}(Q^2) = -2\frac{m\langle\bar{q}q\rangle}{Q^2+m^2}, \qquad \Pi_{\bar{\mathrm{q}}\mathrm{q}}^{(\mathrm{P,V})}(Q^2) = -\Pi_{\bar{\mathrm{q}}\mathrm{q}}^{(\mathrm{S,A})}(Q^2). \tag{15}$$

When the QCD Laplace sum rules are constructed in Sec. III, we will need to calculate the Borel transform $\hat{B}$ of (15) and all additional condensate contributions. The following result is useful in order to calculate Borel transforms of the condensate contributions [49]

$$\frac{\hat{B}}{\tau}\left[\frac{(-Q^2)^k}{Q^2+m^2}\right] = m^{2k}e^{-m^2\tau}. \tag{16}$$

TABLE III. Coefficient functions f_i for the imaginary part of the renormalized perturbative result (14).

J^P	$0^{\pm}$	$1^{\pm}$
f_0	$3(1-x)^2$	$2-3x+x^3$
f_1	$\frac{1}{2}(17-72x+55x^2)$	$\frac{1}{3}(3-33x-x^2+31x^3)$
f_2	$3-16x+12x^2-2x^3$	$\frac{2}{3}x(-7-2x+4x^2)$
f_3	$2(x-4)(1-x)^2$	$-\frac{2}{3}(1-x)^2(5+4x)$
f_4	$2(1-x)^2$	$\frac{2}{3}(2-3x+x^3)$
f_5	$4(1-x)^2$	$\frac{4}{3}(2-3x+x^3)$
f_6	$-3(1-6x+5x^2)$	$6x(1-x^2)$

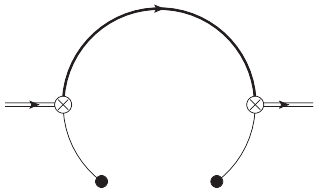

FIG. 3. Feynman diagrams representing the dimension-four quark condensate $m_q\langle\bar{q}q\rangle$ contribution to the heavy-light diquark correlation function. Solid dots represent field condensates. All other notations are identical to Fig. 1.

This result can be extended to cases where the denominator is raised to a higher power by differentiating (16) with respect to m^2. Using this result, the quark condensate contributions to the sum rules are given by

$$\begin{aligned}\mathcal{B}^{(\mathrm{S,A})}_{\bar{\mathrm{q}}\mathrm{q}}(k,\tau) &\equiv \frac{\hat{B}}{\tau}[(-Q^2)^k\Pi^{(\mathrm{S,A})}_{\bar{\mathrm{q}}\mathrm{q}}(Q^2)] \\ &= -2m^{2k}m\langle\bar{q}q\rangle e^{-m^2\tau}, \\ \mathcal{B}^{(\mathrm{P,V})}_{\bar{\mathrm{q}}\mathrm{q}}(k,\tau) &= -\mathcal{B}^{(\mathrm{S,A})}_{\bar{\mathrm{q}}\mathrm{q}}(k,\tau).\end{aligned} \tag{17}$$

Next, we determine contributions from the gluon condensate $\langle\alpha G^2\rangle = \langle\alpha G^a_{\mu\nu}G^{\mu\nu}_a\rangle$, which are shown in Fig. 4. For these contributions we find

$$\begin{aligned}\Pi^{(\mathrm{S,P})}_{\mathrm{GG}}(Q^2) &= \frac{\langle\alpha G^2\rangle}{24\pi}\frac{1}{Q^2+m^2}, \\ \Pi^{(\mathrm{A,V})}_{\mathrm{GG}}(Q^2) &= \frac{\langle\alpha G^2\rangle}{24\pi}\left[\frac{1}{Q^2}-\frac{3}{Q^2+m^2}\right. \\ &\quad \left.-\frac{m^2}{Q^4}\log\left[1+\frac{Q^2}{m^2}\right]\right].\end{aligned} \tag{18}$$

The Borel transforms of these are

$$\begin{aligned}\mathcal{B}^{(\mathrm{S,P})}_{\mathrm{GG}}(k,\tau) &= \frac{\langle\alpha G^2\rangle}{24\pi}m^{2k}e^{-m^2\tau}, \\ \mathcal{B}^{(\mathrm{A,V})}_{\mathrm{GG}}(k,\tau) &= -\frac{\langle\alpha G^2\rangle}{8\pi}m^{2k}e^{-m^2\tau}.\end{aligned} \tag{19}$$

In calculating (19) for the axial vector and vector channels we have not included the logarithmic term in (18). This term will lead to an imaginary part and hence the gluon condensate will have a continuum contribution in these channels. This can be calculated an identical fashion to (14), with the result

$$\mathrm{Im}\,\Pi^{(\mathrm{A,V})}_{\mathrm{GG}}(x) = \frac{\langle\alpha G^2\rangle}{24m^2}x^2, \qquad 0<x<1. \tag{20}$$

The contributions of the mixed condensate $\langle\bar{q}\sigma Gq\rangle = \langle g\bar{q}\frac{\lambda^a}{2}\sigma^{\mu\nu}G^a_{\mu\nu}q\rangle$ are

$$\begin{aligned}\Pi^{(\mathrm{S})}_{\bar{\mathrm{q}}\mathrm{Gq}}(Q^2) &= \frac{1}{2}m\langle\bar{q}\sigma Gq\rangle\left[\frac{m^2-Q^2}{(Q^2+m^2)^3}\right], \\ \Pi^{(\mathrm{P})}_{\bar{\mathrm{q}}\mathrm{Gq}}(Q^2) &= -\frac{1}{2}m\langle\bar{q}\sigma Gq\rangle\left[\frac{3m^2+Q^2}{(Q^2+m^2)^3}\right], \\ \Pi^{(\mathrm{A})}_{\bar{\mathrm{q}}\mathrm{Gq}}(Q^2) &= m\langle\bar{q}\sigma Gq\rangle\left[\frac{m^2}{(Q^2+m^2)^3}\right], \\ \Pi^{(\mathrm{V})}_{\bar{\mathrm{q}}\mathrm{Gq}}(Q^2) &= -\Pi^{(\mathrm{A})}_{\bar{\mathrm{q}}\mathrm{Gq}}(Q^2).\end{aligned} \tag{21}$$

Note that (21) includes a term that arises from the fixed-point gauge expansion of the vacuum expectation value $\langle\bar{q}(x)q(0)\rangle$ in Fig. 3. This is separate and distinct from the term that is represented in Fig. 5. The contributions of the mixed condensate to the sum rules can be calculated using (16), yielding

$$\begin{aligned}\mathcal{B}^{(\mathrm{S})}_{\bar{\mathrm{q}}\mathrm{Gq}}(k,\tau) &= \frac{1}{2}m\langle\bar{q}\sigma Gq\rangle m^{2(k-1)}e^{-m^2\tau} \\ &\quad\times[k^2-2km^2\tau+m^2\tau(m^2\tau-1)], \\ \mathcal{B}^{(\mathrm{P})}_{\bar{\mathrm{q}}\mathrm{Gq}}(k,\tau) &= -\frac{1}{2}m\langle\bar{q}\sigma Gq\rangle m^{2(k-1)}e^{-m^2\tau} \\ &\quad\times[k^2-2k(1+m^2\tau)+m^2\tau(1+m^2\tau)], \\ \mathcal{B}^{(\mathrm{A})}_{\bar{\mathrm{q}}\mathrm{Gq}}(k,\tau) &= \frac{1}{2}m\langle\bar{q}\sigma Gq\rangle m^{2(k+1)}e^{-m^2\tau}\left[\tau^2-\frac{2k\tau}{m^2}+\frac{k(k-1)}{m^4}\right], \\ \mathcal{B}^{(\mathrm{V})}_{\bar{\mathrm{q}}\mathrm{Gq}}(k,\tau) &= -\mathcal{B}^{(\mathrm{A})}_{\bar{\mathrm{q}}\mathrm{Gq}}(k,\tau).\end{aligned} \tag{22}$$

Finally we consider the dimension-six quark condensate, $\alpha\langle\bar{q}q\rangle^2$, which arises purely from a higher order term in the fixed-point gauge expansion of the vacuum expectation value $\langle\bar{q}(x)q(0)\rangle$ in Fig. 3. For this we find

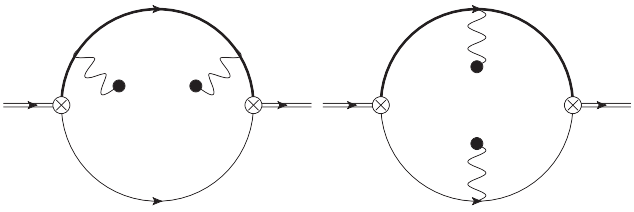

FIG. 4. Feynman diagrams representing the dimension-four gluon condensate $\langle\alpha G^2\rangle$ contribution to the heavy-light diquark correlation function. An additional diagram where the light and heavy quark propagators are exchanged is not shown. All notations are identical to those in Fig. 3.

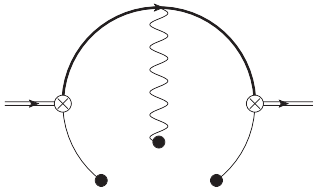

FIG. 5. Feynman diagram representing one of the dimension-five mixed condensate $\langle g\bar{q}\sigma Gq\rangle$ contributions to heavy-light diquark correlation function. All notations are identical to Fig. 1.

$$\Pi^{(S)}_{\bar{q}q\bar{q}q}(Q^2) = -\frac{16\pi}{27}\alpha\langle\bar{q}q\rangle^2\left[\frac{m^4}{(Q^2+m^2)^4}\right],$$
$$\Pi^{(P)}_{\bar{q}q\bar{q}q}(Q^2) = \Pi^{(S)}_{\bar{q}q\bar{q}q}(Q^2),$$
$$\Pi^{(A)}_{\bar{q}q\bar{q}q}(Q^2) = -\Pi^{(S)}_{\bar{q}q\bar{q}q}(Q^2), \quad (23)$$
$$\Pi^{(V)}_{\bar{q}q\bar{q}q}(Q^2) = -\Pi^{(S)}_{\bar{q}q\bar{q}q}(Q^2),$$

where we have assumed vacuum saturation. The contributions of the dimension-six quark condensate to the sum rules are given by

$$\mathcal{B}^{(S,P)}_{\bar{q}q\bar{q}q}(k,\tau) = -\frac{8\pi}{81}\alpha\langle\bar{q}q\rangle m^{2(k+2)}e^{-m^2\tau}\left[\tau^3 - \frac{3k\tau^2}{m^2} + \frac{3k(k-1)\tau}{m^4} - \frac{k(k-1)(k-2)}{m^6}\right],$$
$$\mathcal{B}^{(A,V)}_{\bar{q}q\bar{q}q}(k,\tau) = -\mathcal{B}^{(S,P)}_{\bar{q}q\bar{q}q}(k,\tau). \quad (24)$$

We do not consider the dimension-six gluon condensate in this analysis. In Sec. III we will see that the gluon condensate is a subleading contribution to the heavy-light diquark sum rules, hence we expect higher-dimensional gluon condensates are suppressed and can be ignored.

III. QCD LAPLACE SUM-RULE ANALYSIS

We now proceed to the QCD Laplace sum rules analysis of $J^P = 0^{\pm}, 1^{\pm}$ heavy-light diquarks. Refs. [59,60] are the original papers presenting the QCD sum rules technique, and reviews of its methodology are given in Refs. [61,62]. Using a resonance plus continuum model for the hadronic spectral function

$$\rho^{had}(t) = \rho^{res}(t) + \theta(t-s_0)\mathrm{Im}\Pi(t), \quad (25)$$

where s_0 is the continuum threshold, the Laplace sum rules take the form

$$\mathcal{R}_k(\tau,s_0) = \frac{1}{\pi}\int_{t_0}^{\infty} t^k \exp[-t\tau]\rho^{res}(t)dt, \quad (26)$$

where t_0 is the hadronic threshold. The left-hand side of (26) is given by

$$\mathcal{R}_k(\tau,s_0) \equiv \frac{\hat{B}}{\tau}[(-Q^2)^k\Pi(Q^2)] - \frac{1}{\pi}\times\int_{s_0}^{\infty} t^k\exp[-t\tau]\mathrm{Im}\Pi(t)dt. \quad (27)$$

We now construct the heavy-light diquark sum rules. Using the results obtained above for the perturbative (14), quark condensate (17), gluon condensate (19) and (20), mixed condensate (22), and dimension-six quark condensate (24) contributions, the QCD Laplace sum rules are given by

$$\mathcal{R}^{(i)}_k(\tau,s_0) = \frac{m^2}{\pi}\int_1^{s_0/m^2}(m^2z)^k\left[\mathrm{Im}\Pi^{(i)}_{pert}\left(\frac{1}{z}\right) + \mathrm{Im}\Pi^{(i)}_{GG}\left(\frac{1}{z}\right)\right]\times e^{-m^2\tau z}dz + \mathcal{B}^{(i)}_{\bar{q}q}(k,\tau) + \mathcal{B}^{(i)}_{GG}(k,\tau) + \mathcal{B}^{(i)}_{\bar{q}Gq}(k,\tau) + \mathcal{B}^{(i)}_{\bar{q}q\bar{q}q}(k,\tau). \quad (28)$$

The mass and coupling in (28) are implicitly functions of the renormalization scale μ in the $\overline{\mathrm{MS}}$-scheme and renormalization group improvement may be implemented by setting $\mu = 1/\sqrt{\tau}$ [63]. In order to extract mass predictions for heavy-light diquarks we utilize a single narrow resonance model,

$$\frac{1}{\pi}\rho^{res}(t) = f^2\delta(t-M^2). \quad (29)$$

Equation (26) then yields

$$\mathcal{R}_k(\tau,s_0) = f^2M^{2k}\exp(-M^2\tau), \quad (30)$$

from which the heavy-light diquark mass M can be determined via the ratio

$$M = \sqrt{\frac{\mathcal{R}_1(\tau,s_0)}{\mathcal{R}_0(\tau,s_0)}}. \quad (31)$$

Prior to extracting mass predictions we must discuss the QCD parameters occurring in the sum rules. We use one-loop $\overline{\mathrm{MS}}$ expressions for the running coupling, charm, and bottom quark masses,

$$\alpha(\mu) = \frac{\alpha(M)}{1 + A\frac{\alpha(M)}{\pi}\log\left(\frac{\mu^2}{M^2}\right)}, \qquad m(\mu) = \bar{m}\left(\frac{\alpha(\mu)}{\alpha(\bar{m})}\right)^{1/A},$$
$$\bar{m} = m(\mu = m). \quad (32)$$

In the charm-light diquark analysis we take

$$M = M_\tau = 1.77\ \mathrm{GeV}, \qquad \alpha(M_\tau) = 0.33 \pm 0.01,$$
$$A = A_c = \frac{25}{12}, \qquad \bar{m}_c = 1.28 \pm 0.03\ \mathrm{GeV}, \quad (33)$$

while in the bottom-light diquark analysis we use

$$M = M_Z = 91.188\ \mathrm{GeV}, \qquad \alpha(M_Z) = 0.1184 \pm 0.0007,$$
$$A = A_b = \frac{23}{12}, \qquad \bar{m}_b = 4.18 \pm 0.03\ \mathrm{GeV}. \quad (34)$$

All of these parameters are taken from Ref. [6], apart from A_c and A_b which are given in Ref. [49]. We set $\mu = 1/\sqrt{\tau}$ in order to implement renormalization group improvement as described above.

We now specify the values used for the QCD condensates. Beginning with the quark condensate, we define

$$m\langle\bar{q}q\rangle = \frac{m(2\ \mathrm{GeV})}{m_q(2\ \mathrm{GeV})}m_q\langle\bar{q}q\rangle, \quad (35)$$

where m denotes the charm or bottom quark mass and we use the PCAC relation $m_q\langle\bar{q}q\rangle = -\frac{1}{2}f_\pi^2m_\pi^2$. The numerical values are again taken from Ref. [6],

$$m_q(2\ \mathrm{GeV}) = \frac{1}{2}[m_u(2\ \mathrm{GeV}) + m_d(2\ \mathrm{GeV})] = 0.0038 \pm 0.0006\ \mathrm{GeV}, \qquad f_\pi = 0.093\ \mathrm{GeV}, \qquad m_\pi = 0.139\ \mathrm{GeV}, \tag{36}$$

$$r_c = \frac{m_c(2\ \mathrm{GeV})}{m_q(2\ \mathrm{GeV})} = 305 \pm 59, \qquad r_b = \frac{m_b(2\ \mathrm{GeV})}{m_q(2\ \mathrm{GeV})} = 1229 \pm 210, \tag{37}$$

where the heavy quark mass at 2 GeV is determined using (32). The mixed condensate is similarly defined as

$$m\langle\bar{q}\sigma Gq\rangle = M_0^2 m\langle\bar{q}q\rangle, \tag{38}$$

where $M_0^2 = (0.8 \pm 0.1)\ \mathrm{GeV}^2$ [64] and $m\langle\bar{q}q\rangle$ is as defined in (35). The gluon condensate is taken to be [65]

$$\langle\alpha G^2\rangle = (7.5 \pm 2.0) \times 10^{-2}\ \mathrm{GeV}^4. \tag{39}$$

Finally, the dimension-six quark condensate is

$$\alpha\langle\bar{q}q\rangle^2 = (5.8 \pm 0.9) \times 10^{-4}\ \mathrm{GeV}^6, \tag{40}$$

which implicitly includes deviation from ideal vacuum saturation [66]. In condensate contributions there are additional factors of the quark mass that are not included in the definitions (35) or (38), such as the factors of m^{2k} in (17), for instance. We define these masses in terms of the pole mass following the approach of Ref. [67], utilizing the known relationship between the pole mass and $\overline{\mathrm{MS}}$ mass [68–71],

$$m = m(\mu)\left[1 + \left(\frac{4}{3} - \log\left[\frac{\bar{m}^2}{\mu^2}\right]\right)\frac{\alpha(\mu)}{\pi}\right], \tag{41}$$

where $m(\mu)$ and $\alpha(\mu)$ are determined via (32) and $\bar{m}$ is the one-loop $\overline{\mathrm{MS}}$ charm or bottom quark mass.

In order to extract mass prediction for heavy-light diquarks using (31) we must first establish a permissible range of values for the Borel scale τ and the continuum threshold s_0. We adopt the approach developed in Ref. [72], whereby the Hölder inequalities [73,74]

$$\left|\int_{t_1}^{t_2} f(t)g(t)d\mu\right| \le \left[\int_{t_1}^{t_2} |f(t)|^p d\mu\right]^{1/p} \times \left[\int_{t_1}^{t_2} |g(t)|^q d\mu\right]^{1/q}, \qquad \frac{1}{p} + \frac{1}{q} = 1, \qquad p, q \ge 1, \tag{42}$$

are used to constrain the values of τ and s_0. The key observation of Ref. [72] is that because $\mathrm{Im}\Pi(Q^2)$ is related to a physical hadronic spectral function via duality, $\mathrm{Im}\Pi(Q^2)$ must be positive and hence it can serve as the integration measure in (42). It can be shown that the sum rules (28) must satisfy

$$\frac{\mathcal{R}_2(\tau, s_0)/\mathcal{R}_1(\tau, s_0)}{\mathcal{R}_1(\tau, s_0)/\mathcal{R}_0(\tau, s_0)} \ge 1, \qquad \frac{\mathcal{R}_3(\tau, s_0)/\mathcal{R}_2(\tau, s_0)}{\mathcal{R}_2(\tau, s_0)/\mathcal{R}_1(\tau, s_0)} \ge 1, \tag{43}$$

where the first and second inequalities come from requiring that $\mathcal{R}_0(\tau, s_0)$ and $\mathcal{R}_1(\tau, s_0)$ satisfy the Hölder inequalities, respectively. The inequalities in (43) can be used to set a lower bound on the Borel mass $M_B = 1/\sqrt{\tau}$ or to set a lower bound on the continuum threshold s_0. The constraints set by the first inequality in (43) are more restrictive than those set by the second, hence we rely solely upon the first. We fix an upper bound on M_B by requiring that continuum contributions are less than 50% of total contributions to the sum rule [60],

$$f_{\mathrm{cont}}(\tau, s_0) = \frac{\mathcal{R}_1(\tau, s_0)/\mathcal{R}_0(\tau, s_0)}{\mathcal{R}_1(\tau, \infty)/\mathcal{R}_0(\tau, \infty)}, \tag{44}$$

and require that $f_{\mathrm{cont}} \ge 0.5$. Using (43) and (44) we can define a range of M_B values over which the sum rule is considered reliable, i.e., the sum rule window. We also require that the mass prediction $M(\tau, s_0)$ extracted from (31) exhibits τ stability, that is,

$$\frac{d}{d\tau}M(\tau, s_0) = 0 \tag{45}$$

within the sum rule window. However, note that the bounds on the Borel scale that are determined using (43) and (44) will vary depending on the value of s_0. Typically the sum rule window widens as s_0 is increased. Thus we first seek a minimum value s_0^{min}, which we take to be the smallest value of s_0 in whose sum rule window τ stability (45) is

TABLE IV. Mass predictions and sum rule parameters for charm-light ($[cq]$) and bottom-light ($[bq]$) diquarks with positive parity. M_{max} is an upper bound on the mass, determined from $s_0 \to \infty$. The minimal value of the continuum threshold is s_0^{min}, the optimal value determined by(46) is s_0^{opt}, the sum rule window boundaries are M_B^{min} and M_B^{max}.

$[Qq]$	J^P	M (GeV)	M_{max} (GeV)	s_0^{min} (GeV^2)	M_B^{min} (GeV)	M_B^{max} (GeV)	s_0^{opt} (GeV^2)
$[cq]$	0^+	1.86 ± 0.05	2.02	5.0	1.2	1.6	5.0
	1^+	1.87 ± 0.10	2.07	5.0	1.3	1.6	5.0
$[bq]$	0^+	5.08 ± 0.04	5.32	30	2.1	3.8	30
	1^+	5.08 ± 0.04	5.32	30	2.2	3.8	30

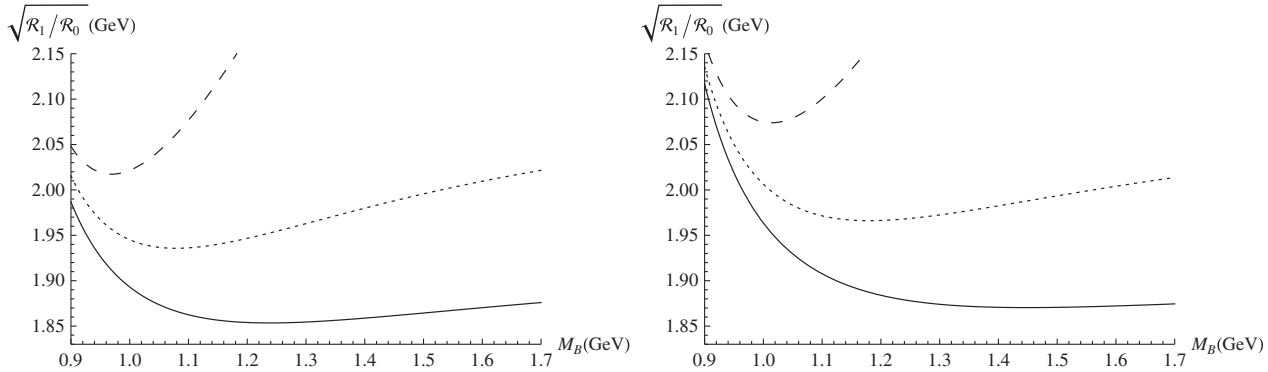

FIG. 6. Mass predictions for $J^P = 0^+$ (left) and 1^+ (right) charm-light diquarks. Solid lines correspond to $s_0^{\rm opt}$, yielding the results in Table IV. In both plots the uppermost dashed lines correspond to $s_0 \to \infty$ which provides an upper mass bound and the middle dotted line corresponds to $s_0 = 6.0$ GeV^2.

satisfied. If there are no values of s_0 that exhibit τ stability, we consider the sum rule to be unstable. Once the minimum value of s_0 has been found, we determine the optimal value $s_0^{\rm opt}$ using the following criterion:

$$\chi^2(s_0) = \sum_j \left(\frac{1}{M} \sqrt{\frac{\mathcal{R}_1(\tau_j, s_0)}{\mathcal{R}_0(\tau_j, s_0)}} - 1 \right)^2, \quad s_0 \geq s_0^{\rm min}. \qquad (46)$$

The optimal value $s_0^{\rm opt}$ is that for which (46) is minimized. We adopt a conservative approach, where (46) is calculated over the sum rule window corresponding to the minimal value of s_0. In some cases we can obtain an upper bound on the mass prediction (31) by taking $s_0 \to \infty$, however in order to extract such a bound the requirements described above must be satisfied.

We also determine the uncertainty in our mass predictions due to uncertainties in the QCD parameters. In order of significance these are r_c (37), $\bar{m}_c$ (33), $\alpha(M_\tau)$ (33), and M_0^2 (38) in the charm analysis, whereas in the bottom analysis they are r_b (37), $\bar{m}_b$ (33), M_0^2 (38), and $\alpha(M_Z)$ (33). Uncertainties in $\langle \alpha G^2 \rangle$ and $\alpha \langle \bar{q} q \rangle^2$ are insignificant in both cases and we have made no attempt to estimate contributions to these uncertainties from higher loop effects. The resulting mass predictions and uncertainties for heavy-light diquarks with positive parity are summarized in Table IV. None of the negative parity heavy-light diquark sum rules exhibit τ stability, therefore we have been unable to extract mass predictions in these channels. Fig. 6 shows the mass predictions for $J^P = 0^+$ and 1^+ charm-light diquarks while those for bottom-light diquarks are shown in Fig. 7.

IV. CONCLUSIONS

In this paper we have used QCD Laplace sum rules to study heavy-light diquarks with $J^P = 0^\pm$, $1^\pm$. Our calculations extend previous sum rule work [33] by including higher-loop perturbative contributions which necessitate renormalization of the diquark currents. We have successfully extracted mass predictions for positive parity charm-light and bottom-light diquarks, which are summarized in Table IV. However, the sum rules derived for negative parity channels are poorly behaved, and do not permit unambiguous mass predictions, similar to what was found for light diquarks [31].

The mass predictions for the $J^P = 0^+$ and 1^+ heavy-light diquarks are degenerate within uncertainty, as would be expected by heavy-quark symmetry [17]. Our predicted $J^P = 0^+$ and 1^+ charm-light diquark masses of 1.86 ± 0.05

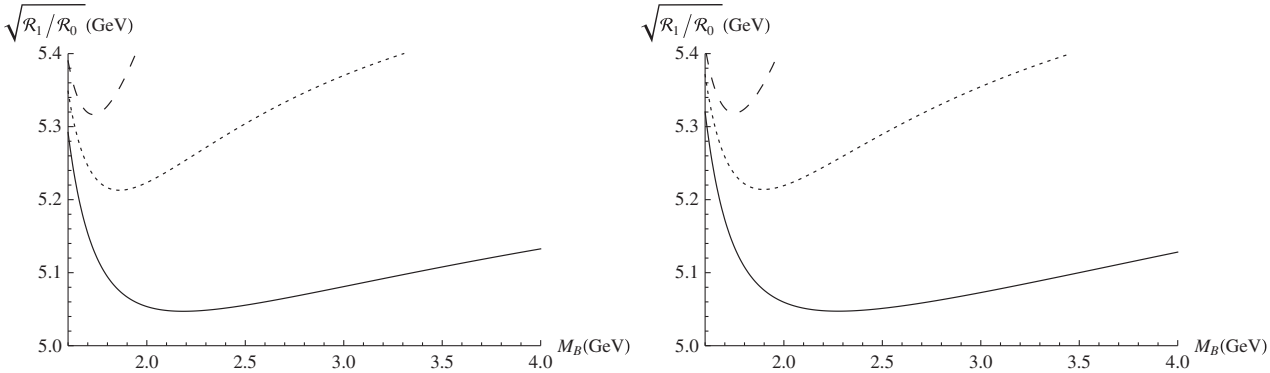

FIG. 7. Mass predictions for $J^P = 0^+$ (left) and 1^+ (right) bottom-light diquarks. Solid lines correspond to $s_0^{\rm opt}$, yielding the results in Table IV. In both plots the uppermost dashed lines correspond to $s_0 \to \infty$ and the middle dotted line corresponds to $s_0 = 35$ GeV^2.

and 1.87 ± 0.10 GeV are in superb agreement with the constituent charm-light diquark mass of 1.93 GeV determined by Maiani *et al.* [17] from a fit to the $X(3872)$. Additionally, we predict both the $J^P = 0^+$ and 1^+ bottom-light diquark masses to be 5.08 ± 0.04 GeV in reasonable agreement with the constituent bottom-light diquark mass of 5.20 GeV determined by Ali *et al.* [42] from a fit to the $Y_b(10890)$. Given the agreement between these constituent diquark masses and our QCD-based calculations, our results provide QCD support for the identification of the $X(3872)$ and $Y_b(10890)$ as $J^{PC} = 1^{++}$ tetraquarks composed of diquark clusters. Furthermore, because the constituent heavy-light diquark is such an important input for constituent diquark models of tetraquarks, we interpret this agreement as indirect support for the predictions of these models. Specifically, our results strengthen the case for the tetraquark interpretation of the charged XYZ states $Z_c^{\pm}(3895)$, $Z_b^{\pm}(10610)$, and $Z_b^{\pm}(10650)$.

In this work we have focused on heavy-light diquarks so as to examine the constituent diquark masses determined in Refs. [17,42]. However, the methods used in this paper could be extended to doubly-heavy diquarks to study diquark clustering within other tetraquarks or within heavy baryons.

ACKNOWLEDGMENTS

T. G. S. and R. T. K. are grateful for the hospitality of Shanghai University where this work was initiated and partially completed. T. G. S. is grateful for financial support from the Natural Sciences and Engineering Research Council of Canada (NSERC). Ailin Zhang is supported by the National Natural Science Foundation of China (11075102) and the Innovation Program of Shanghai Municipal Education Commission under Grant No. 13ZZ066.

[1] S. K. Choi *et al.* (Belle Collaboration), Phys. Rev. Lett. **91**, 262001 (2003).
[2] D. Acosta *et al.* (CDF Collaboration), Phys. Rev. Lett. **93**, 072001 (2004).
[3] V. M. Abazov *et al.* (D0 Collaboration), Phys. Rev. Lett. **93**, 162002 (2004).
[4] B. Aubert *et al.* (*BABAR* Collaboration), Phys. Rev. Lett. **93**, 041801 (2004).
[5] R. Aaij *et al.* (LHCb Collaboration), Eur. Phys. J. C **72**, 1972 (2012).
[6] J. Beringer *et al.* (Particle Data Group Collaboration), Phys. Rev. D **86**, 010001 (2012).
[7] R. Aaij *et al.* (LHCb Collaboration), arXiv:1302.6269.
[8] E. S. Swanson, Phys. Rep. **429**, 243 (2006).
[9] F. E. Close and P. R. Page, Phys. Lett. B **578**, 119 (2004).
[10] M. B. Voloshin, Phys. Lett. B **579**, 316 (2004).
[11] E. S. Swanson, Phys. Lett. B **588**, 189 (2004).
[12] N. A. Tornqvist, Phys. Lett. B **590**, 209 (2004).
[13] M. T. AlFiky, F. Gabbiani, and A. A. Petrov, Phys. Lett. B **640**, 238 (2006).
[14] C. E. Thomas and F. E. Close, Phys. Rev. D **78**, 034007 (2008).
[15] X. Liu, Z.-G. Luo, Y.-R. Liu, and S.-L. Zhu, Eur. Phys. J. C **61**, 411 (2009).
[16] I. W. Lee, A. Faessler, T. Gutsche, and V. E. Lyubovitskij, Phys. Rev. D **80**, 094005 (2009).
[17] L. Maiani, F. Piccinini, A. D. Polosa, and V. Riquer, Phys. Rev. D **71**, 014028 (2005).
[18] D. Ebert, R. N. Faustov, and V. O. Galkin, Phys. Lett. B **634**, 214 (2006).
[19] R. D'E. Matheus, S. Narison, M. Nielsen, and J. M. Richard, Phys. Rev. D **75**, 014005 (2007).
[20] K. Terasaki, Prog. Theor. Phys. **118**, 821 (2007).
[21] S. Dubnicka, A. Z. Dubnickova, M. A. Ivanov, and J. G. Korner, Phys. Rev. D **81**, 114007 (2010).
[22] N. Brambilla, S. Eidelman, B. K. Heltsley, R. Vogt, G. T. Bodwin, E. Eichten, A. D. Frawley, and A. B. Meyer *et al.*, Eur. Phys. J. C **71**, 1534 (2011).
[23] M. Anselmino, E. Predazzi, S. Ekelin, S. Fredriksson, and D. B. Lichtenberg, Rev. Mod. Phys. **65**, 1199 (1993).
[24] R. L. Jaffe, Phys. Rep. **409**, 1 (2005).
[25] A. Zhang, T. Huang, and T. G. Steele, Phys. Rev. D **76**, 036004 (2007).
[26] M. Nielsen, F. S. Navarra, and S. H. Lee, Phys. Rep. **497**, 41 (2010).
[27] S. Narison and R. Tarrach, Phys. Lett. B **125**, 217 (1983).
[28] M. Jamin and M. Kremer, Nucl. Phys. **B277**, 349 (1986).
[29] R. T. Kleiv and T. G. Steele, J. Phys. G **38**, 025001 (2011); **39**, 039501(E) (2012).
[30] H. G. Dosch, M. Jamin, and B. Stech, Z. Phys. C **42**, 167 (1989).
[31] M. Jamin and M. Neubert, Phys. Lett. B **238**, 387 (1990).
[32] Z.-G. Wang, Commun. Theor. Phys. **59**, 451 (2013).
[33] Z.-G. Wang, Eur. Phys. J. C **71**, 1524 (2011).
[34] Z. G. Wang, S. L. Wan, and W. M. Yang, Commun. Theor. Phys. **47**, 287 (2007).
[35] Y.-M. Yu, H.-W. Ke, Y.-B. Ding, X.-H. Guo, H.-Y. Jin, X.-Q. Li, P.-N. Shen, and G.-L. Wang, Commun. Theor. Phys. **46**, 1031 (2006).
[36] P. Maris, Few-Body Syst. **32**, 41 (2002).
[37] K. Kim, D. Jido, and S. H. Lee, Phys. Rev. C **84**, 025204 (2011).
[38] R. Faccini, L. Maiani, F. Piccinini, A. Pilloni, A. D. Polosa, and V. Riquer, arXiv:1303.6857.
[39] M. Ablikim *et al.* (BESIII Collaboration), arXiv:1303.5949.
[40] Z. Q. Liu *et al.* (Belle Collaboration), arXiv:1304.0121.

[41] T. Xiao, S. Dobbs, A. Tomaradze, and K. K. Seth, arXiv:1304.3036.
[42] A. Ali, C. Hambrock, and W. Wang, Phys. Rev. D **85**, 054011 (2012).
[43] K. F. Chen *et al.* (Belle Collaboration), Phys. Rev. Lett. **100**, 112001 (2008).
[44] A. Bondar *et al.* (Belle Collaboration), Phys. Rev. Lett. **108**, 122001 (2012).
[45] R. Berg, D. Harnett, R. T. Kleiv, and T. G. Steele, Phys. Rev. D **86**, 034002 (2012).
[46] D. Harnett, R. T. Kleiv, T. G. Steele, and H.-y. Jin, J. Phys. G **39**, 125003 (2012).
[47] E. E. Boos and A. I. Davydychev, Teor. Mat. Fiz. **89**, 56 (1991) [Theor. Math. Phys. **89**, 1052 (1991)].
[48] A. I. Davydychev, J. Math. Phys. (N.Y.) **33**, 358 (1992).
[49] P. Pascual and R. Tarrach, *QCD: Renormalization for the Practitioner* (Springer-Verlag, New York, 1984).
[50] R. Mertig and R. Scharf, Comput. Phys. Commun. **111**, 265 (1998).
[51] O. V. Tarasov, Phys. Rev. D **54**, 6479 (1996).
[52] O. V. Tarasov, Nucl. Phys. **B502**, 455 (1997).
[53] T. Huber and D. Maitre, Comput. Phys. Commun. **175**, 122 (2006).
[54] T. Huber and D. Maitre, Comput. Phys. Commun. **178**, 755 (2008).
[55] L. Lewin, *Polylogarithms and Associated Functions* (Elsevier North Holland, New York, 1981).
[56] D. Harnett, R. T. Kleiv, K. Moats, and T. G. Steele, Nucl. Phys. **A850**, 110 (2011).
[57] J. C. Collins, *Renormalization: An Introduction to Renormalization, the Renormalization Group and the Operator-Product Expansion* (Cambridge University Press, New York, 1984).
[58] E. Bagan, M. R. Ahmady, V. Elias, and T. G. Steele, Z. Phys. C **61**, 157 (1994).
[59] M. A. Shifman, A. I. Vainshtein, and V. I. Zakharov, Nucl. Phys. **B147**, 385 (1979).
[60] M. A. Shifman, A. I. Vainshtein, and V. I. Zakharov, Nucl. Phys. **B147**, 448 (1979).
[61] L. J. Reinders, H. Rubinstein, and S. Yazaki, Phys. Rep. **127**, 1 (1985).
[62] S. Narison, *QCD as a Theory of Hadrons From Partons to Confinement*, (Cambridge University Press, Cambridge, England, 2004).
[63] S. Narison and E. de Rafael, Phys. Lett. **103B**, 57 (1981).
[64] H. G. Dosch, M. Jamin, and S. Narison, Phys. Lett. B **220**, 251 (1989).
[65] S. Narison, Phys. Lett. B **693**, 559 (2010); **705**, 544(E) (2011).
[66] S. Narison, Phys. Lett. B **626**, 101 (2005).
[67] S. Narison, Phys. Lett. B **718**, 1321 (2013).
[68] N. Gray, D. J. Broadhurst, W. Grafe, and K. Schilcher, Z. Phys. C **48**, 673 (1990).
[69] D. J. Broadhurst, N. Gray, and K. Schilcher, Z. Phys. C **52**, 111 (1991).
[70] J. Fleischer, F. Jegerlehner, O. V. Tarasov, and O. L. Veretin, Nucl. Phys. **B539**, 671 (1999); **B571**, 511(E) (2000).
[71] K. G. Chetyrkin and M. Steinhauser, Nucl. Phys. **B573**, 617 (2000).
[72] M. Benmerrouche, G. Orlandini, and T. G. Steele, Phys. Lett. B **356**, 573 (1995).
[73] E. F. Beckenbach and R. Bellman, *Inequalities* (Springer, Berlin, 1961).
[74] S. K. Berberian, *Measure and Integration* (MacMillan, New York, 1965).
[75] D. Binosi and L. Theussl, Comput. Phys. Commun. **161**, 76 (2004).

Chapter 5
Scalar Diquark Operator Renormalization

5.1 Introduction

The research in this chapter is based upon the publication:

- R.T. Kleiv and T.G. Steele, Two-loop QCD renormalization and anomalous dimension of the scalar diquark operator, J. Phys. G38 (2011) 025001.

In QSR calculations hadronic states are probed by currents which are composite local operators constructed from quark and gluon fields. As discussed in Chapter 1, composite operators can mix under renormalization with operators of lower dimension and the same quantum numbers. This presents a significant challenge to extending QSR studies to higher orders. However, some composite operators are protected from this mixing by the fact that there are no lower dimensional operators with which they could mix. Such operators must renormalize multiplicatively, and the renormalization factor can be determined using the methods described in Chapter 1. Therefore it is much easier to perform higher order QSR analyses using operators that do not mix under renormalization.

An example of a composite operator that does not mix under renormalization is the scalar diquark operator, which is given by

$$J^d_\alpha = \epsilon_{\alpha\beta\gamma} Q^T_\beta C\gamma_5 q_\gamma \tag{5.1}$$

where the notation used here is identical to that of Eq. (4.3). The current couples to diquarks with $J^P = 0^+$. However, because diquarks have a net colour there are no lower dimensional operators that could mix with the scalar diquark current (5.1). Therefore, the scalar diquark

operator must renormalize multiplicatively. The publication above (Ref. [70]) determines the renormalization factor of the scalar $\left(J^P = 0^+\right)$ diquark operator to second (two-loop) order in the strong coupling α. This builds upon the work of Ref. [42], which gives the scalar diquark renormalization factor to first order.

5.2 Results

The renormalization factor of the scalar diquark operator can be determined by considering the correlation function

$$\Gamma^d = \langle\Omega| T\left[Q\left(x\right) J^d\left(0\right) q\left(y\right)\right] |\Omega\rangle\,, \tag{5.2}$$

where J^d is the scalar diquark operator (5.1) and colour indices have been omitted for brevity. The correlation function can be calculated using the perturbative expansion (1.19) in momentum space with the external quark propagators amputated. Because we are calculating a renormalization factor which is momentum independent, the diquark operator inserted into Eq. (5.2) can be taken to have zero momentum without loss of generality. We will use the $\overline{\text{MS}}$ renormalization scheme which is mass independent so we can work in the chiral limit, ignoring the quark masses in Eq. (5.2). The bare and renormalized correlation functions are related by

$$\Gamma^d_R\left(q\,; m_R\,, a_R\,, \alpha_R\right) = \lim_{\epsilon\to 0}\left[Z_{\text{d}}\, Z^{-1}_{\text{2F}} \Gamma^d_B\left(q\,; m_B\,, a_B\,, \alpha_B\right)\right]\,. \tag{5.3}$$

As discussed in Chapter 1, the scalar diquark renormalization factor Z_{d} is the additional renormalization factor that is required in order to evaluate the limit in Eq. (5.3). This relationship can be used to calculate the scalar diquark operator renormalization factor Z_{d} to any order in the coupling α.

In order to calculate scalar diquark operator renormalization factor, it is helpful to exploit the similarity between the scalar diquark and scalar meson operators. The scalar meson

operator renormalizes as

$$J^s = \bar{Q}q\,, \quad [J^s]_R = Z_m\,[J^s]_B\ , \tag{5.4}$$

where Z_m corresponds to the quark mass renormalization factor in the $\overline{\text{MS}}$ scheme and this expression is valid to all orders in the coupling α. The renormalization factor Z_{m} is given to $\mathcal{O}\left(\alpha^2\right)$ in Ref. [97]. Equivalently, the scalar meson operator renormalization factor can be calculated directly using the relation

$$\Gamma^s_R\left(q\,; m_R\,, a_R\,, \alpha_R\right) = \lim_{\epsilon\to 0}\left[Z_{\text{m}}\, Z^{-1}_{2\text{F}}\Gamma^s_B\left(q\,; m_B\,, a_B\,, \alpha_B\right)\right]\ , \tag{5.5}$$

where Γ^s is a correlation function similar to that in Eq. (5.2), except with a zero momentum insertion of J^s rather than J^d. Because the scalar diquark (5.1) and scalar meson (5.4) operators are very similar in structure, the correlation functions given in Eqs. (5.3) and (5.5) are closely related. In fact, to any order in perturbation theory, each diagram contributing to the scalar diquark correlation function is proportional to a corresponding diagram contributing to the scalar meson operator. This relationship and the known two loop expression for the scalar meson operator renormalization factor provide a useful benchmark for the direct calculation of the scalar diquark renormalization factor via Eq. (5.3). At one-loop order, there is only one diagram that contributes to each correlation function, so the one-loop renormalization factors are proportional. However, at two-loop order there are eleven Feynman diagrams that contribute to each correlation function. Thus the simple proportionality between the scalar diquark and scalar meson operator renormalization factors does not persist at two-loop level. The complete expression for the two-loop scalar diquark renormalization factor in the $\overline{\text{MS}}$ scheme is determined to be

$$\begin{aligned} Z_{\text{d}} = 1 + \frac{\alpha}{\pi}\left[\frac{3-a}{6\epsilon}\right] + \left(\frac{\alpha}{\pi}\right)^2\left[\frac{1}{\epsilon}\left(\frac{1545-40n_f}{2880} - \frac{a}{8} - \frac{a^2}{64}\right)\right. \\ \left. + \frac{1}{\epsilon^2}\left(\frac{234-12n_f}{288} - \frac{17a}{96} - \frac{5a^2}{288}\right)\right]\ , \end{aligned} \tag{5.6}$$

where a is the covariant gauge parameter, n_f is the number of quark flavours and dimensional regularization with $d = 4 + 2\epsilon$ has been used.

The two-loop scalar diquark operator renormalization factor given in Eq. (5.6) can be used to extend existing QSR studies of diquarks to higher order. It is possible that these higher order corrections could have a significant effect on QSR mass predictions for diquarks. Note that the renormalization factor was calculated in the $\overline{\text{MS}}$ renormalization scheme, where all quark flavours renormalize in the same way. Therefore the renormalization factor determined in Ref. [70] applies to all scalar diquark operators, regardless of the flavour of the quarks composing the diquark operator. In Chapter 4, mass predictions were determined for heavy-light diquarks with $J^P = 0^\pm\,, 1^\pm$. The unknown renormalization factors for the pseudoscalar (0^-), axial vector (1^+) and vector (1^-) diquark operators were determined by utilizing the one-loop relationship between diquark and quark meson operators established in this chapter.

Although this research presented in this chapter is not directly relevant to the heavy quarkonium-like states, it has been applied in the QSR study of heavy-light diquarks in Chapter 4. The renormalization of the diquark current is an essential aspect of the renormalization methodology used in Chapter 4. In order to calculate the two-loop scalar diquark operator renormalization factor, a large number of loop integrals must be calculated. Because the $\overline{\text{MS}}$ renormalization scheme is mass independent, these integrals can be evaluated in the chiral limit. The loop integration methods discussed in Chapter 2 are needed in order to evaluate these integrals. Finally, the result presented here for the two-loop scalar diquark renormalization factor could permit higher order QSR studies of scalar diquarks.

5.3 Published Article

The two-loop scalar diquark renormalization paper was published in the Journal of Physics G in 2011. Note that a corrigendum correcting a minor error was published in the same journal in 2012. The following pages include the corrigendum followed by the original article in the journal format.

- R.T. Kleiv and T.G. Steele, Two-loop QCD renormalization and anomalous dimension of the scalar diquark operator, J. Phys. G38 (2011) 025001.

Two-loop QCD renormalization and anomalous dimension of the scalar diquark operator

2011 J. Phys. G: Nucl. Part. Phys. 38 025001

(http://iopscience.iop.org/0954-3899/38/2/025001)

J. Phys. G: Nucl. Part. Phys. **39** (2012) 039501 (2pp) doi:10.1088/0954-3899/39/3/039501

Corrigendum: Two-loop QCD renormalization and anomalous dimension of the scalar diquark operator

2011 *J. Phys. G: Nucl. Part. Phys.* **38** 025001

R T Kleiv and T G Steele

Department of Physics and Engineering Physics, University of Saskatchewan, Saskatoon, SK S7N 5E2, Canada

E-mail: Tom.Steele@usask.ca

Received 29 November 2011
Published 19 January 2012
Online at stacks.iop.org/JPhysG/39/039501

Abstract
We present a corrected result for the two-loop $\overline{\text{MS}}$ scalar diquark renormalization factor and anomalous dimension. Our conclusions relating to the QCD renormalization scale dependence of diquark matrix elements of the $\Delta S = 1$ effective weak Hamiltonian are unchanged.

In [1], the colour factor corresponding to diagram 10 was incorrectly given in table 1 as $\frac{2}{5}$. The correct value for this diagram is in fact $\frac{5}{2}$. With the corrected colour factor, we now find the following result for the two-loop $\overline{\text{MS}}$ QCD diquark renormalization constant:

$$Z_d = 1 + \frac{\alpha}{\pi}\left[\frac{3-\xi}{6\epsilon}\right] + \left(\frac{\alpha}{\pi}\right)^2\left[\frac{1}{\epsilon}\left(\frac{1545-40n_f}{2880} - \frac{\xi}{8} - \frac{\xi^2}{64}\right) + \frac{1}{\epsilon^2}\left(\frac{234-12n_f}{288} - \frac{17\xi}{96} - \frac{5\xi^2}{288}\right)\right]. \quad (1)$$

The two-loop $\overline{\text{MS}}$ QCD anomalous dimension for the diquark operator is now found to be

$$\gamma_d(\alpha) = \gamma_1\frac{\alpha}{\pi} + \gamma_2\left(\frac{\alpha}{\pi}\right)^2, \quad \gamma_1 = 1 - \frac{\xi}{3}, \quad \gamma_2 = \frac{1545-40n_f}{720} - \frac{\xi}{2} - \frac{\xi^2}{16}. \quad (2)$$

This result still satisfies the renormalization group (RG) constraint discussed in [1].

As mentioned in [1], the QCD renormalization scale dependence of the diquark matrix elements of the $\Delta S = 1$ effective weak Hamiltonian is governed by the combination of the Wilson coefficient $c_-(\mu)$ [3] and the scalar diquark decay constant $g_+(\mu)$ [2]. Using our revised result (2) for the scalar diquark operator anomalous dimension and performing an analysis identical to that in [1], we find

$$c_-(\mu)g_+(\mu)g_+(\mu) = 1 - \frac{35}{54}\frac{\alpha(\mu)}{\pi}. \quad (3)$$

Our revised result (3) again shows that the cancellation of the scale dependence of this quantity found in [2] does not persist at next-to-leading order. In addition, the scale dependence of (3) still has the correct behaviour to counter the residual scale dependence from non-perturbative contributions found in [2]. Thus, our conclusions regarding the renormalization scale dependence of diquark matrix elements of the $\Delta S = 1$ effective weak Hamiltonian are unchanged.

0954-3899/12/039501+02$33.00

Acknowledgment

We thank John Gracey for making us aware of this error.

References

[1] Kleiv R T and Steele T G 2011 *J. Phys. G: Nucl. Part. Phys.* **38** 025001
[2] Jamin M and Neubert M 1990 *Phys. Lett.* B **238** 387
[3] Buras A J and Weisz P H 1990 *Nucl. Phys.* B **333** 66

Two-loop QCD renormalization and anomalous dimension of the scalar diquark operator

2011 J. Phys. G: Nucl. Part. Phys. 38 025001

(http://iopscience.iop.org/0954-3899/38/2/025001)

J. Phys. G: Nucl. Part. Phys. **38** (2011) 025001 (8pp) doi:10.1088/0954-3899/38/2/025001

Two-loop QCD renormalization and anomalous dimension of the scalar diquark operator

R T Kleiv and T G Steele

Department of Physics and Engineering Physics, University of Saskatchewan, Saskatoon, SK, S7N 5E2, Canada

Received 14 October 2010
Published 5 January 2011
Online at stacks.iop.org/JPhysG/38/025001

Abstract
The renormalization of the scalar diquark operator and its anomalous dimension is calculated at two-loop order in QCD, enabling higher-order QCD studies of diquarks. As an application of our result, the two-loop diquark anomalous dimension in the $\overline{\text{MS}}$ scheme is used to study the QCD renormalization scale dependence of diquark matrix elements of the $\Delta S = 1$ effective weak Hamiltonian.

1. Introduction

Four-quark (or tetraquark) $qq\bar{q}\bar{q}$ states explain the inverted mass hierarchy of the scalar mesons compared to a $q\bar{q}$ nonet in a variety of theoretical approaches [1–5]. With the inclusion of a gluonium (glueball) state [6], the scalar spectrum below 2 GeV is then understood as mixtures of gluonium, the $q\bar{q}$ nonet, and the $qq\bar{q}\bar{q}$ nonet. The $X(3872)$ [7] and $Y(4260)$ [8] mesons can also be interpreted as four-quark states [9].

Diquark (qq) clusters are relevant to the internal structure of hadrons (see e.g. [10, 11]). In particular, [9] uses constituent models for diquark clusters to study four-quark states. The constituent (scalar) diquark masses that emerge in [9] are in good agreement with QCD sum-rule analyses of diquarks [12, 13], providing QCD corroboration for the diquark model of four-quark states.

In this paper, we study the renormalization of scalar diquark operators to two-loop order in QCD and thereby obtain the two-loop anomalous dimension of the scalar diquark current. As discussed below, the renormalization of the diquark operator is an essential component of QCD sum-rule analyses, and the anomalous dimension is also necessary for determining the scale dependence of matrix elements of the effective weak Hamiltonian for non-leptonic strange particle decays [14]. Our two-loop results thus enable future QCD studies of diquarks to higher loop order.

The scalar diquark operator in an anti-triplet colour configuration (the 'good' diquark in the terminology of [11]) is given by [12]

$$J_\gamma = \epsilon_{\alpha\beta\gamma}\, Q_i^\alpha\, (C\gamma_5)_{ij}\, q_j^\beta = \epsilon_{\alpha\beta\gamma}\, Q_\alpha^T C\gamma_5 q_\beta, \tag{1}$$

0954-3899/11/025001+08$33.00

Figure 1. Feynman diagram for the tree-level vertex of the diquark operator with the quark fields $\bar{Q}$ and $\bar{q}$. The double line represents the Q field that is transposed and the diquark operator is denoted by $\otimes$. This and all subsequent Feynman diagrams were drawn with JaxoDraw [15].

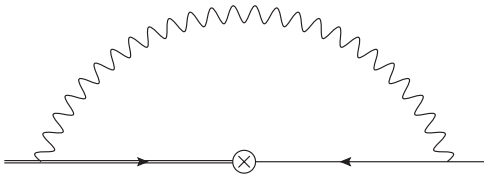

Figure 2. One-loop Feynman diagram for the renormalization of J_γ. As in figure 1, the double line represents the (transposed) Q field and the diquark operator is denoted by $\otimes$.

where the greek and latin indices respectively represent colour and spin degrees of freedom for the quark fields Q and q, and C is the charge conjugation operator. The presence of a transposed quark field in (1) implies that the Feynman rule for the three-point function of the diquark operator and $\bar{Q}, \bar{q}$ fields shown in figure 1,

$$\Gamma_d^{(0)} = -\epsilon_{\alpha\beta\gamma} C\gamma_5, \tag{2}$$

implicitly transposes the external propagator associated with the Q field.

2. One-loop renormalization

Although the diquark operator is gauge dependent, the theory of composite-operator renormalization [16] implies that the diquark operator is multiplicatively renormalizable because there are no lower-dimensional operators with the same quantum numbers as (1).[1] The one-loop renormalization of the diquark operator can thus be determined by figure 2, which results in the following one-particle irreducible (1PI) Green's function for a zero-momentum insertion of J_γ in D dimensions (dimensional regularization):

$$\Gamma_d^{(1)} = \mathrm{i}\frac{g^2}{4}\lambda^a_{\sigma\alpha}\lambda^a_{\tau\beta}\epsilon_{\sigma\tau\gamma}\frac{1}{\nu^{2\epsilon}}\int\frac{\mathrm{d}^D k}{(2\pi)^D}(\gamma^\rho)^T \times \frac{(\not{p}+\not{k})^T}{(p+k)^2}C\gamma_5\frac{(\not{p}+\not{k})}{(p+k)^2}\gamma^\mu\left[-\frac{g_{\mu\rho}}{k^2}+(1-\xi)\frac{k_\mu k_\rho}{k^4}\right], \tag{3}$$

where ν is the renormalization scale, the quark mass has been ignored because dimensional regularization is a mass-independent scheme, $\alpha_s = g^2/(4\pi)$, colour indices have been explicitly shown for the Gell–Mann matrices λ^a, and a covariant gauge with gauge parameter ξ has been used. Working in normal (or naïve) dimensional regularization[2], where $\{\gamma^\mu, \gamma_5\} = 0$ [17] in $D = 4 + 2\epsilon$ dimensions, and using the (D-dimensional) properties of the charge conjugation operator $CC = -1$ and $C(\gamma_\mu)^T C = \gamma_\mu$ [19] we find

$$\Gamma_d^{(1)} = \frac{8}{3}[-\epsilon_{\alpha\beta\gamma}C\gamma_5]\mathrm{i}\frac{g^2}{4}\frac{1}{\nu^{2\epsilon}}\int\frac{\mathrm{d}^D k}{(2\pi)^D}\gamma^\rho\frac{(\not{p}+\not{k})}{(p+k)^2}\frac{(\not{p}+\not{k})}{(p+k)^2}\gamma^\mu\left[-\frac{g_{\mu\rho}}{k^2}+(1-\xi)\frac{k_\mu k_\rho}{k^4}\right]. \tag{4}$$

[1] We are grateful for discussions with John Dixon clarifying this point.

[2] We have chosen to work in normal dimensional regularization (as opposed to, e.g., the 't Hooft-Veltman scheme [18]) because QCD sum-rule analyses of diquarks [12, 14] have used the normal dimensional regularization scheme.

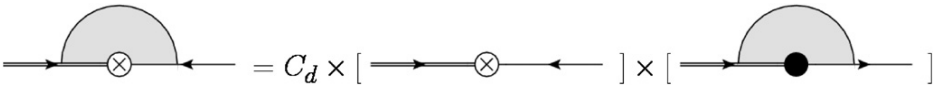

Figure 3. Diagrammatic representation of the relationship (5) between two-point functions with scalar and diquark operator insertions. The scalar operator is denoted by the solid circle.

By comparison with the one-loop process determining the renormalization of the scalar current $J_s = \bar{Q}q$, we see that (4) can be related to the (one-loop) 1PI result for the scalar current $\Gamma_s^{(1)}$ apart from a numerical factor C_d representing the ratio of the different colour factors that occur in the two processes:

$$\Gamma_d^{(1)} = \tfrac{1}{2}\Gamma_d^{(0)}\Gamma_s^{(1)} \equiv C_d\Gamma_d^{(0)}\Gamma_s^{(1)}, \tag{5}$$

as represented diagrammatically in figure 3.

The renormalized diquark operator $[J_\gamma]_R$ is defined via the renormalization constant Z_d:

$$[J_\gamma]_R = Z_d J_\gamma. \tag{6}$$

Similarly, the well-known renormalization of the scalar operator is

$$[J_s]_R = Z_m J_s, \tag{7}$$

where Z_m is the quark mass renormalization constant. Using (5) it is easy to see that to one-loop order in the minimal-subtraction (MS) and associated schemes

$$Z_d = Z_{2F}^{1/2} Z_m^{1/2}, \tag{8}$$

where Z_{2F} is the renormalization constant for the quark fields. Landau gauge ($\xi = 0$) is of particular interest in the QCD sum-rule analysis of diquark currents, because the Schwinger string used for a gauge-invariant formulation of the two-point diquark correlation function vanishes in this gauge [12]. Combining the one-loop Landau-gauge result $Z_{2F} = 1$ with (8) leads to the one-loop Landau gauge MS-scheme result

$$Z_d = Z_m^{1/2} = 1 + \frac{1}{2}\frac{\alpha}{\pi}\frac{1}{\epsilon}, \tag{9}$$

where we use the dimensional regularization convention $D = 4 + 2\epsilon$. Equation (9) agrees with the (one-loop) renormalization and renormalization-group improvement implicitly implemented in [12, 14].

3. Two-loop renormalization

The two-loop diagrams for the renormalization of the diquark operator are shown in figure 4. As in the one-loop analysis and shown in figure 3, each diagram is given by a colour factor C_d multiplying the bare diquark vertex and the equivalent diagram with a scalar current. The divergent parts for each of the two-loop diagrams in figure 4 are expressed in table 1 in terms of the corresponding scalar diagram $\Gamma_{s,i}^{(2)}$ in the modified minimal-subtraction ($\overline{\text{MS}}$) scheme:

$$\Gamma_{s,i}^{(2)} = \left(\frac{\alpha_b}{\pi}\right)^2 \left[\frac{A_i}{\epsilon} + \frac{B_i}{\epsilon^2}\right], \qquad i \in \{1, 2, \ldots, 11\}, \tag{10}$$

where n_f is the number of active quark flavours and α_b and ξ_b are the bare coupling and gauge parameter. A number of the Feynman diagrams are clearly related by the exchange of Q and q fields, and hence table 1 exhibits anticipated symmetries $\Gamma_4 = \Gamma_6$, $\Gamma_7 = \Gamma_8$ and $\Gamma_9 = \Gamma_{11}$. Note that the colour factors C_d that relate the scalar and diquark diagrams are not universally

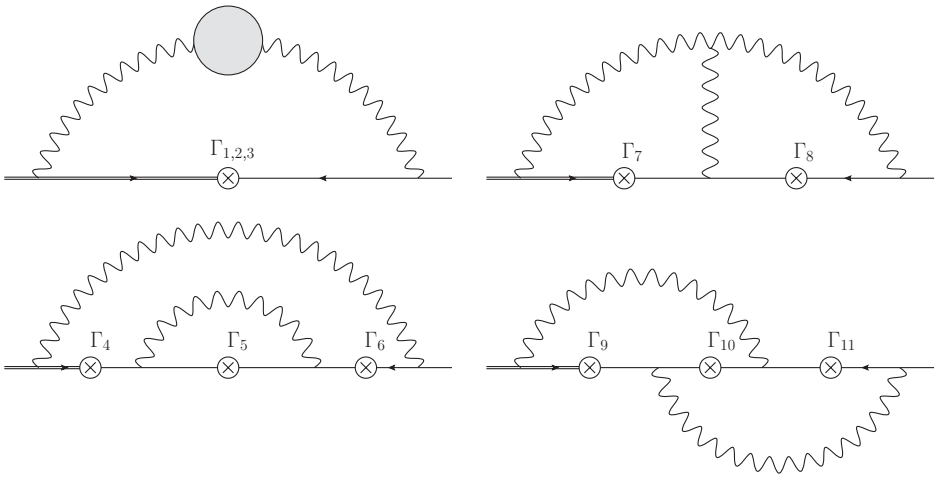

Figure 4. Two-loop diagrams for the renormalization of the diquark operator where Γ_1 denotes a quark loop, Γ_2 a ghost loop and Γ_3 a gluon loop. Implicitly, the Q (double) line extends to the insertion of the diquark operator.

Table 1. Results for the two-loop diagrams in figure 4. The quantity $L = \log(-p^2/\nu^2)$ and the notations for A_i and B_i are defined in equation (10).

i	C_d	A_i	B_i
1	$\frac{1}{2}$	$\frac{n_f(2-L)}{6}$	$-\frac{n_f}{12}$
2	$\frac{1}{2}$	$\frac{(2L-5)\left(1+\xi_b^2\right)}{32}$	$\frac{1+\xi_b^2}{32}$
3	$\frac{1}{2}$	$\frac{\xi_b^2+4\xi_b-44-L\left(\xi_b^2+6\xi_b-25\right)}{16}$	$\frac{25-6\xi_b-\xi_b^2}{32}$
4	$\frac{1}{2}$	$\frac{\xi_b[5+2\xi_b-L(3+\xi_b)]}{9}$	$-\frac{\xi_b(3+\xi_b)}{18}$
5	$\frac{1}{4}$	$\frac{(3+\xi_b)[2L(3+\xi_b)-11-5\xi_b]}{18}$	$\frac{(3+\xi_b)^2}{18}$
6	$\frac{1}{2}$	$\frac{\xi_b[5+2\xi_b-L(3+\xi_b)]}{9}$	$-\frac{\xi_b(3+\xi_b)}{18}$
7	$\frac{1}{2}$	$\frac{3L\left(\xi_b^2+4\xi_b+3\right)-5\xi_b^2-17\xi_b-24}{16}$	$\frac{3\left(\xi_b^2+4\xi_b+3\right)}{32}$
8	$\frac{1}{2}$	$\frac{3L\left(\xi_b^2+4\xi_b+3\right)-5\xi_b^2-17\xi_b-24}{16}$	$\frac{3\left(\xi_b^2+4\xi_b+3\right)}{32}$
9	$\frac{1}{2}$	$-\frac{(3+\xi_b)[1+\xi_b(L-2)]}{72}$	$-\frac{\xi_b(3+\xi_b)}{144}$
10	$\frac{2}{5}$	$\frac{3-6\xi_b-\xi_b^2}{144}$	0
11	$\frac{1}{2}$	$-\frac{(3+\xi_b)[1+\xi_b(L-2)]}{72}$	$-\frac{\xi_b(3+\xi_b)}{144}$

equal to the one-loop result $C_d = 1/2$, implying that one cannot expect the simple pattern of the one-loop result (9) to persist at two-loop order. The diagrams that are the exception to the one-loop pattern (Γ_5 and Γ_{10}) require multiple applications of colour algebra identities unique to the Feynman rule (2); all other diagrams contain a single application of these identities combined with standard colour algebra factors occurring in the renormalization of the scalar operator.

The two-loop renormalization procedure first involves the replacement of α_b and ξ_b with their (one-loop) renormalized expressions (see, e.g., [20]):

$$Z_\alpha = 1 + \frac{\alpha}{\pi}\left[\frac{33 - 2n_f}{12\epsilon}\right], \qquad \alpha_b = Z_\alpha \alpha; \tag{11}$$

$$Z_\xi = 1 + \frac{\alpha}{\pi}\left[\frac{4n_f - 39 + 9\xi}{24\epsilon}\right], \qquad \xi_b = Z_\xi \xi. \tag{12}$$

in the two-loop 1PI Green's function

$$\Gamma_d = \Gamma_d^{(0)} + \Gamma_d^{(1)} + \Gamma_d^{(2)}. \tag{13}$$

For consistency at two-loop level, (13) requires inclusion of the finite parts of the one-loop calculation (5):

$$\Gamma_s^{(1)} = \frac{1}{3}\left(\frac{\alpha_b}{\pi}\right)\left[-\frac{3+\xi_b}{\epsilon} + 2(2+\xi_b) - L(3+\xi_b)\right], \qquad L = \log\left[-\frac{p^2}{\nu^2}\right]. \tag{14}$$

The renormalization constant Z_d is then constrained by the requirement that it cancel the divergences in

$$Z_d Z_{2F}\left[\Gamma_d^{(0)} + \Gamma_d^{(1)} + \Gamma_d^{(2)}\right], \tag{15}$$

where the two-loop $\overline{\text{MS}}$ quark field renormalization constant is [21]

$$Z_{2F} = 1 + \frac{\alpha}{\pi}\frac{\xi}{3\epsilon} + \left(\frac{\alpha}{\pi}\right)^2\left[\frac{\xi\,(27+17\xi)}{144\epsilon^2} + \frac{201 - 12n_f + 72\xi + 9\xi^2}{288\epsilon}\right]. \tag{16}$$

As a benchmark to ensure accuracy in our calculations in table 1, we have verified that our results for the scalar diagrams lead to the required two-loop $\overline{\text{MS}}$ result $Z_s = Z_m$ [22]

$$Z_m = 1 + \frac{\alpha}{\pi\epsilon} + \left(\frac{\alpha}{\pi}\right)^2\left[\frac{1}{\epsilon^2}\left(\frac{15}{8} - \frac{n_f}{12}\right) + \frac{1}{\epsilon}\left(\frac{101}{48} - \frac{5n_f}{72}\right)\right]. \tag{17}$$

The final QCD result for the two-loop $\overline{\text{MS}}$ diquark renormalization constant is

$$Z_d = 1 + \frac{\alpha}{\pi}\left[\frac{3-\xi}{6\epsilon}\right] + \left(\frac{\alpha}{\pi}\right)^2\left[\frac{1}{\epsilon}\left(\frac{1671 - 40n_f}{2880} - \frac{17\xi}{80} - \frac{29\xi^2}{960}\right) + \frac{1}{\epsilon^2}\left(\frac{234 - 12n_f}{288} - \frac{17\xi}{96} - \frac{5\xi^2}{288}\right)\right]. \tag{18}$$

The cancellation of the L/ϵ terms in Z_d that are generated by (14) provides another consistency check on our calculation. Note that the two-loop Landau gauge result does not uphold the one-loop ($\xi = 0$) pattern $Z_d = Z_m^{1/2}$.

The anomalous dimension for the diquark operator defined by

$$\gamma_d = \frac{\nu}{Z_d}\frac{\mathrm{d}Z_d}{\mathrm{d}\nu} \tag{19}$$

is easily extracted from (18) to obtain the two-loop $\overline{\text{MS}}$ QCD anomalous dimension for the diquark operator:

$$\gamma_d(\alpha) = \gamma_1\frac{\alpha}{\pi} + \gamma_2\left(\frac{\alpha}{\pi}\right)^2, \tag{20}$$

$$\gamma_1 = 1 - \frac{\xi}{3}, \qquad \gamma_2 = \frac{1671 - 40n_f}{720} - \frac{17\xi}{20} - \frac{29\xi^2}{240}. \tag{21}$$

In the extraction of the anomalous dimension we have verified that the two-loop coefficients of Z_d

$$Z_d = 1 + \frac{Z_{d,1}}{\epsilon} + \frac{Z_{d,2}}{\epsilon^2} + \cdots \tag{22}$$

satisfy the renormalization-group constraint

$$2\alpha \frac{\partial Z_{d,2}}{\partial \alpha} = \left[\gamma_d(\alpha) - \beta(\alpha)\alpha \frac{\partial}{\partial \alpha} - \delta(\alpha, \xi)\xi \frac{\partial}{\partial \xi} \right] Z_{d,1}, \tag{23}$$

where we are working in the conventions of [20] with the (one-loop) β function and anomalous dimension δ of the gauge parameter given by

$$\beta(\alpha) = \beta_1 \frac{\alpha}{\pi}, \qquad \beta_1 = -\frac{11}{2} + \frac{n_f}{3} \tag{24}$$

$$\delta(\alpha, \xi) = \delta_1 \frac{\alpha}{\pi}, \qquad \delta_1 = \frac{1}{4}(13 - 3\xi) - \frac{n_f}{3}. \tag{25}$$

Confirmation of this renormalization-group constraint provides another verification of the accuracy of our results given in table 1.

4. Application and conclusions

It has previously been noted that at leading order, the renormalization scale dependence cancels between the QCD perturbative contributions to the diquark decay constants and the $\Delta S = 1$ effective weak Hamiltonian, although there remains some residual scale dependence from non-perturbative terms [14]. As an application of our two-loop results, we can explore this scale dependence at next-to-leading order. Following [14], we consider the combination

$$c_-(\mu) g_+(\mu) g_+(\mu), \tag{26}$$

where $c_-(\mu)$ represents the renormalization scale dependence of the Wilson coefficient in the $\Delta S = 1$ effective weak Hamiltonian [23] and $g_+(\mu)$ is the scale-dependent scalar diquark decay constant emerging from QCD sum-rules [14]. The renormalization-group (RG) factor arising from c_- is [23]

$$c_-(\mu) \sim \exp\left[-\int \frac{\gamma_-(\alpha)}{\beta(\alpha)} \frac{\mathrm{d}\alpha}{\alpha} \right], \tag{27}$$

where in the normal dimensional regularization scheme with $n_f = 3$, the anomalous dimension $\gamma_-(\alpha)$ is[3]

$$\gamma_-(\alpha) = \tilde{\gamma}_1 \frac{\alpha}{\pi} + \tilde{\gamma}_2 \left(\frac{\alpha}{\pi} \right)^2 \tag{28}$$

$$\tilde{\gamma}_1 = -2, \qquad \tilde{\gamma}_2 = -\frac{50}{48}. \tag{29}$$

Similarly, the anomalous dimension for the diquark operator leads to the following RG factor for the (scalar) diquark decay constants:

$$g_+(\mu) g_+(\mu) \sim \exp\left[-2 \int \frac{\gamma_d(\alpha)}{\beta(\alpha)} \frac{\mathrm{d}\alpha}{\alpha} \right]. \tag{30}$$

As mentioned above, QCD sum-rule calculations with diquark currents extract gauge-invariant information from the two-point correlation function through the insertion of a Schwinger string,

[3] Note that we have converted the expressions in [23] into our conventions.

which becomes trivial for a line geometry in Landau gauge [12]. Thus for applications to RG behaviour of the diquark decay constants, we use (21) with $n_f = 3$ and $\xi = 0$:

$$\gamma_1 = 1, \qquad \gamma_2 = \tfrac{517}{240}. \tag{31}$$

The resulting RG behaviour of (26) is

$$c_-(\mu)g_+(\mu)g_+(\mu) \sim \exp\left[\int \frac{4}{9}\frac{\left[1+\frac{\tilde{\gamma}_2}{\tilde{\gamma}_1}\frac{\alpha}{\pi}\right]}{\left[1+\frac{\beta_2}{\beta_1}\frac{\alpha}{\pi}\right]}\frac{\mathrm{d}\alpha}{\alpha}\right]\exp\left[-\int \frac{4}{9}\frac{\left[1+\frac{\gamma_2}{\gamma_1}\frac{\alpha}{\pi}\right]}{\left[1+\frac{\beta_2}{\beta_1}\frac{\alpha}{\pi}\right]}\frac{\mathrm{d}\alpha}{\alpha}\right]$$
$$= 1 - \frac{98}{135}\frac{\alpha(\mu)}{\pi}. \tag{32}$$

Thus the leading-order cancellation of scale dependence in (26) for the perturbative contributions to g_+ does not persist to second order. However, the residual scale dependence associated with (32), which decreases with increasing $\alpha(\mu)$, does have the right qualitative behaviour to counter the residual scale dependence encountered in [14]. A more detailed analysis of the residual scale dependence is beyond the scope of this paper because it would require a full next-order sum-rule analysis of the diquark decay constants.

In conclusion, we have determined the $\overline{\mathrm{MS}}$ renormalization constant and associated anomalous dimension for the scalar diquark operator at two-loop order in QCD in an arbitrary covariant gauge for normal dimensional regularization. This result enables future QCD sum-rule studies of diquarks to higher orders in perturbation theory. For example, the divergent terms in the diquark renormalization constant (18) combined with lower-loop terms $\mathcal{O}(\epsilon)$ and $\mathcal{O}(\epsilon^2)$ generate finite parts corresponding to renormalization-induced physical contributions to the diquark correlation function. Furthermore, the anomalous dimension of the diquark operator appearing in the renormalization-group equation governing scale dependence of the diquark correlation function is an essential feature of QCD Laplace sum-rule analyses [24]. Given the relative size of the one- and two-loop terms in (18) and (31), these renormalization-induced and anomalous dimension effects could be significant in higher-loop extensions of [14].

Acknowledgments

We are grateful for financial support from the Natural Sciences and Engineering Research Council of Canada (NSERC). We thank John Dixon and Derek Harnett for valuable discussions.

References

[1] Jaffe R L 1977 *Phys. Rev.* D **15** 267
[2] Weinstein J D and Isgur N 1982 *Phys. Rev. Lett.* **48** 659
[3] Fariborz A H, Jora R and Schechter J 2009 *Phys. Rev.* D **79** 074014
Black D, Fariborz A H, Sannino F and Schechter J 1999 *Phys. Rev.* D **59** 074026
[4] 't Hooft G, Isidori G, Maiani L, Polosa A D and Riquer V 2008 *Phys. Lett.* B **662** 424
[5] Forkel H 2010 *Phys. Lett.* B **694** 252
[6] Narison S and Veneziano G 1989 *Int. J. Mod. Phys.* A **4** 2751
Amsler C and Close F E 1996 *Phys. Rev.* D **53** 295 (http://prd.aps.org/abstract/PRD/v53/i1/p295_1)
Burakovsky L and Page P R 1999 *Phys. Rev.* D **59** 014022
Minkowski P and Ochs W 1999 *Eur. Phys. J.* C **9** 283 (www.springerlink.com/content/k29dcfbt3v6jt9vb/)
Fariborz A H 2006 *Phys. Rev.* D **74** 054030
[7] Choi S-K *et al* (Belle Collaboration) 2003 *Phys. Rev. Lett.* **91** 262001
Acosta D *et al* (CDF II Collaboration) 2004 *Phys. Rev. Lett.* **93** 072001
Abazov V M *et al* (D0 Collaboration) 2004 *Phys. Rev. Lett.* **93** 162002

Aubert B *et al* (BaBar Collaboration) 2005 *Phys. Rev.* D **71** 071103
[8] Aubert B *et al* (BaBar Collaboration) 2005 *Phys. Rev. Lett.* **95** 142001
[9] Maiani L, Piccinini F, Polosa A D and Riquer V 2005 *Phys. Rev.* D **71** 014028
Maiani L, Riquer V, Piccinini F and Polosa A D 2005 *Phys. Rev.* D **72** 031502
[10] Anselmino M, Predazzi E, Ekelin S, Fredriksson S and Lichtenberg D B 1993 *Rev. Mod. Phys.* **65** 1199
[11] Jaffe R L 2005 *Phys. Rep.* **409** 1
[12] Dosch H G, Jamin M and Stech B 1989 *Z. Phys.* C **42** 167
[13] Zhang A, Huang T and Steele T G 2007 *Phys. Rev.* D **76** 036004
[14] Jamin M and Neubert M 1990 *Phys. Lett.* B **238** 387
[15] Binosi D and Theußl L 2004 *Comput. Phys. Commun.* **161** 76
[16] Dixon J A and Taylor J C 1974 *Nucl. Phys.* B **78** 552
Kluberg-Stern H and Zuber J B 1975 *Phys. Rev.* D **12** 467
[17] Chanowitz M S, Furman M and Hinchliffe I 1979 *Nucl. Phys.* B **159** 225
[18] 't Hooft G and Veltman M J G 1972 *Nucl. Phys.* B **44** 189
[19] Akyeampong D A and Delbourgo R 1973 *Nuovo Cimento* A **17** 578
[20] Pascual P and Tarrach R 1984 *QCD: Renormalization for the Practitioner* (New York: Springer)
[21] Egoryan E Sh and Tarasov O V 1979 *Theor. Math. Phys.* **41** 863
[22] Tarrach R 1981 *Nucl. Phys.* B **183** 384
[23] Buras A J and Weisz P H 1990 *Nucl. Phys.* B **333** 66
[24] Narison S and de Rafael E 1981 *Phys. Lett.* B **103** 57

Chapter 6

Mixing of Scalar Gluonium and Quark Mesons

6.1 Introduction

The research in this chapter is based upon the publication:

- D. Harnett, R.T. Kleiv, K. Moats and T.G. Steele, Near-maximal mixing of scalar gluonium and quark mesons: a Gaussian sum-rule analysis, Nucl. Phys. A850 (2011) 110.

The publication above (Ref. [59]) explores mixing between scalar $\left(J^{PC} = 0^{++}\right)$ glueballs and quark mesons. As described in Chapter 1, glueballs (or gluonia) are hadrons that are composed entirely of gluons. The scalar glueball is predicted to be the lightest glueball, with a mass in the range of approximately $1.0 - 1.7\,\text{GeV}$. The heavy quarkonium-like states have masses in the range $3.8 - 4.7\,\text{GeV}$, therefore the research in this chapter is not directly relevant to the heavy quarkonium-like states. Rather, the research in this chapter is related to the problem of the light scalar mesons. Below $2.0\,\text{GeV}$, there are too many hadrons with $J^{PC} = 0^{++}$ to be explained in terms of conventional mesons. It is widely suspected that some of these supernumerary states could be exotic hadrons, with the scalar glueball among them. The research in this chapter considers the possibility that some of the light scalars could be mixtures of a glueball and a conventional quark meson. Refs. [87, 96] review the current experimental and theoretical status of glueballs.

6.2 Results

The emphasis of this chapter is on the field-theoretic aspects of the publication above. As mentioned in Chapter 1, multiple currents may couple to a single hadronic state. For instance, consider a state $|h\rangle$ that couples to both scalar meson and glueball currents:

$$\langle\Omega|J_q|h\rangle \neq 0\,, \quad \langle\Omega|J_g|h\rangle \neq 0\,. \tag{6.1}$$

Hadrons that couple to multiple currents can be studied within QSR using non-diagonal correlation functions. In this case the non-diagonal correlation function contains scalar glueball and quark meson currents

$$\Pi_{gq}\left(Q^2\right) = i\int d^4x\, e^{iq\cdot x}\,\langle\Omega|T\left[\, J_g\left(x\right) J_q\left(0\right)\,\right]|\Omega\rangle\,, \quad Q^2 = -q^2\,, \tag{6.2}$$

$$J_q = m_q\left(\bar{u}u + \bar{d}d\right)\,, \quad J_g = \alpha G^2\,, \quad G^2 = G^a_{\mu\nu}G^{\mu\nu}_a\,. \tag{6.3}$$

This correlation function can be calculated using the perturbative expansion (1.19) and the OPE (1.99) as usual. However, the leading order contribution to the perturbative Wilson coefficient contains a non-local divergence. Because this divergence arises at leading order, it cannot be canceled through a multiplicative renormalization.

This problem can be solved by considering the renormalization of the composite operator representing the scalar glueball current, which mixes with the scalar meson current under renormalization. The renormalized scalar glueball operator is given by

$$G^2_R = \left[1 + \frac{1}{\epsilon}\frac{\alpha}{\pi}\left(\frac{11}{4} - \frac{n_f}{6}\right)\right] G^2_B - \frac{4}{\epsilon}\frac{\alpha}{\pi}\left[m_u\bar{u}u + m_d\bar{d}d\right]_B\,, \tag{6.4}$$

where n_f is the number of quark flavours and the subscripts R and B denote renormalized and bare quantities, respectively. [97, 89]. The renormalized scalar glueball operator must be used in order to renormalize the non-diagonal correlation function (6.3). Note the appearance of the second term in Eq. (6.4) which is divergent and proportional to the scalar meson current. This arises due to operator mixing and must be included in the QSR analysis. This term amounts to a renormalization-induced contribution to the non-diagonal correlation

function, and serves to precisely cancel the non-local divergence that appears in the bare non-diagonal correlation function. The renormalized non-diagonal correlation function is free of divergences, as it must be. This represents the perturbative contribution to the OPE of the non-diagonal correlation function (6.3), and hence represents purely perturbative contributions to the mixing between scalar mesons and gluonia.

The research presented in this chapter emphasizes the renormalization methodology used in QSR analyses. In particular, the composite local operators used to represent currents that probe hadronic states can mix under renormalization. Divergent terms that appear at leading order in the expansion of Wilson coefficients cannot be renormalized multiplicatively and hence must be due to operator mixing. Conversely, when divergent terms appear in higher order terms in the Wilson coefficients, such as in Chapter (4) they can be removed through a multiplicative renormalization. In both cases renormalization-induced contributions are generated and must be included. The loop integration techniques developed in Chapter 2 are needed in order to perform these calculations. In addition, the techniques used here have been extended to investigate mixing effects among the heavy quarkonium-like states [32].

6.3 Published Article

The scalar glueball and quark meson mixing paper was published in Nuclear Physics A in 2011. The paper is presented on the following pages in the journal format.

- D. Harnett, R.T. Kleiv, K. Moats and T.G. Steele, Near-maximal mixing of scalar gluonium and quark mesons: a Gaussian sum-rule analysis, Nucl. Phys. A850 (2011) 110.

Available online at www.sciencedirect.com
ScienceDirect
Nuclear Physics A 850 (2011) 110–135
NUCLEAR PHYSICS A
www.elsevier.com/locate/nuclphysa

Near-maximal mixing of scalar gluonium and quark mesons: A Gaussian sum-rule analysis

D. Harnett [a], R.T. Kleiv [b], K. Moats [c], T.G. Steele [b,*]

[a] *Department of Physics, University of the Fraser Valley, Abbotsford, BC, V2S 7M8, Canada*
[b] *Department of Physics and Engineering Physics, University of Saskatchewan, Saskatoon, SK, S7N 5E2, Canada*
[c] *Department of Physics, Carleton University, Ottawa, ON, K1S 5B6, Canada*

Received 6 June 2008; received in revised form 9 November 2010; accepted 13 December 2010

Available online 17 December 2010

Abstract

Gaussian QCD sum-rules are ideally suited to the study of mixed states of gluonium (glueballs) and quark ($q\bar{q}$) mesons because of their capability to resolve widely-separated states of comparable strength. The analysis of the Gaussian QCD sum-rules (GSRs) for all possible two-point correlation functions of gluonic and non-strange ($I = 0$) quark scalar ($J^{PC} = 0^{++}$) currents is discussed. For the non-diagonal sum-rule of gluonic and $q\bar{q}$ currents we show that perturbative and gluon condensate contributions are chirally suppressed compared to non-perturbative effects of the quark condensate, mixed condensate, and instantons, implying that the mixing of quark mesons and gluonium is of non-perturbative origin. The independent predictions of the masses and relative coupling strengths from the non-diagonal and the two diagonal GSRs are remarkably consistent with a scenario of two states with masses of approximately 1 GeV and 1.4 GeV that couple to significant mixtures of quark and gluonic currents. The mixing is nearly maximal with the heavier mixed state having a slightly larger coupling to gluonic currents than the lighter state.

Keywords: Gluonium; Glueballs; QCD sum-rules

1. Introduction

The interpretation of the nature of the lightest scalar mesons is one of the most fascinating problems in hadronic physics. The plethora of scalar ($J^{PC} = 0^{++}$) states below 2 GeV [1] can-

* Corresponding author.
E-mail address: tom.steele@usask.ca (T.G. Steele).

0375-9474/$ – see front matter
doi:10.1016/j.nuclphysa.2010.12.005

not be described by a simple $q\bar{q}$ nonet, a situation indicative of exotic states such as gluonium (glueballs) or multi-quark ($q\bar{q}q\bar{q}$) states amongst the known scalar mesons. In the gluonium scenario, two-body decays to pseudoscalars suggest that the $f_0(1370)$, $f_0(1500)$ and $f_0(1710)$ contain strong mixtures of gluonium and $q\bar{q}$ mesons [2], with the $f_0(1500)$ favoured as the dominant glueball state [3]. Analyses based on chiral Lagrangians [4,5] suggest that the $f_0(1500)$ and $f_0(1710)$ are mainly gluonium states with a small gluonium component of the $f_0(980)$ [4]. Other phenomenological approaches present a scenario of mixing between a 1 GeV glueball and the $f_0(980)$, $f_0(1500)$ states of a $q\bar{q}$ nonet [6]. Lattice QCD calculations lead to a scalar gluonium state of approximately 1.6 GeV with quenched quarks [7]. However, with dynamical quarks the mixing with $q\bar{q}$ states appears to be very strong, driving the mass of the lightest flavour-singlet meson down toward 1 GeV with tentative identification of an excited state on the order of 1.5 GeV [8]. The vast literature on mixing of gluonia in QCD sum-rules is reviewed in detail in [9]. The key findings of QCD Laplace sum-rules are that admixtures of scalar gluonium and $q\bar{q}$ ($I = 0$) states exist with masses of approximately 1 GeV and 1.6 GeV [9–12], a conclusion that is also upheld by studies based on Gaussian QCD sum-rules [13–15]. In particular, the mixing that results from QCD sum-rules is very large [9,10], with comparable couplings of these states to gluonic and $q\bar{q}$ currents [13–15].

The results of these different approaches suggest that a consistent scenario of $q\bar{q}$–gluonium mixing is manifested in the scalar hadronic spectrum as two states on the order of 1 GeV and 1.5 GeV that couple to a significant mixture of $q\bar{q}$ and gluonium currents. From both the QCD sum-rule and lattice perspectives, this implies that the non-diagonal correlation function between $q\bar{q}$ and gluonic currents must be large enough to describe this behaviour. However, perturbative contributions to the non-diagonal correlation function (and hence mixing between gluonium and quark mesons) are chirally suppressed [16–19]. Non-diagonal correlation functions have been analyzed in detail for pseudoscalar gluonium leading to a small mixing angle even in the presence of chiral-violating condensates [16]; given the similarities in field-theoretical structure between the scalar and pseudoscalar channels, a similarly small mixing angle in the scalar channel seems unavoidable [16,19]. However, the mixed condensate effects, which are zero at leading order in the pseudoscalar channel [16], are shown below to be non-zero for the scalar channel providing a scale for large mixing. In addition, we consider instanton effects in our analysis; such effects have been argued to be essential for studies of gluonium [20]. As will be seen below (and as argued in [21] for glueball decays), the full inclusion of chiral-violating effects of QCD condensates and instantons provide the dominant contributions to the non-diagonal correlator in the scalar channel. These chiral-violating effects in the non-diagonal correlator are essential for a self-consistent scenario of two states coupling to a strong (near maximal) mixture of gluonium and $q\bar{q}$ currents; this scenario emerges from all possible correlation functions of gluonic and $q\bar{q}$ quark currents (i.e., diagonal gluonic, diagonal $q\bar{q}$, non-diagonal gluonic–$q\bar{q}$).

The formulation and analysis of Gaussian sum-rules is reviewed in Section 2. In Section 3 the leading-order perturbative, QCD condensate, and instanton contributions to the non-diagonal correlation function of $q\bar{q}$ and gluonic currents are calculated along with the associated Gaussian QCD sum-rules. The analysis of the Gaussian sum-rules and the pattern of state coupling mixing is then presented in Section 4.

2. Review of Gaussian sum-rules

Gaussian sum-rules associated with QCD two-point correlation functions have been shown to be sensitive to the hadronic spectral functions over a broad energy range, and analysis techniques

have been developed to exploit this dependence to determine how resonance strength is distributed in the spectral function [13–15]. Thus Gaussian sum-rules are well-suited to situations such as $q\bar{q}$–gluonium mixing where multiple hadronic states could contribute to a correlation function.

The ($k = 0$) Gaussian sum-rule (GSR), introduced in [22], is given by

$$G_0(\hat{s},\tau) = \frac{1}{\sqrt{4\pi\tau}} \int_{t_0}^{\infty} \exp\left[\frac{-(t-\hat{s})^2}{4\tau}\right] \frac{1}{\pi}\rho(t)\,\mathrm{d}t, \quad \tau > 0 \tag{1}$$

and relates a QCD calculation $G_0(\hat{s},\tau)$ to a weighted integral of its associated hadronic spectral function $\rho(t)$ from its threshold t_0. The Gaussian kernel peaked at $t = \hat{s}$ smears the spectral function through an (approximate) interval $\hat{s} - 2\sqrt{\tau} \leqslant t \leqslant \hat{s} + 2\sqrt{\tau}$. This smearing provides a clear conceptual implementation of quark-hadron duality. The width of this duality interval is constrained from below by QCD because renormalization-group improvement of $G_0(\hat{s},\tau)$ sets the renormalization scale ν through $\nu^2 = \sqrt{\tau}$ [14,22]; therefore it is not possible to achieve the formal $\tau \to 0$ limit where complete knowledge of the spectral function could be obtained through

$$\lim_{\tau\to 0} G_0(\hat{s},\tau) = \frac{1}{\pi}\rho(\hat{s}), \quad \hat{s} > t_0. \tag{2}$$

In contrast, the variable $\hat{s}$ in (1) is unconstrained by QCD and can be varied to probe excited and ground states with similar sensitivity. Any features of the spectral function strong enough to be isolated from the continuum will be revealed through the GSR. This behaviour should be compared to that of the Laplace sum-rules

$$R\big(\Delta^2\big) = \int_{t_0}^{\infty} \exp\left(-\frac{t}{\Delta^2}\right) \frac{1}{\pi}\rho(t)\,\mathrm{d}t \tag{3}$$

which exponentially suppress excited states relative to the ground state.[1]

Sum-rules analyses start from the calculation of an appropriate QCD correlation function of renormalized composite operators. We focus on two-point functions of scalar operators J_1 and J_2

$$\Pi\big(Q^2\big) = \mathrm{i}\int \mathrm{d}^4x\, \mathrm{e}^{\mathrm{i}q\cdot x}\langle 0|T\big[J_1(x)J_2(0)\big]|0\rangle, \qquad Q^2 \equiv -q^2 \tag{4}$$

where J_1 and J_2 can be the same (diagonal) or different (non-diagonal). The correlator (4) is related to a hadronic spectral function $\rho(t)$ through a dispersion relation with a number of subtraction constants. For example, in the diagonal scalar gluonic case, we have

$$\Pi\big(Q^2\big) - \Pi(0) - Q^2\Pi'(0) - \frac{1}{2}Q^4\Pi''(0) = -\frac{Q^6}{\pi}\int_{t_0}^{\infty} \frac{\rho(t)}{t^3(t+Q^2)}\,\mathrm{d}t. \tag{5}$$

Unknown subtraction constants and field-theoretical divergences can be eliminated by constructing the GSRs[2]

[1] The configuration–space correlation function in (4) as used in lattice QCD involves exponential suppression of excited states similar to that occurring for Laplace sum-rules.

[2] This definition is a natural generalization of that given in [22]. To recover the original GSR, we simply let $k = 0$ in (6).

$$G_k(\hat{s},\tau) \equiv \sqrt{\frac{\tau}{\pi}}\mathcal{B}\left\{\frac{(\hat{s}+\mathrm{i}\Delta)^k \Pi(-\hat{s}-\mathrm{i}\Delta) - (\hat{s}-\mathrm{i}\Delta)^k \Pi(-\hat{s}+\mathrm{i}\Delta)}{\mathrm{i}\Delta}\right\} \tag{6}$$

where $k \in \{-1, 0, 1, \ldots\}$ and where the Borel transform $\mathcal{B}$ is defined by

$$\mathcal{B} \equiv \lim_{\substack{N,\Delta^2\to\infty \\ \Delta^2/N\equiv 4\tau}} \frac{(-\Delta^2)^N}{\Gamma(N)}\left(\frac{\mathrm{d}}{\mathrm{d}\Delta^2}\right)^N. \tag{7}$$

Applying (6) to (5) yields the following one-parameter family of GSRs (see [13] for further details):

$$G_k(\hat{s},\tau) + \delta_{k,-1}\frac{1}{\sqrt{4\pi\tau}}\exp\left(\frac{-\hat{s}^2}{4\tau}\right)\Pi(0) = \frac{1}{\sqrt{4\pi\tau}}\int_{t_0}^{\infty} t^k \exp\left[\frac{-(\hat{s}-t)^2}{4\tau}\right]\frac{1}{\pi}\rho(t)\,\mathrm{d}t. \tag{8}$$

Note that the $k=-1$ sum-rule can only be used in situations where there exists an appropriate low-energy theorem from which we can determine the subtraction constant $\Pi(0)$. Such is the case, for instance, with the diagonal scalar gluonic two-point function [18].

On the right-hand side of (8), we impose a fairly general resonance(s) plus continuum model

$$\rho(t) = \rho^{\mathrm{had}}(t) + \theta(t-s_0)\,\mathrm{Im}\,\Pi^{\mathrm{QCD}}(t) \tag{9}$$

where s_0 represents the onset of the QCD continuum. The resulting continuum contribution

$$G_k^{\mathrm{cont}}(\hat{s},\tau,s_0) = \frac{1}{\sqrt{4\pi\tau}}\int_{s_0}^{\infty} t^k \exp\left[\frac{-(\hat{s}-t)^2}{4\tau}\right]\frac{1}{\pi}\,\mathrm{Im}\,\Pi^{\mathrm{QCD}}(t)\,\mathrm{d}t \tag{10}$$

is then moved to the left-hand side of (8). The total QCD contribution

$$G_k^{\mathrm{QCD}}(\hat{s},\tau,s_0) \equiv G_k(\hat{s},\tau) - G_k^{\mathrm{cont}}(\hat{s},\tau,s_0) \tag{11}$$

then satisfies

$$\begin{aligned} &G_k^{\mathrm{QCD}}(\hat{s},\tau,s_0) + \delta_{k,-1}\frac{1}{\sqrt{4\pi\tau}}\exp\left(\frac{-\hat{s}^2}{4\tau}\right)\Pi(0) \\ &\quad = \frac{1}{\sqrt{4\pi\tau}}\int_{t_0}^{\infty} t^k \exp\left[\frac{-(\hat{s}-t)^2}{4\tau}\right]\frac{1}{\pi}\rho^{\mathrm{had}}(t)\,\mathrm{d}t. \end{aligned} \tag{12}$$

Integrating both sides of (12) with respect to $\hat{s}$ gives

$$\int_{-\infty}^{\infty} G_k^{\mathrm{QCD}}(\hat{s},\tau,s_0)\,\mathrm{d}\hat{s} + \delta_{k,-1}\Pi(0) = \int_{t_0}^{\infty} t^k \frac{1}{\pi}\rho^{\mathrm{had}}(t)\,\mathrm{d}t, \tag{13}$$

in which the right-hand side is recognized as the kth member of the finite-energy sum-rule (FESR) family. Thus, the information contained in the GSRs which is independent of the FESRs can be isolated by considering the *normalized* Gaussian sum-rules (NGSRs) [14]

$$N_k^{\rm QCD}(\hat{s},\tau,s_0)=\frac{G_k^{\rm QCD}(\hat{s},\tau,s_0)+\delta_{k,-1}\frac{1}{\sqrt{4\pi\tau}}\exp\left(\frac{-\hat{s}^2}{4\tau}\right)\Pi(0)}{M_{k,0}(\tau,s_0)+\delta_{k,-1}\Pi(0)}, \tag{14}$$

$$M_{k,n}(\tau,s_0)=\int_{-\infty}^{\infty}\hat{s}^n G_k^{\rm QCD}(\hat{s},\tau,s_0)\,{\rm d}\hat{s} \tag{15}$$

which are related to the hadronic spectral function via

$$N_k^{\rm QCD}(\hat{s},\tau,s_0)=\frac{\frac{1}{\sqrt{4\pi\tau}}\int_{t_0}^{\infty}t^k\exp\left[\frac{-(\hat{s}-t)^2}{4\tau}\right]\rho^{\rm had}(t)\,{\rm d}t}{\int_{t_0}^{\infty}t^k\rho^{\rm had}(t)\,{\rm d}t}. \tag{16}$$

For diagonal correlation functions the spectral function obeys a positivity constraint so the NGSR must exist. For non-diagonal correlators the possibility of state mixing implies that $\rho^{\rm had}(t)$ could change sign, so it is possible that either $M_{k,0}(\tau,s_0)$ or the denominator on the right-hand sides of (14) or (16) could be zero. In such situations, the GSRs would have to be analyzed instead of the NGSRs.

We next consider the currents that will be used to probe the gluonic and $q\bar{q}$ aspects of the scalar hadronic states. Refs. [10,23] argue eloquently that the mixing of $q\bar{q}$ mesons and gluonium is unavoidable because of the trace anomaly for the energy–momentum tensor $T_{\mu\nu}$ [24]

$$T^{\mu}_{\mu}=\frac{1}{4}\beta(\alpha)G^a_{\mu\nu}G^{a\mu\nu}+\left[1+\gamma(\alpha)\right]\sum_f m_f\bar{\psi}_f\psi_f \tag{17}$$

where

$$2\pi\alpha\beta(\alpha)=\nu^2\frac{\rm d}{{\rm d}\nu^2}\left(\frac{\alpha}{\pi}\right)=-\beta_0\left(\frac{\alpha}{\pi}\right)^2-\beta_1\left(\frac{\alpha}{\pi}\right)^3+\cdots, \tag{18}$$

$$\beta_0=\frac{11}{4}-\frac{1}{6}n_f,\qquad \beta_1=\frac{51}{8}-\frac{19}{24}n_f, \tag{19}$$

$$-2m\gamma(\alpha)=\nu^2\frac{{\rm d}m}{{\rm d}\nu^2}. \tag{20}$$

Eq. (17) actually contains *two* multiplicatively-renormalizable (renormalization-group invariant) composite operators: $m\bar{\psi}\psi$ and $\beta G^2+4\gamma m\bar{\psi}\psi$. From a strictly field theoretical perspective, both are suitable choices for currents. However, the gluonic and/or $q\bar{q}$ nature of states which couple to the current $\beta G^2+4\gamma m\bar{\psi}\psi$ would be difficult to disentangle. As such, we instead follow [16] and use renormalized currents

$$J_g=\alpha G^2,\qquad G^2_R=\left(1+\frac{\beta_0}{\epsilon}\frac{\alpha}{\pi}\right)G^2_B-4\frac{\alpha}{\pi}\frac{1}{\epsilon}(m_u\bar{u}u+m_d\bar{d}d)_B+\cdots, \tag{21}$$

$$J_q=m_q(\bar{u}u+\bar{d}d),\qquad m_q=\frac{1}{2}(m_u+m_d), \tag{22}$$

where R denotes a renormalized composite operator and B denotes bare quantities. Our convention for dimensional regularization uses $D=4+2\epsilon$ spacetime dimensions. Of course the form of the renormalized operator (21) necessarily underlies the renormalization-group invariance of the trace anomaly (17) (see e.g. [25]). However, the advantage of the current J_g is that its tree-level expansion is purely gluonic allowing a qualitative separation of gluonic and $q\bar{q}$ degrees of freedom. Note that the use of a scalar tri-gluonium current, with three factors of the field strength

rather than two as in (21), does not seem to couple to the lightest state and mixes weakly [26]. The non-strange current J_q has isospin $I = 0$ and is renormalization-group invariant.

We define diagonal correlators corresponding to (21) and (22) as follows:

$$\Pi_{gg}\big(Q^2\big) = \mathrm{i}\int \mathrm{d}^4x\, \mathrm{e}^{\mathrm{i}q\cdot x}\langle 0|T\big[J_g(x)J_g(0)\big]|0\rangle, \tag{23}$$

$$\Pi_{qq}\big(Q^2\big) = \mathrm{i}\int \mathrm{d}^4x\, \mathrm{e}^{\mathrm{i}q\cdot x}\langle 0|T\big[J_q(x)J_q(0)\big]|0\rangle \tag{24}$$

where $Q^2 \equiv -q^2$. Although both correlation functions are probes of scalar mesons, those states which have a more significant overlap with the gluonic current should predominate in (23); those states which are dominantly of a non-strange quark ($q\bar{q}$) nature should be more significant in (24). A mixed state with substantial gluonic and quark components (i.e., a state that couples to both the gluonic and quark currents) should self-consistently appear in an analysis of both correlation functions. In particular, independent predictions of identical-mass states from QCD sum-rule analyses of both (23) and (24) would be indicative of mixing. Note that the currents are simply probes of the actual hadronic spectrum and do not impose a particular interpretation on the states: any state that has non-strange $\bar{q}q$ content would be probed by J_q, and any state with gluonic content would be probed by J_g regardless of any additional content (e.g., $s\bar{s}$) in the states.

In the scalar gluonic channel, a low-energy theorem (LET) [18]

$$\Pi_{gg}(0) \equiv \lim_{Q^2\to 0}\Pi_{gg}\big(Q^2\big) = \frac{8\pi}{\beta_0}\langle\alpha G^2\rangle \tag{25}$$

allows construction of the $k = -1$ GSR. The significance of instanton contributions in the overall consistency of the LET-sensitive $k = -1$ sum-rule and the LET-insensitive $k \geqslant 0$ sum-rules was first demonstrated for Laplace sum-rules [27,28]. A similar consistency is observed for Gaussian sum-rules, but theoretical uncertainties are better controlled in the $k \geqslant 0$ GSRs [13]; hence, we focus here on the $k = 0$ GSRs for both the diagonal gluonic and quark channels. QCD expressions for the GSRs $G_0^{(gg)}(\hat{s},\tau,s_0)$ and $G_0^{(qq)}(\hat{s},\tau,s_0)$ corresponding to the diagonal correlation functions (23), (24) can be found in [13,14].

3. Non-diagonal correlation function and GSRs of $q\bar{q}$ and gluonic currents

The non-diagonal correlation function for quark and gluonic currents

$$\Pi_{gq}\big(Q^2\big) = \mathrm{i}\int \mathrm{d}^4x\, \mathrm{e}^{\mathrm{i}q\cdot x}\langle 0|T\big[J_q(x)J_g(0)\big]|0\rangle, \qquad Q^2 \equiv -q^2, \tag{26}$$

contains perturbative, QCD condensate, and instanton contributions

$$\Pi_{gq}\big(Q^2\big) = \Pi_{gq}^{pert}\big(Q^2\big) + \Pi_{gq}^{cond}\big(Q^2\big) + \Pi_{gq}^{inst}\big(Q^2\big). \tag{27}$$

The leading-order perturbative diagrams that contribute to $\Pi_{gq}^{pert}(Q^2)$ are given in Fig. 1. The first diagram, a two-loop calculation, corresponds to the (bare) gluonic term in (21). The second, a one-loop calculation, corresponds to the (bare) quark term arising from composite-operator renormalization (i.e., it is a renormalization-induced diagram). Despite the differing

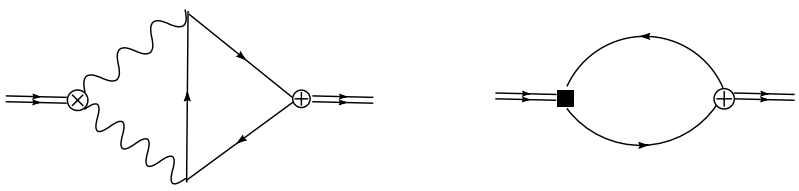

Fig. 1. Leading-order perturbative diagrams for the non-diagonal correlation function. The symbol $\otimes$ denotes the bare current αG_B^2 within J_g and $\oplus$ denotes the bare current J_q. In the second diagram, the solid square represents the $q\bar{q}$ term arising in the renormalization of J_g. The Feynman diagrams were drawn with JaxoDraw [29].

number of loops, both diagrams are $\mathcal{O}(\alpha^2)$.[3] Also, both diagrams have the same $\mathcal{O}(m_q^2)$ leading chiral behaviour because the quark loop in the first diagram provides a $\mathcal{O}(m_q)$ chiral suppression factor. The perturbative contributions can thus be separated into these bare and renormalization-induced diagrams

$$\Pi_{gq}^{pert}\big(Q^2\big) = \Pi_{gq}^{bare}\big(Q^2\big) + \Pi_{gq}^{renorm}\big(Q^2\big). \tag{28}$$

At leading chiral order in the $\overline{\text{MS}}$ scheme, the result for Π_{gq}^{bare} (corresponding to the two-loop diagram in Fig. 1) is

$$\Pi_{gq}^{bare}\big(Q^2\big) = \alpha^2 m_q^2\left[\frac{3Q^2L}{\pi^3}\frac{1}{\epsilon} + \frac{3Q^2L}{\pi^3}\left(L - \frac{35}{6}\right)\right], \quad L = \log\left(\frac{Q^2}{\nu^2}\right) \tag{29}$$

where ν is the renormalization scale. We have ignored non-logarithmic terms in (29) as they correspond to dispersion relation subtraction constants which are eliminated upon forming the GSRs. The $\frac{L}{\epsilon}$ term in (29) is problematic since it cannot be renormalized away or absorbed into a dispersion-relation subtraction constant. However, the leading chiral order contribution Π_{gq}^{renorm} arising from the one-loop renormalization-induced diagram of Fig. 1 is

$$\Pi_{gq}^{renorm} = -3m_q^2Q^2L\frac{\alpha^2}{\pi^3}\frac{1}{\epsilon} + 3m_q^2Q^2\frac{\alpha^2}{\pi^3}\left(-\frac{L^2}{2} + 2L\right) \tag{30}$$

where we have again ignored non-logarithmic terms. An important, but subtle, aspect in the calculation of Π_{gq}^{renorm} is retaining order ϵ contributions from the loop integrals that lead to finite terms when combined with the renormalization constant appearing in (21). This methodology is necessary and can be verified for well-known correlation functions (e.g., light-quark pseudoscalar currents). The offending $\frac{L}{\epsilon}$ term in (29) is thus cancelled by a compensating term in (30), and we are left with the leading-order $\overline{\text{MS}}$-scheme perturbative contribution to the non-diagonal correlation function[4]:

$$\Pi_{gq}^{pert}\big(Q^2\big) = m_q^2Q^2\big[A_0L + A_1L^2\big], \tag{31}$$

$$A_0 = -\frac{23}{2\pi}\left(\frac{\alpha}{\pi}\right)^2, \qquad A_1 = \frac{3}{2\pi}\left(\frac{\alpha}{\pi}\right)^2. \tag{32}$$

[3] Strange (and heavier) quarks originating from composite operator renormalization in (21) will be suppressed by an additional factor of α^2.

[4] The numerical coefficients in this result disagree with those presented in Ref. [16], although the overall chiral and logarithmic dependence is identical. We have checked our calculational methodology by verifying the pseudoscalar results in [16] and believe that (32) is correct.

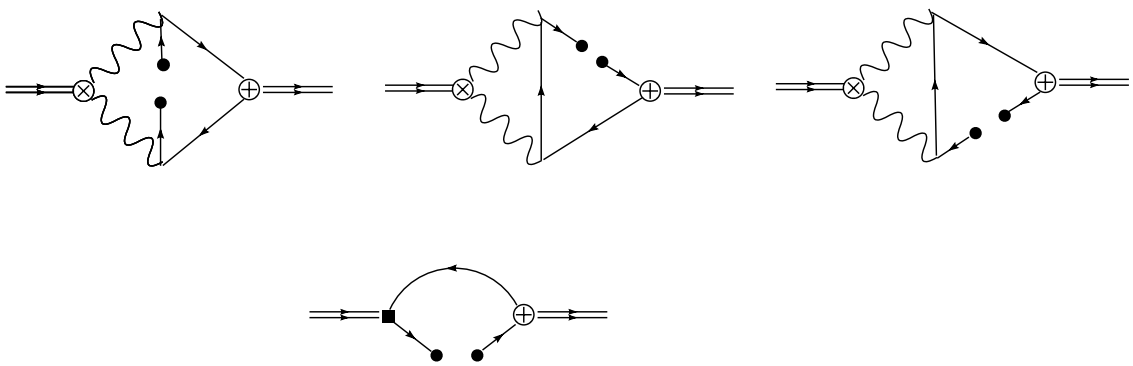

Fig. 2. Leading α order quark condensate diagrams for the non-diagonal correlation function. The solid circles on the quark lines denote insertion of plane-wave states or coordinate space vacuum expectation values for evaluation of the operator-product expansion coefficients. All other notations are identical to Fig. 1.

The QCD condensate contributions [30] to the non-diagonal correlator, including operators up to dimension-five, can be written as an operator-product expansion (OPE)

$$\Pi_{gq}^{cond}\big(Q^2\big) = C_{QQ}\langle\bar{q}q\rangle + C_{GG}\big\langle\alpha G^2\big\rangle + C_{QGQ}\langle\bar{q}\sigma Gq\rangle, \tag{33}$$

$$\langle\bar{q}q\rangle = \frac{1}{2}\langle\bar{u}u + \bar{d}d\rangle, \qquad \big\langle\alpha G^2\big\rangle = \big\langle\alpha G^a_{\mu\nu}G^{a\mu\nu}\big\rangle,$$

$$\langle\bar{q}\sigma Gq\rangle = \left\langle\bar{q}g\frac{\lambda^a}{2}\sigma^{\mu\nu}G^a_{\mu\nu}q\right\rangle. \tag{34}$$

As will be shown below, the chiral violating effects of the quark condensate $\langle\bar{q}q\rangle$ and mixed condensate $\langle\bar{q}\sigma Gq\rangle$ will dominate that of the gluon condensate $\langle\alpha G^2\rangle$. To obtain the leading chiral order behaviour of the OPE coefficients, it is necessary to include higher-order mass contributions that result in operator mixing [31,32]. In particular, the naively-calculated unmixed OPE coefficients E_{QQ}, E_{GG}, and E_{QGQ} are related to the coefficients in (33) by [31]

$$E_{QQ} = C_{QQ}, \qquad E_{QGQ} = C_{QGQ}, \tag{35}$$

$$C_{GG} = E_{GG} + \frac{1}{12\pi m_q}C_{QQ} - \frac{m_q}{2\pi}\log\left(\frac{m_q^2}{\nu^2}\right)C_{QGQ}. \tag{36}$$

In principle, the coefficient of the identity operator (i.e., perturbative contributions) also mix with the quark condensate coefficients, but such terms are proportional to $m_q^3 C_{QQ}$ and are therefore sub-leading in the quark mass compared with (32).

The quark condensate contribution to the non-diagonal correlator is easily calculated to leading chiral order using any of the equivalent methods for evaluating OPE coefficients [33]. As in the perturbative case, in principle there are two classes of diagrams, both of which are depicted in Fig. 2. However, the renormalization-induced diagram of Fig. 2 is chirally-suppressed relative to (37) and so represents subleading effects. Computing the first set of diagrams in Fig. 2 therefore gives the leading-order quark-condensate contributions

$$C_{QQ} = -\frac{8}{\pi}\alpha^2 m_q \log\left(\frac{Q^2}{\nu^2}\right). \tag{37}$$

Fig. 3 shows two of the diagrams that contribute to the mixed condensate OPE coefficient. Within fixed-point gauge methods, the two-quark vacuum expectation value appearing in the

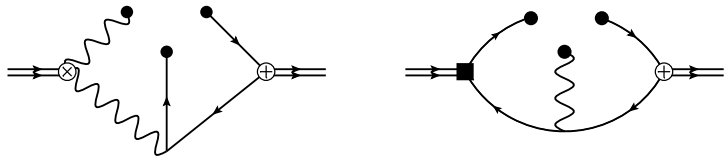

Fig. 3. Leading-order mixed condensate diagrams for the non-diagonal correlation function. The solid circles on the quark lines denote insertion of plane-wave states or coordinate space vacuum expectation values for evaluation of the operator-product expansion coefficients. All other notations are identical to Fig. 1.

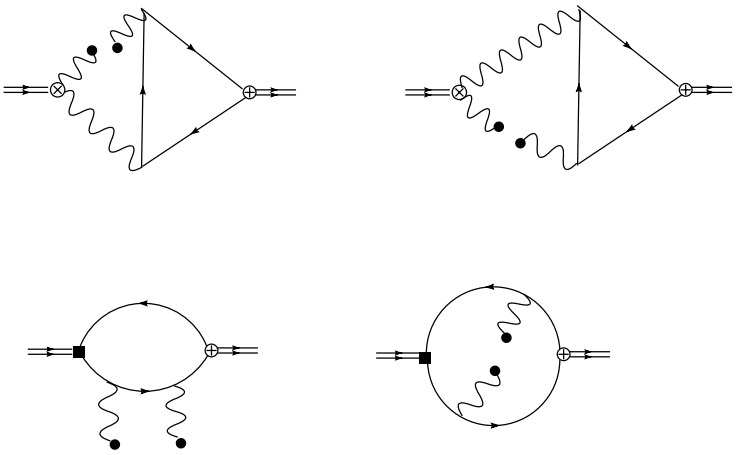

Fig. 4. Leading-order gluon condensate diagrams for the non-diagonal correlation function. The solid circles on the gluon lines denote insertion of plane-wave states for evaluation of the operator-product expansion coefficients. All other notations are identical to Fig. 1.

renormalization-induced diagram of Fig. 2 also introduces the mixed condensate (see, e.g., Ref. [34]). However, the two renormalization-induced diagrams are suppressed by a factor of α and additional factors of the quark mass compared with the first diagram of Fig. 3, resulting in the following leading-order OPE coefficient

$$C_{QGQ} = \frac{4\alpha m_q}{Q^2}. \tag{38}$$

In the absence of operator mixing, the diagrams that could lead to the gluon condensate OPE coefficient E_{GG} are shown in Fig. 4. However, the renormalization-induced diagrams are higher-order in α and hence are subleading. Because of infrared divergences, it is necessary to retain the quark mass until the last steps of the calculation and then extract the leading chiral behaviour. Using plane-wave methods with $m_u = m_d = m$ we find

$$E_{GG} = 2i\frac{32\pi\alpha m_q^2}{D^2q^2}\big[m^2(8-4D)I_1 - 2DI_2 + \big(D^2-4D+8\big)I_3\big], \tag{39}$$

where

$$\begin{aligned} I_1 &= \frac{1}{\nu^{2\epsilon}}\int \frac{\mathrm{d}^D k}{(2\pi)^D}\frac{1}{(k^2-m^2)^2[(q-k)^2-m^2]} \\ &= \frac{\mathrm{i}}{16\pi^2}\frac{1}{q^2\sqrt{1-4m^2/q^2}}\log\left[\frac{\sqrt{1-4m^2/q^2}+1}{\sqrt{1-4m^2/q^2}-1}\right], \end{aligned} \tag{40}$$

$$I_2 = \frac{1}{\nu^{2\epsilon}} \int \frac{\mathrm{d}^D k}{(2\pi)^D} \frac{1}{(k^2 - m^2)^2} = \frac{\mathrm{i}}{16\pi^2} \left(\frac{m^2}{4\pi\nu^2} \right)^{\epsilon} \Gamma(-\epsilon), \tag{41}$$

$$\begin{aligned} I_3 &= \frac{1}{\nu^{2\epsilon}} \int \frac{\mathrm{d}^D k}{(2\pi)^D} \frac{1}{(k^2 - m^2)[(q-k)^2 - m^2]} \\ &= \frac{\mathrm{i}}{16\pi^2} \left(-\frac{1}{\epsilon} - \gamma - \log\left(\frac{m^2}{4\pi\nu^2} \right) + 2 \right. \\ &\quad \left. - \sqrt{1 - 4m^2/q^2} \log\left[\frac{\sqrt{1 - 4m^2/q^2} + 1}{\sqrt{1 - 4m^2/q^2} - 1} \right] \right). \end{aligned} \tag{42}$$

The divergences in I_3 and I_2 cancel, leaving a finite result as required given the m_q^2/q^2 prefactor. The logarithmic correction from I_1 is seen to be subleading compared with the logarithmic correction from I_3. Thus the leading-chiral gluon condensate contribution to the non-diagonal unmixed OPE coefficient is

$$E_{GG} = \frac{2\alpha m_q^2}{\pi Q^2} \left[3 - \log\left(\frac{Q^2}{m^2} \right) \right]. \tag{43}$$

The $\log(m^2)$ infrared divergence in (43) is now cancelled when (43) and (38) are substituted in (36), resulting in the leading-order contribution to the gluon condensate OPE coefficient

$$C_{GG} = \frac{2\alpha m_q^2}{\pi Q^2} \left[3 - \log\left(\frac{Q^2}{\nu^2} \right) \right]. \tag{44}$$

The cancellation of the infrared divergence follows from the methodology of [31], and provides a consistency check on our calculation of the OPE coefficients.

Finally, the result of our calculation for the single instanton [35] contributions (i.e., multi-instanton effects are negligible [36]) to the non-diagonal correlator in the dilute instanton liquid model [27] are:

$$\Pi_{gq}^{inst}(Q^2) = -8\sqrt{3n_c} m_q \rho Q^2 \sqrt{\rho^2 Q^2} K_1\left(\sqrt{\rho^2 Q^2} \right) K_2\left(\sqrt{\rho^2 Q^2} \right), \tag{45}$$

where K_n is a modified Bessel function in the conventions of [37].

Combining Eqs. (32), (37), (38), (44), and (45), we have the leading-order chiral and α contributions to the non-diagonal correlation function of gluonic and (non-strange) $I = 0$ quark currents in the $\overline{\mathrm{MS}}$ scheme:

$$\begin{aligned} \Pi_{gq}(Q^2) &= m_q^2 Q^2 \left[A_0 L + A_1 L^2 \right] \\ &\quad + m_q \langle \bar{q} q \rangle C_0 L + m_q^2 \langle \alpha G^2 \rangle \frac{1}{Q^2} [B_0 + B_1 L] + m_q \langle \bar{q} \sigma G q \rangle \frac{D_0}{Q^2} \\ &\quad - 8\sqrt{3n_c} m_q \rho Q^2 \sqrt{\rho^2 Q^2} K_1\left(\sqrt{\rho^2 Q^2} \right) K_2\left(\sqrt{\rho^2 Q^2} \right), \end{aligned} \tag{46}$$

$$C_0 = -8\pi \left(\frac{\alpha}{\pi} \right)^2, \qquad D_0 = 4\alpha, \tag{47}$$

$$B_0 = 6\frac{\alpha}{\pi}, \qquad B_1 = -2\frac{\alpha}{\pi}, \tag{48}$$

with A_0, A_1 given in (32). From the correlation function, the $k = 0$ GSR can be calculated as outlined in Section 2 and Ref. [13]:

$$
\begin{aligned}
G_0^{(gq)}(\hat{s},\tau,s_0) = {} & \frac{m_q^2}{\sqrt{4\pi\tau}}\int_0^{s_0} \mathrm{d}t\,\exp\left[-\frac{(t-\hat{s})^2}{4\tau}\right] t\left(A_0 + 2A_1\log\left[\frac{t}{\sqrt{\tau}}\right]\right) \\
& + B_0 m_q^2\langle\alpha G^2\rangle\frac{1}{\sqrt{4\pi\tau}}\exp\left(-\frac{\hat{s}^2}{4\tau}\right) \\
& + B_1 m_q^2\langle\alpha G^2\rangle\frac{1}{\sqrt{4\pi\tau}}\lim_{\eta\to 0}\left\{\int_\eta^{s_0}\mathrm{d}t\,\frac{1}{t}\exp\left[-\frac{(t-\hat{s})^2}{4\tau}\right]\right. \\
& \left. + \log\left(\frac{\eta}{\sqrt{\tau}}\right)\exp\left(-\frac{\hat{s}^2}{4\tau}\right)\right\} \\
& - C_0 m_q\langle\bar{q}q\rangle\frac{1}{\sqrt{4\pi\tau}}\int_0^{s_0}\mathrm{d}t\,\exp\left[-\frac{(t-\hat{s})^2}{4\tau}\right] \\
& + D_0 m_q\langle\bar{q}\sigma Gq\rangle\frac{1}{\sqrt{4\pi\tau}}\exp\left(-\frac{\hat{s}^2}{4\tau}\right) \\
& + 2\sqrt{3n_c}\pi m_q\rho^2\frac{1}{\sqrt{4\pi\tau}}\int_0^{s_0}\mathrm{d}t\,\exp\left[-\frac{(t-\hat{s})^2}{4\tau}\right]t\sqrt{t} \\
& \times\left[J_1(\rho\sqrt{t})Y_2(\rho\sqrt{t}) + J_2(\rho\sqrt{t})Y_1(\rho\sqrt{t})\right]
\end{aligned}
\tag{49}
$$

where in practice, the limit $\eta \to 0$ is implemented numerically with values of $\eta < 10^{-4}$ GeV^2. Due to renormalization-group scaling of the GSRs [14,22], we have set $\nu^2 = \sqrt{\tau}$ in (49), and hence m_q and α are implicitly the leading-order versions of the running quantities evaluated at the scale $\nu^2 = \sqrt{\tau}$ for three active flavours in the $\overline{\mathrm{MS}}$ scheme

$$
\begin{aligned}
&\frac{\alpha(\nu^2)}{\pi} = \frac{1}{\beta_0 L}, \qquad m_q\left(\nu^2\right) = \frac{\hat{m}_q}{(\frac{1}{2}L)^{\frac{4}{9}}}, \\
&L = \log\left(\frac{\nu^2}{\Lambda^2}\right), \qquad \beta_0 = \frac{9}{4}
\end{aligned}
\tag{50}
$$

where $\hat{m}_q$ is the renormalization-group invariant quark mass parameter and $\Lambda_{\overline{MS}} \approx 300$ MeV consistent with current estimates of $\alpha(M_\tau)$ [1]. The normalized GSR $N_0^{(gq)}(\hat{s},\tau,s_0)$ associated with (49) is defined by (14):

$$
N_0^{(gq)}(\hat{s},\tau,s_0) = \frac{G_0^{(gq)}(\hat{s},\tau,s_0)}{M_{0,0}^{(gq)}(\tau,s_0)}, \qquad M_{0,0}^{(gq)}(\tau,s_0) = \int_{-\infty}^{\infty} G_0^{(gq)}(\hat{s},\tau,s_0)\,\mathrm{d}\hat{s}. \tag{51}
$$

Since a low-energy theorem exists for the non-diagonal correlator [18]

$$
\Pi_{gq}(0) = \frac{48\pi}{9} m_q\langle\bar{q}q\rangle, \tag{52}
$$

the LET-sensitive $k = -1$ GSR is also relevant. Again using the methods outlined in Section 2 and Ref. [13], the corresponding results for the $k = -1$ GSR are

$$
\begin{aligned}
G_{-1}^{(gq)}(\hat{s},\tau,s_0) = {} & \frac{m_q^2}{\sqrt{4\pi\tau}}\int_0^{s_0} \mathrm{d}t\,\exp\left[-\frac{(t-\hat{s})^2}{4\tau}\right]\left(A_0+2A_1\log\left[\frac{t}{\sqrt{\tau}}\right]\right)\\
& - C_0 m_q\langle\bar{q}q\rangle\frac{1}{\sqrt{4\pi\tau}}\lim_{\eta\to 0}\left\{\int_\eta^{s_0}\mathrm{d}t\,\frac{1}{t}\exp\left[-\frac{(t-\hat{s})^2}{4\tau}\right]\right.\\
& \left.+\log\left(\frac{\eta}{\sqrt{\tau}}\right)\exp\left(-\frac{\hat{s}^2}{4\tau}\right)\right\}\\
& + B_1 m_q^2\langle\alpha G^2\rangle\frac{1}{\sqrt{4\pi\tau}}\lim_{\eta\to 0}\left\{\int_\eta^{s_0}\mathrm{d}t\,\frac{1}{t^2}\exp\left[-\frac{(t-\hat{s})^2}{4\tau}\right]-\frac{1}{\eta}\exp\left(-\frac{\hat{s}^2}{4\tau}\right)\right\}\\
& + B_0 m_q^2\langle\alpha G^2\rangle\frac{1}{\sqrt{4\pi\tau}}\frac{\hat{s}}{2\tau}\exp\left(-\frac{\hat{s}^2}{4\tau}\right)\\
& + D_0 m_q\langle\bar{q}\sigma Gq\rangle\frac{1}{\sqrt{4\pi\tau}}\frac{\hat{s}}{2\tau}\exp\left(-\frac{\hat{s}^2}{4\tau}\right)\\
& + 2\sqrt{3n_c}\pi m_q\rho^2\frac{1}{\sqrt{4\pi\tau}}\int_0^{s_0}\mathrm{d}t\exp\left[-\frac{(t-\hat{s})^2}{4\tau}\right]\sqrt{t}\\
& \times\left[J_1(\rho\sqrt{t})Y_2(\rho\sqrt{t})+J_2(\rho\sqrt{t})Y_1(\rho\sqrt{t})\right]\\
& + \frac{1}{\sqrt{4\pi\tau}}\exp\left(-\frac{\hat{s}^2}{4\tau}\right)\frac{16\sqrt{3n_c}m_q}{\rho}. \qquad (53)
\end{aligned}
$$

Note that the last term in (53) has a functional dependence identical to the LET term in (14), and hence there is an LET-like instanton contribution for the non-diagonal GSR similar to the diagonal gluonic case [13]. The NGSR $N_{-1}^{(gq)}(\hat{s},\tau,s_0)$ associated with (53) is defined by (14):

$$
\begin{aligned}
N_{-1}^{(gq)}(\hat{s},\tau,s_0) &= \frac{G_{-1}^{(gq)}(\hat{s},\tau,s_0)+\frac{1}{\sqrt{4\pi\tau}}\exp\left(\frac{-\hat{s}^2}{4\tau}\right)\Pi_{gq}(0)}{M_{-1,0}^{(gq)}(\tau,s_0)+\Pi_{gq}(0)},\\
M_{-1,0}^{(gq)}(\tau,s_0) &= \int_{-\infty}^{\infty} G_{-1}^{(gq)}(\hat{s},\tau,s_0)\,\mathrm{d}\hat{s}. \qquad (54)
\end{aligned}
$$

The QCD input parameters appearing within the non-diagonal NGSRs will now be specified. For the gluon condensate we employ the (central) value from [38]

$$\langle\alpha G^2\rangle = (0.07\pm 0.01)\ \mathrm{GeV}^4, \qquad (55)$$

and the quark condensate is determined by the PCAC relation

$$m_q\langle\bar{q}q\rangle = -\frac{1}{2}f_\pi^2 m_\pi^2, \qquad f_\pi = 93\ \mathrm{MeV}. \qquad (56)$$

For our purpose, the expression of the mixed condensate in terms of the quark condensate [39] is the most useful:

$$\langle\bar{q}\sigma Gq\rangle = M_0^2\langle\bar{q}q\rangle, \qquad M_0^2 = (0.8\pm 0.1)\ \mathrm{GeV}^2. \qquad (57)$$

In addition, the dilute instanton liquid (DIL) model parameters (which have an estimated uncertainty of about 15%) [27]

$$n_c = 8.0 \times 10^{-4}\ \text{GeV}^4, \qquad \rho = \frac{1}{0.6}\ \text{GeV}^{-1} \tag{58}$$

will be employed. The NGSRs for the diagonal correlators do not require knowledge of the quark masses; in the diagonal gluonic case this occurs because the leading chiral behaviour is independent of the quark masses, while the diagonal $q\bar{q}$ case is proportional to m_q^2 and hence the quark mass dependence cancels when forming the NGSR. However, the non-diagonal case has terms of differing chiral order and therefore requires input of the quark mass. Unfortunately, m_q is not known very accurately; we will use the Particle Data Group range for the 2 GeV $\overline{\text{MS}}$ mass [1]:

$$2.5\ \text{MeV} < m_q(2\ \text{GeV}) < 5.5\ \text{MeV}. \tag{59}$$

The implications of the large uncertainty in m_q within our analysis will be discussed in more detail below.

The non-diagonal correlator and its associated GSR have quite distinct chiral behaviour compared with the diagonal correlators. In the diagonal case, the perturbative, condensate, and instanton corrections all appear with identical powers of the quark mass. However, in the non-diagonal case the perturbative and gluon condensate corrections are chirally-suppressed compared with the quark condensate, mixed condensate, and instanton terms. One can understand this chiral behaviour in the non-diagonal case by recognizing that the operator $\bar{u}(x)u(x)+\bar{d}(x)d(x)$ appearing in J_q violates chiral symmetry, and hence the chiral-conserving gluon condensate (and perturbative corrections) must have an additional chiral suppression because the gluon condensate would be non-zero in the limit of vanishing quark mass. Similarly, the chiral-violating condensates (and instanton) do not require an additional mass chiral suppression because chiral symmetry is restored when the condensates are zero. The implications of the quark mass suppression of the chiral-preserving terms, and the comparative enhancement of chiral-violating effects, will be discussed below.

4. Analysis of Gaussian sum-rules for $q\bar{q}$ and gluonic currents

The general strategy for analysis of NGSRs involves matching the QCD expression with a parametrized model for $\rho^{\text{had}}(t)$ in (16). Correlation functions of vector and axial-vector $q\bar{q}$ currents can be directly related to experimental data (e.g., $R(s)$, τ decays), but in the case of gluonium there is no direct connection with experimental observables. The narrow resonance approximation is the most common choice made for Laplace sum-rule analyses of gluonium, with either a single (narrow) resonance [12,40–42] to examine the dominant gluonic state or two (narrow) resonances [10,11,43] to explore the possibility of $q\bar{q}$–gluonium mixtures. Laplace sum-rule gluonium analyses which go beyond the narrow width approximation include a single Breit–Wigner resonance skewed by kinematic factors [44], and an interpolation between the LET and continuum behaviour [23]. Finite-energy sum-rule analyses of scalar gluonium include narrow resonance models [45] and incorporate resonance widths through step functions [46] and Breit–Wigner resonances [47] with kinematic skewing.[5]

[5] Ref. [47] also uses the Gaussian sum-rule diffusion equation analysis to constrain the QCD continuum. As discussed in Section 2, our approach based on NGSRs provides information that is *independent* of the FESR duality constraint.

GSR analyses of gluonium have employed single and double narrow resonance models in addition to a variety of models that incorporate resonance widths [13,15]. However, inclusion of width effects do not lead to appreciable improvement in the agreement between the QCD expression and phenomenological model. We attribute this to the large value of the QCD-limited width of the Gaussian kernel $2\sqrt{\tau} \geqslant 2$ GeV^2 in (1) which obscures resonance-width effects. As in our previous combined analysis of the diagonal quark and gluonic GSRs [15], we thus choose a double narrow resonance model for capturing the essential features of the analysis.

In general, the analysis of NGSRs in the double narrow resonance model has the form

$$\frac{1}{\pi}\rho^{\text{had}}(t) = f_1^2\delta\big(t-m_1^2\big) + f_2^2\delta\big(t-m_2^2\big), \tag{60}$$

$$N_0^{\text{QCD}}(\hat{s},\tau,s_0) = \frac{1}{\sqrt{4\pi\tau}}\left\{r_1\exp\left[-\frac{(\hat{s}-m_1^2)^2}{4\tau}\right] + r_2\exp\left[-\frac{(\hat{s}-m_2^2)^2}{4\tau}\right]\right\}, \tag{61}$$

$$r_1 = \frac{f_1^2}{f_1^2+f_2^2}, \qquad r_2 = \frac{f_2^2}{f_1^2+f_2^2}, \qquad r_1+r_2 = 1 \tag{62}$$

where f_1, f_2 denote the couplings of the resonances to the currents under consideration and $m_1 < m_2$. As outlined in Refs. [13,15]. The GSR moments (15) are the most useful quantities for extracting the resonance parameters from the QCD expression. In particular, the first-order moments provide a measure of the peak of the GSR

$$P(\tau,s_0) = \frac{M_{0,1}(\tau,s_0)}{M_{0,0}(\tau,s_0)}, \tag{63}$$

second-order moments provide a measure of the GSR width

$$\sigma^2(\tau,s_0) = \frac{M_{0,2}(\tau,s_0)}{M_{0,0}(\tau,s_0)} - \big[P(\tau,s_0)\big]^2, \tag{64}$$

and the third-order moments provide a measure of the GSR asymmetry

$$A(\tau,s_0) = \frac{M_{0,3}(\tau,s_0)}{M_{0,0}(\tau,s_0)} - 3\sigma^2(\tau,s_0)P(\tau,s_0) - \big[P(\tau,s_0)\big]^3. \tag{65}$$

The double-resonance phenomenological parameters defined by

$$r = r_1 - r_2, \qquad y = m_1^2 - m_2^2, \qquad z = m_1^2 + m_2^2, \tag{66}$$

are then related to the moments by

$$z = 2P + \frac{A}{\sigma^2-2\tau}, \tag{67}$$

$$y = \frac{-\sqrt{A^2+4(\sigma^2-2\tau)^3}}{\sigma^2-2\tau}, \tag{68}$$

$$r = \frac{A}{\sqrt{A^2+4(\sigma^2-2\tau)^3}}, \tag{69}$$

where the τ, s_0 dependence of the moments has been suppressed for brevity. The quantity $\sigma^2-2\tau$ appearing in Eqs. (67)–(69) is particularly important because it is a clear diagnostic of multiple resonances. This can be seen from

$$\sigma^2 - 2\tau = \frac{1}{4}y^2\big(1-r^2\big) > 0, \tag{70}$$

Table 1
Analysis results from the diagonal and non-diagonal NGSRs of gluonic and $\bar{q}q$ currents in the double narrow resonance model. Central values of the QCD input parameters have been employed.

Sum-rule	m_1 (GeV)	m_2 (GeV)	r_1	r_2	s_0 (GeV^2)
diagonal: gluonic–gluonic	0.98	1.4	0.28	0.72	2.30
diagonal: $\bar{q}q$–$\bar{q}q$	0.97	1.4	0.63	0.37	2.60
non-diagonal: gluonic–$\bar{q}q$	0.84	1.4	0.44	0.56	2.75

which indicates that a second resonance cannot be absorbed into the continuum if the QCD value of the second-order GSR moments exceed the natural Gaussian width of 2τ.

In general, the resonance parameters depend on τ and s_0 through the QCD values of the moments. Apart from the previously-discussed QCD constraints, τ is a free parameter and therefore the resonance parameters should be largely independent of τ; residual τ dependence can be interpreted as a source of theoretical uncertainty. However, the continuum threshold s_0 appears within the QCD expression, so a criterion must be established for optimizing s_0. Various approaches to this optimization will be discussed below.

In the case of the diagonal quark and gluonic cases, s_0 was constrained by studying the τ dependence of the value $\hat{s}_{peak}$ at which the QCD expression for the NGSR reaches its maximum value. This τ dependence is then compared with that arising from a double-resonance model, and s_0 is constrained by optimizing the agreement between them. This procedure for optimizing s_0 and determining the resonance parameters has been confirmed by a more numerically-intensive multi-parameter fit of s_0 and the resonance parameters [14,48]. The resonance parameters resulting from our previous analyses of the diagonal gluonic and diagonal quark NGSRs [13–15] are summarized in Table 1 (the details of the non-diagonal case will be discussed below). The double narrow resonance model results in excellent agreement with the QCD expression as illustrated in Fig. 5 [13]; there is no indication of discrepancies that would require a more elaborate phenomenological model (e.g., additional states, resonance widths). For the diagonal NGSRs, the uncertainties associated with the QCD input parameters have been found to be 10% for $\{r_2^{(gg)}, r_1^{(gg)}\}$, and at most 0.2 GeV for the masses with a correlated effect that leads to a relatively stable mass splitting $m_2 - m_1 \approx 0.4$ GeV [13].

The remarkable agreement between the resonance masses resulting from independent analysis of the diagonal gluonic and diagonal $q\bar{q}$ NGSRs suggests the existence of states with masses of approximately 1.0 GeV and 1.4 GeV that couple to mixtures of gluonium and $q\bar{q}$ currents, with the heavier state being slightly more gluonic because of its stronger coupling to gluonic currents and weaker coupling to $q\bar{q}$ currents. This consistency of the mass predictions in the two channels is precisely what is expected for hadronic states that couple to both gluonium and quark currents. The results also indicate that the mixing is rather strong (consistent with the conclusions of [9,10]) because r_1 and r_2 are not appreciably different, and hence the non-diagonal correlator must also contain clear signals of this strong mixing to validate this scenario. In other words, a definitive signal of states that are $q\bar{q}$–gluonic mixtures is their consistent appearance with the same mass in *all three* cases (diagonal gluonic, diagonal quark, and non-diagonal gluonic–quark) since such mixtures would necessarily couple to both the gluonic and $q\bar{q}$ currents.

Before proceeding with a detailed analysis of the non-diagonal correlator, we consider the approximate scales associated with the couplings of the resonances to the gluonic and scalar currents. The perturbative corrections in the diagonal correlators (see Refs. [13,14]) imply that

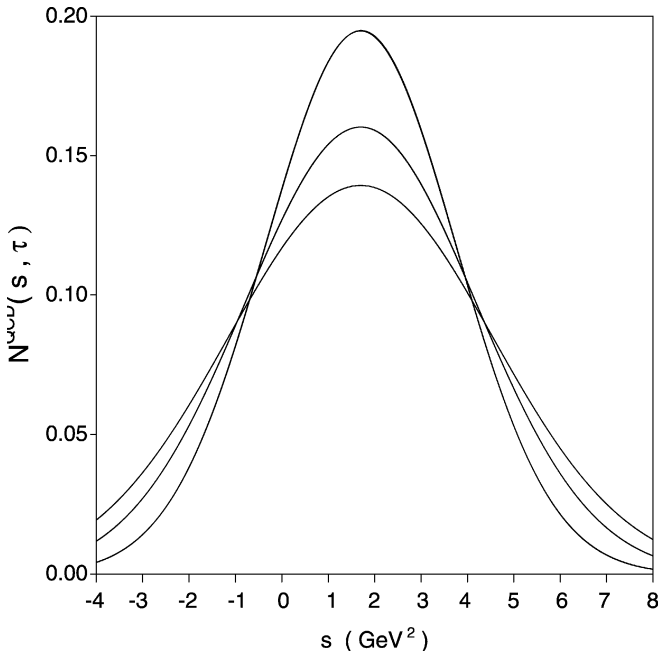

Fig. 5. Comparison of the QCD theoretical expression for $N_0^{(gg)}(\hat{s},\tau,s_0)$ with the double narrow resonance phenomenological model in the diagonal gluonic case. The τ values used for the three pairs of curves, from top to bottom in the figure, are respectively $\tau = 2.0$ GeV^4, $\tau = 3.0$ GeV^4, and $\tau = 4.0$ GeV^4. Note the almost perfect overlap between the theoretical expression and the phenomenological model. A qualitatively similar agreement between the double narrow resonance model and the QCD expression exists for the diagonal quark NGSR.

$$f_g^2 \sim \left(\frac{\alpha}{\pi}\right)^2 E^4, \qquad f_q^2 \sim m_q^2 E^2, \tag{71}$$

where f_g and f_q respectively denote the resonance couplings to the gluonic and $q\bar{q}$ currents and E is a characteristic sum-rule energy scale of order $E \sim 1$ GeV. In the simplest single-angle mixing scenario, the non-diagonal correlator will be proportional to $f_g f_q \sin 2\theta$ where θ is the mixing angle. The perturbative corrections to the non-diagonal correlator (46) then imply

$$f_g f_q \sin 2\theta \sim m_q^2 \left(\frac{\alpha}{\pi}\right)^2 E^2. \tag{72}$$

Combining (71) and (72) then leads to a chirally-suppressed mixing angle for perturbative contributions

$$\sin 2\theta \sim \frac{\alpha}{\pi}\frac{m_q}{E} \ll 1. \tag{73}$$

A similar chiral suppression exists for the gluon condensate contributions

$$\sin 2\theta \sim \frac{m_q}{E}\frac{\langle \alpha G^2\rangle}{E^4} \ll 1. \tag{74}$$

However, for the quark and mixed condensate contributions we find

$$\sin 2\theta \sim \frac{\alpha}{\pi}\frac{\langle \bar{q}q\rangle}{E^3}, \tag{75}$$

$$\sin 2\theta \sim \frac{\langle \bar{q}\sigma Gq\rangle}{E^5} = \frac{M_0^2}{E^2}\frac{\langle \bar{q}q\rangle}{E^3}\ . \tag{76}$$

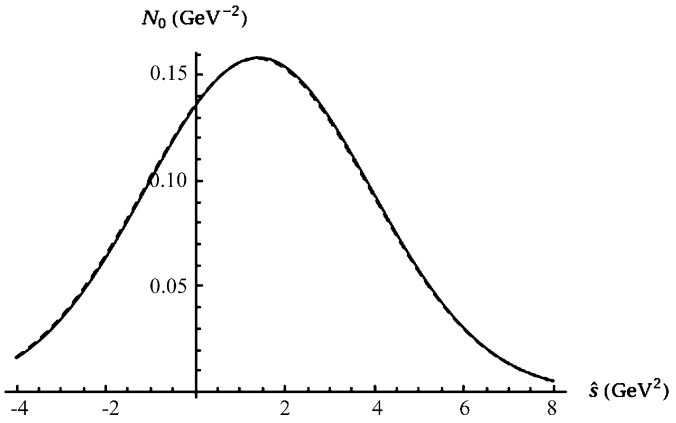

Fig. 6. Comparison of the full contributions (solid curve) to the GSR $N_0^{(gq)}(\hat{s},\tau,s_0)$ with its leading-order chiral contributions (dashed curve) from the quark condensate, mixed condensate and instanton arising from $\chi_0^{(gq)}(\hat{s},\tau,s_0)$. The two curves overlap almost completely. Central values of the QCD input parameters have been employed along with $s_0 = 2.5\ \text{GeV}^2$ and $\tau = 3\ \text{GeV}^4$.

These estimates illustrate that the chiral-violating condensates avoid the chiral suppression of the mixing angle. However, since $M_0 \sim E$ the mixing angle generated by the quark condensate will be suppressed compared to the mixed condensate by a factor of α/π. As noted earlier, the mixed condensate is zero at leading order in the non-diagonal pseudoscalar case [16] and hence there is a qualitative distinction between the scalar and pseudoscalar channels. Although it is not as simple to estimate the order of magnitude of the mixing generated by the instanton contributions, one already sees from (76) that a substantive mixing angle is anticipated.

The apparent contradiction between the strong mixing found in the GSRs for the diagonal correlators and the basic perturbative scales in the non-diagonal GSR is therefore resolved by a detailed analysis of the non-diagonal case which demonstrates that the chiral-violating terms (i.e., quark condensate, mixed condensate, and instanton) dominate the perturbative and gluon condensate corrections. We first define the leading $\mathcal{O}(m_q)$ chiral terms in (49) as

$$\begin{aligned}\chi_0^{(gq)}(\hat{s},\tau,s_0) = {} & -C_0 m_q \langle\bar{q}q\rangle \frac{1}{\sqrt{4\pi\tau}} \int_0^{s_0} \mathrm{d}t \exp\left[-\frac{(t-\hat{s})^2}{4\tau}\right] \\ & + D_0 m_q \langle\bar{q}\sigma Gq\rangle \frac{1}{\sqrt{4\pi\tau}} \exp\left(-\frac{\hat{s}^2}{4\tau}\right) \\ & + 2\sqrt{3n_c}\pi m_q \rho^2 \frac{1}{\sqrt{4\pi\tau}} \int_0^{s_0} \mathrm{d}t \exp\left[-\frac{(t-\hat{s})^2}{4\tau}\right] t\sqrt{t} \\ & \times \left[J_1(\rho\sqrt{t})Y_2(\rho\sqrt{t}) + J_2(\rho\sqrt{t})Y_1(\rho\sqrt{t})\right]. \end{aligned} \tag{77}$$

Fig. 6 demonstrates that these leading chiral terms are actually the dominant contribution to the non-diagonal GSR, avoiding the chiral suppression occurring in (73), and obviating the chiral suppression of the mixing angle that would occur for dominantly perturbative corrections. We thus have the intriguing result that the underlying mixing mechanism is fundamentally non-perturbative, i.e., perturbative analyses do not provide the essential phenomenological scales.

Because PCAC fixes the combination $m_q\langle\bar{q}q\rangle$, the quark condensate term in (77) is effectively independent of m_q, so in principle $N_0^{(gq)}$ could be strongly dependent on m_q. Fig. 7 shows that

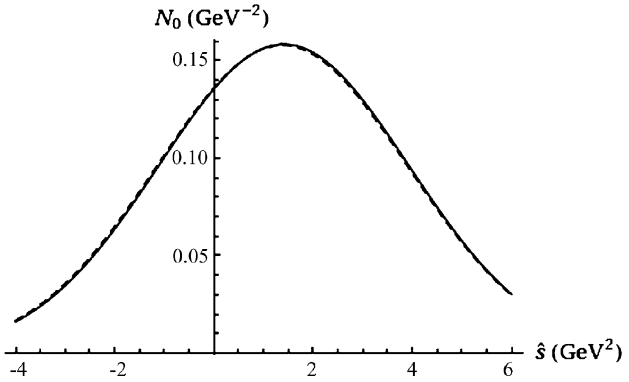

Fig. 7. Comparison of the NGSR $N_0^{(gq)}(\hat{s}, \tau, s_0)$ for the upper and lower ranges of the quark mass specified in (59). Central values of the other QCD input parameters have been employed along with $\tau = 3$ GeV^4 and $s_0 = 2.5$ GeV^2. The two curves overlap almost completely.

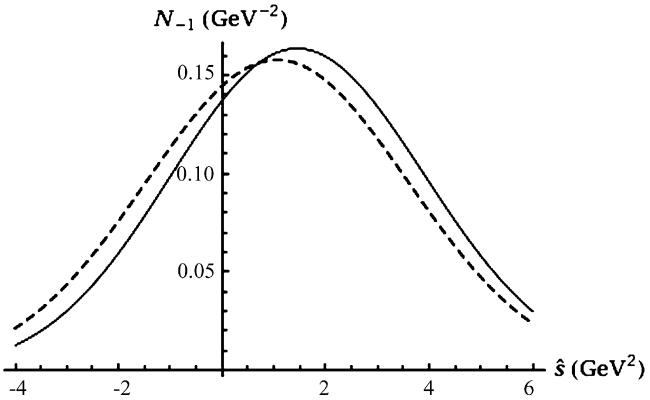

Fig. 8. Comparison of the NGSR $N_{-1}^{(gq)}(\hat{s}, \tau, s_0)$ for the upper and lower ranges of the quark mass specified in (59). Central values of the other QCD input parameters have been employed along with $\tau = 3$ GeV^4 and $s_0 = 2.5$ GeV^2. The solid and dotted curves respectively correspond to the lower and upper bound on the quark mass.

this is not the case; the NGSR $N_0^{(gq)}$ is relatively insensitive to the range (59) for m_q. However, Fig. 8 shows that this is not the case for the LET-sensitive NGSR $N_{-1}^{(gq)}$ which exhibits stronger dependence on m_q. Thus we focus our analysis on the $k = 0$ NGSR $N_0^{(gq)}$ as it is less affected by quark-mass uncertainties. However, it is significant that Figs. 7 and 8 do demonstrate qualitative agreement between N_0 and N_{-1}, particularly for m_q at the upper bound of (59).

Our detailed analysis of the non-diagonal GSR begins with an exploration of its consistency with the results of the diagonal cases. In the double narrow resonance model, the non-diagonal NGSR has the form

$$N_0^{(gq)}(\hat{s}, \tau, s_0) = \frac{1}{\sqrt{4\pi\tau}} \left\{ r_1^{(gq)} \exp\left[-\frac{(\hat{s} - m_1^2)^2}{4\tau} \right] + r_2^{(gq)} \exp\left[-\frac{(\hat{s} - m_2^2)^2}{4\tau} \right] \right\}, \tag{78}$$

$$r_1^{(gq)} = \frac{f_{1g} f_{1q}}{f_{1g} f_{1q} + f_{2g} f_{2q}}, \qquad r_2^{(gq)} = \frac{f_{2g} f_{2q}}{f_{1g} f_{1q} + f_{2g} f_{2q}}, \qquad r_1^{(gq)} + r_2^{(gq)} = 1. \tag{79}$$

From the analysis of the diagonal cases [13–15], we have found (see Table 1) $m_1 \approx 1$ GeV, $m_2 \approx 1.4$ GeV, and

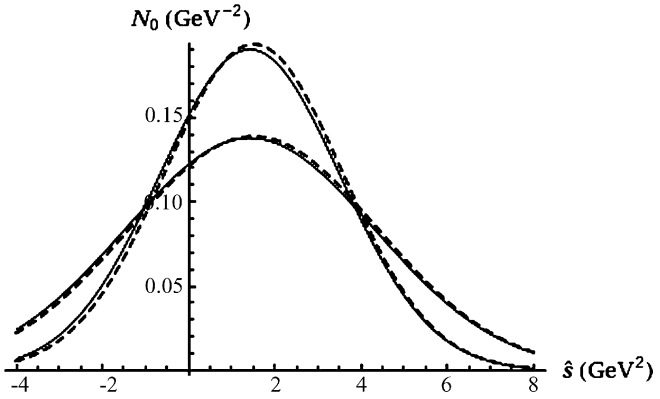

Fig. 9. Comparison of the best fit of theoretical expression for the normalized GSR $N_0^{(gq)}(\hat{s}, \tau, s_0)$ (solid curves) to the double narrow resonance phenomenological model (dashed curves). Resonance parameters resulting from the analyses of the diagonal NGSRs have been employed (the solution $r_1 = 0.45$ from (82), along with $m_1 = 0.98$ GeV and $m_2 = 1.4$ GeV). The optimized value of the continuum for these (inputted) resonance parameters is $s_0 = 2.75$ GeV^2. The upper set of curves are for $\tau = 2$ GeV^4 and the bottom set of curves is for $\tau = 4$ GeV^4. The phenomenological and QCD expressions overlap to a large extent.

$$r_1^{(gg)} = 0.28 = \frac{{f_{1g}}^2}{{f_{1g}}^2 + {f_{2g}}^2}, \qquad r_2^{(gg)} = 1 - 0.28 = \frac{{f_{2g}}^2}{{f_{1g}}^2 + {f_{2g}}^2}, \tag{80}$$

$$r_1^{(qq)} = 0.63 = \frac{{f_{1q}}^2}{{f_{1q}}^2 + {f_{2q}}^2}, \qquad r_2^{(qq)} = 1 - 0.63 = \frac{{f_{2q}}^2}{{f_{1q}}^2 + {f_{2q}}^2}. \tag{81}$$

Thus the parametrization of the mixed gluonic–$\bar{q}q$ system has four couplings of the states to the various currents as in Ref. [11]. The four equations (80) and (81) representing the diagonal results determine the four couplings up to an overall sign, leading to two possible solutions for the non-diagonal case:

$$r_1^{(gq)} = \begin{cases} +0.45, \\ -4.4. \end{cases} \tag{82}$$

Apart from the ambiguity arising from the sign of the couplings, all the phenomenological parameters in the non-diagonal NGSR (78) are determined except for the continuum s_0 which can be determined by performing a least-squares fit of the $\hat{s}$, τ dependence of (78) in the region -4 GeV$^2 < \hat{s} < 8$ GeV^2 and 2 GeV$^4 < \tau < 4$ GeV^4. The best fit for the two cases in (82) are shown in Figs. 9 and 10. From these figures we see that the positive case in (82) is demonstrably most consistent with the QCD expression.

At this point we reach an important conclusion: the non-diagonal GSR is consistent with the results of the diagonal gluonic GSR analyses [13–15], providing strong evidence for a consistent scenario of mixed gluonic–$\bar{q}q$ states with masses of $m_1 \approx 1$ GeV and $m_2 \approx 1.4$ GeV that couple to mixtures of gluonium and $q\bar{q}$ currents, with the heavier state having a slightly larger gluonic coupling. A significant feature of our analysis is the nearly-identical masses that have resulted independently from the diagonal gluonic and diagonal $\bar{q}q$ cases. Although we have demonstrated that the non-diagonal case is consistent with these results, an independent analysis of the non-diagonal case is necessary for further confirmation of this gluonic–$\bar{q}q$ mixing scenario.

The moments (67)–(69) will be used to determine the QCD predictions of the resonance parameters arising from the non-diagonal NGSR $N_0^{(gq)}$. In Figs. 11 and 12 we show the s_0, τ dependence of these moments. As required in a reliable sum-rule analysis, the resulting resonance parameters show almost no τ dependence. The predicted value of the resonance parameters

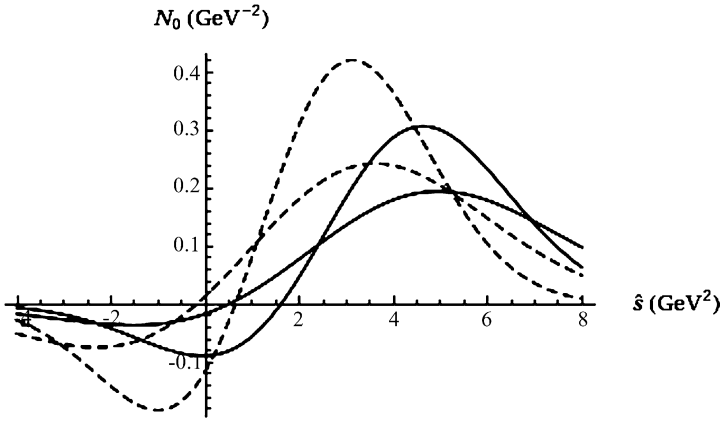

Fig. 10. Comparison of the best fit of theoretical expression for the normalized GSR $N_0^{(gq)}(\hat{s}, \tau, s_0)$ (solid curves) to the double narrow resonance phenomenological model (dashed curves). Resonance parameters resulting from the analyses of the diagonal NGSRs have been employed (the solution $r_1 = -4.4$ from (82), along with $m_1 = 0.98$ GeV and $m_2 = 1.4$ GeV). The optimized value of the continuum for these (inputted) resonance parameters is $s_0 = 4.9$ GeV^2. The upper set of curves are for $\tau = 2$ GeV^4 and the bottom set of curves is for $\tau = 4$ GeV^4.

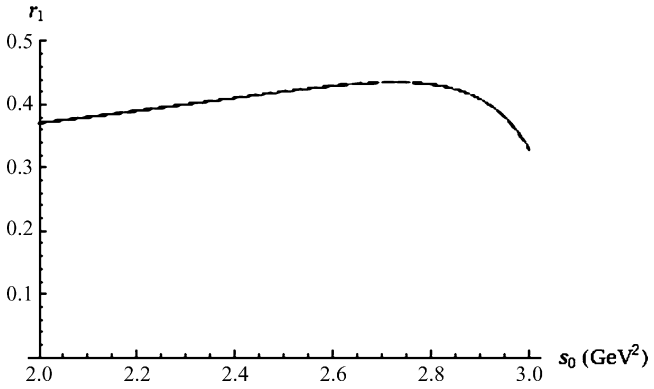

Fig. 11. The resonance parameter $r_1^{(gq)}$ extracted from the moments (69) of $N_0^{(gq)}$ as a function of s_0 for $\tau = 2$ GeV^4 (solid curve) and $\tau = 4$ GeV^4 (dashed curve). The dashed and sold curves overlap almost completely.

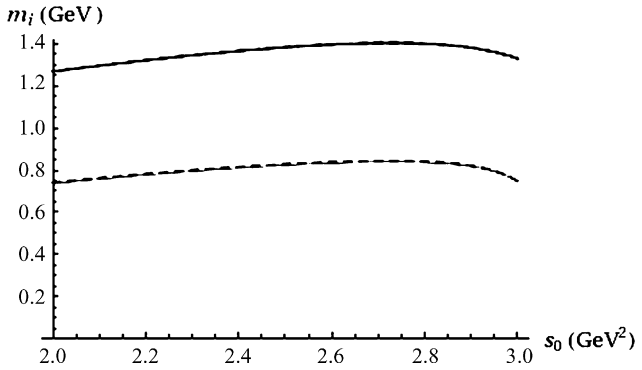

Fig. 12. The resonance parameters m_1 and m_2 extracted from the moments (67) and (68) of $N_0^{(gq)}$ as a function of s_0 for $\tau = 2$ GeV^4 (solid curves) and $\tau = 4$ GeV^4 (dashed curves). The dashed and sold curves overlap almost completely in both cases. The upper pair of curves represent m_2 and the lower set represent m_1.

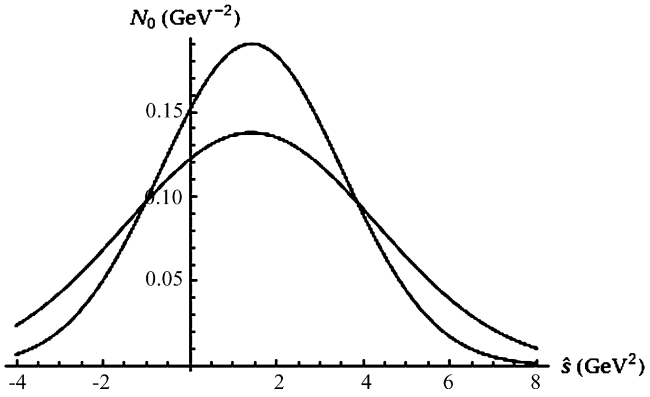

Fig. 13. Comparison of the theoretical expression (solid curves) for the non-diagonal NGSR $N_0^{(gq)}(\hat{s}, \tau, s_0)$ with the double narrow resonance phenomenological model (dashed curves) for the predicted values of the resonance parameters and continuum s_0 of Table 1. The upper set of curves are for $\tau = 2$ GeV^4 and the bottom set of curves is for $\tau = 4$ GeV^4. The dashed and solid curves overlap almost completely in both cases.

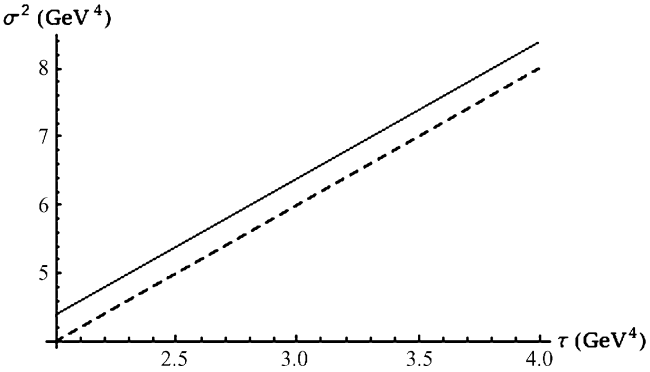

Fig. 14. Comparison of the theoretical value of the moment $\sigma^2(\tau, s_0)$ (solid curve) with 2τ (dashed curve). The optimized value $s_0 = 2.75$ GeV^2 has been used along with central values of QCD input parameters.

is then obtained from the point where they are stable against variations in s_0. This point of stability is approximately $s_0 = 2.75$ GeV^2 in all cases and is comparable in scale to that resulting from the diagonal analysis (see Table 1), confirming the reliability of the procedure. The results of the analysis of the non-diagonal NGSR are given in Table 1. Although the theoretical uncertainties for the non-diagonal sum-rule have not yet been discussed, it is evident that the independent predictions of the masses from all possible sum-rules show exceptional agreement, particularly for the heavier state. Furthermore, the prediction $r_1^{(gq)} = 0.44$ from the non-diagonal sum-rule is in excellent agreement with the positive solution of Eq. (82) emerging from the diagonal sum-rules.

For the non-diagonal NGSR, the double narrow resonance model results in excellent agreement with the QCD expression as illustrated in Fig. 13; as in the diagonal case (see Fig. 5) there is no indication of discrepancies that would require a more elaborate phenomenological model (e.g., additional states, resonance widths). As a further diagnostic, Fig. 14 illustrates that the optimized value $s_0 = 2.75$ GeV^2 leads to excellent agreement between the τ dependence of the QCD expression σ^2 and its expected dependence (70) from the two resonance model: a straight line with slope 2 and a positive intercept.

Because the non-diagonal sum-rule is dominated by the chiral-violating contributions, the Table 1 predictions of the resonance parameters only depend on the quark mass, mixed condensate, instanton size, and instanton density. The quantity $r_1^{(gq)}$ is most dependent on $\hat{m}_q$ and

ρ, whereas m_1 and m_2 are most dependent on ρ. By comparison, the resonance parameters are relatively unaffected by uncertainties in the mixed condensate and n_c. In aggregate, the resulting uncertainties in the mass parameters are comparable to those found in the diagonal case: approximately 0.2 GeV with a correlated effect that leads to a relatively stable mass splitting $0.5\ \text{GeV} < m_2 - m_1 < 0.6\ \text{GeV}$. However, in comparison to the diagonal analyses, the couplings have greater sensitivity to the input parameters in the non-diagonal case, with an uncertainty in $r_1^{(gq)}$ of approximately 0.1. Across the entire parameter space considered, s_0 continues to stabilize at the same value for all the resonance parameters, demonstrating that our methodology is robust.

Taking into account the uncertainties in the values of the resonance parameters for the diagonal and non-diagonal NGSRs associated with Table 1, we see that the non-diagonal case leads to predictions that are consistent with those of the diagonal analyses, so that all possible GSRs of gluonic and $\bar{q}q$ currents independently confirm the existence of two states with approximate masses of 1 GeV and 1.4 GeV that couple to mixtures of gluonium and $q\bar{q}$ currents. In particular, there is excellent agreement between the central value $r_1^{(gq)} = 0.44$ obtained from analysis of the non-diagonal NGSR and the positive solution $r_1^{(gq)} = 0.45$ in Eq. (82) resulting from the diagonal NGSRs.

Another inherent source of uncertainty in our analysis is the narrow resonance approximation. One can qualitatively model the effect of resonance widths and kinematic distortions by studying their effect on the moments (63)–(65). For example, a Gaussian resonance (which introduces an effective Breit–Wigner width Γ_{BW}) with a t^2 kinematic distortion [44,47] can be modelled by decreasing the QCD values of the moments systematically as a function of the ratio $\xi = \sqrt{2\log 2}\Gamma_{BW}/m$ [13] and then exploring the effect on the resonance parameters as a series in ξ. The leading-order deviations of m_1 and m_2 from their narrow-width values are proportional to ξ^2 with a negative coefficient of $\mathcal{O}(1)$ in GeV units. From this we can conclude that the narrow-width approximation tends to overestimate the masses if the underlying resonances are broad and kinematically-skewed (see, e.g., [49] for similar conclusions in other contexts). In this situation, the mass predictions in Table 1 can be conservatively interpreted as an upper bound on the masses in a more complicated models [44,47].

We now examine the pattern of mixing of the couplings for these states as contained in the quantities r_i for the various cases. If the couplings obey a single-angle mixing pattern, then one would expect $r_2^{(gg)} = \cos^2\theta = r_1^{(qq)}$. Although such a scenario could be possible given the 10% uncertainty in these quantities in Table 1, the non-diagonal case provides a more sensitive test because single-angle mixing leads to

$$G_0^{(gq)}(\hat{s}, \tau, s_0) \sim \frac{\sin 2\theta}{\sqrt{4\pi\tau}}\left[\exp\left[-\frac{(\hat{s}-m_1^2)^2}{4\tau}\right] - \exp\left[-\frac{(\hat{s}-m_2^2)^2}{4\tau}\right]\right]. \tag{83}$$

In this situation, the integral of the right-hand side of (83) is zero which then requires $M_{0,0}^{(gq)}(\tau, s_0) = 0$ in (51). A value of $s_0 = 4.18\ \text{GeV}^2$ can be found to satisfy this constraint over the considered range $2\ \text{GeV}^4 < \tau < 4\ \text{GeV}^4$. However, as shown in Fig. 15 the $\hat{s}$, τ dependence of the QCD expression $G_0^{(gq)}(\hat{s}, \tau, s_0)$ is not consistent with mass scales $m_1 \approx 1$ GeV and $m_2 \approx 1.4$ GeV. We thus conclude that the pattern of mixing for the couplings is not consistently described by a single mixing angle, and hence the situation must be similar to the two-angle scenario that has been found for the couplings (decay constants) of the η–η' system in the singlet–octet basis [50]. Implicitly this is the same result found in [8,11], where four independent couplings are found necessary in the study of the mixed gluonic–$q\bar{q}$ system rather

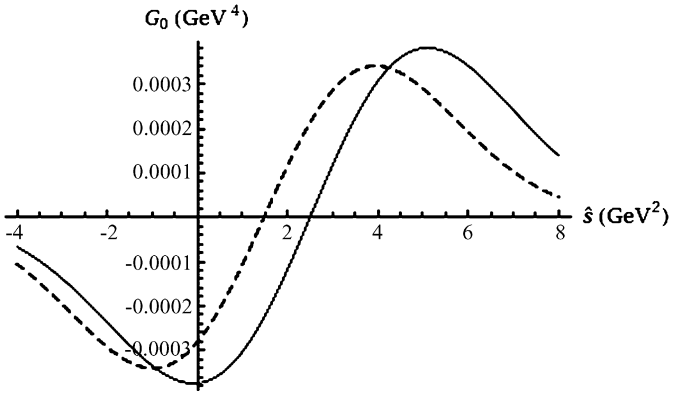

Fig. 15. Comparison of the best fit of theoretical expression for the GSR $G_0^{(gq)}(\hat{s}, \tau, s_0)$ to the double narrow resonance phenomenological model for a single mixing angle. Resonance masses $m_1 = 1$ GeV and $m_2 = 1.4$ GeV resulting from the analyses of the diagonal NGSRs have been employed. The continuum leading to $M_{0,0}^{(gq)} = 0$ for the central values of QCD input parameters is $s_0 = 4.18$ GeV^2. The solid curve represents the QCD expression $G_0^{(gq)}(\hat{s}, \tau, s_0)$ and the dashed curve represents the phenomenological model; $\tau = 3.0$ GeV^4 has been used in both cases.

than the three-parameter system of two couplings and one mixing angle. Following Ref. [8], we then define an effective mixing angle ϕ

$$\tan^2\phi = \left| \frac{\langle 0|J_g|1\rangle\langle 0|J_q|2\rangle}{\langle 0|J_g|2\rangle\langle 0|J_q|1\rangle} \right|, \tag{84}$$

where $|1\rangle$ and $|2\rangle$ respectively correspond to the states with mass m_1 and m_2. Taking into account the uncertainties in the Table 1 values leads to $\phi = 54^\circ \pm 4^\circ$. Thus we find that the effective mixing angle corresponds to nearly maximal mixing ($\phi = 45^\circ$) where each of the two states are equally coupled to the $q\bar{q}$ and gluonic currents, a result in excellent agreement with the conclusions of [9,10]. The deviation of our effective mixing angle from the maximal angle indicates that the heavier (1.4 GeV) state $|2\rangle$ is somewhat more gluonic in comparison to the lighter (1.0 GeV) state $|1\rangle$.

5. Discussion and conclusions

Gaussian QCD sum-rules are able to probe hadronic spectral functions over a broad range of energy, and are thus ideally suited to exploring the possibility of states that couple to mixtures of gluonium and $q\bar{q}$ currents exist amongst the light scalar mesons. We have studied the NGSRs for all possible combinations of scalar gluonic and scalar $I = 0$ (non-strange) $q\bar{q}$ currents (diagonal gluonic, diagonal $q\bar{q}$, and non-diagonal $q\bar{q}$–gluonic) and find that all three cases independently predict the existence of two states with masses of approximately 1 GeV and 1.4 GeV. This is precisely what one would expect from hadronic states that couple to mixtures of gluonium and $q\bar{q}$ currents. Given the uncertainties in our mass predictions, it is not clear whether our lighter state should be interpreted as the $f_0(980)$ or σ (at the heavier end of its range [1]) and it is also not clear whether the heavier state should be interpreted as the $f_0(1370)$ or the $f_0(1500)$. However, because the approximate 0.5 GeV mass splitting between the states is relatively stable under QCD uncertainties, our results do suggest identifying either the lighter pair of states [σ and $f_0(1370)$] or the heavier pair [$f_0(980)$ and $f_0(1500)$] as states coupling to mixtures of gluonium–$q\bar{q}$ currents.

The non-diagonal sum-rule provides important insights into the mixing of the $q\bar{q}$ and gluonic aspects of these two states. Because of chiral suppression factors associated with the light (non-strange) quarks, perturbative effects are unable to generate any significant amount of mixing. However, the chiral-violating contributions of the quark condensate, mixed condensate, and instantons do not suffer from this chiral suppression and provide the dominant contribution to the non-diagonal correlation function, implying that mixing of gluonic and $q\bar{q}$ degrees of freedom has a non-perturbative origin. Qualitatively, this conclusion is similar to that obtained for glueball decays [21] and to that of Ref. [51] which demonstrated that instantons can lead to a significant mixing between glueballs and (heavy quark) mesons in the pseudoscalar channel.

The state couplings that result from the analysis of the various GSRs provide an additional means to examine the self-consistency of the scenario of two states with masses of approximately 1 GeV and 1.4 GeV that couple to mixtures of $q\bar{q}$ and gluonic currents. In particular, the relative couplings between the states in the non-diagonal case is constrained by the relative couplings in the diagonal cases. The independent prediction of these couplings from the non-diagonal NGSR is found to satisfy this constraint extremely well, providing strong evidence for the validity of the mixing scenario.

The state couplings also provide a means to study the pattern of mixing associated with the couplings to gluonic and $q\bar{q}$ currents. The resulting pattern is similar to the two-angle mixing that occurs for the couplings (decay constants) for the η–η' system in the singlet–octet basis [50], and result in an effective mixing angle of $\phi \approx 54^\circ$ in excellent agreement with the sum-rule analyses of Refs. [9,10]. Because this mixing angle is in the region near maximal mixing ($\phi = 45^\circ$), there is only a slight preference for the heavier 1.4 GeV state to couple to gluonic currents and a concomitantly slight preference for the lighter 1.0 GeV state to couple to $q\bar{q}$ currents. Indeed, the existence of such strong mixing implies that qualitative features that would distinguish pure gluonic and $q\bar{q}$ states would be obscured for strongly-mixed states and the experimental signal of gluonium would thus be elusive.

In summary, our results provide strong QCD evidence to support the scenario where the mixing of $q\bar{q}$ and gluonium is manifested in the scalar hadronic spectrum as a lighter state on the order of 1 GeV and a heavier state on the order of 1.5 GeV [4,6,8–12,15]. In particular, our conclusion that there exists a strong mixing between gluonium and $q\bar{q}$ states is similar to the results from a variety of approaches [6,8–10] and our result for the heavier state's preference for gluonic channels provides QCD support for the findings of a large gluonic component of the $f_0(1500)$ [2,3].

Acknowledgements

The authors are grateful for financial support from the Natural Sciences and Engineering Research Council of Canada (NSERC). Many thanks to Hong-Ying Jin for helpful discussions. T.G.S. dedicates this work to the memory of Victor Elias.

References

[1] W.-M. Yao, et al., J. Phys. G 33 (2006) 1.
[2] F.E. Close, A. Kirk, Phys. Lett. B 483 (2000) 245;
De-Min Li, Hong Yu, Qi-Xing Shen, Mod. Phys. Lett. A 15 (2000) 1781.
[3] C. Amsler, F.E. Close, Phys. Rev. D 53 (1996) 295;
L. Burakovsky, P.R. Page, Phys. Rev. D 59 (1999) 014022;
F.E. Close, Qiang Zhao, Phys. Rev. D 71 (2005) 094022.

[4] A.H. Fariborz, Phys. Rev. D 74 (2006) 054030;
A.H. Fariborz, Int. J. Mod. Phys. A 19 (2004) 2095.
[5] M. Albaladejo, J.A. Oller, Phys. Rev. Lett. 101 (2008) 252002.
[6] P. Minkowski, W. Ochs, Eur. Phys. J. C 9 (1999) 283;
P. Minkowski, W. Ochs, arXiv:hep-ph/0209225.
[7] C.J. Morningstar, M. Peardon, Phys. Rev. D 60 (1999) 034509;
A. Vaccarino, D. Weingarten, Phys. Rev. D 60 (1999) 114501;
Y. Chen, et al., Phys. Rev. D 73 (2006) 014516.
[8] UKQCD Collaboration, A. Hart, C. McNeile, C. Michael, J. Pickavance, Phys. Rev. D 74 (2006) 114504.
[9] S. Narison, Nucl. Phys. B 509 (1998) 312.
[10] G. Mennessier, S. Narison, N. Paver, Phys. Lett. B 158 (1985) 153;
S. Narison, G. Veneziano, Int. J. Mod. Phys. A 4 (1989) 2751;
A. Bramon, S. Narison, Mod. Phys. Lett. A 4 (1989) 1113;
S. Narison, Phys. Rev. D 73 (2006) 114024.
[11] Tao Huang, Hong Ying Jin, Ai-lin Zhang, Phys. Rev. D 59 (1998) 034026.
[12] L.S. Kisslinger, J. Gardner, C. Vanderstraeten, Phys. Lett. B 410 (1997) 1.
[13] D. Harnett, T.G. Steele, Nucl. Phys. A 695 (2001) 205.
[14] G. Orlandini, T.G. Steele, D. Harnett, Nucl. Phys. A 686 (2001) 261.
[15] T.G. Steele, D. Harnett, G. Orlandini, AIP Conf. Proc. 688 (2004) 128, arXiv:hep-ph/0308074.
[16] S. Narison, N. Pak, N. Paver, Phys. Lett. B 147 (1984) 162.
[17] M.S. Chanowitz, Phys. Rev. Lett. 95 (2005) 172001.
[18] V.A. Novikov, M.A. Shifman, A.I. Vainshtein, V.I. Zakharov, Nucl. Phys. B 191 (1981) 301.
[19] S. Narison, QCD as a Theory of Hadrons, Cambridge University Press, 2004.
[20] H. Forkel, Phys. Rev. D 71 (2005) 054008.
[21] Z.F. Zhang, H.Y. Jin, arXiv:hep-ph/0511252v3.
[22] R.A. Bertlmann, G. Launer, E. de Rafael, Nucl. Phys. B 250 (1985) 61.
[23] P. Pascual, R. Tarrach, Phys. Lett. B 113 (1982) 495.
[24] N.K. Nielsen, Nucl. Phys. B 120 (1977) 212;
J.C. Collins, A. Duncan, S.D. Joglekar, Phys. Rev. D 16 (1977) 438.
[25] R. Tarrach, Nucl. Phys. B 196 (1982) 45.
[26] J.I. Latorre, S. Narison, S. Paban, Phys. Lett. B 191 (1987) 437.
[27] E.V. Shuryak, Nucl. Phys. B 203 (1982) 93.
[28] H. Forkel, Phys. Rev. D 64 (2001) 034015;
D. Harnett, T.G. Steele, V. Elias, Nucl. Phys. A 686 (2001) 393.
[29] D. Binosi, L. Theußl, Comp. Phys. Comm. 161 (2004) 76.
[30] M.A. Shifman, A.I. Vainshtein, V.I. Zakharov, Nucl. Phys. B 147 (1979) 385, 448.
[31] M. Jamin, M. Muenz, Z. Phys. C 60 (1993) 569.
[32] E. Bagan, J.I. Latorre, P. Pascual, Z. Phys. C 32 (1986) 43.
[33] E. Bagan, M.R. Ahmady, V. Elias, T.G. Steele, Z. Phys. C 61 (1994) 157.
[34] V. Elias, T.G. Steele, M.D. Scadron, Phys. Rev. D 38 (1988) 1584.
[35] A. Belavin, A. Polyakov, A. Schwartz, Y. Tyupkin, Phys. Lett. B 59 (1975) 85;
G. 't Hooft, Phys. Rev. D 14 (1976) 3432.
[36] T. Schäefer, E.V. Shuryak, Phys. Rev. Lett. 75 (1995) 1707.
[37] M. Abramowitz, I.E. Stegun, Mathematical Functions with Formulas, Graphs, and Mathematical Tables, National Bureau of Standards Applied Mathematics Series, National Bureau of Standards, Washington, 1972.
[38] S. Narison, Nucl. Phys. B (Proc. Suppl.) 54A (1997) 238.
[39] H.G. Dosch, M. Jamin, S. Narison, Phys. Lett. B 220 (1989) 251.
[40] V.A. Novikov, M.A. Shifman, A.I. Vainshtein, V.I. Zakharov, Nucl. Phys. B 165 (1980) 67.
[41] L.S. Kisslinger, M.B. Johnson, Phys. Lett. B 523 (2001) 127.
[42] S. Narison, Z. Phys. C 26 (1984) 209;
H. Forkel, Phys. Rev. D 71 (2005) 054008.
[43] E. Bagan, T.G. Steele, Phys. Lett. B 243 (1990) 413.
[44] J. Bordes, V. Gimènez, J.A. Peñarrocha, Phys. Lett. B 223 (1989) 251;
J.L. Liu, D. Liu, J. Phys. G 19 (1993) 373.
[45] N.V. Krasnikov, A.A. Pivovarov, N.N. Tavkhelidze, Z. Phys. C 19 (1983) 301.
[46] M.A. Shifman, Z. Phys. C 9 (1981) 347.

[47] C.A. Dominguez, N. Paver, Z. Phys. C 31 (1986) 591.
[48] Ailin Zhang, T.G. Steele, Nucl. Phys. A 728 (2003) 165.
[49] V. Elias, A.H. Fariborz, Fang Shi, T.G. Steele, Nucl. Phys. A 633 (1998) 279.
[50] A.V. Kisselev, V.A. Petrov, Z. Phys. C 58 (1993) 595;
Th. Feldmann, P. Kroll, B. Stech, Phys. Rev. D 58 (1998) 114006;
Th. Feldmann, P. Kroll, B. Stech, Phys. Lett. B 449 (1999) 339.
[51] N. Kochelev, Dong-Pil Min, Phys. Rev. D 72 (2005) 097502.

Chapter 7

Conclusions

Heavy quarkonium spectroscopy is a rapidly changing field, both experimentally and theoretically. In recent years many heavy quarkonium-like states have been discovered by the Babar, Belle, BES-III, CDF, CLEO, D0, and LHCb experiments. It is entirely possible that more heavy quarkonium-like states will be discovered by these experiments, or by new experiments being planned such as Belle-II [15] and $\overline{\mathrm{P}}$ANDA [83]. The heavy quarkonium sector provides perhaps the most promising "hunting ground" for exotic hadrons. Firm theoretical predictions for the properties of exotic hadrons are needed in order to determine the true nature of the heavy quarkonium-like states.

The main theme of research presented in this thesis has been to utilize QSR techniques to determine mass predictions for exotic hadrons that could exist among the heavy quarkonium-like states. This work has direct implications for the XYZ states. In Chapter 3 the mass of the $J^{PC} = 0^{-+}$ charmonium hybrid was found to be $3.82 \pm 0.13\,\mathrm{GeV}$, which is compatible with the $Y(3940)$. In Ref. [5] it was suggested that this particle could be a charmonium hybrid, and the mass prediction extracted in Chapter 3 is compatible with this interpretation. More experimental work is needed to establish the J^{PC} quantum numbers of this state. Similarly, the 1^{++} charmonium hybrid mass was predicted to be $5.13 \pm 0.25\,\mathrm{GeV}$ in Chapter 3. The LHCb collaboration has confirmed that the $X(3872)$ has $J^{PC} = 1^{++}$ [2], therefore the mass prediction in Chapter 3 helps to rule out the pure charmonium hybrid interpretation of this state [77]. In Chapter 4 the $J^P = 0^+$ and 1^+ charm-light diquark masses were predicted to be $1.86 \pm 0.05\,\mathrm{GeV}$ and $1.87 \pm 0.10\,\mathrm{GeV}$. In Ref. [84] the $X(3872)$ was interpreted as a tetraquark using a constituent diquark model. The $J^P = 0^+$ and 1^+ charm-light diquark masses were determined to be $1.93\,\mathrm{GeV}$, which is compatible with the mass predictions extracted in Chapter 4. This agreement provides QCD support for the predictions of the

constituent diquark model developed in Ref. [84]. In particular, this agreement provides indirect support for the tetraquark interpretation of the $Z_c^{\pm}(3895)$. The $J^P = 0^+$ and 1^+ bottom-light diquark masses were also extracted in Chapter 4, finding a common mass of $5.08 \pm 0.04\,\text{GeV}$. This is in reasonable agreement with the constituent bottom-light diquark mass of $5.20\,\text{GeV}$ determined from a constituent diquark model of the $Y_b(10890)$ in Ref. [10]. Therefore the bottom-light diquark mass prediction extracted in Chapter 4 supports the tetraquark interpretations of the $Y_b(10890)$, $Z_b^{\pm}(10610)$ and $Z_b^{\pm}(10650)$.

A secondary theme in this research has been renormalization methodology. QSR calculations involve correlation functions of composite local operators. The renormalization of these composite operators can significantly complicate QSR calculations. In Chapter 4, next-to-leading order perturbative contributions to the heavy-light diquark correlation function were calculated. In order to renormalize these contributions the heavy quark mass and diquark current must be renormalized. The scalar diquark operator renormalization factor was determined in Chapter 5. A QSR analysis of mixing between scalar mesons and gluonium was performed in Chapter 6. The leading order perturbative contribution to the bare non-diagonal correlation function was found to contain a non-local divergence. This problem was resolved through the use of the renormalized scalar glueball operator, which mixes under renormalization with the scalar meson operator. The renormalization induced contributions of the scalar meson operator served to cancel the divergence in the bare non-diagonal correlation function. The research in Chapters 4 and 6 illustrates the two distinct ways in which composite operator renormalization can complicate QSR calculations: it can be required in leading order contributions due to operator mixing or in higher order contributions due to the multiplicative renormalization of the current being used.

The QSR calculations in this thesis have largely been concerned with heavy quarkonium-like states that contain heavy quarks. Unlike calculations that involve only light quarks whose masses can be neglected, the heavy quark mass cannot be ignored. In practice this means that loop integrals that involve heavy quarks are much more complicated than those that involve only light quarks. The loop integration techniques developed in Chapter 2 are crucial to the QSR analyses in Chapters 3 and 4. In addition, the renormalization methodology used in Chapters 4 and 6 is dependent upon the loop integration methods discussed in Chapter 2.

The research presented in this thesis can be extended in several ways. First, the QSR studies of $J^{PC} = 1^{++}$ and 0^{-+} heavy quarkonium hybrids in Chapter 3 have been extended to additional J^{PC} channels in Ref. [33]. This will provide useful information regarding the spectrum of heavy quarkonium hybrids, enabling a comparison between QSR and lattice QCD predictions [78]. Second, the heavy-light diquark analysis in Chapter 4 can be generalized to doubly-heavy diquarks, which could be used to study heavy baryons as well as doubly-charmed or doubly-bottomed tetraquarks. Third, the scalar diquark operator renormalization factor determined in Chapter 5 could be used to extend existing QSR studies of scalar diquarks to higher orders. Finally, the renormalization methodology applied to the mixing between scalar mesons and gluonia in Chapter 6 can be applied to study possible mixing among the heavy quarkonium-like states. These methods have been used to study mixing between heavy quarkonium hybrids and four-quark states in Ref. [32].

The unanticipated XYZ states have heralded a golden age in hadron spectroscopy. In order to determine if any of these states are exotic hadrons, theoretical calculations are needed to clearly establish the expected properties of exotic hadrons that may coexist with heavy quarkonia. The QSR method is a powerful, QCD-based technique that can be used to perform these calculations. To date, there have been many QSR studies of heavy quarkonium-like states. However most of these have focused on four-quark states and have only included leading order perturbative contributions in the OPE. It is desirable to extend QSR calculations to higher order so that more complete and accurate predictions for the properties of exotic hadrons can be obtained. In order to do so, the renormalization methodology and loop integration techniques discussed in this thesis are essential. The techniques used in this thesis can be used to extract more accurate QSR predictions of the properties of exotic hadrons and therefore aid in efforts to determine the true natures of the heavy quarkonium-like states.

References

[1] G. Aad et al., Phys. Lett. **B716** (2012), 1.

[2] R Aaij et al., arXiv:1302.6269 [hep-ex].

[3] R. Aaij et al., Eur. Phys. J. **C72** (2012), 1972.

[4] V.M. Abazov et al., Phys. Rev. Lett. **93** (2004), 162002.

[5] K. Abe et al., Phys. Rev. Lett. **94** (2005), 182002.

[6] M. Ablikim et al., Phys. Rev. Lett. **110** (2013), 252001.

[7] M. Abramowitz and I.A. Stegun, *Handbook of Mathematical Functions*, Dover, 1964.

[8] D. Acosta et al., Phys. Rev. Lett. **93** (2004), 072001.

[9] M.T. AlFiky, F. Gabbiani, and A.A. Petrov, Phys. Lett. **B640** (2006), 238.

[10] A. Ali, C. Hambrock, and W. Wang, Phys. Rev. **D85** (2012), 054011.

[11] M. Anselmino, E. Predazzi, S. Ekelin, S. Fredriksson, and D. B. Lichtenberg, Rev. Mod. Phys. **65** (1993), 1199–1234.

[12] T. Appelquist and J. Carazzone, Phys. Rev. **D11** (1975), 2856.

[13] B. Aubert et al., Phys. Rev. Lett. **93** (2004), 041801.

[14] B. Aubert et al., Phys. Rev. Lett. **101** (2008), 082001.

[15] T. Aushev, W. Bartel, A. Bondar, J. Brodzicka, T.E. Browder, et al., arXiv:1002.5012 [hep-ex].

[16] E. Bagan, M.R. Ahmady, V. Elias, and T.G. Steele, Z. Phys. **C61** (1994), 157.

[17] T. Barnes, F.E. Close, and E.S. Swanson, Phys. Rev. **D52** (1995), 5242–5256.

[18] C. Becchi, A. Rouet, and R. Stora, Ann. Phys. **98** (1976), 287.

[19] R. Berg, D. Harnett, R.T. Kleiv, and T.G. Steele, Phys. Rev. **D86** (2012), 034002.

[20] J. Beringer et al., Phys. Rev. **D86** (2012), 010001.

[21] R.A. Bertlmann, G. Launer, and E. de Rafael, Nucl. Phys. **B250** (1985), 61.

[22] S. Bethke, Eur. Phys. J. **C64** (2009), 689.

[23] D. Binosi and L. Theussl, Comput. Phys. Commun. **161** (2004), 76.

[24] J.D. Bjorken and S.D. Drell, *Relativistic Quantum Mechanics*, McGraw-Hill, 1964.

[25] C.G. Bollini and J.J. Giambiagi, Phys. Lett. **B40** (1972), 566.

[26] A. Bondar et al., Phys. Rev. Lett. **108** (2012), 122001.

[27] E.E. Boos and A.I. Davydychev, Theor. Math. Phys. **89** (1991), 1052.

[28] N. Brambilla, S. Eidelman, B.K. Heltsley, R. Vogt, G.T. Bodwin, et al., Eur. Phys. J. **C71** (2011), 1534.

[29] D.J. Broadhurst, J. Fleischer, and O.V. Tarasov, Z. Phys. **C60** (1993), 287.

[30] S. Chatrchyan et al., Phys. Lett. **B716** (2012), 30.

[31] K.F. Chen et al., Phys. Rev. Lett. **100** (2008), 112001.

[32] W. Chen, H.Y. Jin, R.T. Kleiv, T.G. Steele, M. Wang, et al., arXiv:1305.0244 [hep-ph].

[33] W. Chen, R.T. Kleiv, T.G. Steele, B. Bulthuis, D. Harnett, J. Ho, T. Richards, and S.L. Zhu, arXiv:1304.4522 [hep-ph].

[34] K.G. Chetyrkin, A.L. Kataev, and F.V. Tkachov, Nucl. Phys. **B174** (1980), 345.

[35] K.G. Chetyrkin and F.V. Tkachov, Nucl. Phys. **B192** (1981), 159.

[36] S.K. Choi et al., Phys. Rev. Lett. **91** (2003), 262001.

[37] F.E. Close and P.R. Page, Phys. Lett. **B578** (2004), 119–123.

[38] P. Colangelo and A. Khodjamirian, arXiv:0010175 [hep-ph].

[39] John C. Collins, *Renormalization: an Introduction to Renormalization, the Renormalization Group and the Operator-Product Expansion*, Cambridge University Press, 1984.

[40] A.I. Davydychev, J. Math. Phys. **33** (1992), 358.

[41] H.G. Dosch, M. Jamin, and S. Narison, Phys. Lett. **B220** (1989), 251.

[42] H.G. Dosch, M. Jamin, and B. Stech, Z. Phys. **C42** (1989), 167.

[43] S. Dubnicka, A.Z. Dubnickova, M.A. Ivanov, and J.G. Korner, Phys. Rev. **D81** (2010), 114007.

[44] D. Ebert, R.N. Faustov, and V.O. Galkin, Phys. Lett. **B634** (2006), 214.

[45] G. Ecker, Prog. Part. Nucl. Phys. **35** (1995), 1.

[46] V. Elias, A.H. Fariborz, F. Shi, and T.G. Steele, Nucl. Phys. **A633** (1998), 279.

[47] A. Erdelyi, *Higher Transcendental Functions (Bateman Manuscript Project)*, vol. 1, McGraw-Hill Book Company, Inc., 1953.

[48] R. Faccini, L. Maiani, F. Piccinini, A. Pilloni, A.D. Polosa, et al., arXiv:1303.6857 [hep-ph].

[49] L. D. Faddeev and V. N. Popov, Phys. Lett. **25B** (1967), 19.

[50] R.P Feynman and A.R. Hibbs, *Quantum Mechanics and Path Integrals*, McGraw-Hill, 1965.

[51] M. Gell-Mann, Phys. Lett. **8** (1964), 214.

[52] M. Gell-Mann, R.J Oakes, and B. Renner, Phys. Rev. **175** (1968), 2195.

[53] S. Godfrey, arXiv:0910.3409 [hep-ph].

[54] J. Govaerts, L.J. Reinders, P. Francken, X. Gonze, and J. Weyers, Nucl. Phys. **B284** (1987), 674.

[55] J. Govaerts, L.J. Reinders, H.R. Rubinstein, and J. Weyers, Nucl. Phys. **B258** (1985), 215.

[56] J. Govaerts, L.J. Reinders, and J. Weyers, Nucl. Phys. **B262** (1985), 575.

[57] O.W. Greenberg, Phys. Rev. Lett. **13** (1964), 598–602.

[58] D.J. Griffiths, *Introduction to Elementary Particles*, John Wiley & Sons, Inc., 1987.

[59] D. Harnett, R.T. Kleiv, K. Moats, and T.G. Steele, Nucl. Phys. **A850** (2011), 110.

[60] D. Harnett, R.T. Kleiv, T.G. Steele, and H.Y. Jin, J. Phys. **G39** (2012), 125003.

[61] D. Harris and K. Riesselmann, *Deconstruction: Standard Model Discoveries*, Symmetry Magazine **6** (2009), 30.

[62] T. Huber and D. Maitre, Comput. Phys. Commun. **175** (2006), 122.

[63] Tobias Huber and D. Maitre, Comput. Phys. Commun. **178** (2008), 755.

[64] M.Z. Iofa and I.V. Tyutin, Theor. Math. Phys. **27** (1976), 316.

[65] M. Jamin and M. Kremer, Nucl. Phys. **B277** (1986), 349.

[66] M. Jamin and B.O. Lange, Phys. Rev. **D65** (2002), 056005.

[67] M. Jamin and M. Neubert, Phys. Lett. **B238** (1990), 387.

[68] M.Y. Kalmykov, JHEP **0604** (2006), 056.

[69] Y. Kim, I.J. Shin, and T. Tsukioka, Prog. Part. Nucl. Phys. **68** (2013), 55.

[70] R.T. Kleiv and T.G. Steele, J. Phys. **G38** (2011), 025001.

[71] R.T. Kleiv, T.G. Steele, A. Zhang, and I. Blokland, Phys. Rev. **D87** (2013), 125018.

[72] E. Klempt and A. Zaitsev, Phys. Rept. **454** (2007), 1.

[73] A.S. Kronfeld, Ann. Rev. Nucl. Part. Sci. **62** (2012), 265.

[74] W. Kwong, J.L. Rosner, and C. Quigg, Ann. Rev. Nucl. Part. Sci. **37** (1987), 325.

[75] I.W. Lee, A. Faessler, T. Gutsche, and V.E. Lyubovitskij, Phys. Rev. **D80** (2009), 094005.

[76] L. Lewin, *Polylogarithms and Associated Functions*, North-Holland, 1981.

[77] B.A. Li, Phys. Lett. **B605** (2005), 306–310.

[78] L. Liu et al., JHEP **1207** (2012), 126.

[79] L. Liu, S.M. Ryan, M. Peardon, G. Moir, and P. Vilaseca, arXiv:1112.1358 [hep-lat].

[80] X. Liu, Z.G. Luo, Y.R. Liu, and S.L. Zhu, Eur. Phys. J. **C61** (2009), 411.

[81] Z.Q. Liu et al., Phys. Rev. Lett. **110** (2013), 252002.

[82] Y.L. Luke, *The Special Functions and their Approximations*, vol. 1, Academic Press, 1969.

[83] M.F.M. Lutz et al., arXiv:0903.3905 [hep-ex].

[84] L. Maiani, F. Piccinini, A.D. Polosa, and V. Riquer, Phys. Rev. **D71** (2005), 014028.

[85] P. Maris and C.D. Roberts, Int. J. Mod. Phys. **E12** (2003), 297.

[86] R. Matheus, S. Narison, M. Nielsen, and J.M. Richard, Phys. Rev. **D75** (2007), 014005.

[87] V. Mathieu, N. Kochelev, and V. Vento, Int. J. Mod. Phys. **E18** (2009), 1.

[88] R. Mertig and R. Scharf, Comput. Phys. Commun. **111** (1998), 265.

[89] S. Narison, *QCD as a Theory of Hadrons: From Partons to Confinement*, Cambridge University Press, 2007.

[90] S. Narison, Phys. Lett. **B693** (2010), 559–566.

[91] S. Narison, Phys. Lett. **B706** (2012), 412.

[92] S. Narison and R. Tarrach, Phys. Lett. **B125** (1983), 217.

[93] M. Neubert, Phys. Rept. **245** (1994), 259.

[94] M. Nielsen, F.S. Navarra, and S.H. Lee, Phys. Rept. **497** (2010), 41.

[95] V.A. Novikov, M.A. Shifman, A.I. Vainshtein, and V.I. Zakharov, Fortsch. Phys. **32** (1984), 585.

[96] W. Ochs, J. Phys. G **40** (2013), 043001.

[97] P. Pascual and R. Tarrach, *QCD: Renormalization for the Practitioner*, Springer-Verlag, 1984.

[98] G. Passarino and M.J.G. Veltman, Nucl. Phys. **B160** (1979), 151.

[99] S. Perantonis and C. Michael, Nucl. Phys. **B347** (1990), 854–868.

[100] M.E. Peskin and D.V. Schroeder, *An Introduction to Quantum Field Theory*, Westview Press, 1995.

[101] G. Pólya and G. Latta, *Complex Variables*, Wiley, 1974.

[102] C.F. Qiao, L. Tang, G. Hao, and X.Q. Li, J. Phys. **G39** (2012), 015005.

[103] E.D. Rainville, *Special Functions*, The Macmillan Company, 1960.

[104] L.J. Reinders, H. Rubinstein, and S. Yazaki, Phys. Rept. **127** (1985), 1.

[105] J.M. Richard, arXiv:1205.4326 [hep-ph].

[106] M.A. Shifman, A.I. Vainshtein, and V.I. Zakharov, Nucl. Phys. **B147** (1979), 385.

[107] M.A. Shifman, A.I. Vainshtein, and V.I. Zakharov, Nucl. Phys. **B147** (1979), 448.

[108] L.J. Slater, *Generalized Hypergeometric Functions*, Cambridge University Press, 1966.

[109] A.A. Slavnov, Sov. Jour. Part. Nucl. **5** (1975), 303.

[110] V.A. Smirnov, *Evaluating Feynman Integrals*, vol. 211, Springer, 2004.

[111] Mark Srednicki, *Quantum Field Theory*, Cambridge University Press, 2007.

[112] M. Steinhauser, Phys. Rept. **364** (2002), 247–357.

[113] E.S. Swanson, Phys. Lett. **B588** (2004), 189.

[114] E.S. Swanson, Phys. Rept. **429** (2006), 243.

[115] G. 't Hooft and M.J.G. Veltman, Nucl. Phys. **B44** (1972), 189.

[116] G. 't Hooft and M.J.G. Veltman, Nucl. Phys. **B50** (1972), 318.

[117] O.V. Tarasov, Phys. Rev. **D54** (1996), 6479–6490.

[118] O.V. Tarasov, Nucl. Phys. **B502** (1997), 455–482.

[119] O.V. Tarasov, Acta Phys. Polon. **B29** (1998), 2655.

[120] J.C. Taylor, Nucl. Phys. **B33** (1971), 436.

[121] K. Terasaki, Prog. Theor. Phys. **118** (2007), 821–826.

[122] C.E. Thomas and F.E. Close, Phys. Rev. **D78** (2008), 034007.

[123] N.A. Tornqvist, Phys. Lett. **B590** (2004), 209–215.

[124] M.B. Voloshin, Phys. Lett. **B579** (2004), 316.

[125] Z.G. Wang, Eur. Phys. J. **C71** (2011), 1524.

[126] Z.G. Wang, Commun. Theor. Phys. **59** (2013), 451.

[127] K.G. Wilson, Phys. Rev. **179** (1969), 1499.

[128] T. Xiao, S. Dobbs, A. Tomaradze, and K.K. Seth, arXiv:1304.3036 [hep-ex].

[129] A. Zhang, T. Huang, and T.G. Steele, Phys. Rev. **D76** (2007), 036004.

[130] S.L. Zhu, Phys. Lett. **B625** (2005), 212.

[131] G. Zweig, CERN-TH **412** (1964), 80.

Appendix A

Conventions

For brevity four-vectors are often written without a Lorentz index, that is, it is to be understood that $x = (x^0\,, x^1\,, x^2\,, x^3)$. When used, three-vectors are denoted as $\mathbf{x} = (x^1\,, x^2\,, x^3)$. The following convention is used for the four-dimensional Minkowski space metric:

$$g_{\mu\nu} = \begin{bmatrix} 1 & 0 & 0 & 0 \\ 0 & -1 & 0 & 0 \\ 0 & 0 & -1 & 0 \\ 0 & 0 & 0 & -1 \end{bmatrix}, \quad g_{\mu\nu}\, p^\mu k^\nu = p \cdot k = p^0 k^0 - \mathbf{p} \cdot \mathbf{k}\,. \tag{A.1}$$

In d-dimensions, the metric is defined such that $g^{\mu\nu} g_{\mu\nu} = d$. The Einstein summation convention is assumed on all indices, that is, a product containing repeated spinor, colour, Lorentz or SU(3) indices is summed over the full range of the indices. Apart from Lorentz indices, no distinction is made between raised and lowered indices. That is, $A^a_\mu = A_{\mu\, a}$, for instance.

We use the conventions of Ref. [24] for the Dirac gamma matrices. In what follows each matrix element is itself a two by two matrix (*i.e.* the two by two identity matrix is denoted as 1). The specific forms are

$$\gamma^0 = \begin{bmatrix} 1 & 0 \\ 0 & -1 \end{bmatrix}, \quad \gamma^i = \begin{bmatrix} 0 & \sigma^i \\ -\sigma^i & 0 \end{bmatrix}, \quad i = \{1\,, 2\,, 3\}\,, \tag{A.2}$$

where σ^i is a Pauli matrix. In these conventions,

$$\gamma^5 = i\gamma^0\gamma^1\gamma^2\gamma^3 = \begin{bmatrix} 0 & 1 \\ 1 & 0 \end{bmatrix}, \tag{A.3}$$

from which it follows that $(\gamma_5)^2 = 1$. Ref. [39] discusses various approaches to defining γ_5

in d-dimensions. In QSR calculations using dimensional regularization it is conventional to define γ_5 such that $\{\gamma_5\,,\gamma_\mu\}=0$ [89]. The charge conjugation operator is defined as

$$C = i\gamma^2\gamma^0\,. \tag{A.4}$$

The following properties are useful in Chapters 4 and 5:

$$C^{-1}=C^T=-C\,,\quad C^2=-1\,,\quad C\gamma_\mu^T C=\gamma_\mu\,,\quad [C\,,\gamma_5]=0\,, \tag{A.5}$$

where T denotes the transpose.

Natural units are used, where $\hbar=c=1$. Using the relativistic invariant it can be shown that

$$E^2=(\mathbf{p}c)^2+\left(mc^2\right)^2\,,\quad \xrightarrow{c=1}\quad [E]=[\mathbf{p}]=[m]\,, \tag{A.6}$$

so that energy, momentum and mass have identical dimensions in this system of units. It is conventional to chose energy units as the base unit for all quantities. For instance, in natural units the masses of the electron and proton are approximately $0.511\,\mathrm{MeV}$ and $938\,\mathrm{MeV}$, respectively.

Dimensional analysis in natural units is straightforward. We define $[m]=1$, from which it follows that $[E]=[\mathbf{p}]=[p_\mu]=1$. Because momenta and derivatives are related through Fourier transforms, $[\partial_\mu]=[p_\mu]=1$. From the expression for a plane wave it can be shown that

$$e^{ip\cdot x}\quad\rightarrow\quad [p\cdot x]=0\,,\quad\rightarrow\quad [x]=-1\,, \tag{A.7}$$

and consequently $\left[d^d x\right] = -d$. By a similar argument it can be shown that

$$\exp\left[i\int d^d x\,\mathcal{L}\right] \quad \rightarrow \quad \left[\int d^d x\,\mathcal{L}\right] = 0 \quad \rightarrow \quad [\mathcal{L}] = d\,. \tag{A.8}$$

This can be used to determine the dimensions of the fields and parameters appearing in the QCD Lagrangian (1.40). For instance, from the quark term we can show that

$$\left[\bar{Q}\gamma^\mu\partial_\mu Q\right] = d \quad \rightarrow \quad \left[\bar{Q}\right] = [Q] = \frac{d-1}{2}\,, \tag{A.9}$$

because the Dirac Gamma matrix is dimensionless. From the gluon term we find that

$$\left[G^{\mu\nu}_a G^a_{\mu\nu}\right] = d \quad \rightarrow \quad \left[G^a_{\mu\nu}\right] = \left[\partial_\mu A^a_\mu\right] = \frac{d}{2} \quad \rightarrow \quad \left[A^a_\mu\right] = \frac{d-2}{2}\,. \tag{A.10}$$

The units of the coupling can be determined from the quark-gluon interaction term:

$$\left[g\bar{Q}\frac{\lambda^a}{2}\gamma^\mu A^a_\mu Q\right] = d\,, \quad \rightarrow \quad [g] = \frac{4-d}{2}\,, \tag{A.11}$$

because the Gell-Mann matrix is dimensionless. The renormalization scale has $[\mu] = 1$, therefore

$$[\alpha] = \left[g^2\mu^{d-4}\right] = 0\,, \tag{A.12}$$

and hence α is an appropriate expansion parameter in d-dimensions.

Appendix B

Mathematical Functions

This appendix briefly summarizes the relevant properties of the special functions that are used in Chapters 2, 3, 4, 5 and 6. The material in Section B.1 is taken from Refs. [101, 7], that of Section B.2 can be found in Refs. [47, 108, 82, 103], and Ref. [76] contains the material in Section B.3.

B.1 The Gamma Function

As we have seen, the Gamma function arises frequently in dimensional regularization. A plot of the Gamma function is shown in Fig. B.1.

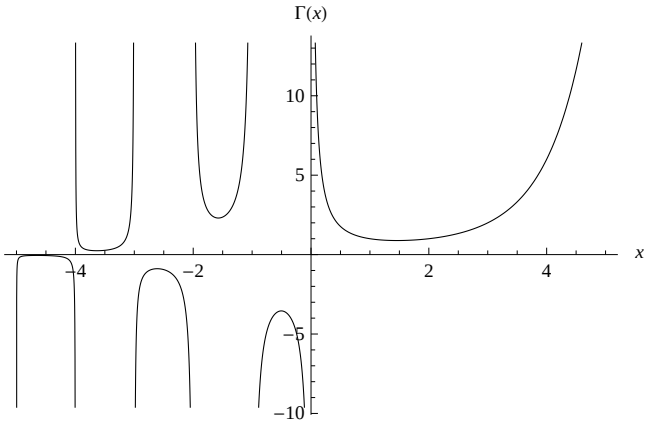

Figure B.1: The Gamma function.

The Gamma function provides an extension of the factorial to non-integers:

$$\Gamma(n) = (n-1)!\,, \quad \Gamma(z+1) = z\Gamma(z)\,. \tag{B.1}$$

$\Gamma(z)$ has a simple pole when its argument is zero or a negative integer, the residue of which

is

$$\mathrm{Res}\,\Gamma\,(\mathrm{z})|_{z\to -n} = \frac{(-1)^n}{n!}\,. \tag{B.2}$$

Note that there is no value of z for which $\Gamma\,(z) = 0$, hence $[\Gamma\,(z)]^{-1}$ is an entire function. An integral representation is given by

$$\Gamma\,(z) = \int_0^\infty dt\, t^{z-1} e^{-t}\,, \quad \mathrm{Re}(z) > 0\,. \tag{B.3}$$

Using (B.3), it can be shown that $\Gamma\left(\frac{1}{2}\right) = \sqrt{\pi}$. The argument of the Gamma function can be simplified using the identity

$$\Gamma\,(2z) = \frac{2^{2x-\frac{1}{2}}}{\sqrt{2\pi}}\Gamma\,(z)\,\Gamma\left(z+\frac{1}{2}\right)\,. \tag{B.4}$$

In order to construct series expansions of the Gamma function, it is helpful to introduce the Digamma function

$$\psi\,(z) = \frac{1}{\Gamma\,(z)}\frac{d}{dz}\Gamma\,(z)\,, \tag{B.5}$$

and the closely related Polygamma function

$$\psi^{(n)}\,(z) = \frac{d^n}{dz^n}\psi\,(z)\,. \tag{B.6}$$

Numerical values of these functions at $z = 1$ are

$$\psi\,(1) = -\gamma_E\,, \quad \psi^{(n)}\,(1) = (-1)^n\; n!\,\zeta\,(n+1)\,, \tag{B.7}$$

where $\gamma_E \simeq 0.577$ is the Euler-Mascheroni constant and $\zeta\,(z)$ is the Riemann Zeta function.

Using these results, it is easy to show that

$$\Gamma(1+z) = 1 - \gamma_E z + \frac{1}{2}\left[\gamma_E^2 + \zeta(2)\right] z^2 + \mathcal{O}\left(z^3\right) . \tag{B.8}$$

Using (B.1) and (B.8), it can be shown that

$$\Gamma(z) = \frac{1}{z} - \gamma_E + \frac{1}{2}\left[\gamma_E^2 + \zeta(2)\right] z + \mathcal{O}\left(z^2\right) . \tag{B.9}$$

The Beta function is defined in terms of the Gamma function as

$$B(a\,,b) = \frac{\Gamma(a)\,\Gamma(b)}{\Gamma(a+b)} . \tag{B.10}$$

Integral representations of the Beta function are

$$B(a\,,b) = \int_0^1 dx\, x^{a-1}\,(1-x)^{b-1} = \int_0^\infty dx\, \frac{x^{a-1}}{(1+x)^{a+b}} . \tag{B.11}$$

B.2 Hypergeometric Functions

The generalized hypergeometric function is defined as

$$\begin{aligned} {}_pF_q\left[a_1\,,a_2\,,\ldots a_p\,;b_1\,,b_2\,,\ldots b_q\,;z\right] &= {}_pF_q\left[\left.\begin{matrix} a_1\,,a_2\,,\ldots a_p \\ b_1\,,b_2\,,\ldots b_q \end{matrix}\right| z\right] \\ = \frac{\Gamma(b_1)\,\Gamma(b_2)\ldots\Gamma(b_q)}{\Gamma(a_1)\,\Gamma(a_2)\ldots\Gamma(a_p)} &\sum_{n=0}^{\infty} \frac{\Gamma(a_1+n)\,\Gamma(a_2+n)\ldots\Gamma(a_p+n)}{\Gamma(b_1+n)\,\Gamma(b_2+n)\ldots\Gamma(b_q+n)} \frac{z^n}{n!} , \end{aligned} \tag{B.12}$$

where the constants a_i, b_i are called indices and uniquely define each generalized hypergeometric function. From this definition it is clear that the ordering of the indices is irrelevant and that if any $a_i = b_j$ $(1 \le i \le p\,,\, 1 \le j \le q)$, the generalized hypergeometric function ${}_pF_q$ reduces to ${}_{p-1}F_{q-1}$. When $p = q+1$, the generalized hypergeometric function has a branch cut on the interval $z \in [1\,,\infty)$. Generalized hypergeometric functions can also be

represented in terms of Mellin-Barnes contour integrals. For instance, the following contour integral representation

$$
\begin{aligned}
&{}_pF_q\left[a_1\,,a_2\,,\ldots a_p\,;b_1\,,b_2\,,\ldots b_q\,;z\right] \\
&\quad=\frac{\Gamma\left(b_1\right)\Gamma\left(b_2\right)\ldots\Gamma\left(b_q\right)}{\Gamma\left(a_1\right)\Gamma\left(a_2\right)\ldots\Gamma\left(a_p\right)}\int_{-i\infty}^{i\infty}\frac{ds}{2\pi i}\frac{\Gamma\left(a_1+s\right)\Gamma\left(a_2+s\right)\ldots\Gamma\left(a_p+s\right)}{\Gamma\left(b_1+s\right)\Gamma\left(b_2+s\right)\ldots\Gamma\left(b_q+s\right)}\Gamma\left(-s\right)\left(-z\right)^s
\end{aligned}
\tag{B.13}
$$

is completely equivalent to the series representation (B.12). The integral can be evaluated using the residue theorem, and the integration along the imaginary axis can be shifted to avoid poles if needed. Note that the Gamma functions of the form $\Gamma\left(c+s\right)$ have poles in the left half plane, while the Gamma function $\Gamma\left(-s\right)$ has poles in the right half plane. In order to reproduce (B.12), the contour should be closed in the right half plane, and the residues can be calculated using (B.2). If the integration contour is closed appropriately, it can be shown that all contributions apart from the integration along the imaginary axis are zero. The proof of this is rather delicate and is not given here (see Refs. [108, 103]). Using (B.13), we can write

$$
{}_1F_0\left[n\,;\,;z\right]=\frac{1}{\left(1-z\right)^n}=\frac{1}{\Gamma\left(n\right)}\int_{-\infty}^{i\infty}\frac{ds}{2\pi i}\Gamma\left(n+s\right)\Gamma\left(-s\right)\left(-z\right)^s\,. \tag{B.14}
$$

This identity permits massive propagators to be expressed as contour integrals of massless propagators and is the foundation of the Mellin-Barnes techniques used in Chapter 2 to calculate loop integrals with two massive propagators. An important identity for contour integrals of the form (B.13) is Barnes' Lemma:

$$
\int_{-\infty}^{i\infty}\frac{ds}{2\pi i}\Gamma\left(a+s\right)\Gamma\left(b+s\right)\Gamma\left(c+s\right)\Gamma\left(d+s\right)=\frac{\Gamma\left(a+c\right)\Gamma\left(a+d\right)\Gamma\left(b+c\right)\Gamma\left(b+d\right)}{\Gamma\left(a+b+c+d\right)}\,. \tag{B.15}
$$

Most special functions encountered in Mathematical Physics can be expressed in terms of generalized hypergeometric functions (see Ref. [82] for a partial list). The most commonly

known hypergeometric function is the Gauss hypergeometric function, ${}_2F_1\left[a\,,b\,;c\,;z\right]$, of which the Chebyshev, Gegenbauer, Jacobi and Legendre polynomials are special cases. The Gauss hypergeometric function has the integral representation

$$ {}_2F_1\left[a\,,b\,;c\,;z\right] = \frac{\Gamma\left(c\right)}{\Gamma\left(a\right)\Gamma\left(c-b\right)} \int_0^1 dt\, t^{b-1}\left(1-t\right)^{c-b-1}\left(1-tz\right)^{-a}\,, \quad \mathrm{Re}\left(c\right) > \mathrm{Re}\left(b\right) > 0\,. \tag{B.16} $$

At $z=1$, the Gauss hypergeometric function reduces to

$$ {}_2F_1\left[a\,,b\,;c\,;1\right] = \frac{\Gamma\left(c\right)\Gamma\left(c-a-b\right)}{\Gamma\left(c-a\right)\Gamma\left(c-b\right)}\,, \quad \mathrm{Re}\left(c-a-b\right) > 0\,. \tag{B.17} $$

It is interesting to note that there are recurrence relations relating ${}_2F_1\left[a\,,b\,;c\,;z\right]$ and the contiguous functions ${}_2F_1\left[a\pm 1\,,b\pm 1\,;c\pm 1\,;z\right]$ (See Ref. [7]). In Ref. [119] it is pointed out that these are closely related to the generalized recurrence relations discussed in Chapter 2.

B.3 Polylogarithms

In Chapter 2 it was pointed out that loop integrals that include an external momentum and a mass often lead to generalized hypergeometric functions whose indices of are d-dependent. Higher order terms in the epsilon expansion of these often involve Polylogarithm functions [76]. The simplest Polylogarithm is the Dilogarithm, which is defined as

$$ \mathrm{Li}_2\left(z\right) = -\int_0^z ds\,\frac{\log\left(1-s\right)}{s}\,, \tag{B.18} $$

which has the same branch cut as the generalized hypergeometric function (B.12). The numerical value at $z=1$ is given by

$$ \mathrm{Li}_2\left(1\right) = \frac{\pi^2}{6}\,. \tag{B.19} $$

In general, the Polylogarithm is defined recursively:

$$\mathrm{Li}_n(z) = \int_0^z ds\, \frac{\mathrm{Li}_{n-1}(s)}{s}\,, \tag{B.20}$$

which for $n = 3$ is called the Trilogarithm. The Dilogarithm satisfies the identity

$$\mathrm{Li}_2(1-z) = \frac{\pi^2}{6} - \log(z)\log(1-z) - \mathrm{Li}_2(z)\ . \tag{B.21}$$

The Trilogarithm satisfies a similar identity,

$$\begin{aligned}\mathrm{Li}_3(1-z) = \frac{\pi^2}{6}\log(1-z) + \frac{1}{6}\log^3(1-z) - \frac{1}{2}\log^2(1-z)\log(z) - \mathrm{Li}_3(z) \\ - \mathrm{Li}_3\left(\frac{z}{z-1}\right) + \zeta(3)\ .\end{aligned} \tag{B.22}$$

As mentioned previously, the Mathematica package HypExp can perform epsilon expansions of some generalized hypergeometric functions. This was used in the heavy-light diquark calculation in Chapter 4. However, when this package was used some functions with an inappropriate branch cut structure were generated. Using the identities (B.21) and (B.22), the functions with this branch structure can be canceled identically, and those that remain have the appropriate branch cut structure.